DEVELOPMENT OF INTERMOLECULAR C-H FUNCTIONALIZATION METHODS FOR ACCEPTOR-ACCEPTOR DIAZO COMPOUNDS

A Dissertation
Presented to
The Academic Faculty

by

Brett D. McLarney

In Partial Fulfillment
of the Requirements for the Degree
Doctor of Philosophy in the
School of Chemistry and Biochemistry

Georgia Institute of Technology
August, 2018

DEVELOPMENT OF INTERMOLECULAR C-H FUNCTIONALIZATION METHODS FOR ACCEPTOR-ACCEPTOR DIAZO COMPOUNDS

Approved by:

Dr. Stefan France, Advisor
School of Chemistry and Biochemistry
Georgia Institute of Technology

Dr. Joseph Sadighi
School of Chemistry and Biochemistry
Georgia Institute of Technology

Dr. Djamaladdin Musaev, Co-Advisor
Cherry L. Emerson Center for Scientific Computation
Emory University

Dr. William Gutekunst
School of Chemistry and Biochemistry
Georgia Institute of Technology

Dr. Charles Liotta
School of Chemistry and Biochemistry
Georgia Institute of Technology

Date Approved: April 13, 2018

To scientists

ACKNOWLEDGEMENTS

I acknowledge the support of my committee members, especially that of Stefan France and Jamal Musaev, two who played distinct and critical roles in my development as a scientist. These two individuals have different personalities, and working between them provided me with the best-of-both-worlds in terms of mentorship. I thank Charlie Liotta for being an excellent career mentor as well as teacher – Charlie's enthusiasm for physical organic chemistry is contagious and inspired my physical organic chemistry-infused approach toward research. I thank Joseph Sadighi, whose class on organometallic chemistry was invaluable during my graduate career. Seth Marder, an original member of my committee, also deserves recognition for his guidance early on in my graduate experience. By the same token, Will Gutekunst, Seth's replacement, deserves recognition for not only joining my committee on short notice, but also contributing valuable insight during discussions of my projects.

However, perhaps my biggest thanks are extended to Paul Rablen, my former advisor in the Chemistry Department of Swarthmore College. The first chemistry class I ever enjoyed was taught by Paul, my first research experience was under Paul's tutelage, and my first copy of Exploring Chemistry with Electronic Structure Methods: A Guide to Using Gaussian was bestowed to me by Paul. Many thanks go to Paul.

My family, of course, deserves thanks for providing me with an environment in which my passion for science could be cultivated. Martha, Rich, Matthew and Jane, I thank you. I also thank my Rottweiler, Jabba the Pup, who has been very supportive of my career goals.

Furthermore, all those working alongside me in the trenches at Georgia Tech deserve the highest praises. From the custodian, Shelina, who was always wishing me a good day, to amazing mentors, Ray Shenje, Cynthia Martin, Joel Aponte-Guzman, Marchello Cavitt, Corey Williams, and George Ward, to undergraduates, Steven Hanna, Vanessa Cupil-Garcia, Theodore Donnell, and Marilyn Nduke, to peers Matthew Sandridge and Kimberley Osborne, these people deserve credit for dedicating their lives to pushing science forward and making the Georgia Institute of Technology a fondly remembered home.

By the same token, I thank the computational team at Emory lead by Jamal. Jamal Musaev, Brandon Haines, Alex Kaledin and Shen Tan welcomed me into their group and showed me how to use a real computer. For this, I am very grateful.

I thank the National Science Foundation for funding my research with graduate fellowship (DGE-1148903), as well as the Center for C-H Functionalization (CHE-1205646).

Lastly, I would like to give the talented soccer super-star, Raynold Shenje, and the amazing singer, Cynthia Martin, a second round of applause. They deserve it.

TABLE OF CONTENTS

LIST OF TABLES

LIST OF FIGURES

LIST OF SCHEMES

LIST OF SYMBOLS AND ABBREVIATIONS

ΔG	Change in Gibbs free energy
ΔH	Change in Enthalpy
^{1}H	Standard isotope of hydrogen
^{13}C	Carbon isotope with a nucleus containing six protons and seven neutrons
A	Acceptor
A-A	Acceptor-acceptor
ABL	α-Heteroatom-γ-butyrolactone
acac	Acetylacetonate
Boc	*tert*-Butyloxycarbonyl
BPCP	(1-(biphenyl)-2,2-diphenylcyclopropanecarboxylate)
Bu	Butyl
Cat.	Catalyst
Cbz	Carboxybenzyl
cod	1,5-Cyclooctadiene
Cp*	Pentamethylcyclopentadiene
Cu(II)	Copper in the second oxidation state
D	Donor
D-A	Donor-acceptor
DCE	1,2 Dichloroethane
DCM	Dichloromethane
DEA	U.S. Drug Enforcement Administration
DFT	Density Functional Theory

DHF	Dihydrofuran
DHP	Dihydro-2*H*-pyran
dmpe	1,2-Bis(dimethylphosphino)ethane
d.r.	Diastereomeric ratio
ee	Enantiomeric excess
e.r.	Enantiomeric ratio
esp	α,α,α',α'-tetramethyl-1,3-benzenedipropionic acid
Func.	Functionalization
hfacac	Hexafluoroacetylacetone
HRMS	High-resolution mass spectrometry
i-Pr	Iso-propyl
IEF-PCM	Polarizable ontinuum model implemented by integral equation formalism
IRC	Intrinsic reaction coordinate
L	Ligand
LA	Lewis acid
LG	Leaving group
LSF	Late-stage functionalization
M	Molar (unit of concentration)
NMR	Nuclear magnetic resonance
NTTL	*N*-1,2-Naphthoyl-*tert*-leucinate
PA	Proton affinity
phen	Phenanthroline
pin	Pinacolato
PTTL	*N*-5-*t*-butyl-phthaloyl-*tert*-leucinato
r	A geometric parameter

r'	A geometric parameter
Rh_2	Dimeric rhodium catalyst
Rh(II)	Rhodium in the second oxidation state
Rh(III)	Rhodium in the third oxidation state
R/S-BTPCP	(*R/S*)-(-/+)-[(1*R/S*)-1-(4-bromophenyl)-2,2-diphenylcyclopropanecarboxylato
R/S-DOSP	(*R/S*)-(+/-)-N-(*p*-dodecylphenylsulfonyl)prolinato
R/S-PTAD	(*R/S*)-(-/+)-(1-adamantyl)-(N-phthalimido)acetato
r.t.	Room temperature
σ_p	Hammett coefficient
t-Bu	Tertiary-butyl
TEA	Triethylamine
tert	Tertiary
Tf	Triflate
TFA	Trifluoroacetate
THF	Tetrahydrofuran
X	Non-hydrogen atom

SUMMARY

Given the recent progress made with donor-acceptor (D-A) carbene C-H functionalization, as well as the functional diversity of acceptor-acceptor (A-A) carbenes, surprisingly little effort has been made by the chemical community toward uncovering the latent potential of these species to functionalize C-H bonds under intermolecular manifolds. This Ph.D. thesis highlights several synthetic and computational investigations that result in the advancement of acceptor-acceptor carbene mediated intermolecular sp^2 and sp^3 C-H functionalization methodology. Together, the advancements in this thesis provide the seed and structure for further growth in this promising field.

In the first project, this thesis showcases the development of a catalytic intermolecular C(sp^2)-H functionalization through the pursuit of β,γ-unsaturated-γ-heteroatom carbonyl frameworks. Density functional theory (DFT) calculations provide insight that expands the scope of the reaction and enables the tuning of selectivity. The product space is elaborated with further chemistry including a novel Lewis acid catalyzed cyclization to construct naphthol building blocks. DFT plays a more prominent role in the second project where it is used to build chemical space map describing how the intermolecular sp^3 C-H insertion reactivity of A-A carbenes varies with the steric and electronic nature of the acceptor groups. This insight is then leveraged to discover a new synthetically useful class of H-bonding A-A carbenes. Synthetic utility is demonstrated through substrate scope, site- and enantioselective C-H insertions, and cyclopropanation using a 2° N-aryl diazomalonamide. In the third project, a dual C-H functionalization

protocol is developed to access highly substituted indoles from α-diazo-β-keto nitrile and enol ether starting materials.

CHAPTER 1. INTRODUCTION

The two permeating themes of this thesis are: (1) C-H functionalization and (2) metal carbene species for organic synthesis. Thus, it is the intent of this introductory chapter to acquaint the reader with pertinent background associated with these topics.

1.1 C-H Functionalization

C-H functionalization is the process by which a carbon-hydrogen bond is broken and a new bond is formed between the carbon and a non-hydrogen atom (Scheme 1).

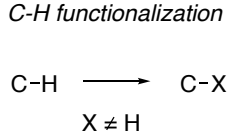

Scheme 1 – C-H Functionalization Definition

This process is old – nature has been performing C-H functionalization for an innumerable length of time – and even in the lab, C-H functionalization reactions can be so pedestrian that we overlook their beauty and power: radical halogenation, directed metalation, and enolate chemistry are all examples of the functionalization of the carbon-hydrogen bond. Yet this old field is experiencing a Renaissance, introducing sophisticated tools, namely transition metal catalysts with complex ligand environments, to achieve exotic selectivity for the functionalization of carbon-hydrogen bonds. This movement is known as Modern C-H Functionalization, for now, and is not only the subject of this introduction but also the field to which this author has dedicated his graduate school efforts.

1.1.1 The C-H Functionalization Renaissance

Robert Crabtree, Phil Baran, and Huw Davies have separately written nice pieces on the development of Modern C-H Functionalization in which seminal reactions in the field dating back to Fenton (1898), Dimroth (1902), and Chatt (1965) (Scheme 2) all the way to the recent advancements of Jin-Quan Yu, Nakamura, Itami and others are chronicled alongside insightful commentary regarding their applications in synthesis.[1-4]

Fenton, 1898

$$Fe(II) + H_2O_2 = Fe(III) + OH^- + {}^{\bullet}OH$$

$$R\text{-}H + {}^{\bullet}OH = R^{\bullet} + H_2O$$

$$R^{\bullet} + O_2 = R\text{-}O\text{-}O^{\bullet}$$

Dimroth, 1902

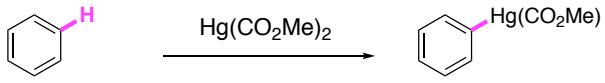

Chatt, 1965

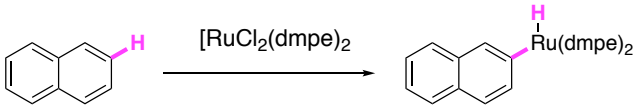

Scheme 2 – Seminal Examples of Metal Mediated C-H Activation

Examples of state-of-the-art C-H functionalization methods are shown in Scheme 3. Recent highlights in the field include the C-H insertion of donor-acceptor carbenes into methyl groups using 3rd generation dirhodium catalysts,[5] C-H borylation of agro- and pharmaceutically relevant heterocycles accompanied by selectivity models,[6] and total syntheses that rely on multiple C-H functionalization steps.[7]

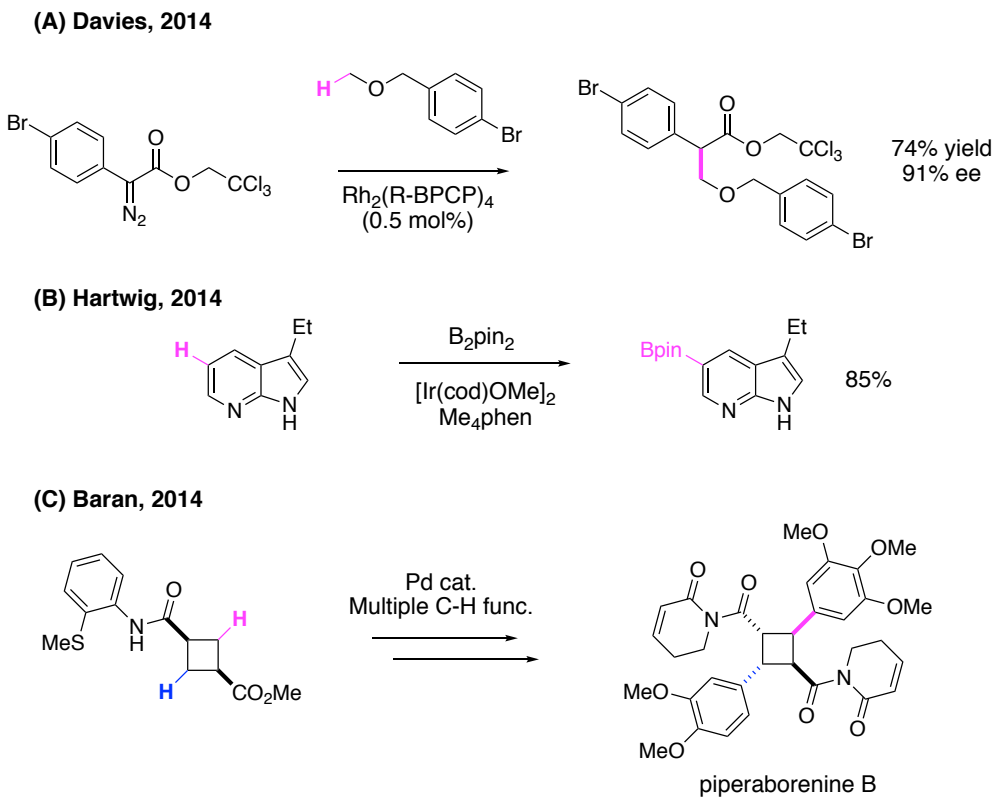

Scheme 3 – Examples of State-of-the-Art C-H Functionalization

It is also important to note that the advancement of this field was not only driven by the discovery of these seminal methods, but, as Will Gutekunst and Phil Baran state in their critical review of Modern C-H Functionalization, by the associated "philosophical precepts and implications [that] were clearly articulated by visionaries."[1f] In other words, C-H functionalization is an intellectual movement as much as it is a set of chemical transformations.

As humans became increasingly aware of the limited time and natural resources on this planet, we were likewise awakened to the power of C-H functionalization reactions, which promise shorter and more atom economic synthetic pursuits that rely on intuitive disconnection strategies and cheaper starting materials compared to tradition methods.

1.1.2 Understanding the Utility of C-H Functionalization by Analogy

A simple way to view traditional synthesis is through the analogy of the sculptor. A sculptor begins with a big rock, and, as he chisels away, his creation begins to take form. In this analogy, the rock chiseled away represents functional groups used by the chemist to complete a synthesis. The chemist must begin his pursuit with enough functionality – a big enough rock – to make his molecule. If he begins with too little, then inevitably he will reach a point where the molecule can no longer be manipulated into the desired target – just as a sculptor realizes that he cannot build a 6-foot-tall statue with a 5-foot rock. Why is this the case? It is the case because both the functional group-oriented chemist and the sculptor envision their art through a *subtractive* approach. C-H functionalization is important because it represents an *additive* synthetic logic that defies this traditional view of molecular sculpting (Scheme 4).

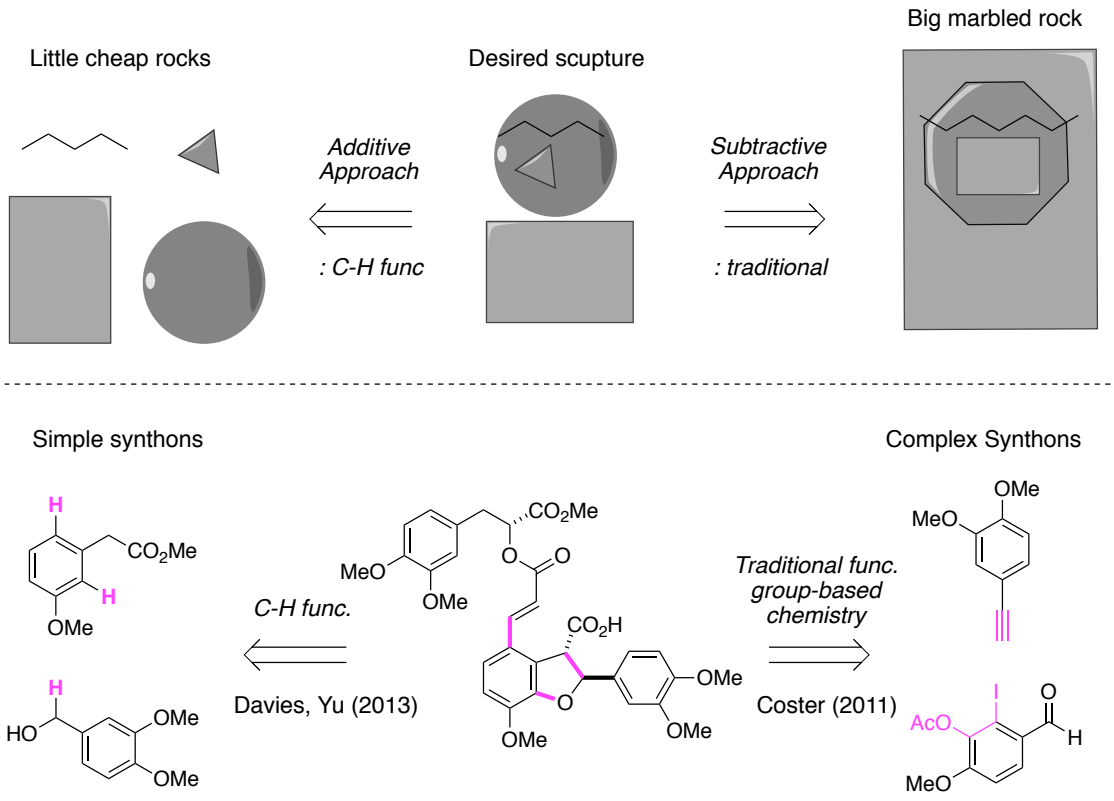

Scheme 4 – Explaining C-H Functionalization[8,9] through the Sculpture Analogy

C-H functionalization is equivalent to a hammer that puts rock back on the statue rather than chiseling it off. With this hammer, a sculptor would not need to start each sculpture with an enormous rock; he could begin with smaller pieces that were more cheaply sourced and easier to handle while adding functionality to them as need. He would never fret over making the nose of David too small; he could always add rock to the nose and chisel it into Cyrano de Bergerac later.[10] The ability of C-H functionalization to create functionality on molecules where it does not yet exist has applications in many areas of chemistry – but which applications depends on the molecular complexity the substrate possesses.[11]

1.1.3 Applications of C-H Functionalization

As substrate complexity increases, the breadth of application for a related C-H functionalization method decreases – in other words, applications become more niche (Figure 1). Functionalization of chemical feedstock is important as it converts cheap and simple molecules into powerful synthons which could conceivably be used toward any synthetic pursuit. Oxidation of methane has long been considered a "holy-grail," as such technology could have an influence on the synthesis of any organic molecule.[12] However, recently, Jin Quan Yu argued that the ability to selectively functionalize pivalic acid's methyl groups also represents a grand challenge as it would provide a streamlined route to quaternary carbon stereocenters, an oft challenging moiety of retrosynthesis.[13] C-H functionalization methods that feature substrates of medium complexity would enable target syntheses in places where traditional methods fall short.[7] Meanwhile, late-stage C-H functionalization enables new drug discovery strategies.[14]

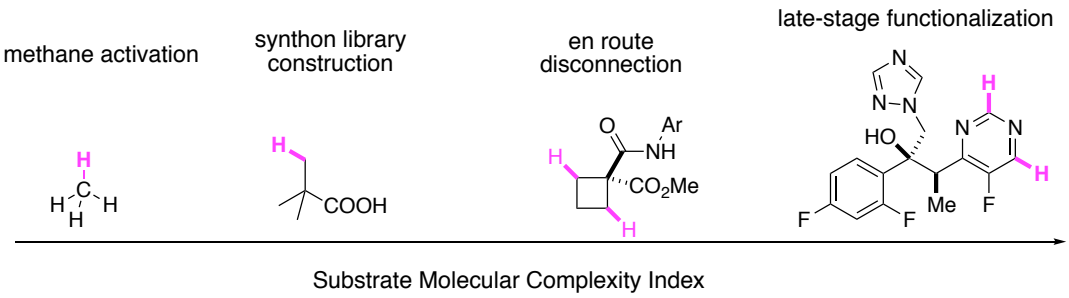

Figure 1 – C-H Functionalization Applications as a Function of Molecular Complexity

One industry that stands to benefit from C-H functionalization methods in all areas along the spectrum of substrate molecular complexity is that of bioactive molecules.

1.1.3.1 Applications of C-H Functionalization in the Pharmaceutical Industry

One of the major proponents of C-H functionalization chemistry is the pharmaceutical industry. Many pharmaceutical companies are actively engaged in pre-competitive C-H functionalization research, provide funding to and contract consulting services from academic laboratories with experience in this field.[1d] In fact, the Center for C-H Functionalization, a Phase III National Science Foundation Center for Chemical Innovation, has partnerships with Abbvie, Novartis, Merck, Pfizer, and Bristol-Myers Squibb, among other pharmaceutical companies which provide resources for C-H functionalization research.[15] Meanwhile, several industrial chemists, such as Tim Cernak (Merck), Eric Voight (Abbvie), and John Macor (Sanofi), have become champions for C-H functionalization, publicizing the impact this field continues to have in the development of bioactive molecules.[1d,14a,15]

C-H functionalization is valuable to the pharmaceutical industry not only because it offers atom economic routes to target molecules, but it is also the synthetic vehicle to implementing an efficient drug discovery strategy known as late-stage functionalization (LSF). LSF is the process of installing functional groups onto molecules late in their synthetic route. LSF synthetic methods allow medicinal chemists to convert lead molecules into derivatives, thus enabling the construction of libraries of similar drug-like molecules – an activity that is often prohibitively resource-consuming if the *de novo* synthesis of derivatives is required (Figure 2).

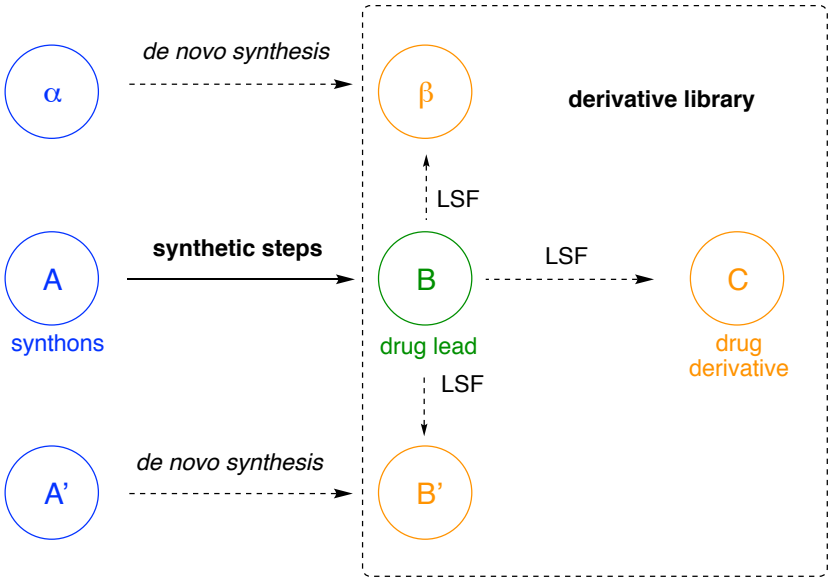

Figure 2 – Late-Stage Functionalization Streamlines the Construction of Drug Derivative Libraries by Eliminating *de Novo* Syntheses

These libraries are instrumental in drug discovery as they not only thoroughly probe the chemical space surround a lead, but they also provide a platform for determining structure activity relationships and understanding more about the binding target of these drugs and their mechanisms of action.[14a]

1.1.4 The Challenge of Modern C-H Functionalization

In a C-H functionalization process, two events must occur: (1) the carbon-hydrogen bond must be broken, or activated, and (2) a carbon-X bond must form with enough selectivity to procure the desired product in useful quantities. The arch problem precluding chemists from leveraging C-H functionalization to its full potential is the second event. Chemists have possessed the tools, strong bases, radical initiators, transition metals, carbenes, etc., capable of activating C-H bonds for a long time. Today, those in the field of C-H functionalization focus on harnessing those tools to generate C-H functionalized

products with the chemo-, regio-, and/or stereochemical control required by their increasingly ambitious synthetic contexts.

1.2 Metal Carbenes in Intermolecular C-H Functionalization Manifolds

1.2.1 Overview of Metal Carbene Species

One set of chemical species that has high potential of meeting these ambitious synthetic goals is the carbene.[16] Carbenes can exist in triplet or singlet electronic states, the latter of which describes the carbenes featured in this thesis work (Figure 3).[17]

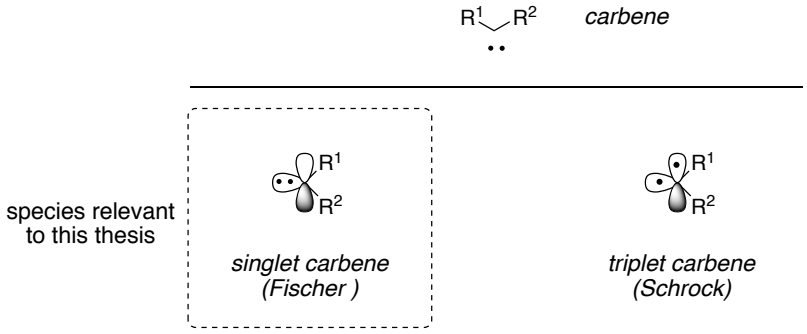

Figure 3 – Two Types of Carbene Species: Fischer and Schrock

When coordinated to a metal, singlet carbenes are stabilized by σ donation into the metal dz^2 orbital and π back-donation from the metal π-d orbitals to the carbene p-orbital (Scheme 5).[18] These species exhibit a variety of chelotropic and chameleonic reactivity including cyclopropanation with olefins,[19] C-H and X-H bond activation,[16] and a host of [3+2] cycloaddition chemistry.[20]

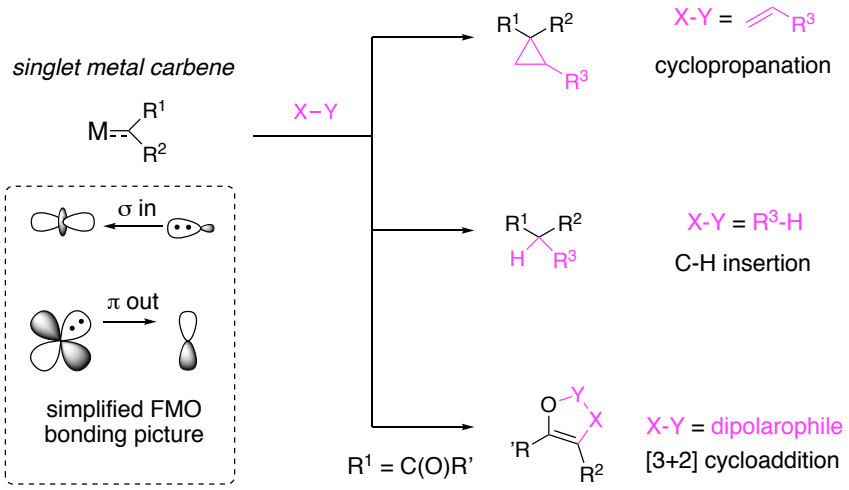

Scheme 5 – Common Reactivity of Singlet Metal Carbenes: Cyclopropanation, C-H Insertion, and [3+2] Cycloaddition

In these cases, the empty p-like orbital of the carbene welcomes attack from a nucleophile, meanwhile the filled sp^2 orbital behaves as a Lewis base toward acidic frontier orbitals revealed in the process. In a C-H insertion mechanism, this process is concerted, albeit asynchronous with negative charge accumulating on the carbene and positive charge accumulating on the carbon losing its C-H bond in the transition state (Figure 4).[18b] For this reason, C-H insertions occur at higher rates for C-H bonds at positions where positive charge accumulation is stabilized, such as benzylic positions and carbons alpha to heteroatoms.[21] Methylene C-H bonds react faster than methyl bonds for this electronic reason, but methines react slower than methylenes due to sterics hindrance negating the electronic preference.

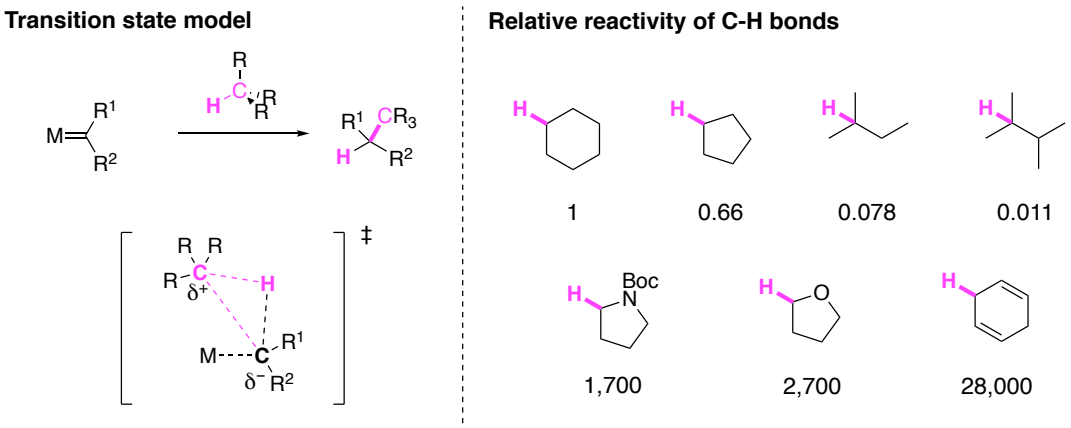

Figure 4 – Transition State Model Shows Positive Charge Accumulation on the Carbon Donating the H-Bond

Furthermore, C-H insertions are, for heuristic purposes, frequently treated as hydride transfers in discussions regarding reactivity trends. However, it is important to note the distinction between "C-H functionalization" and "C-H insertion," the latter of which is a subset of the former. Many metal carbene mediated C-H functionalization reactions rely on the general electrophilic behavior of the carbene p-orbital and activate a C-H bond in a non-chelotropic, step-wise process; examples of such reactivity are discussed in Section 1.2.3.1.

Note, carbenes without metal coordination will be referred to as "free-carbenes" throughout this thesis to highlight the absence of a metal. Generally, free-carbenes can exhibit the same behavior as metal carbenes, but are not typically used in selective synthesis given their highly reactive nature.

1.2.2 Synthesis of Metal Carbenes

1.2.2.1 Precursors

The most popular carbene precursors in the C-H functionalization community are α-carbonyl diazo compounds (Scheme 6). These species are prepared via deprotonation at the α-position of a carbonyl bearing molecule followed by electrophilic attack of a diazo transfer reagent. Common diazo transfer reagents include tosyl azide **1**, 4-acetomidobenzenesulfonyl azide **2**, 1*H*-imidazole-1-sulfonylazide HCl salt **3**, and perfluorobutanesulfonyl azide **4**. For more on the synthesis of α-diazo carbonyl compounds, see McKervey's review.[22]

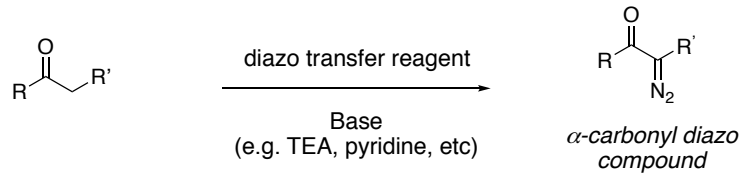

Common diazo transfer reagents:

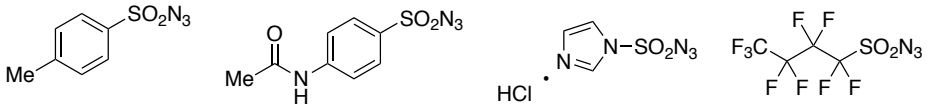

1 **2** **3** **4**

Scheme 6 – General Approach to α-Carbonyl Diazo Compound Synthesis

Nitrogen gas is extruded from the diazo compound by coordination of a metal catalyst, typically copper or rhodium, to generate the metal carbene (Scheme 7).[18b]

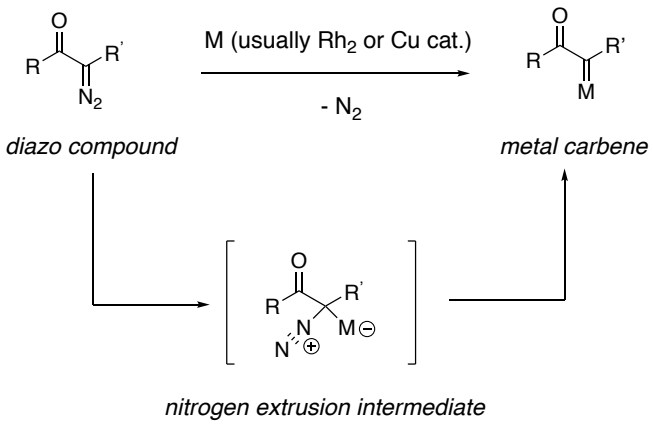

Scheme 7 – Generating Metal Carbenes from Diazo Compounds

More recently, *N*-sulfonyl-1,2,3-triazoles have been gaining traction because they form synthetically useful imino-carbenes and increase the reaction scope beyond carbonyl containing compounds (Scheme 8).[23] Note, both diazo compounds and sulfonyl triazoles utilize the formation of nitrogen gas as an irreversible energetic driving force for carbene formation.

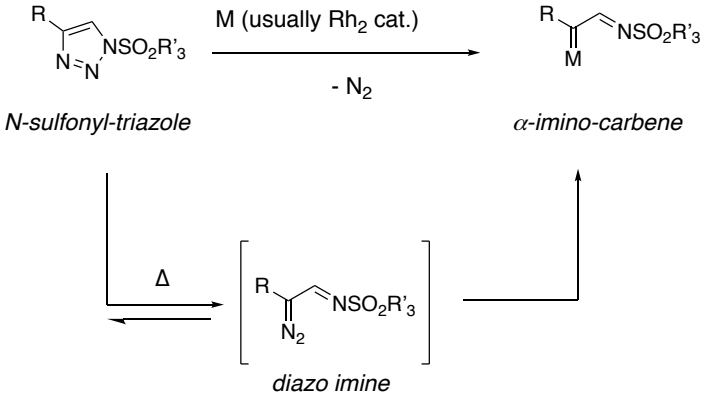

Scheme 8 – Generating α-Imino-Carbenes from Sulfonyl Triazoles

1.2.2.2 Dirhodium Catalysts

While diazo compounds can be degraded thermally or by light activation, the resulting free carbene is prone to its inherent reactivity which leads to undesirable side reactions in many cases. To temper this reactivity and add a ligand environment to influence selectivity, dimeric ligand-bridged rhodium species, derivatives of dirhodium tetraacetate, or copper catalysts are used for the extrusion of nitrogen gas from diazo compounds and *N*-sulfonyl-1,2,3-triazoles to form metal carbenes.[16,20] To tune the reactivity of the carbene, intricate ligands continue to be developed for these catalysts. A short list of popular and emergent dirhodium catalysts is shown in Table 1.

Table 1 – Popular Dimeric Rhodium Catalysts for Carbene Formation

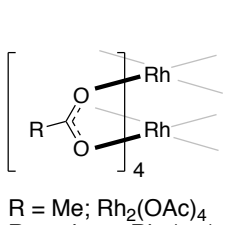

R = Me; $Rh_2(OAc)_4$
R = *n*-hept; $Rh_2(oct)_4$
R = tBu; $Rh_2(piv)_4$
R = CF_3; $Rh_2(TFA)_4$

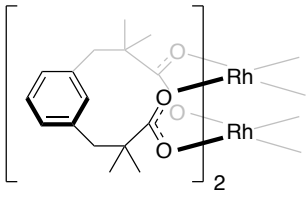

$Rh_2(esp)_2$

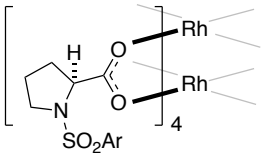

Ar = 4-$C_{12}H_{25}C_6H_4$;
Rh_2(*S*-DOSP)$_4$

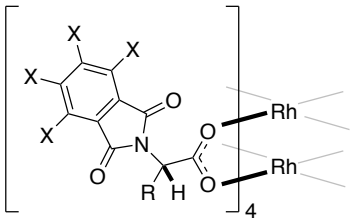

X = H, R = tBu; Rh_2(*S*-PTTL)$_4$
X = Cl, R = tBu; Rh_2(*S*-TCPTTL)$_4$
X = H, R = Ad; Rh_2(*S*-PTAD)$_4$
X = H, R = Bn; Rh_2(*S*-PTPA)$_4$

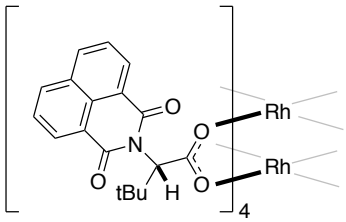

Rh_2(*S*-NTTL)$_4$

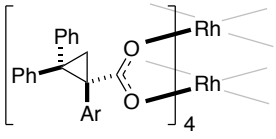

Ar = 4-PhC_6H_4;
Rh_2(*R*-BPCP)$_4$

1.2.3 Traditional Classes of Metal Carbenes: Donor-Acceptors, Acceptors, and Acceptor-Acceptors

Traditionally, metal carbenes are divided into three categories depending on which α-diazo carbonyl precursor is used in their formation: acceptors, donor-acceptors, and acceptor-acceptors (Table 2). Each of these carbenes has a representative substrate that is commonly invoked in discussions describing the behaviour of each class: methyl 2-diazo-2-phenylacetate (**5**), ethyl diazoacetate (**6**), and dimethyl diazomalonate (**7**).

Table 2 – Classes of Diazo Compounds and Carbenes and Their Representative Species

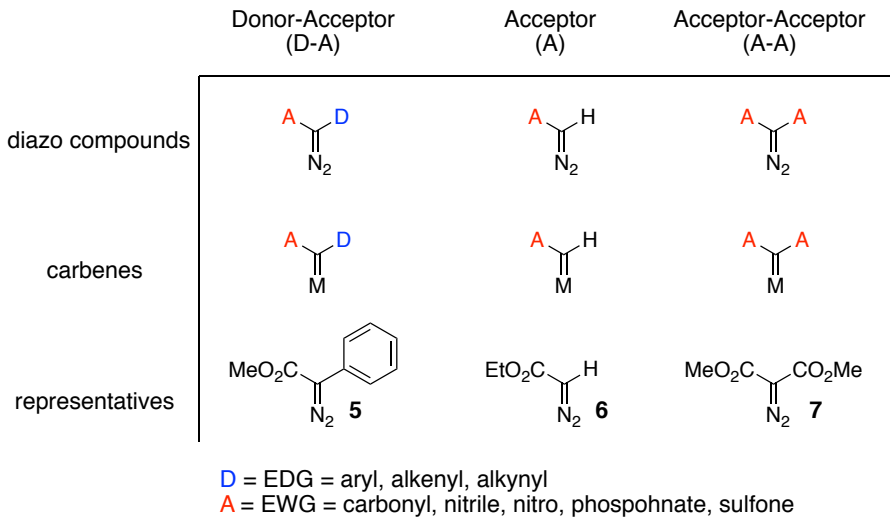

The classification was established to provide the community with intuition about the characteristic behavior of carbenes in each class, but these generalizations are heavily biased toward the three class representatives which were studied alongside each other in seminal reports by Davies and Muller (Scheme 9).[24,25] In these reports, the donor-acceptor species outperformed both acceptors and acceptor-acceptors in terms of yield and selectivity. Moreover, dimeric Rh(II) catalysts became favored by the community over copper catalysts for C-H insertion processes. Notably, donor-donor species and alkyl

substitution were not studied in these early reports and were frequently, as Doyle noted, left out of discussion in concurrent literature.[20]

(A) Muller and Tohill, 2000

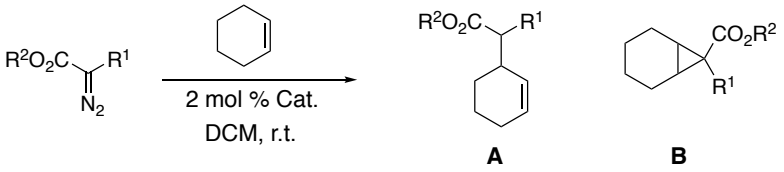

Carbene Class	R^1	R^2	Catalyst	Yield (%)	**A : B**
D-A	Ph	Me	$Rh_2(OAc)_4$	50	75 : 25
A	H	Et	$Rh_2(OAc)_4$	80	20 : 80
A	H	Et	$[Cu(OMe)_3PI]$	9	5 : 95
A-A	CO_2Me	Me	$Rh_2(OAc)_4$	96	38 : 62
A-A	CO_2Me	Me	$[Cu(OMe)_3PI]$	63	10 : 90

(B) Davies, 1997

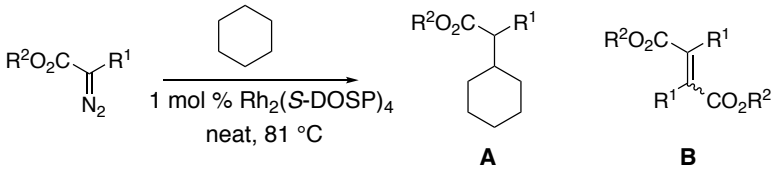

Carbene Class	R^1	R^2	Yield **A** (%)	Yield **B** (%)	ee **A** (%)
D-A	Ph	Me	83	0	81
A	H	Et	34	29	–
A-A	COMe	Me	51	0	3

Scheme 9 – Seminal Reports by Muller and Davies on the Comparative Selectivity of D-A, A, and A-A Carbenes

These findings, along with others[18b] have been used to build a qualitative picture associating the reactivity of these species with steric and electronic profiles (Figure 5).[16] According to this picture, the alignment of the phenyl group with the empty carbene p-orbital stabilizes the donor-acceptor carbene while providing a rigid, sterically unhindered

route for approaching nucleophiles. The rigidness of the phenyl group can work in tandem with catalyst ligands to offer excellent stereo- and regioselectivity.

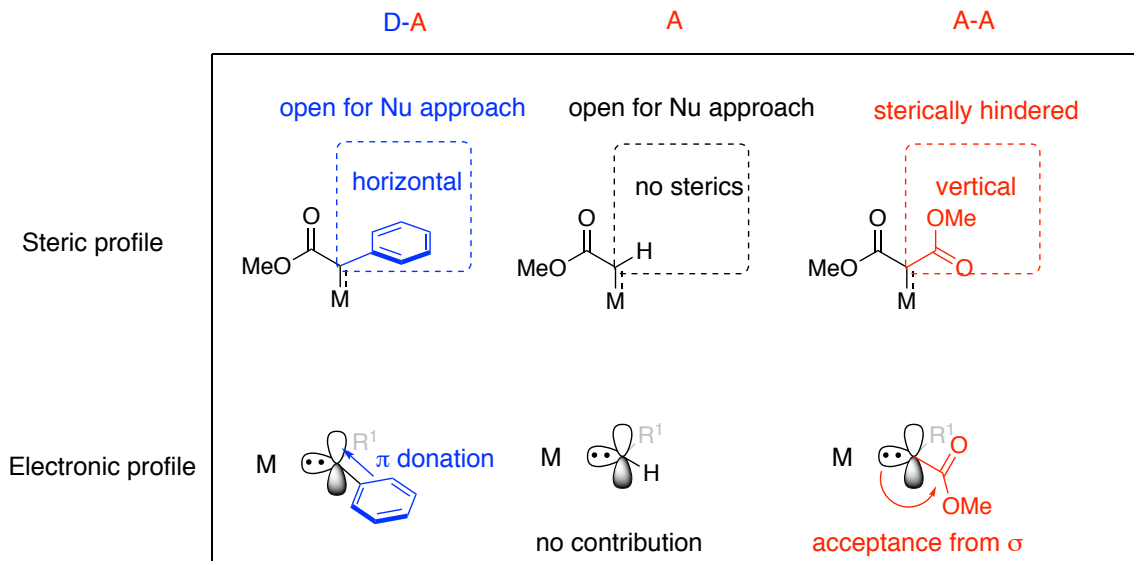

Figure 5 – Qualitative Comparison of D-A and A-A Carbene Steric and Electronic Profiles

On the other hand, the acceptor carbene is the most reactive as it lacks any stabilizing orbital communication with the hydrogen atom and lacks any steric environment to guide incoming nucleophiles. For these reason, this carbene class has experienced challenges in finding useful applications in intermolecular C(sp^3)-H functionalization reactions – it was not until 2016 that the first example was reported.[26] Acceptor-acceptor carbenes are considered more electrophilic than donor-acceptors because stabilizing influences on the carbene are less pronounced compared to the π-donation of a phenyl group. The two carbonyl groups pose reactivity issues for this class. The second carbonyl group maintains parallel geometry to the carbene's electrophilic lobe, which hinders nucleophilic approach; furthermore, the second carbonyl creates symmetry in the molecule and thus makes the development of chiral catalysts for this class a challenge. Lastly, the

second carbonyl render these species more likely to undergo side reactions – the carbonyl acts as a nucleophile in these cases.[27,28] Like the acceptor class, acceptor-acceptors have yet to find useful applications in synthetic intermolecular C(sp^3)-H functionalization methods, but they have been successfully utilized in intramolecular C-H insertion methods as well as intermolecular C(sp^2)-H functionalization protocols by relying on stepwise processes discussed further in Section 1.2.3.1.[29]

Given these profiles, much of the past two decades has been dedicated to the development of donor-acceptor dirhodium-carbene methods – and to fruitful results. Today, when paired with intricate derivatives of dirhodium tetraacetate catalysts, donor-acceptor carbenes will insert into aliphatic C-H bonds with fantastic selectivity. An example of such selectivity is shown in Scheme 10.[30]

Davies (2014)

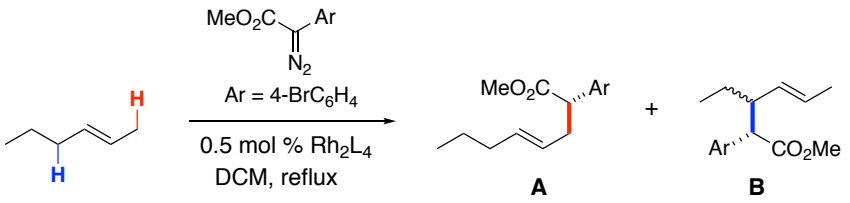

catalyst	ratio **A:B**	yield (%)	ee (%)
Rh_2(*R*-DOSP)$_4$	**1 : 9**	75	–
Rh_2(*R*-BPCP)$_4$	**8 : 1**	80	95

Scheme 10 – Example of Finely Tuning Selectivity for C-H Bonds with Advanced Dirhodium Catalysts

Likewise, donor-acceptor carbenes are frequently utilized in total syntheses and demonstrations of late stage functionalization (Scheme 11).[31,32] However, it is important to note that while the D-A, A, A-A categorization system has been used to generalize the reactivity observed, surprisingly little evidence exists to support these conclusions for non-

class representative species– especially those in the acceptor and acceptor-acceptor classes which have received less attention than their successful donor-acceptor siblings.

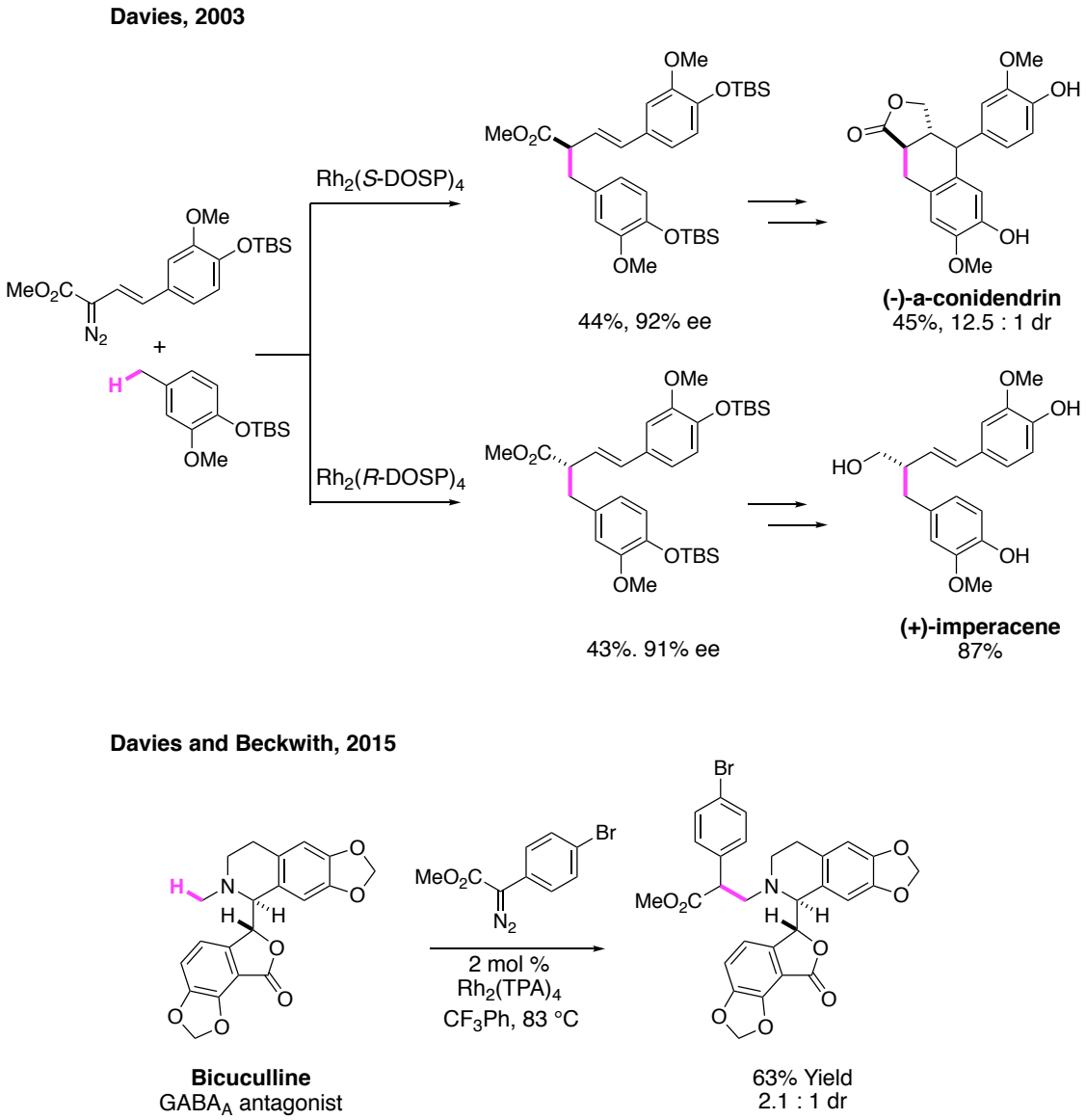

Scheme 11 – Donor-Acceptor Carbenes in Late-Stage Functionalization and Total Synthesis

1.2.3.1 Acceptor-Acceptor Carbenes

While numerous selective intramolecular C-H insertion protocols exist featuring acceptor-acceptor carbenes,[21a] these species have experienced slow uptake into intermolecular C-H functionalization methods. The limited methods that have been developed predominantly feature the dimethyl malonate carbene and do not rely on the direct C-H insertion potential of this compound. Instead of relying on C-H insertion reactivity of the carbene, these methods activate C-H bonds in other manners. For example, in 1989 Alonso utilized an addition-elimination mechanism to functionalize the C(sp^2)-H bond of an enol ether with a dimethyl malonate carbene (Scheme 12 A).[27] This is the same strategy exploited by the methodology in Chapter 2 of this thesis. Additionally, as exemplified by Kim and co-workers in 2015, monomeric Rh(III) catalysts can be used to activate C-H bonds first before a carbene unit is created on the metal and migrates into the metal-carbon bond (Scheme 12 B).[28]

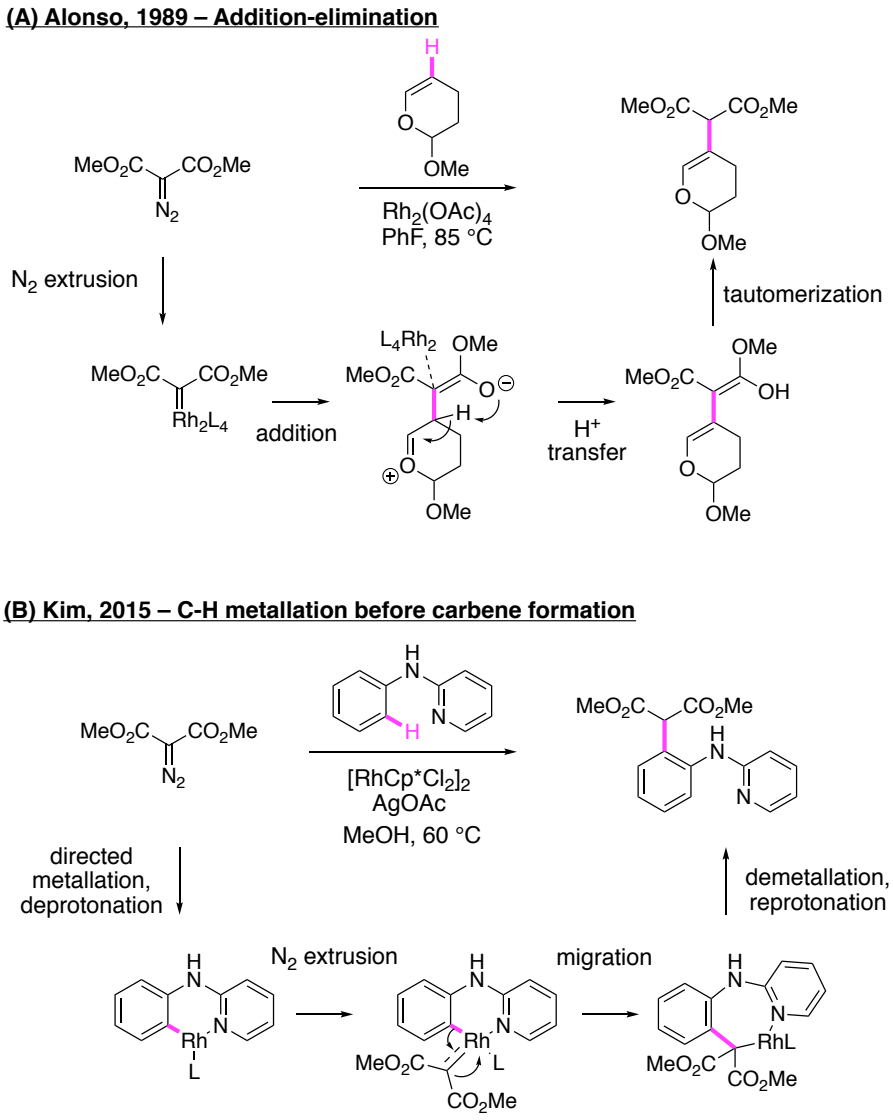

Scheme 12 – Examples of Carbene-Mediated C-H Functionalizations that Eschew Direct Carbene C-H Insertion and the Associated Selectivity Issues

These two examples not only represent mechanistic strategies that can be leveraged in the development of intermolecular C-H functionalization methods for A-A carbenes, but they also highlight a void in the field, and thus an opportunity: no intermolecular C(sp^3)-H functionalization methods exist for acceptor-acceptor carbenes, and the community has yet to articulate *why*, if it is the case, these methods cannot be developed.

1.3 References

[1] (a) Crabtree, R. H. *Journal of the American Chemical Society, Dalton Transactions* **2001**, 2437; (b) Crabtree, R. H.; Lei, A. *Chemical Rev*iews **2017**, *117*, 8481; (c) Davies, H. M. L.; Morton, D. *Journal of Organic Chemistry* **2016**, *81*, 343; (d) Davies, H. M. L.; Morton, D. *ACS Central Science* **2017**, *3*, 936; (e) Davies, H. M. L.; Morton, D. *Chemical Society Reviews* **2011**, *40*, 1857; (f) GuteKunst, W. R.; Baran, P S. *Chemical Society Reviews* **2001**, *40*, 1976.

[2] H. S. H. Fenton, *Journal of the Chemical Society* **1898**, 65, 899.

[3] Chatt, J.; Davidson,J. M. *Journal of the Chemical Society* **1965**, 843.

[4] Dimroth, O. *Berichte der deutschen chemischen Gesellschaft* **1902**, *35*, 2032.

[5] Qin, C.; Davies, H. M. L. *Journal of the American Chemical Society* **2014,** *136*, 9792.

[6] (a) Larsen, M. A.; Hartwig, J. F. *Journal of the American Chemical Society* **2014**, *136*, 4287; (b) Mitch Smith's contributions to C-H borylation, while not discussed in this thesis, should also be recognized for their importance to this field: Smith, K. T.; Berritt, S.; González-Moreiras, M.; Ahn, S.; Smith, M. R.; Baik, M.-H.; Mindiola, D. J. *Science* **2016**, *351*, 1424.

[7] Gutekunst, W. R.; Baran, P. S. *Journal of the American Chemical Society* **2011**, *133*, 19076.

[8] Fischer, J.; Savage, G. P.; Coster, M. J. *Organic Letters* **2011**, *13*, 3376.

[9] Wang, H.; Li, G.; Engle, K. M.; Yu, J.-Q.; Davies, H. M. L. *Journal of the American Chemical Society* **2013**, *135*, 6774.

[10] Cyrano de Bergerac is a fictional character known for having a very large nose. The play, Cyrano de Bergerac: A Heroic Comedy in Five Acts, was written by Edmond Rostand and first premiered in France in 1897.

[11] For discussions on molecular complexity index, see: (a) Bertz, S. H. *Journal of the American Chemical Society* **1981**, *103*, 3599; (b) Böttcher, T. *Journal of Chemical Information and Modeling* **2016**, *56*, 462; (c) Qiu, F. *Canadian Journal of Chemistry*, **2008**, 86, 903.

[12] Caballero, A.; Perez, P. J. *Chemical Society Reviews* **2013**, *42*, 8809.

[13] Jin-Quan Yu. Accelerated C-H Activation Reactions: A Shortcut to Molecular Complexity from Chemical Feedstock. *The Scripps Research Institute Faculty Lecture Series*, May 09, **2012**

[14] (a) Cernak, T.; Dykstra, K. D.; Tyagarajan, S.; Vachal, P.; Krska, S. W. *Chemical Society Reviews* **2016**, *45*, 546; (b) Fier, P. S.; Hartwig, J. F. *Journal of the American Chemical Society* **2014**, *136*, 10139.

[15] Davies, H. M. L.; Morton, D. *Center for Selective C-H Functionalization.* March 28, **2018**. http://www.nsf-cchf.com/index.html.

[16] Doyle, M. P.; Duffy, R.; Ratnikov, M.; Zhou, L. *Chemical Reviews* **2010**, *110*, 704.

[17] For studies on singlet and triplet carbenes see: (a) Hopkinson, A. C.; Lien, M. H. *Canadian Journal of Chemistry* **1985**, *63*, 3582; (b) Irikura, K. K.; Goddard III, W. A.; Beauchamp, J. L. *Journal of the American Chemical Society* **1992**, *114*, 48; (c) Mueller, P. H.; Rondan, N. G.; Houk, K. N.; Harrison, J. F.; Hooper, D.; Willen, B. H.; Liebman, J. F. *Journal of the American Chemical Society* **1981**, 10*3*, 5049.

[18] For discussion of metal carbene bonding see (a) Berry, J. F. *Dalton Tranaction.* **2012**, *41*, 700; (b) Nakamura, E.; Yoshikai, N.; Yamanaka, M. *Journal of the American Chemical Society* **2002**, *124*, 7181.

[19] Brookhart, M.; Studabaker, W. B. *Chemical Reviews* **1987**, *87*, 411.

[20] Doyle, M. P.; Forbes, D. C. *Chemical Reviews* **1998**, *98*, 911.

[21] (a) Taber, D. F.; Ruckle, R. E., Jr. *J. Am. Chem. Soc.* **1986**, *108*, 7686; (b) Doyle, M. P.; Westrum, L. J.; Wolthuis, W. N. E.; See, M. M.; Boone, W. P.; Bagheri, V.; Pearson, M. M. *Journal of the American Chemical Society* **1993**, *115*, 958; (c) Davies, H. M. L.; Ren, P.; Jin, Q. *Organic Letters* **2001**, *3*, 3587.

[22] Ye, T.; McKervey. M. A. *Chemical Reviews* **1994**, 94, 1091.

[23] Davies, H. M. L.; Alford, J. S. *Chemical Society Reviews* **2014**, *43*, 5151-5162

[24] Davies, H. M. L.; Hansen, T. *Journal of the American Chemical Society* **1997**, *119*, 9075.

[25] Muller, P.; Tohill, S. *Tetrahedron* **2000**, *56*, 1725.

[26] Weldy, N. M.; Schafer, A. G.; Owens, C. P.; Herting, C. J.; Varela-Alvarez, A.; Chen, S.; Niemeyer, Z.; Musaev, D. G.; Sigman, M. S.; Davies, H. M. L.; Blakey, S. B. *Chemical Science* **2016**, *7*, 3142.

[27] Audia, J. E.; Droste J. J.; Gevorgyan, V.; Rubin, M.; Chan, W.; Yu, W.; McLarney, B.; France, S. "Dimethyl Diazomalonate." *Encyclopedia of Reagents for Organic Synthesis.* **2016**.

[28] Mishra, N. K.; Choi, M.; Jo, H.; Oh, Y.; Sharma, S.; Han, S. H.; Jeong, T.; Han, S.; Lee, S.-Y.; Kim, I. S. *Chemical Communications* **2015**, *51*, 17229.

[29] M. E. Alonso; R. Fernandez, *Tetrahedron* **1989**, 45, 3313.

[30] Qin, C.; Davies, H. M. L. *Journal of the American Chemical Society* **2014**, *136*, 9792.

[31] Davies, H. M. L.; Jin, Q. *Tetrahedron: Asymmetry*, **2003**, *14*, 941.

[32] Davies, H. M. L.; Beckwith, R. E. J. *Nature Communications* **2015**, *6*, 5943.

CHAPTER 2. DIMERIC RH(II) CATALYZED β-C(SP^2)-H ALKYLATION OF ENOL ETHERS, ENAMIDES, AND ENECARBAMATES WITH α-DIAZO DICARBONYL COMPOUNDS

With the publisher's permission, this chapter was adapted from the original manuscript: McLarney, B. D.; Cavitt, M. A.; Donnell, T. M.; Musaev, D. G.; France, S. A. *Chemistry: A European Journal.* **2017**, *23*, 1129.

2.1 Introduction

2.1.1 γ-Heteroatom-β,γ-Unsaturated Carbonyl Framework

The γ-alkoxy- or γ-amino-β,γ-unsaturated carbonyl moiety **1** represents a unique structural framework that is present in a variety of compounds of broad interest (Figure 6).[1] This structural unit represents a powerful synthetic building block because of the presence of and spatial relationship between the carbonyl group and the olefin fragment, which can be selectively derivatized.

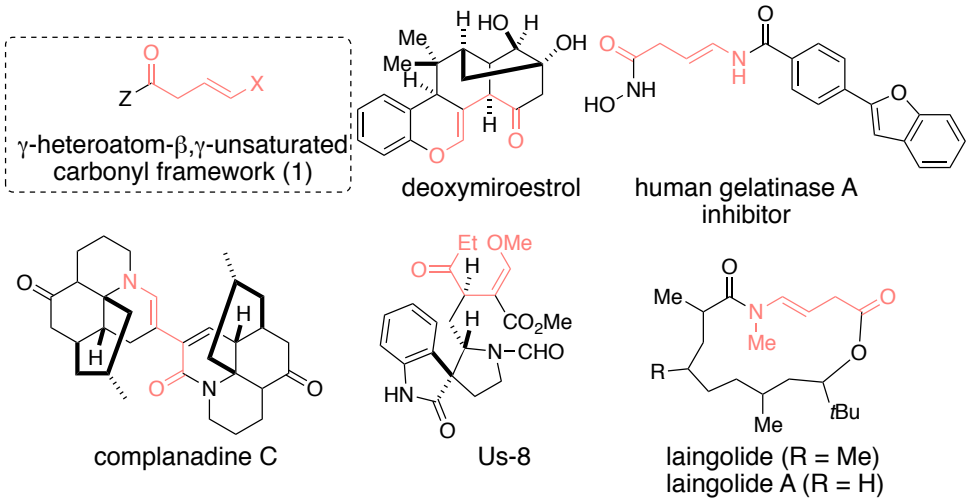

Figure 6 – Biologically Relevant Examples of the γ-Heteroatom-β,γ-Unsaturated Carbonyl Framework

2.1.2 Strategies for Accessing the γ-Heteroatom-β,γ-Unsaturated Carbonyl Framework

Currently, three common strategies have been employed to access the γ-heteroatom-β,γ-unsaturated carbonyl framework.[2] The first two strategies are: (1) oxidative coupling (anodic or with ceric ammonium nitrate) of enamines,[3] glycals,[4] and uracil derivatives[5] with 1,3-dicarbonyls; and (2) β-alkylation of enamides and enecarbamates with α-bromo-1,3-dicarbonyls using visible-light photoredox catalysis.[6] The first strategy is limited by poor substrate scope, low to modest yields, harsh reaction conditions, and the need for stoichiometric reagent quantities. The second strategy is specific to enamides/enecarbamates, requires added base, and is complicated by the decomposition of desired framework into C=C bond migration products.

A latent third strategy exists in the application of diazoacetates as β-alkylating agents for enol ethers and enamides. In a seminal report, Alonso showed that the Cu^{II}-catalyzed reaction of dimethyl α-diazomalonate with 2-methoxy-3,4-dihydro-2*H*-pyrans

afforded β-alkylated dihydropyrans in up to 79% yield (Scheme 13, right).[7] In the article, two examples of this interesting reaction were reported.[7a] More recently, Yan and co-workers disclosed the $Cu(hfacac)_2$-catalyzed reactions of aryldiazoacetates with enamines (Scheme 13, left).[8] The initially formed β-alkylated enamines were shown to be moisture sensitive, and, as a result, the corresponding γ-ketoesters were isolated instead.[8-10]

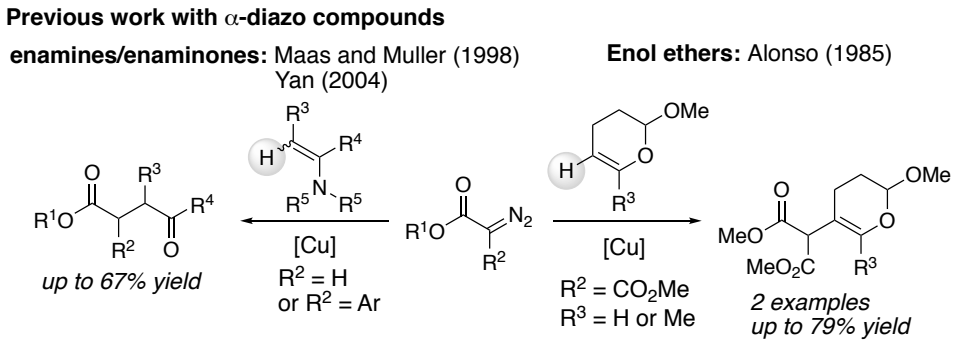

Scheme 13 – Previous Strategies Employing α-Diazo Compounds

2.1.3 Hypothesis

With precedent, however limited, for the β-C(sp^2)-H alkylation of enol ethers and enamides by carbenes generated from diazoacetates, we hypothesized that a broadly useful synthetic method furnishing the γ-heteroatom-β,γ-unsaturated carbonyl moiety utilizing this strategy and a diverse set of acceptor-acceptor diazoacetates could be developed (Scheme 14).

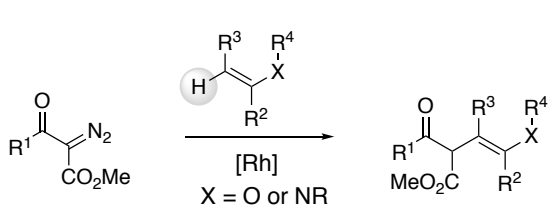

Scheme 14 – France Lab Approach to Accessing the γ-Heteroatom-β,γ-Unsaturated Carbonyl Framework

2.2 Results and Discussion

2.2.1 Reaction Optimization

In a previous study,[11] treatment of *N*-indolyl α-diazomalonamide **2a** with 3,4-dihydro-2H-pyran (DHP; **3a**) in the presence of $Rh_2(esp)_2$ formed β-alkylated DHP **4aa** in 43% yield. Given this interesting result, we sought to directly address the limitations of previously reported functionalizations of enol ethers, enamines, and enecarbamates with α-diazo-1,3-dicarbonyls through systematic optimization of this diazomalonamide–DHP coupling transformation.

By using Alonso's work as a guide, we began the optimization by performing the reactions in fluorobenzene at 85 °C (Table 3). As expected, without a catalyst, no reaction was observed after 24 h (entry 1). No desired alkylated DHP **4aa** was detected with $Cu(acac)_2$ (entry 2). We believe that catalyst deactivation may be occurring because of deleterious coordination between the indole nitrogen and the intermediate copper complex. $Rh_2(OAc)_4$ and chiral dimeric Rh(II) complexes $Rh_2(DOSP)_4$ and $Rh_2(BTPCP)_4$) gave fair yields (24–29%) of **4aa** (entries 3, 5, and 6). $Rh_2(PTAD)_4$, in contrast, yielded no alkylated product (entry 7). Better yield was observed with $Rh_2(esp)_2$ (49%, entry 8). We later determined that the best working ratio for diazomalonamide **2a** to DHP **3a** was 1.3:1 (56%

yield, entry 9). The same yield of **4aa** was observed when the catalyst loading was reduced to 0.3 mol%, which was the lower limit of accurately weighing out the catalyst without making a stock solution. After further screening (concentration, temperature and solvent), the optimized reaction conditions were determined to be $Rh_2(esp)_2$ (0.3–0.5 mol %) and a 1.3:1 ratio of diazomalonamide to DHP in CH_2Cl_2 (0.2 M) at reflux. Slow addition of **2a** ultimately provided β-alkylated DHP **4aa** in 80% yield (entry 19).

Table 3 – Optimization of the β-Alkylation Reaction

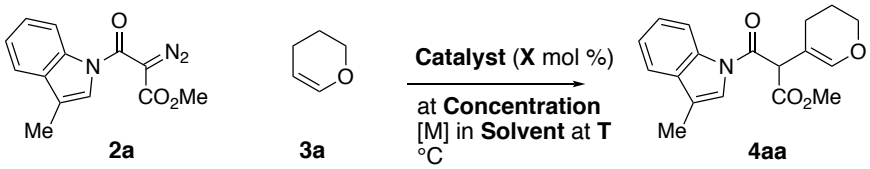

Entry[a]	Catalyst	X (mol %)	2a:3a	Solvent	Conc. [M]	T (°C)	Add.	Yield[b]
1	None	–	1 : 2	C_6H_5F	0.13	85	one shot	0[c]
2	$Cu(acac)_2$	1	1 : 2	C_6H_5F	0.13	85	one shot	0[d]
3	$Rh_2(OAc)_4$	1	1 : 2	C_6H_5F	0.13	85	one shot	28
4	$Rh_2(OAc)_4$	1	1 : 2	C_6H_5F	0.13	65	one shot	15
5	$Rh_2(DOSP)_4$	1	1 : 2	C_6H_5F	0.13	85	one shot	29
6	$Rh_2(BTPCP)_4$	1	1 : 2	C_6H_5F	0.13	85	one shot	24
7	$Rh_2(PTAD)_4$	1	1 : 2	C_6H_5F	0.13	85	one shot	0
8	$Rh_2(esp)_2$	1	1 : 2	C_6H_5F	0.13	85	one shot	49
9	$Rh_2(esp)_2$	1	1.3 : 1	C_6H_5F	0.13	85	one shot	56
10	$Rh_2(esp)_2$	0.3	1.3 : 1	C_6H_5F	0.13	85	one shot	56
12	$Rh_2(esp)_2$	0.3	1.3 : 1	C_6H_5Me	0.13	85	one shot	34
13	$Rh_2(esp)_2$	0.3	1.3 : 1	C_6H_5F	0.13	40	one shot	12
14	$Rh_2(esp)_2$	0.3	1.3 : 1	C_6H_6	0.13	40	one shot	36
15	$Rh_2(esp)_2$	0.3	1.3 : 1	CH_2Cl_2	0.13	40	one shot	66
16	$Rh_2(esp)_2$	0.3	1.3 : 1	CH_2Cl_2	0.13	25	one shot	42
17	$Rh_2(esp)_2$	0.3	1.3 : 1	CH_2Cl_2	0.13	40	6 h	74
18	$Rh_2(esp)_2$	0.3	1.3 : 1	CH_2Cl_2	0.07	40	6 h	73
19	$Rh_2(esp)_2$	0.3	1.3 : 1	CH_2Cl_2	0.20	40	6 h	80
20	$Rh_2(esp)_2$	0.3	1.3 : 1	$CHCl_3$	0.20	60	6 h	73
21	$Rh_2(esp)_2$	0.3	1.3 : 1	1,2-DCE	0.20	85	6 h	73
22	$Rh_2(esp)_2$	0.3	4 : 1	CH_2Cl_2	0.20	40	6 h	85

[a] Reaction conditions: Catalyst (**X** mol%), and **3a** in solvent at indicated temperature and concentration; **2a** (0.66 mmol) added to mixture in one shot or via syringe pump over 6 h. [b] Isolated yields of **3a** after flash column chromatography. [c] No conversion of starting material; >99% **2a** recovered. [d] **2a** was fully consumed, but formation of **4aa** was not observed.

2.2.2 Substrate Scope

2.2.2.1 Substrate Scope of the Alkene Unit

By using the optimized conditions, we explored the β-alkylations of a series of enol ethers, enamides and enecarbamates with diazomalonamide **2a** (Scheme 15).

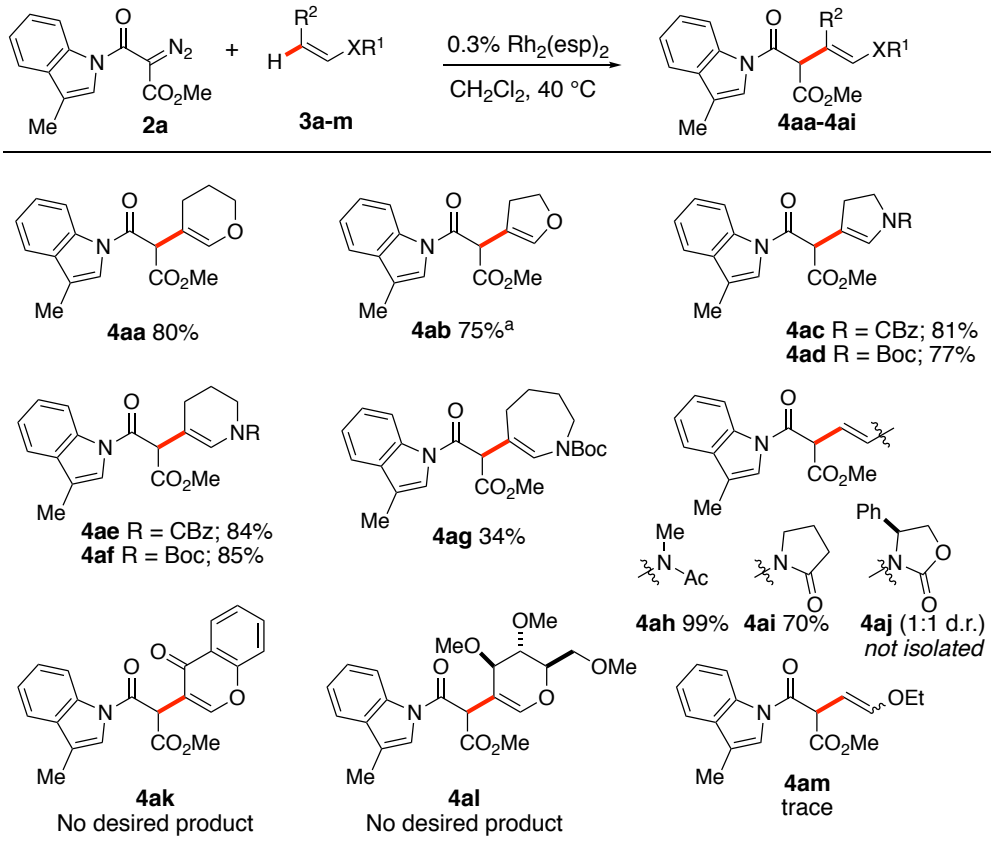

[a]Reaction performed in $CHCl_3$ at 60 °C.

Scheme 15 – Substrate Scope for the β-Alkylation Reaction

2.2.2.2 Substrate Scope of the Diazo Compound

We then examined alkylation reactions by using other α-diazo-1,3-dicarbonyl compounds including dimethyl diazomalonate (**2b**), α-diazomalonamides **2c** and **2d**, and α-diazo-β-ketoesters **2e**–**j** (Scheme 16). Surprisingly, dihydropyran **3a** was the only enol ether to react favorably. Reactions with dihydrofuran **3b** and ethyl vinyl ether **3m** formed almost exclusively a formal [3+2] cycloaddition side product[12] with trace amounts of the desired alkylated products **4ab** and **4am** (see Section 2.2.3 for detailed examination). To circumvent the undesired side reaction, the alkylation of dihydrofuran **3b** was performed

in $CHCl_3$ at 60 °C (Scheme 18) and provided the desired product **4ab** in 75% yield. On the other hand, enamides and enecarbamates did not suffer from the same competitive side reactions. *N*-Cbz- and *N*-Boc-2,3-dihydropyrrole (**3c** and **3d**) were readily converted into their respective β-alkylated enecarbamates, **4ac** and **4ad**, in 81 and 77% yield. Similar results were observed for β-alkylated products **4ae** and **4af** (84 and 85% yield) by using *N*-Cbz- and *N*-Boc-3,4-dihydropyridine (**3e** and **3f**). *N*-Boc-2,3,6,7-tetrahydro-1*H*-azepine (**3g**) afforded a fair yield (34%) of β-alkylated product **4ag**. The low yield may be the result of a steric clash between the indole unit of the carbene and **3g**. Acyclic enamides **3h** and **3i** gave their corresponding β-alkylated products **4ah** and **4ai** in 99 and 70% yield, respectively. Notably, chiral vinyl oxazolidinone **3j** afforded no diastereoselection (a 1:1 mixture of diastereomers was obtained).[13] Reactions of **2a** with chromone and tri-O-Me-*d*-glucal (**3k** and **3l**) failed to provide any discernible alkylated products. This is most likely due to interactions between the rhodium carbene and the adjacent carbonyl or alkoxy groups.

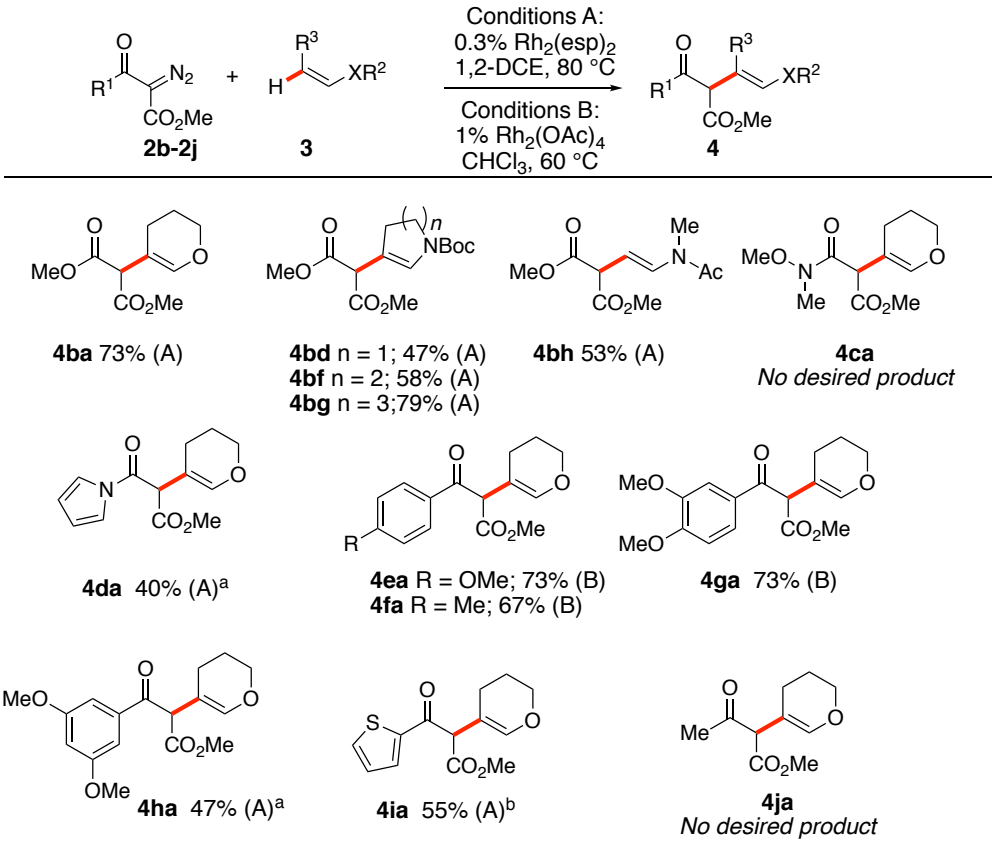

[a]Reaction performed in CH_2Cl_2 at 40 °C. [b]Reaction performed in CH_2Cl_2 at 0 °C → RT.

Scheme 16 – Scope of the Diazo Compound in the β-Alkylation Reaction

When α-diazomalonate was subjected to the optimized conditions with DHP, alkylated product **4ba** was not observed. However, upon changing the conditions to 1,2-dichloroethane (DCE) at 80 °C, **4ba** was obtained in 73% yield. Under these modified conditions, enecarbamates **3d**, **3f**, and **3g** each formed **4bd**, **4bf**, and **4bg** in 47, 58, and 79% yield, respectively. Acyclic enamide **3h** afforded its product in a modest 53% yield. Weinreb α-diazomalonamide **2c** provided a trace amount of alkylated product **4ca**.[14] Lastly, *N*-pyrrolyl α-diazomalonamide **2d** provided 40% yield of its product **4da**. Competing product degradation during purification is responsible for the reduced yield.

α-Diazo-β-ketoesters were similarly found to generate the desired β-alkylated products upon exposure to DHP with either $Rh_2(OAc)_4$ or $Rh_2(esp)_2$ (Scheme 16). The reaction conditions were highly dependent upon the stereoelectronics of the ketone substituent. Aryl α-diazo-β-ketoesters **2e**, **2f**, and **2g** gave their respective alkylated products in 73, 67, and 73% with $Rh_2(OAc)_4$ in $CHCl_3$ at reflux. The 3,5-dimethoxy diazo substrate **2h** performed better using $Rh_2(esp)_2$, although only 47% of the alkylated product **4ha** was obtained. The 2-thienyl α-diazo-β-ketoester **2i** afforded its product **4ia** in 55% yield when the reaction was started at 0 °C and warmed to room temperature (ca. 23 °C).[15] Finally, no detectable product was observed with α-diazoacetoacetonate **2j**.[16]

Curious about the extendibility of this β-alkylation reaction beyond diazoacetates, we explored the reactivity of various alkenes with the diazonitrile **2k** (Table 4). The reaction overwhelmingly preferred the formal [3+2] cycloaddition pathway that similarly plagued reactivity between diazoacetate **2a** and the acyclic enol ethers. Dihydrofuran acetal products **5k** were exclusively formed in the reactions between diazonitrile **2k** and dihydropyran **3a** (entry 1), dihydrofuran **3b** (entry 2), *N*-Boc-dihydropyrrole **3d** (entry 4), and *N*-methyl-vinylacetamide **3h** (entry 5). When *N*-Boc-tetrahydropyridine **3f** was used (entry 3), both β-alkylated **4kf** and dihydrofuran acetal product **5kf** were formed in 30% and 67% yield, respectively. This result provides a starting point for optimization toward a β-alkylation protocol using diazonitriles, but such a pursuit lay outside the scope of the current project.

Table 4 – Behavior of the Diazonitrile in the β-Alkylation Reaction

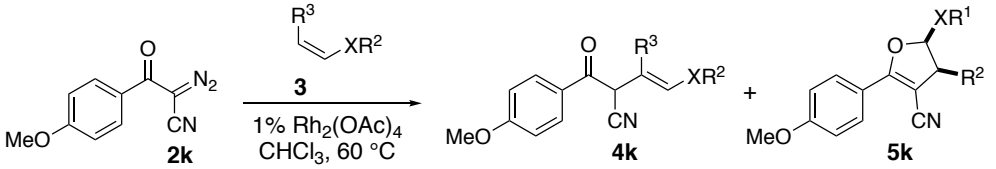

Entry[a]	Alkene	Product(s), Yield
1	 **3a**	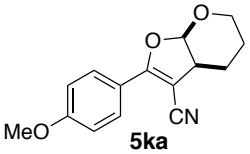 **5ka** 30%
2	 **3b**	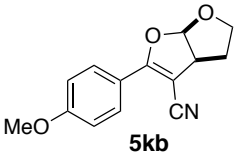 **5kb** 58%
3	 **3f**	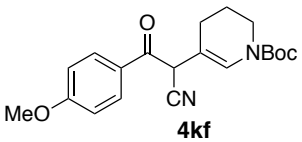 **4kf** 30% 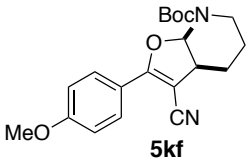 **5kf** 67%
4	 **3d**	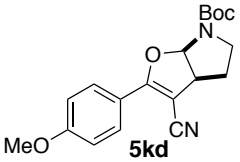 **5kd** 60%
5	 **3h**	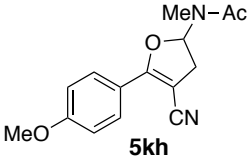 **5kh** 99%

[a]Reaction performed with $Rh_2(OAc)_4$ in $CHCl_3$ (60 °C, 0.2 M) using 1.3 equivalents of **3**.

2.2.3 Understanding Selectivity

The alkylation reaction is proposed to proceed through a commonly accepted addition–elimination mechanism (Scheme 17).[7, 12b]

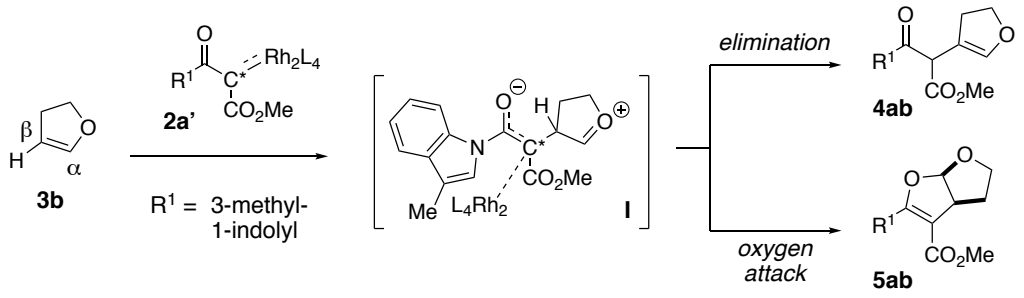

Scheme 17 – Schematic Representations of the Addition-Elimination and Formal [3+2] Cycloaddition Mechanisms Available to the Metal Carbene

For example, in the reaction of **2a** and **3b**, nucleophilic addition of dihydrofuran **3b** to the dirhodium carbene carbon (C*) of **2a'** results in zwitterionic intermediate **I**. The negatively charged fragment of **I** is stabilized by the flanking carbonyl groups, whereas the positive charge is delocalized into the resulting oxonium group. From intermediate **I**, elimination of the β-hydrogen forms an enol before tautomerizing to β-alkylated product **4ab**. Alternatively, attack of the carbonyl oxygen on C_α of the oxonium generates 2,3-dihydrofuran product **5ab** in a formal [3+2] cycloaddition.

2.2.3.1 Synthetic Experiments: Kinetic vs. Thermodynamic Control

To understand the factors that differentiate the reactivity of enol ethers (β-alkylation vs. cycloaddition), we examined the experimental conditions impacting product outcomes for the reaction of 2,3-dihydrofuran **3b** with *N*-indolyl α-diazomalonamide **2a**. As seen in Scheme 18, when $Rh_2(OAc)_4$ was used in either CH_2Cl_2 or $CHCl_3$ at 40 °C, cycloaddition product **5ab** was favorably generated in a 12:1 ratio over the β-alkylated product **4ab**.

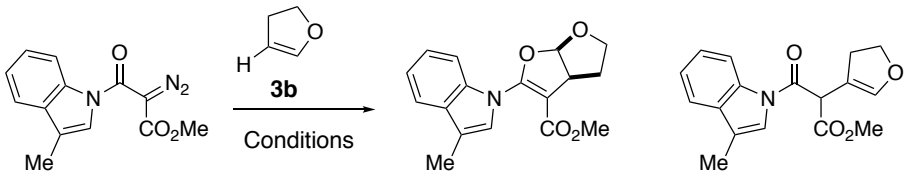

$Rh_2(OAc)_4$ (1.0 mol %), CH_2Cl_2, 40 °C	12	:	1
$Rh_2(OAc)_4$ (1.0 mol %), $CHCl_3$, 40 °C	12	:	1
$Rh_2(OAc)_4$ (1.0 mol %), $CHCl_3$, 60 °C	1	:	17
$Rh_2(esp)_2$ (0.3 mol %), $CHCl_3$, 60 °C	1	:	17 (75% yield)

Scheme 18 – Temperature, Solvent, and Catalyst Effects on the Relative Formation of Alkylated and Cycloaddition Products

In $CHCl_3$ at 60 °C, the ratio switches to 17:1 in favor of the β-alkylated product. Therefore, an increase in temperature alters the reaction outcome. A reaction run with $Rh_2(esp)_2$ showed no catalyst effect on the **4ab** : **5ab** ratio at 60 °C; gratifyingly, product **4ab** was isolated from the latter reaction in 75% yield.

From these experimental data, we hypothesized that alkylation product **4ab** is thermodynamically favorable, whereas cycloaddition (i.e., the formation of **5ab**) is kinetically preferred. To validate this mechanistic hypothesis, two additional control experiments were conducted (Scheme 19). In the first experiment, **5ab** was subjected to 1 mol% $Rh_2(OAc)_4$ in $CHCl_3$ at 60 °C.

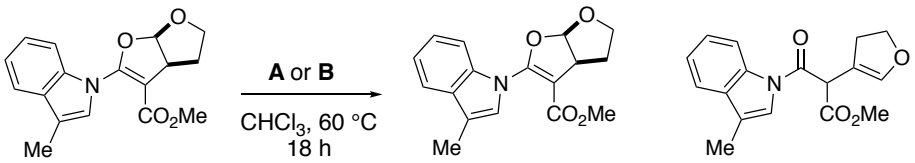

2a		5ab	:	4ab
A: $Rh_2(OAc)_4$ (1.0 mol %)		1	:	14
B: No catalyst		100	:	0

Scheme 19 – Control Experiments Establishing the Dimeric-Rh(II) Catalyst-Mediated Isomerization Pathway Between the Dihydrofuran Acetal and β-Alkylation Products

Equilibration to a 14:1 **4ab** : **5ab** ratio confirmed access to **4ab** from the cyclized intermediate in the presence of dirhodium catalyst (conditions A). The second experiment, performed in the absence of catalyst, demonstrates that the catalyst is necessary for the isomerization to occur (conditions B).

2.2.3.2 Validation from Density Functional Theory

To acquire more insight on the mechanism of the $Rh_2(OAc)_4$-catalyzed reaction of **2a** and **3b**, we utilized DFT calculations (Figure 7).[17–20] The computational investigation focused on the postulated open cyclopropane intermediate **I** featuring a weak Rh–C* interaction (2.42 Å) and lack of a C*-C_α bond (2.41 Å). Transition states **TS-4** and **TS-5**, connecting intermediate **I** with the β-amide ester **4ab** and the bicyclic dihydrofuran acetal **5ab** products, respectively, were also located (Figure 7).

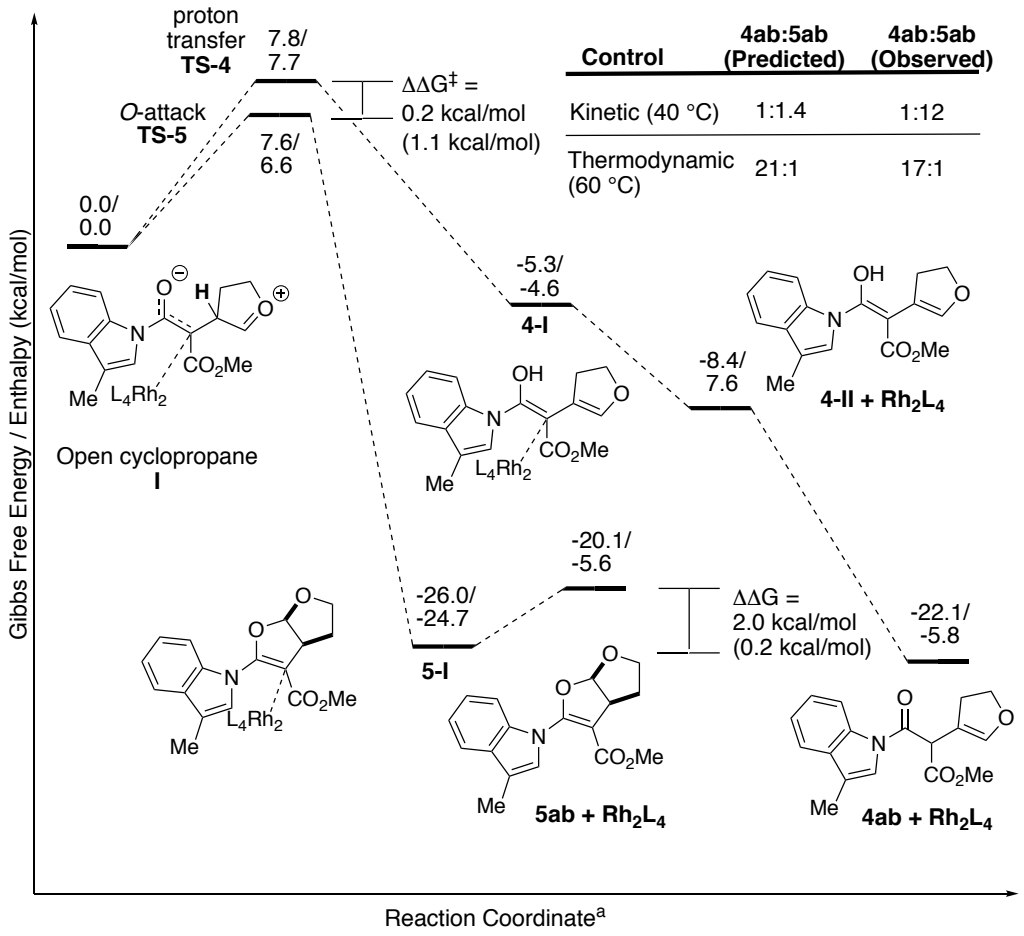

[a]All calculations were performed at the wB97XD/{[6-31++G(d,p)] + LANL2D} level of theory with a polarizable continuum modeled dichloromethane solvent[17,18]

Figure 7 – DFT-Calculated Reaction Coordinate Diagram for the Transformation of the Open Cyclopropane to the Dihydrofuran Acetal and β-Alkylated Products

As seen in Figure 7, the energy barrier associated with **TS-5** is slightly lower than that with **TS-4** with $\Delta\Delta H^{\ddagger}$ =1.1 and $\Delta\Delta G^{\ddagger}$ =0.2 kcal/mo1. While reflecting a smaller $\Delta\Delta G^{\ddagger}$ than the experimental **5ab** : **4ab** ratio of 12:1 suggests (Scheme 18), these data indicate that **5ab** is the kinetically more accessible product in the $Rh_2(OAc)_4$-catalyzed reaction of **2a** and **3b**.

Notably, one of the factors lowering the energy barrier to cyclization relative to alkylation is the relative exergonicities associated with each transformation. The calculated reaction energies for the transformations **I**->**TS-4**->**4-I** and **I**->**TS-5**->**5-I** are $\Delta G/\Delta H$ = -5.3/-4.6 and $\Delta G/\Delta H$ = -26.0/-24.7, respectively (Figure 7). Dissociation of the dirhodium catalyst from **4-I** and subsequent tautomerization generates **4ab**, which lies 2.0 (0.2) kcal/mol in Gibbs free energy (enthalpy) lower than cyclized product **5ab**; this result is in excellent agreement with the thermodynamic control experiments introduced in Scheme 18 and Scheme 19.

The steeply exergonic transformation from **I** into **5-I** is consistent with an early transition state. Hybridization index (i_n) at C_n (n = α or β, respectively) on the dihydrofuran unit was employed to demonstrate progression of **TS-5** and **TS-4** along the reaction coordinate (Figure 8).[19] As seen in Figure 8, **TS-5** is indeed reactant-like: it has an i_α of 2.0 (i.e., features $sp^{2.0}$ geometry about C_α) and bears more geometric similarity to **I** than to **5-I**, where C_α features $sp^{2.6}$ geometry. In contrast, **TS-4** is product-like (i_β = 2.2), resembling the enol **4-I** more so than the open cyclopropane **I**.

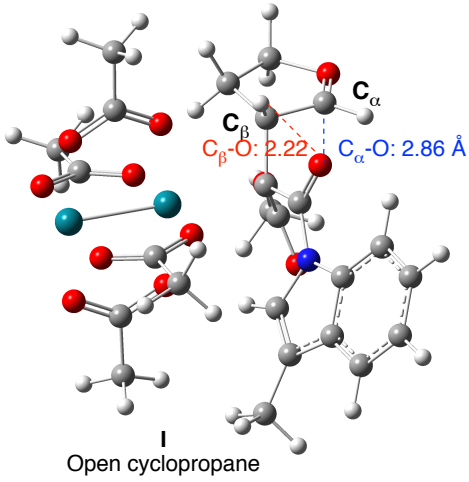

Structure	i_β	i_α
I	2.9	2.0
TS-4	2.2	—
4-I	2.0	—
TS-5	—	2.0
5-I	—	2.6

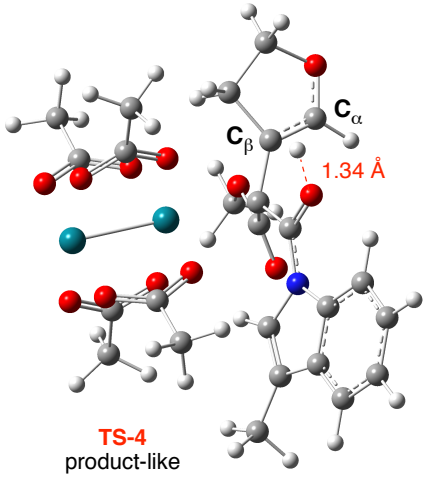

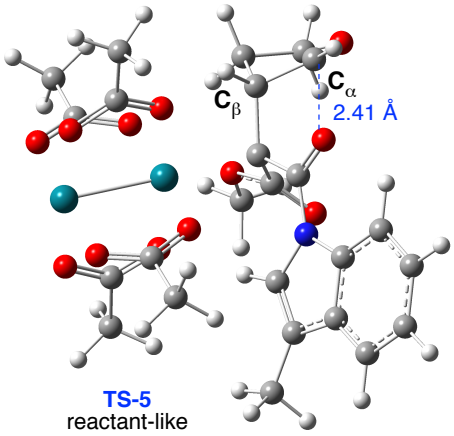

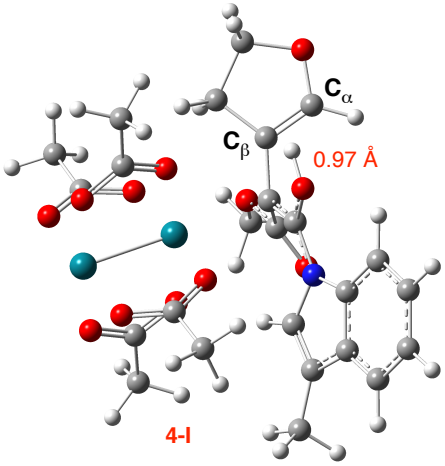

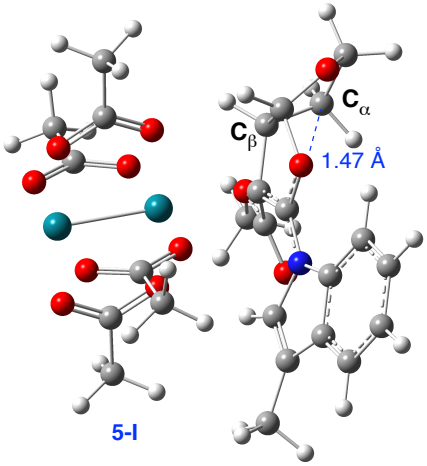

Figure 8 – Tracking Reaction Coordinate Progress through Hybridization Index and Transition-Relevant Bond Lengths

Other mechanistic pathways were also investigated to rationalize the proposed equilibrium between **4ab** and **5ab**. Notably, we investigated non-metal-mediated isomerizations from **5ab** into **4ab**. The resulting barrier to activating the C_α-O bond in **5ab** was prohibitively high (>50 kcal/mol) without rhodium coordination and resulted in fragmentation of the calculated structure. Although never experimentally observed or detected, a closed cyclopropane intermediate was also postulated as part of various isomerization pathways. This intermediate was ultimately ruled out because it was determined to be ca. 10 kcal/mol higher in energy than **5ab** and the calculations yielded high barriers and fragmenting structures, unless the reaction coordinate was retraced back to the open cyclopropane **I**. Several conclusions can be extrapolated from the outcomes of the temperature experiments and DFT calculations. First, an equilibrium pathway linking **4ab** and **5ab** exists that requires catalyst as well as moderate heating (60 °C).[21] Second, K_{eq} favors **4ab**, but a steeply exergonic transformation from **I** into **5-I** lowers **TS-5** relative to **TS-4** rendering **5ab** more favorable at lower temperatures. Finally, the use of temperature provides a means to control product selectivity.

2.2.3.3 Mechanistic Insights Allow for the Alkylation of Mono-Substituted Enol Ethers

Following this mechanistic insight, we pursued the functionalization of acyclic enol ethers (Scheme 20). These systems were reported to produce the corresponding 2,3-dihydrofurans with α-diazo dicarbonyls and dimeric Rh(II) catalysts.[22] In this study, we envisioned that the formation of 2,3-dihydrofuran *in situ* could be coupled with a thermally induced isomerization in the presence of the Rh catalyst to provide β-alkylated products.

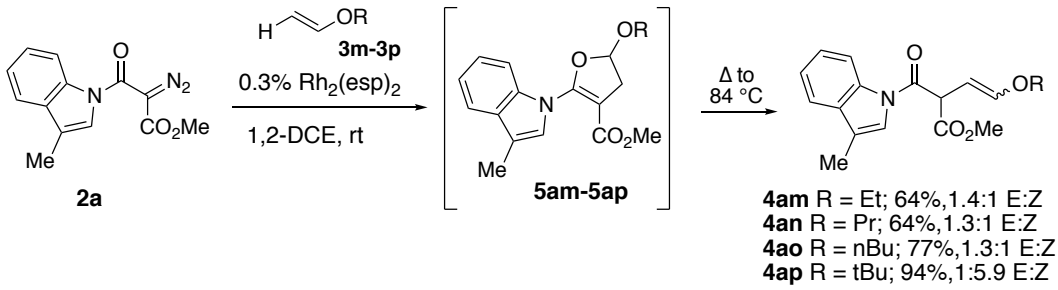

Scheme 20 – Reactions of the α-Diazomalonamide with Acyclic Enol-Ethers

2,3-Dihydrofurans **5am-ap** from the reactions of **2a** with ethyl vinyl ether (**3m**), propyl vinyl ether (**3n**), n-butyl vinyl ether (**3o**), and *tert*-butyl vinyl ether (**3p**) were initially formed at room temperature (ca. 23 °C) in 1,2-DCE and then heated at reflux. By using this sequence, β-alkylated products **4am–ap** were obtained as alkene mixtures in 64, 64, 77, and 94% yield, respectively. In the case of n-alkyl enol ethers, the trans-alkene products were obtained as the major isomers. Conversely, the *tert*-butyl vinyl ether gave predominantly the cis-isomer, which can be attributed to the steric influence of the *tert*-butyl group during the elimination step transition state. Overall, these results are significant and represent the first examples of the β-C-H alkylation of acyclic enol ethers using an α-diazo dicarbonyl compound.

2.2.4 Elaborating the Product Space with Further Chemistry

The β-alkylated products can also serve as synthetic building blocks for target-oriented synthesis (Scheme 21). For example, α-alkylation of β-alkylated product **4ga** gave **6a** or **6b** with modest yield. Ketone **4ga** was quantitatively reduced under chelation-controlled conditions with $NaBH_4$ and $MnCl_2$, providing alcohol **7** in >20:1 d.r.[23] Krapcho decarbalkoxylation provided β,γ-unsaturated ketone **8** in 81% yield.[24]

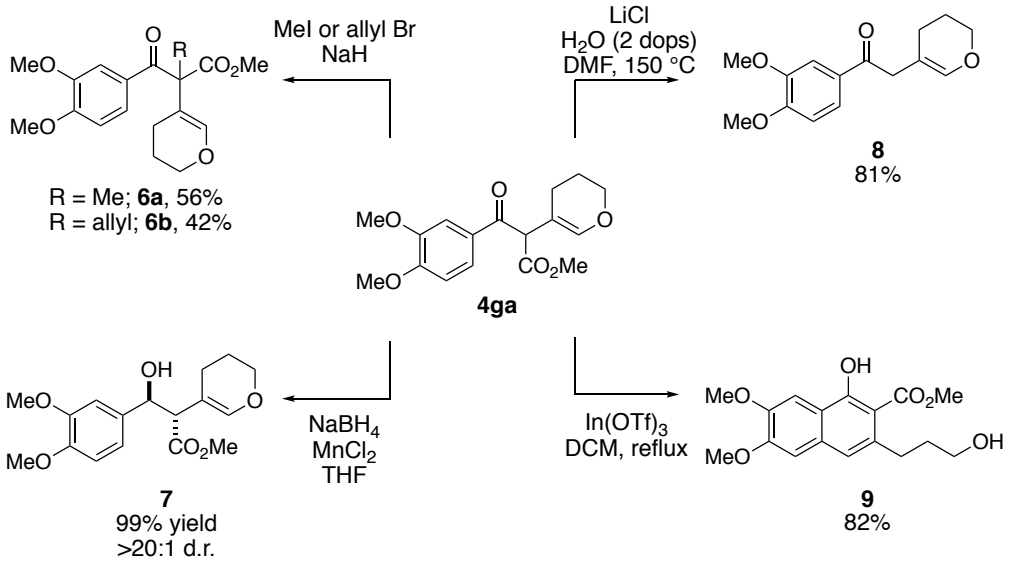

Scheme 21 – Derivatization of a β-Alkylated Product

Finally, functionalized naphthol **9** was formed in 82% yield when **4ga** was treated with 30 mol% $In(OTf)_3$ in CH_2Cl_2 at 40 °C. Presumably, the reaction proceeds through Lewis acid-promoted enol formation, followed by a 6π electrocyclization. Lewis acid-facilitated alcohol elimination results in aromatization to form the naphthyl ring (Scheme 22).[25]

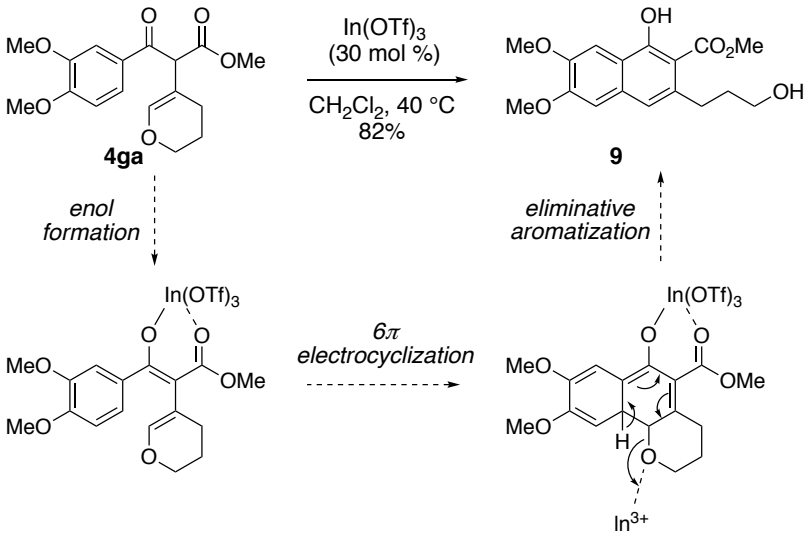

Scheme 22 – Proposed Mechanism for the Lewis Acid Catalyzed 6π-Electrocyclization

2.3 Conclusion

We disclosed an intermolecular, Rh(II)-catalyzed β-C(sp^2)-H alkylation of enols ethers and enamides by using α-diazo-1,3-dicarbonyl compounds. The products are generated in yields of up to 99% by using 0.3–0.5 mol% dimeric Rh(II) catalyst and are readily derivatized. This methodology represents a significant expansion in overall scope, efficiency, and utility when compared with previous approaches. The alkylation reaction works for a variety of α-diazo-1,3-dicarbonyl compounds, including α-diazomalonates, -malonamides, and β-ketoesters. Moreover, both cyclic and acyclic enol ethers and enamides are effectively alkylated. Beyond the reaction scope, the presumptive addition–elimination mechanism was studied both experimentally and computationally and the reaction was determined to proceed under thermodynamic control at higher temperatures. This finding led to the determination of conditions that allowed for the first examples of β-C-H alkylation of acyclic enol ethers using α-diazo-1,3-dicarbonyl compounds to be

reported. Future investigations include: (1) strategic late-stage C-H functionalization of bioactive molecules; (2) expansion of the scope for the Lewis acid-catalyzed 6π-electrocyclization reaction; and (3) use of the β-alkylated products as building blocks for complex synthesis.

2.4 Experimental

See the original manuscript for general methods, computational detail, experimental procedures, and characterization data for all compounds except **5ka**, **5kb**, **5kd**, **5kf**, **5kh**, and **4kf**. See below Sections 2.4.1 and 2.4.2 for experimental procedures and NMR spectra for compounds **5ka**, **5kb**, **5kd**, **5kf**, **5kh**, and **4kf**.

2.4.1 Experimental Procedures

General procedure for formation of **5ka**, **5kb**, **5kd**, **5kf**, **5kh**, and **4kf**: To a dry round-bottom flask containing $Rh_2(OAc)_4$ (1 mol %) and enol ether/enamide (**3a**, **3b**, **3d**, **3f**, or **3h**; 1 equiv) in refluxing chloroform (0.5 M, 60 °C) was added a solution of 2-diazo-3-(4-methoxyphenyl)-3-oxopropanenitrile **2k** (1.3 equiv.) in chloroform (0.33 M) via syringe pump over 6 hours. The reaction was allowed to proceed for 18 hours at 60 °C. The crude mixture was purified via flash silica gel chromatography using 10-20% EtOAc in hexanes as the eluent.

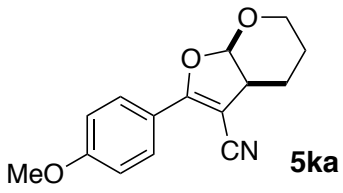

5ka

2-(4-Methoxyphenyl)-3a,5,6,7a-tetrahydro-4*H*-furo[2,3-*b*]pyran-3-carbonitrile (5ka): 29 µl (0.32 mmol) of 3,4-dihydro-2*H*-pyran **3a** was used. **5ka** was afforded as a clear oil (25 mg, 30% yield). **^{1}H NMR** (300 MHz, $CDCl_3$) δ = 7.97 (d, *J* = 8.9 Hz, 2H), 6.95 (d, *J* = 8.8 Hz, 2H), 5.96 (d, *J* = 7.6 Hz, 1H), 3.86 (s, 3H), 3.83 – 3.77 (m, 2H), 3.31 (dt, *J* = 7.6, 5.1 Hz, 1H), 2.03 – 1.84 (m, 2H), 1.82 – 1.67 (m, 2H). **^{13}C NMR** (75 MHz, $CDCl_3$) δ = 166.01, 162.12, 129.07, 120.19, 117.58, 114.07, 103.30, 81.50, 60.18, 55.45, 40.28, 20.24, 18.83.

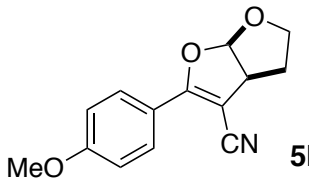

5kb

2-(4-Methoxyphenyl)-3a,4,5,6a-tetrahydrofuro[2,3-*b*]furan-3-carbonitrile (5kb): 29 µl (0.39 mmol) of 2,3-dihydrofuran **3b** was used. **5kb** was afforded as a clear oil (54 mg, 58% yield). **^{1}H NMR** (300 MHz, $CDCl_3$) δ = 7.93 (d, *J* = 9.0 Hz, 2H), 6.93 (d, *J* = 8.7 Hz, 2H), 6.27 (d, *J* = 6.1 Hz, 1H), 4.20 – 4.07 (m, 1H), 3.98 – 3.87 (m, 1H), 3.84 (s, 3H), 3.83 – 3.72 (m, 1H), 2.21 – 2.10 (m, 2H). **^{13}C NMR** (75 MHz, $CDCl_3$) δ = 166.75, 162.16, 129.13, 119.74, 117.63, 114.04, 109.88, 79.21, 67.22, 55.44, 48.86, 31.17.

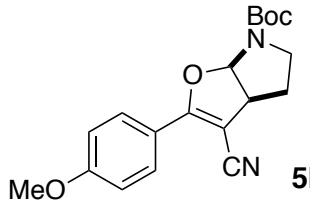

5kd

***tert*-Butyl 3-cyano-2-(4-methoxyphenyl)-3a,4,5,6a-tetrahydro-6*H*-furo[2,3-*b*]pyrrole-6-carboxylate (5kd):** 56 μl (0.33 mmol) of *tert*-butyl 2,3-dihydro-1*H*-pyrrole-1-carboxylate **3d** was used. **5kd** was afforded as a yellow oil (67 mg, 60% yield). **^{1}H NMR** (300 MHz, $CDCl_3$) δ = 7.91 (d, *J* = 8.8 Hz, 2H), 6.92 (d, *J* = 9.0 Hz, 2H), 6.34 (s, 1H), 3.96 (dd, *J* = 10.3, 5.9 Hz, 1H), 3.84 (s, 3H), 3.79 – 3.68 (m, 1H), 3.31 (td, *J* = 10.6, 8.0 Hz, 1H), 2.20 – 2.08 (m, 2H), 1.51 (s, 9H). **^{13}C NMR** (75 MHz, $CDCl_3$) δ = 166.52, 162.23, 152.97, 129.10, 120.19, 117.25, 114.04, 93.78, 80.93, 79.55, 55.33, 48.40, 43.87, 29.19, 28.30.

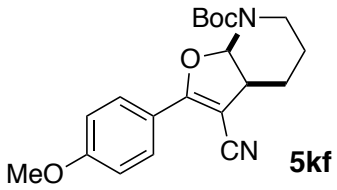

5kf

***tert*-Butyl 3-cyano-2-(4-methoxyphenyl)-3a,5,6,7a-tetrahydrofuro[2,3-*b*]pyridine-7(4*H*)-carboxylate (5kf):** 64 μl (0.32 mmol) of *tert*-butyl 3,4-dihydropyridine-1(2*H*)-carboxylate **3f** was used. **5kf** was afforded as a yellow oil (82 mg, 67% yield. **^{1}H NMR** (300 MHz, $CDCl_3$) δ = ^{1}H NMR (300 MHz, Chloroform-*d*) δ 7.91 (d, *J* = 9.0 Hz, 2H), 6.92 (d, *J* = 9.0 Hz, 2H), 6.58 (m, 1H), 3.84 (s, 3H), 3.73 (m, 1H), 3.30 (m, 1H), 3.16 (m, 1H), 1.82 – 1.61 (m, 4H), 1.51 (s, 9H). **^{13}C NMR** (75 MHz, $CDCl_3$) δ = 165.68, 162.14, 154.88, 129.00, 120.54, 117.47, 114.01, 88.37, 82.03, 81.29, 55.32, 53.24, 40.71, 28.24, 23.66, 18.56.

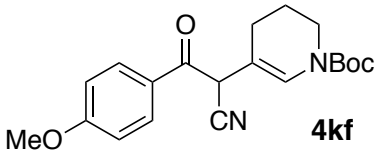

4kf

***tert*-Butyl 5-(1-cyano-2-(4-methoxyphenyl)-2-oxoethyl)-3,4-dihydropyridine-1(2*H*)-carboxylate (4kf):** 64 μl (0.32 mmol) of *tert*-butyl 3,4-dihydropyridine-1(2*H*)-carboxylate **3f** was used. **4kf** was afforded as a clear oil (40 mg, 30% yield). **^{1}H NMR** (300 MHz, $CDCl_3$, 55 °C) δ = 7.96 (d, *J* = 7.1 Hz, 2H), 7.08 (s, 1H), 6.95 (d, *J* = 7.2 Hz, 2H), 4.93 (s, 1H), 3.88 (s, 3H), 3.56 – 3.39 (m, 2H), 2.23 – 2.12 (m, 1H), 2.04 (m, *J* = 6.3 Hz, 1H), 1.81 (m, *J* = 9.9 Hz, 2H), 1.49 (s, 9H). **^{13}C NMR** (75 MHz, $CDCl_3$, 55 °C) δ = 187.28, 168.83, 164.49, 131.26, 127.48, 127.02, 124.99, 116.05, 114.22, 81.40, 55.49, 46.10, 41.83, 28.19, 22.93, 21.22.

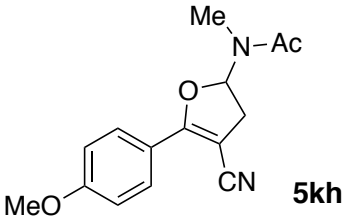

5kh

***N*-(4-cyano-5-(4-methoxyphenyl)-2,3-dihydrofuran-2-yl)-*N*-methylacetamide (5kh):** 36 μl (0.35 mmol) of *N*-methyl-*N*-vinylacetamide **3h** was used. **5kh** was afforded as a clear oil (96 mg, >99% yield). **^{1}H NMR** (300 MHz, $CDCl_3$) δ = 7.89 (d, *J* = 9.0 Hz, 2H), 7.11 (s, 1H), 6.92 (d, *J* = 9.0 Hz, 2H), 3.83 (s, 3H), 3.30 (dd, *J* = 15.9, 10.2 Hz, 1H), 2.88 (s, 3H), 2.16 (s, 3H). **^{13}C NMR** (75 MHz, $CDCl_3$, 55 °C, *asterisk indicates rotomeric peaks)

δ = 171.00, 166.02, 162.29, 128.90, 127.09*, 124.99, 119.81, 116.98*, 114.16, 84.96, 76.33, 55.36, 34.38, 29.56, 21.76.

2.4.2 ^{1}H and ^{13}C NMR Spectra

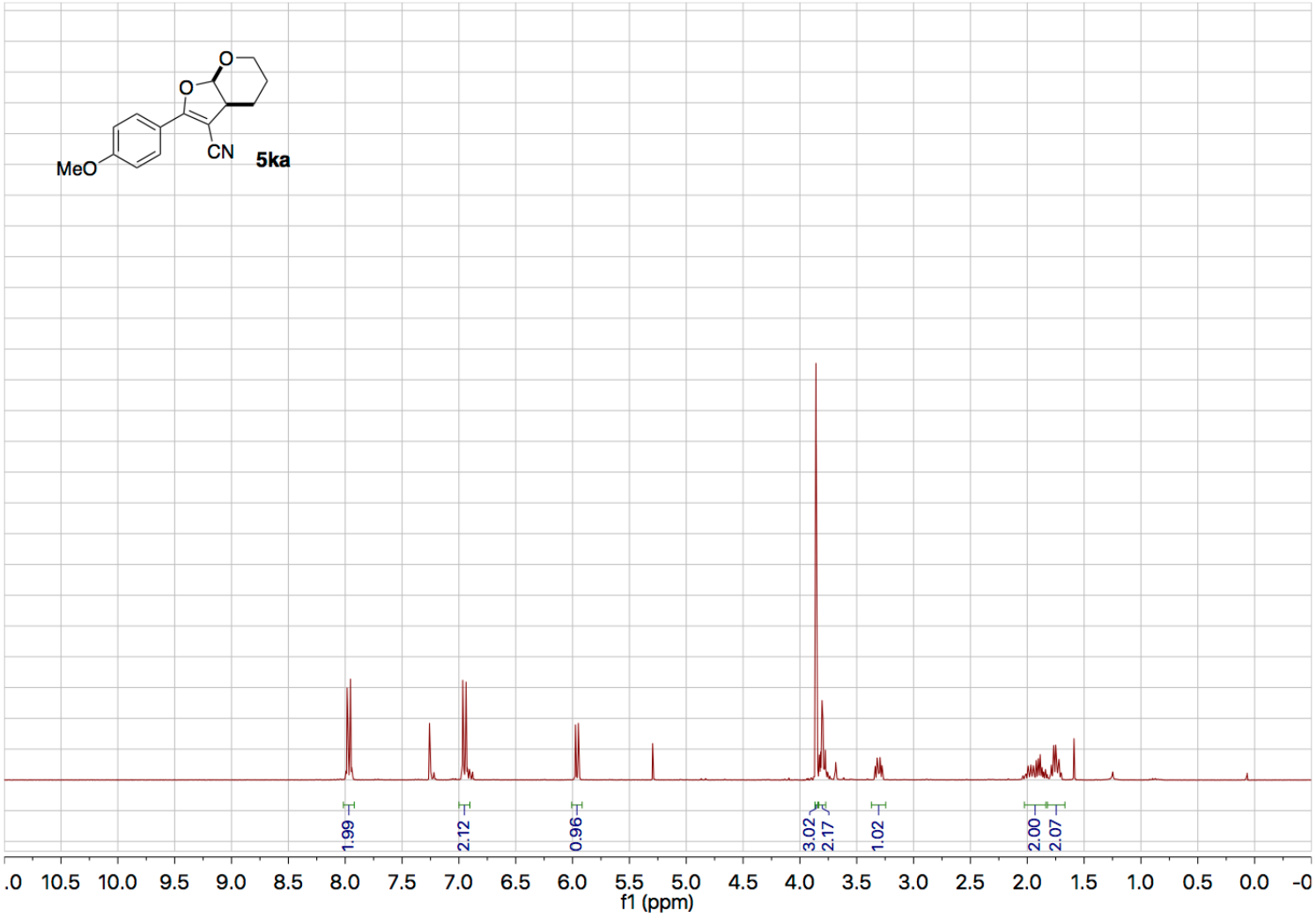
O
O
CN
MeO
5ka
1.99
2.12
0.96
3.02
2.17
1.02
2.00
2.07
.0 10.5 10.0 9.5 9.0 8.5 8.0 7.5 7.0 6.5 6.0 5.5 5.0 4.5 4.0 3.5 3.0 2.5 2.0 1.5 1.0 0.5 0.0 -0
f1 (ppm)

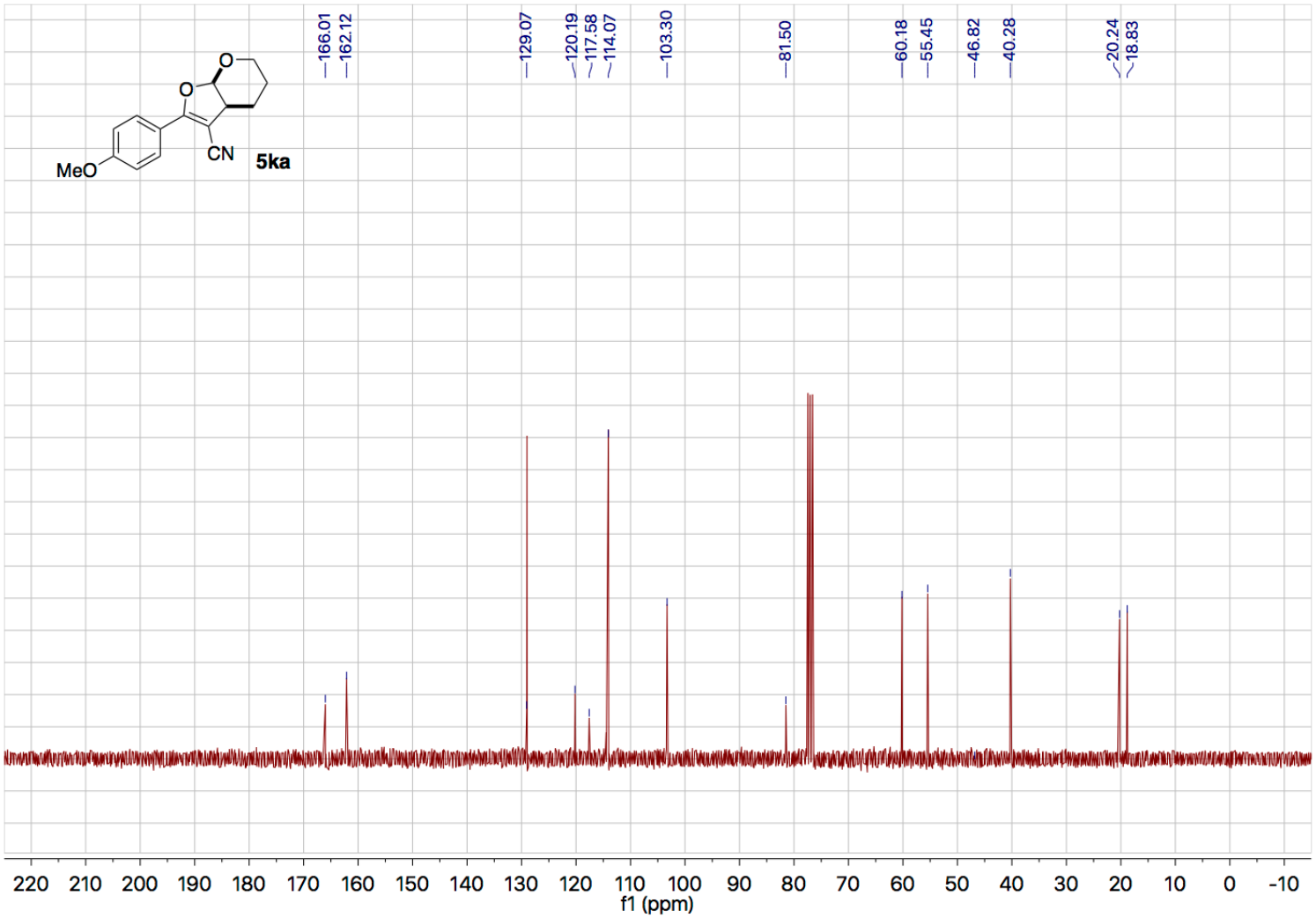
166.01
162.12
129.07
120.19
117.58
114.07
103.30
81.50
60.18
55.45
46.82
40.28
20.24
18.83
MeO
CN
5ka
220 210 200 190 180 170 160 150 140 130 120 110 100 90 80 70 60 50 40 30 20 10 0 -10
f1 (ppm)

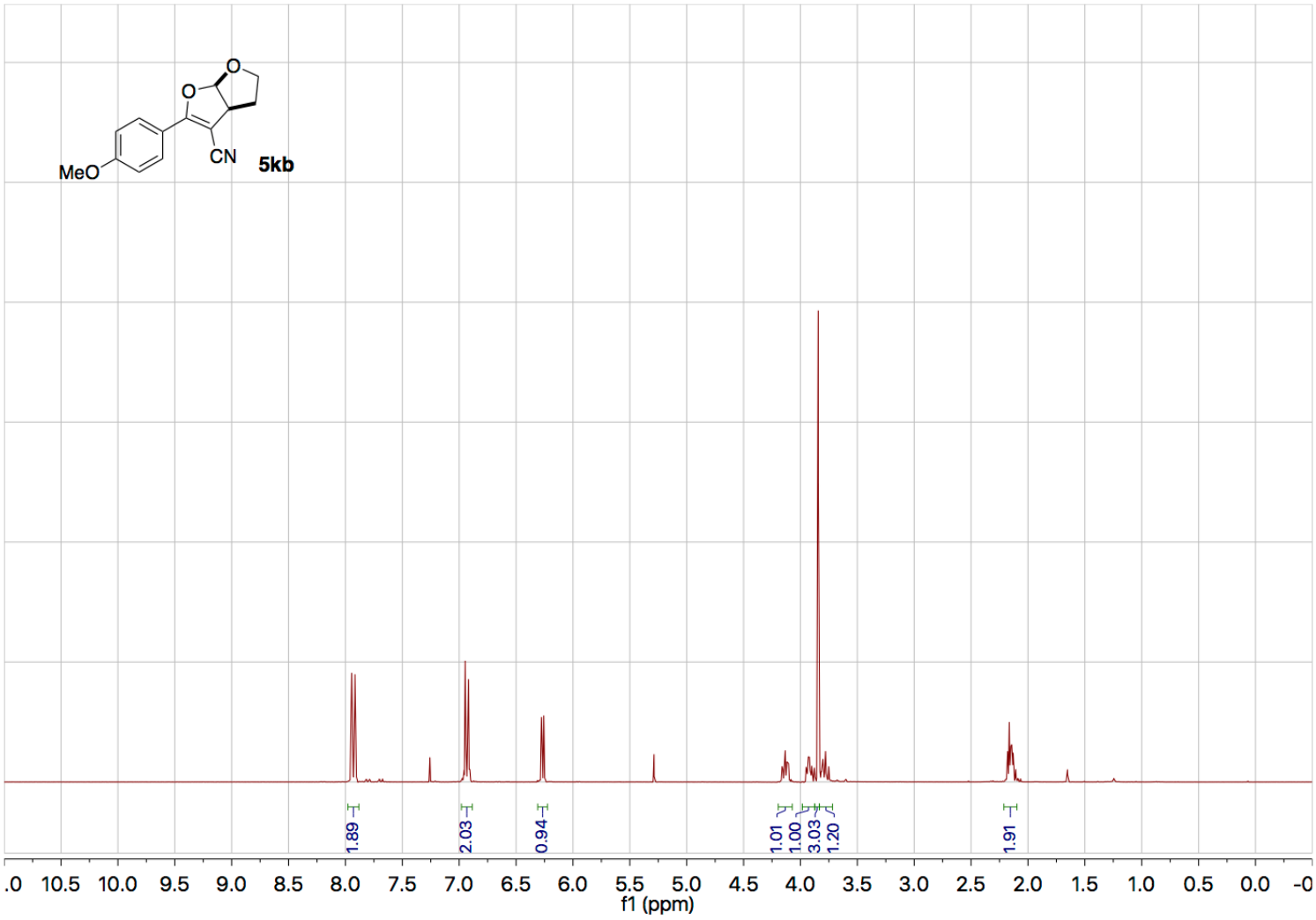
MeO
CN
5kb
1.89
2.03
0.94
1.01
1.00
3.03
1.20
1.91
f1 (ppm)

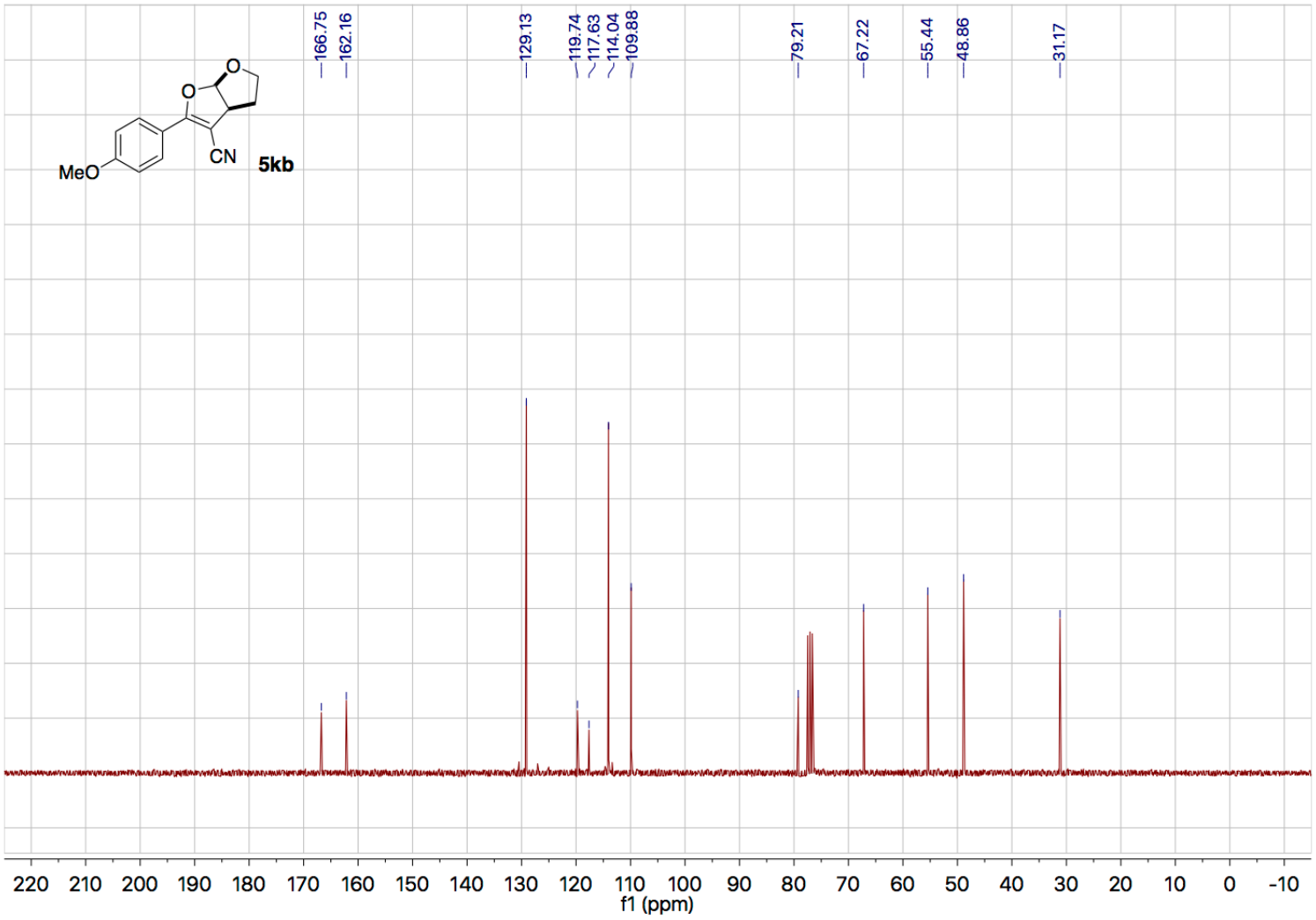
166.75
162.16
129.13
119.74
117.63
114.04
109.88
79.21
67.22
55.44
48.86
31.17
MeO
CN
5kb
220 210 200 190 180 170 160 150 140 130 120 110 100 90 80 70 60 50 40 30 20 10 0 -10
f1 (ppm)

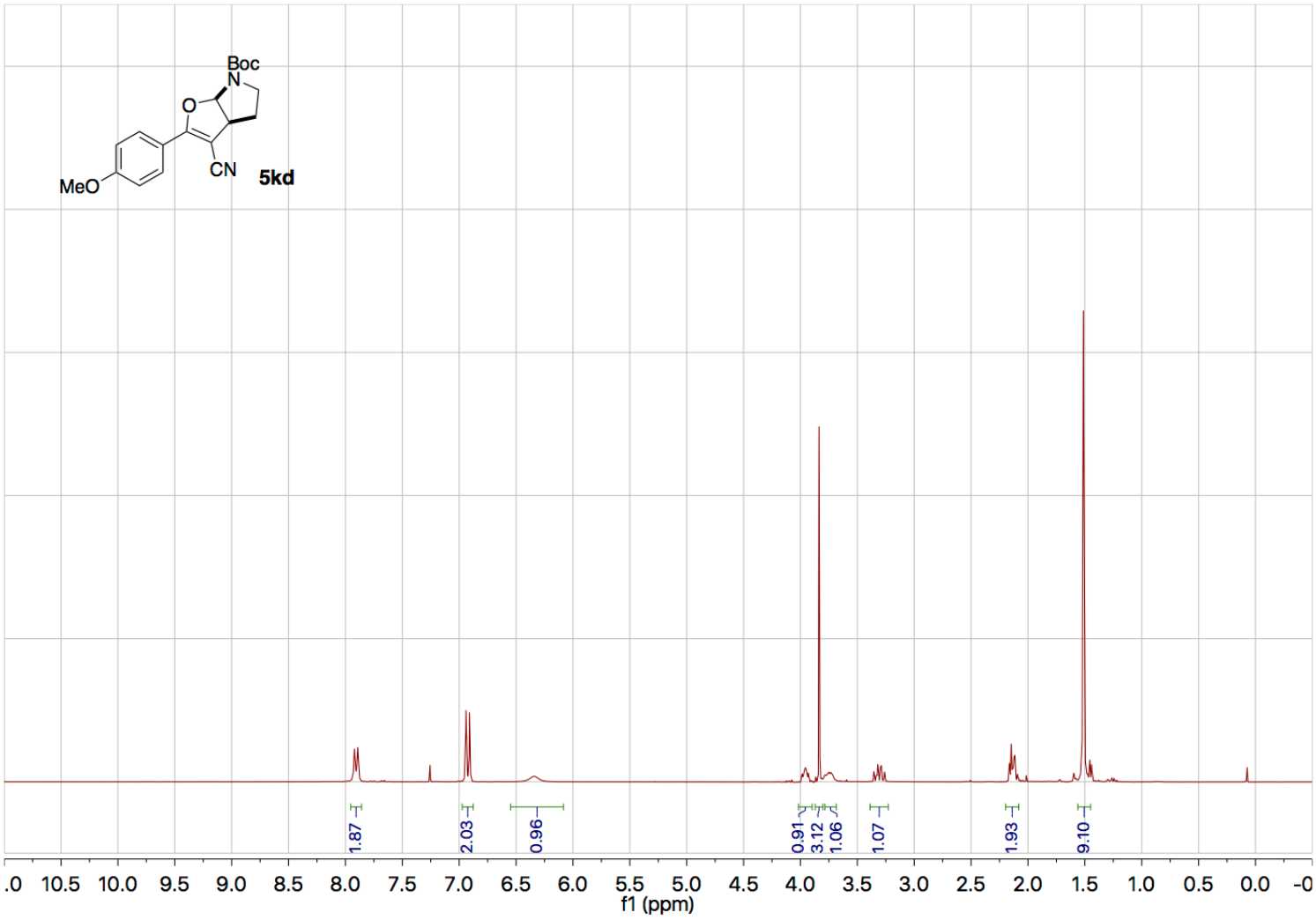
Boc
N
O
CN
MeO
5kd
1.87
2.03
0.96
0.91
3.12
1.06
1.07
1.93
9.10
.0 10.5 10.0 9.5 9.0 8.5 8.0 7.5 7.0 6.5 6.0 5.5 5.0 4.5 4.0 3.5 3.0 2.5 2.0 1.5 1.0 0.5 0.0 -0
f1 (ppm)

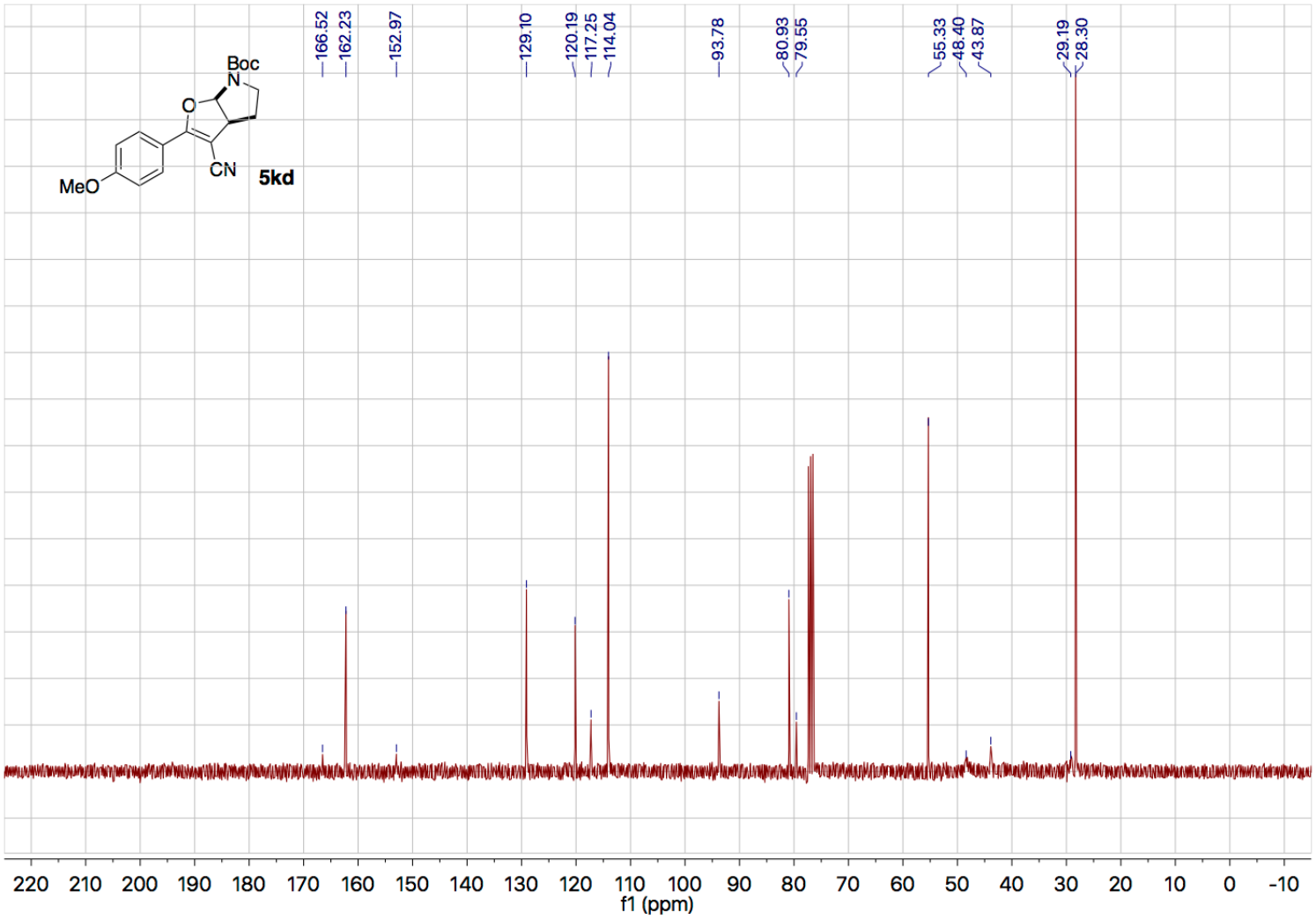
166.52
162.23
152.97
129.10
120.19
117.25
114.04
93.78
80.93
79.55
55.33
48.40
43.87
29.19
28.30
Boc
N
O
CN
MeO
5kd
220 210 200 190 180 170 160 150 140 130 120 110 100 90 80 70 60 50 40 30 20 10 0 -10
f1 (ppm)

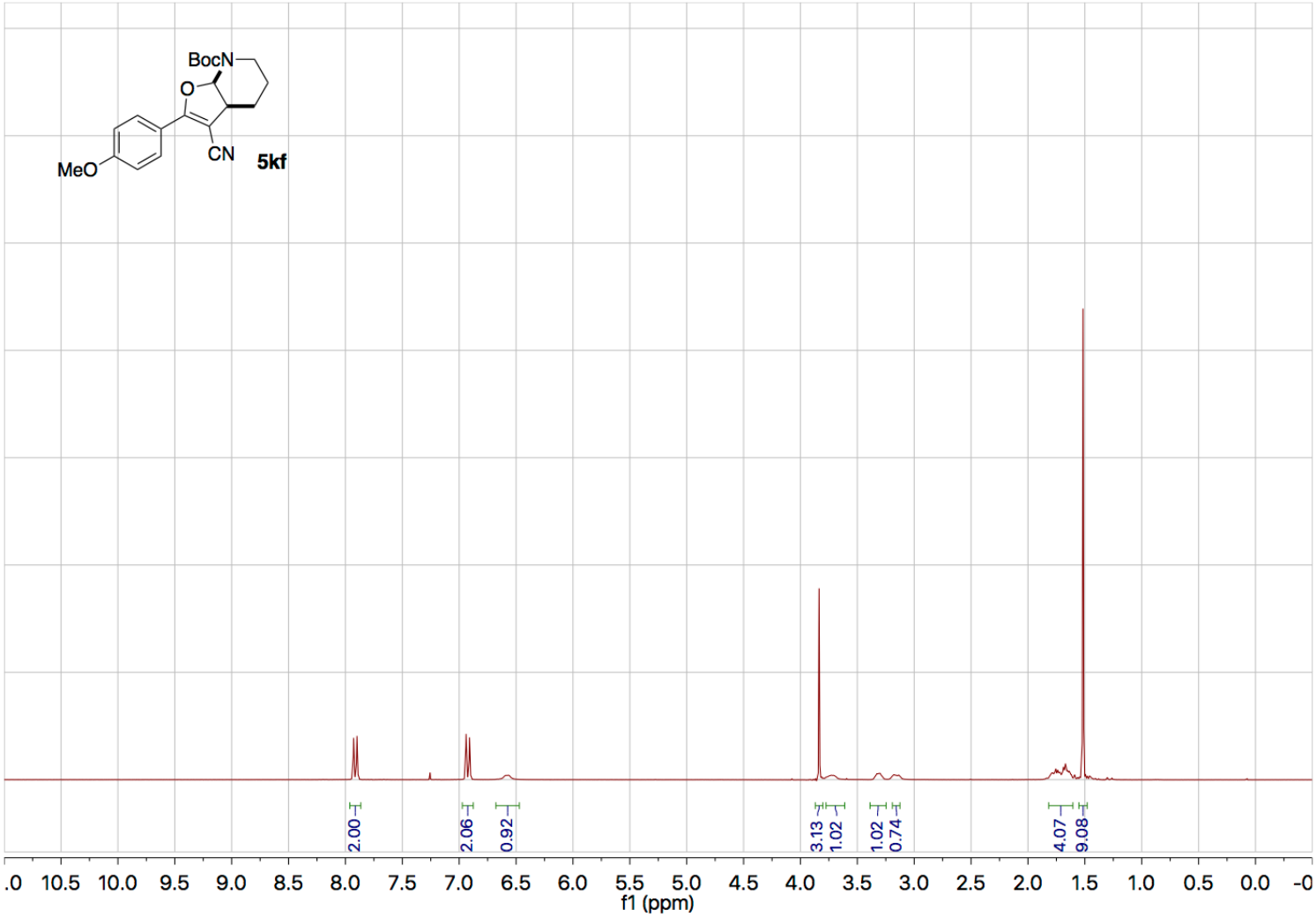
BocN
O
CN
MeO
5kf
2.00
2.06
0.92
3.13
1.02
1.02
0.74
4.07
9.08
.0 10.5 10.0 9.5 9.0 8.5 8.0 7.5 7.0 6.5 6.0 5.5 5.0 4.5 4.0 3.5 3.0 2.5 2.0 1.5 1.0 0.5 0.0 -0
f1 (ppm)

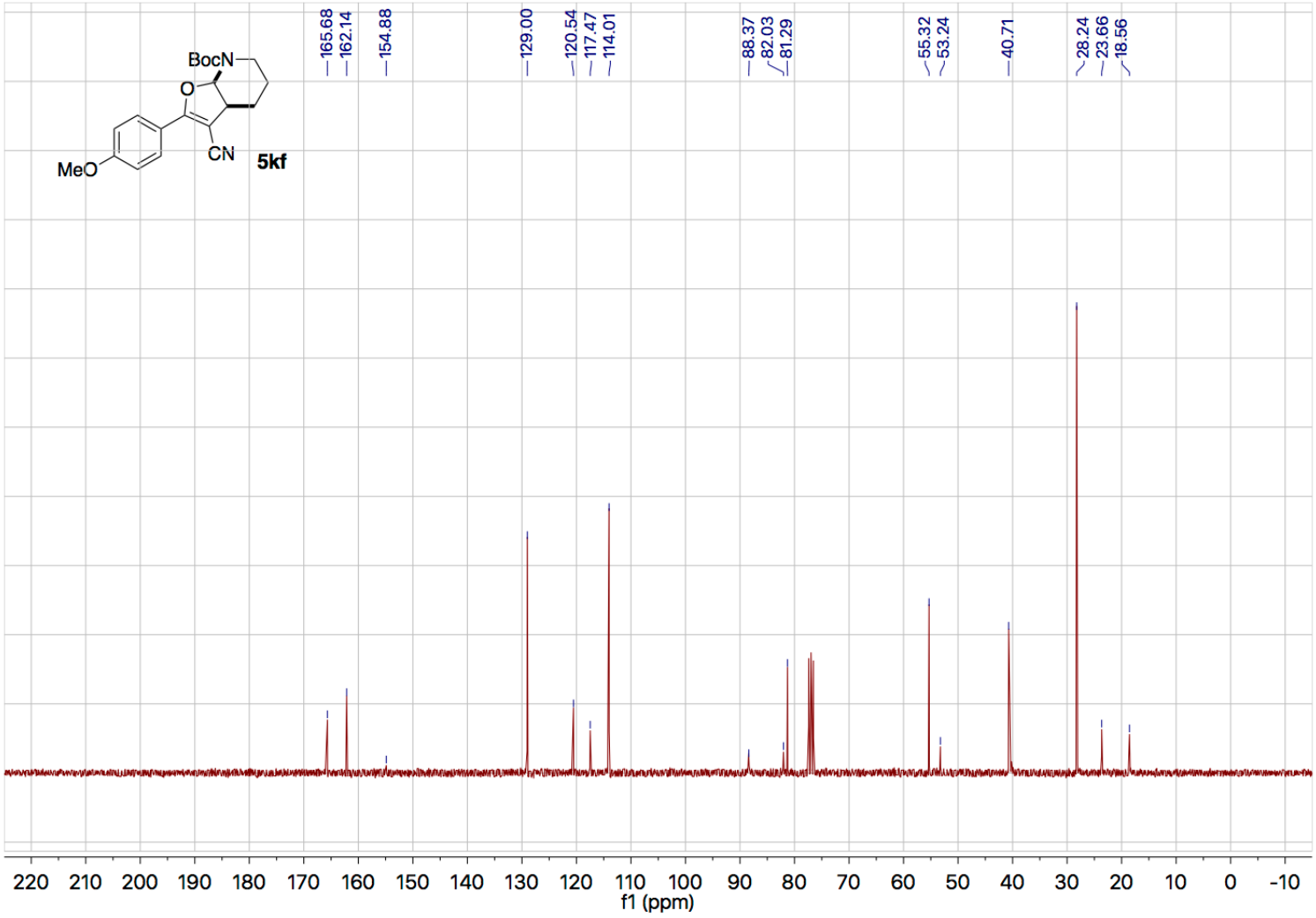
BocN
O
CN
MeO
5kf
165.68
162.14
154.88
129.00
120.54
117.47
114.01
88.37
82.03
81.29
55.32
53.24
40.71
28.24
23.66
18.56
220 210 200 190 180 170 160 150 140 130 120 110 100 90 80 70 60 50 40 30 20 10 0 -10
f1 (ppm)

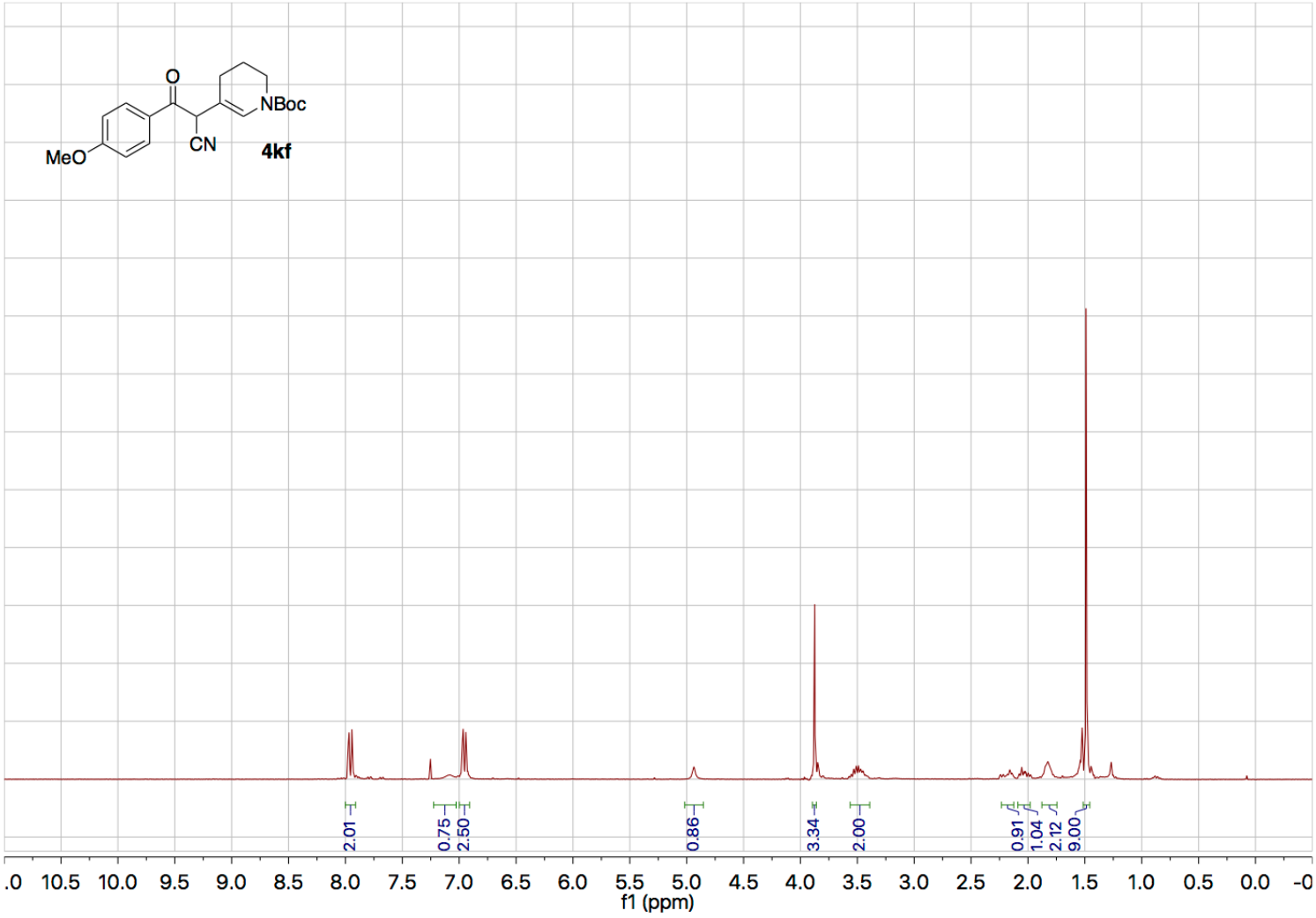
O
NBoc
CN
MeO
4kf
2.01
0.75
2.50
0.86
3.34
2.00
0.91
1.04
2.12
9.00
.0 10.5 10.0 9.5 9.0 8.5 8.0 7.5 7.0 6.5 6.0 5.5 5.0 4.5 4.0 3.5 3.0 2.5 2.0 1.5 1.0 0.5 0.0 -0
f1 (ppm)

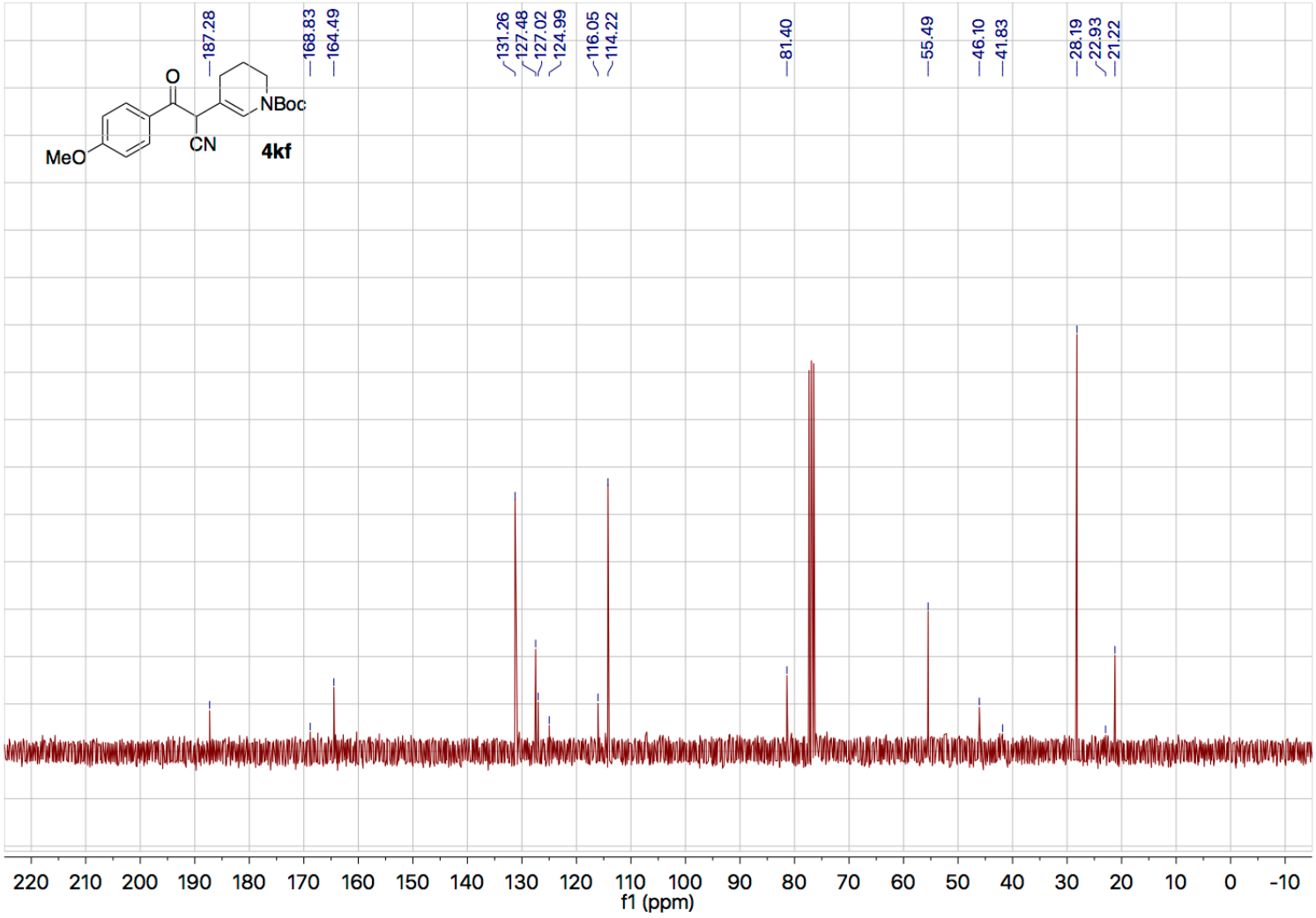
187.28
168.83
164.49
131.26
127.48
127.02
124.99
116.05
114.22
81.40
55.49
46.10
41.83
28.19
22.93
21.22
O
NBoc
CN
MeO
4kf
220 210 200 190 180 170 160 150 140 130 120 110 100 90 80 70 60 50 40 30 20 10 0 -10
f1 (ppm)

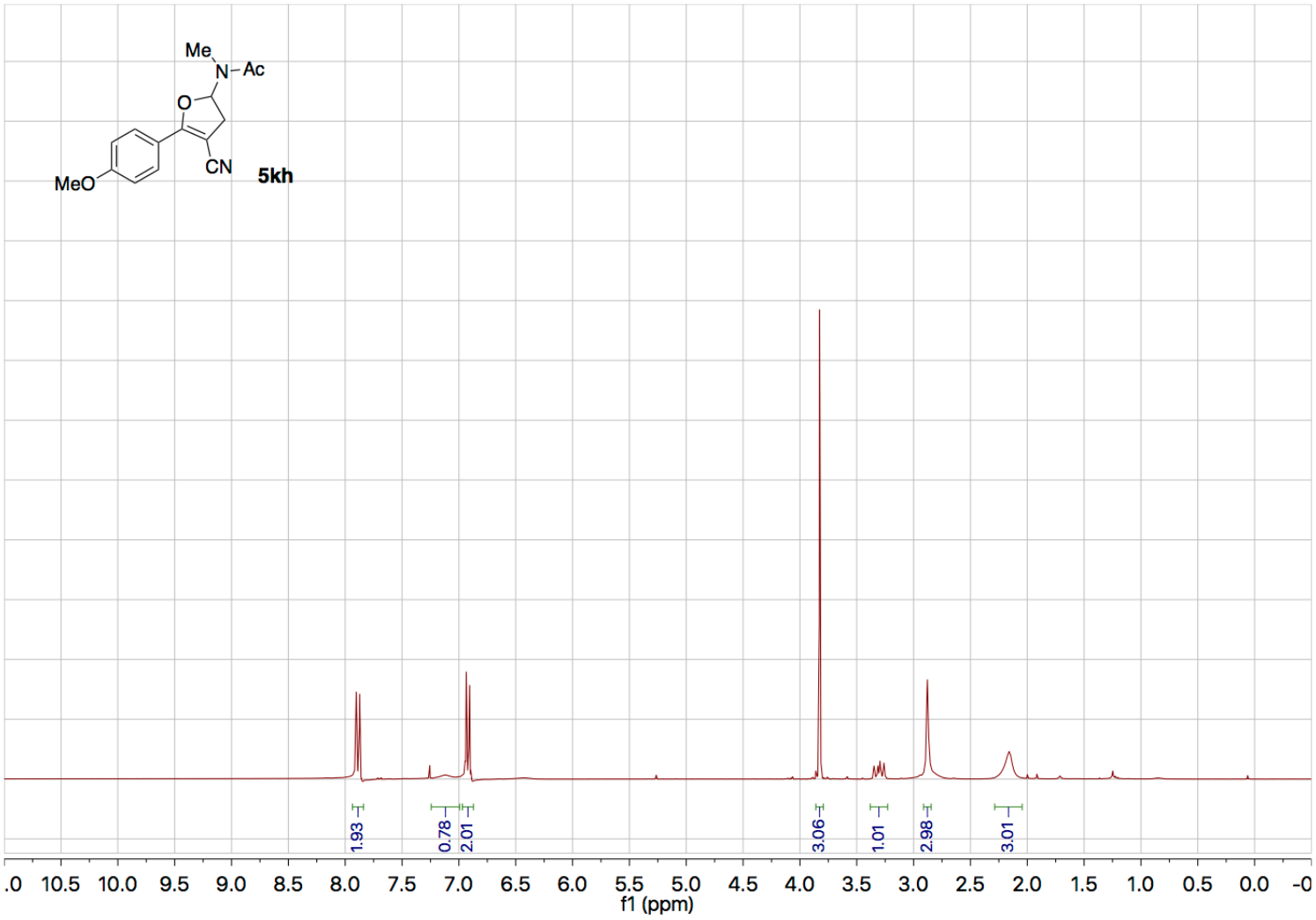
Me
N
Ac
O
CN
MeO
5kh
1.93
0.78
2.01
3.06
1.01
2.98
3.01
.0 10.5 10.0 9.5 9.0 8.5 8.0 7.5 7.0 6.5 6.0 5.5 5.0 4.5 4.0 3.5 3.0 2.5 2.0 1.5 1.0 0.5 0.0 -0
f1 (ppm)

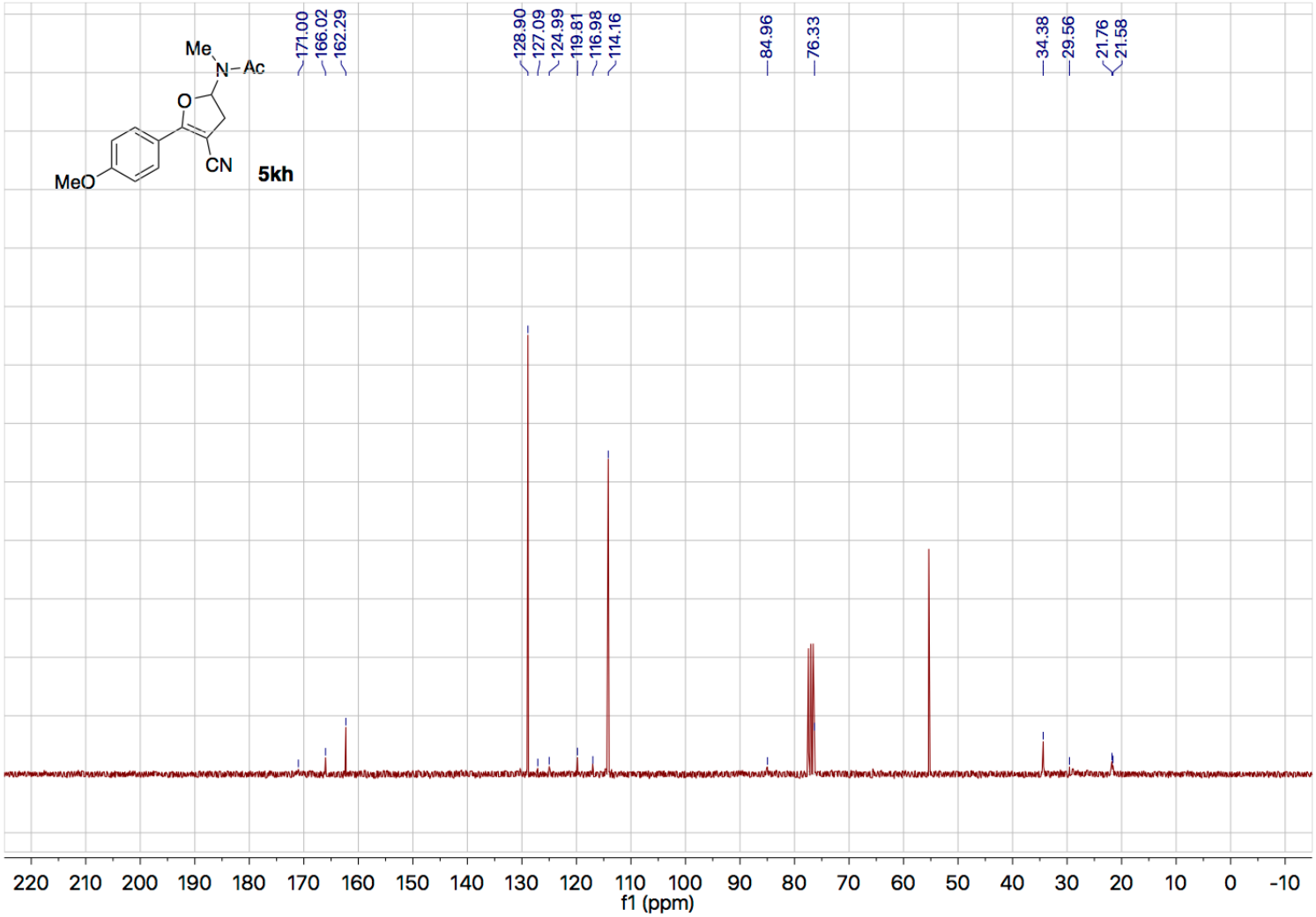
Me
N–Ac
O
CN
MeO
5kh
171.00
166.02
162.29
128.90
127.09
124.99
119.81
116.98
114.16
84.96
76.33
34.38
29.56
21.76
21.58
220 210 200 190 180 170 160 150 140 130 120 110 100 90 80 70 60 50 40 30 20 10 0 -10
f1 (ppm)

2.5 References

[1] a) Chansakaow, S.; Ishikawa, T.; Seki, H.; Sekine, K.; Okada, M.; Chaichantipyuth, C. *Journal of Natural Products* **2000**, *63*, 173; (b) Ishiuchi, K. i.; Kubota, T.; Mikami, Y.; Obara, Y.; Nakahata, N.; Kobayashi, J. i. *Bioorganic & Medicinal Chemistry* **2007**, *15*, 413; (c) Ikura, M.; Nakatani, S.; Yamamoto, S.; Habashita, H.; Sugiura, T.; Takahashi, K.; Ogawa, K.; Ohno, H.; Nakai, H.; Toda, M. *Bioorganic & Medicinal Chemistry* **2006**, *14*, 4241; (d) Takayama, H.; Fujiwara, R.; Kasai, Y.; Kitajima, M.; Aimi, N. *Organic Letters* **2003**, *5*, 2967; (e) Gaetan Pomey and Phannarath Phansavath. Synthesis **2015**, 47, 1016.

[2] Ankner, T.; Cosner, C. C.; Helquist, P. *Chemistry – A European Journal* **2013**, *19*, 1858.

[3] Chiba, T.; Okimoto, M.; Nagai, H.; Takata, Y. *The Journal of Organic Chemistry* **1979**, *44*, 3519.

[4] Elamparuthi, E.; Kim, B. G.; Yin, J.; Maurer, M.; Linker, T. *Tetrahedron* **2008**, *64*, 11925.

[5] Kim, Y. H.; Lee, D. H.; Yang, S. G. *Tetrahedron Letters* **1995**, *36*, 5027.

[6] H. Jiang, H; Huang, C.; Guo, J.; Zeng, C.; Zhang, Y.; Yu, S. *Chemistry – A European Journal* **2012**, *18*, 15158.

[7] (a) Alonso, M. E.; Fernandez, R.; *Tetrahedron* **1989**, *45*, 3313; (b) Alonso, M. E.; Del Carmen Garcia, M. *Journal of Organic Chemistry* **1985**, *50*, 988.

[8] (a) Zhao, W. J.; Yan, M.; Huang, D.; Ji, S.-J. *Tetrahedron* **2005**, *61*, 5585; (b) Yan, M.; Zhao, W.-J.; Huang, D.; Ji, S.-J. *Tetrahedron Lett*. **2004**, *45*, 6365.

[9] Mass and Muller also explored the Cu(OTf)-catalyzed reactions of diazoacetates with acyclic tertiary enaminones to form the corresponding cyclopropanes. Upon treatment of the cyclopropanes with silica gel, enaminoesters were isolated in up to 91% yield. Only three examples were shown. Mass, G.; Mueller, A.; Prakt, J. *Chemiker Zeitung* **1998**, *340*, 315.

[10] Anac and Sezer similarly explored the Cu(II)-catalyzed reactions of enaminones and diazocarbonyl compounds. β-Alkylated products were observed in two cases; both in less than 15% yield: a) Güngçr, F. S.; Anac, O.; Sezer, O. *Tetrahedron Letters*. **2007**, *48*, 4883; (b) Güngçr, F. S.; Hancioğlu, N.; Anac, O. *Helvetica Chimica Acta* **2013**, *96*, 488.

[11] (a) Patil, D. V.; Cavitt, M. A.; Grzybowski, P.; France, S. *Chemical Communications* **2011**, *47*, 10278; For other examples of our use of *N*-indolyl α-diazomalonamides, see: (b) Patil, D. V.; Cavitt, M. A.; France, S. *Heterocycles* **2012**, *84*, 1363; (c) Aponte-Guzmµn, J.; Shenje, R.; Huang, Y.; Woodham, W. H.; Saunders, S. R.; Mostaghimi, S. M.; Flack, K. R.; Pollet, P.; Eckert, C. A.; Liotta, C. L.; France, S. *Industrial and Engineering Chemistry Research* **2015**, *54*, 9550.

[12] (a) Müller, P.; Tohill, S. *Tetrahedron* **2000**, *56*, 1725; (b) Davies, H. M. L.; Ahmed, G.; Calvo, R. L.; Churchill, M. R.; Churchill, D. G. *Journal of Organic Chemistry*. **1998**, *63*, 2641.

[13] This result is not surprising given the proposed involvement of an enol intermediate (Figure 7). Thus, the use of chiral Rh catalysts is also not expected to afford asymmetric products.

[14] Crude ^{1}H NMR reveals a trace amount of **4ca**, however, purification proved unsuccessful. Many side reactions were observed that are likely due to Wolff-type rearrangements and/or unwanted interactions be- tween the carbene and either the Weinreb amide methyl group (C-H insertion to form β-lactam) or the oxygen of the methoxy group (ylide formation and further reactivity).

[15] (a) Phun, L. H.; Patil, D. V.; Cavitt, M. A.; France, S. *Organic Letters* **2011**, *13*, 1952; (b) Phun, L. H.; Patil, D. V.; Cavitt, M. A.; France, S. *Organic Letters* **2012**, *14*, 6379.

[16] No product was detected by crude 1H NMR spectroscopic analysis. The reaction gave an intractable complex mixture that was not further elucidated.

[17] All calculations were performed by using the Gaussian-09 package and the ωB97XD level of density functional theory in conjunction with the 6–311 + + G(d,p) basis sets for all atoms except Rh, for which we used Hay–Wadt pseudopotential and related LanL2DZ basis sets. Transition state calculations were verified to have one imaginary vibrational frequency. For more detail on the computational methods employed, see the Supporting Information from the original manuscript. For pertinent references, see: (a) Gaussian 09, Revision D.01, M. J. Frisch, G. W. Trucks, H. B. Schlegel, G. E. Scuseria, M. A. Robb, J. R. Cheeseman, G. Scalmani, V. Barone, B. Mennucci, G. A. Petersson, H. Nakatsuji, M. Caricato, X. Li, H. P. Hratchian, A. F. Izmaylov, J. Bloino, G. Zheng, J. L. Sonnenberg, M. Hada, M. Ehara, K. Toyota, R. Fukuda, J. Hasegawa, M. Ishida, T. Nakajima, Y. Honda,

O. Kitao, H. Nakai, T. Vreven, J. A. Montgomery, Jr., J. E. Peralta, F. Ogliaro, M. Bearpark, J. J. Heyd, E. Brothers, K. N. Kudin, V. N. Staroverov, R. Kobayashi, J. Normand, K. Raghavachari, A. Rendell, J.C. Burant, S.S. Iyengar, J. Tomasi, M. Cossi, N. Rega, J. M. Millam, M. Klene, J. E. Knox, J. B. Cross, V. Bakken, C. Adamo, J. Jaramillo, R. Gomperts, R. E. Stratmann, O. Yazyev, A. J. Austin, R. Cammi, C. Pomelli, J. W. Ochterski, R. L. Martin, K. Morokuma, V. G. Zakrzewski, G. A. Voth, P. Salvador, J. J. Dannenberg, S. Dapprich, A. D. Daniels, Ö. Farkas, J. B. Foresman, J. V. Ortiz, J. Cioslowski, and D. J. Fox, Gaussian, Inc., Wallingford CT, **2013**; (b) Chai, J.-D. ; Head-Gordon, M. *Physical Chemistry Chemical Physics* **2008**, *10*, 6615; (c) Wadt, W. R.; Hay, P. J. *Journal of Chemical Physics* **1985**, *82*, 284; (d) Hay, P. J.; Wadt, W. R. *Journal of Chemical Physics* **1985**, *82*, 270.

[18] Solvent effects were incorporated into the calculations by using the Polarizable Continuum Model implemented by integral equation formalism (IEF-PCM) with dichloromethane as the solvent. For details, see: (a) Tomasi, J.; Mennucci, B.; Cammi, R. *Chemical Reviews* **2005**, *105*, 2999 and references cited therein; (b) Tomasi, J.; Mennucci, B. Cances, E. *THEOCHEM* **1999**, *464*, 211; (c) Pascal-Ahuir, J.L.; Silla, E.; Tuñoń, I. *Journal of Computational Chemistry* **1994**, *15*, 1127.

[19] Hybridization index i_n at C_n is defined by equation 1, where θ_n is the average bond angle about C_n:

$$i_n = \frac{-1}{\cos(\theta_n)} \quad (1)$$

[20] For formative discussions on the use of the hybridization index as a metric for reaction coordinates, see: (a) Haddon, R. C.; Chow, S.-Y. *Pure and Applied Chemistry* **1999**, *71*, 289; (b) Haddon, R. C.; Chow, S.-Y. *Journal of the American Chemical Society* **1998**, *120*, 10494.

[21] It must be noted that if the predicted isomerization pathway invokes a seemingly high 33.8 kcal mol 1 span in Gibbs free energy, the observed isomerization takes place at 60 °C over 18–24 h, which is sufficient to overcome the barrier.

[22] For seminal reports, see: (a) Lund, E. A.; Kennedy, I. A.; Fallis, A. G. *Tetrahedron Letters* **1993**, *34*, 6841; (b) Wenkert, E.; Ananthanarayan, T. P.; Ferreira, V. F.; Hoffmann, M. G.; Kim, H. S. *Journal of Organic Chemistry* **1990**, *55*, 4975; (c) Alonso, M. E.; Morales, A.; Chitty, A. W. *Journal of Organic Chemistry.* **1982**, *47*, 3747; (d) Wenkert, E.; Alonso, M. E.; Buckwalter, B. L.; Chou, K. J. *Journal of the American Chemical Society* **1977**, *99*, 4778.

[23] For a recent review, see: A. P. Krapcho, *ARKIVOC* (Gainesville, FL, U.S.) **2007**, 54.

[24] Boev, V. I.; Moskalenko, A. I.; Belopukhov, S. L.; Przheval'skii, S. M. *Russian Journal of Organic Chemistry* **2015**, *51*, 1253.

[25] Aponte-Guzman, J.; Phun, L. H.; Cavitt, M. A.; Taylor, J. E.; Davy, J. C.; France, S. *Chemistry – A European Journal* **2016**, *22*, 10405.

CHAPTER 3. DESIGNING CARBENES

3.1 Introduction

3.1.1 Donor-Acceptor vs. Acceptor-Acceptor Carbenes

Diazo derived metal carbenes have been a cornucopia of synthetically useful reactivity. The reactivity of these species prominently features C–H and X–H bond activation, cyclopropanation, and a host of [3+2] cycloaddition chemistry.[1-6] Traditionally, metal carbene compounds have been subdivided between three categories: acceptor only (A), acceptor-acceptor (A-A), and donor-acceptor (D-A) (Figure 9).[7] To date, studies on D-A carbenes feature a panoply of selective C(sp^3)–H functionalization chemistry in which the donor group is credited with stabilizing the metal–carbene interaction.[8] On the other hand, whilst their functional diversity renders them a promising source of synthetic building blocks, A-A diazo compounds have found little application in the budding field of intermolecular selective C(sp^3)–H functionalization chemistry due to several challenges.

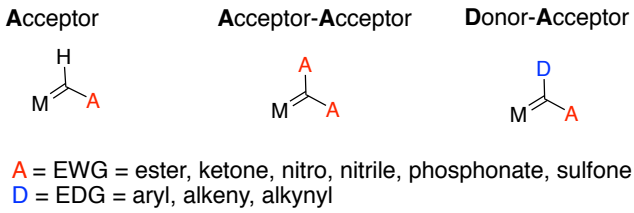

Figure 9 – The Three Traditional Classes of Metal Carbenes

3.1.1.1 Challenges with Studying Acceptor-Acceptor Carbenes

These challenges include, but are not limited to: (a) high energy barriers for A-A diazo decomposition, or nitrogen extrusion; (b) endergonic carbenoid formation upon the

reaction of transition metal complexes with A-A diazo compounds; (c) weak metal–carbene interactions; and (d) relatively small singlet-triplet energy splitting in the A-A carbenes.[9-13] These challenges often preclude the A-A carbenes from regio- and stereoselective addition to nucleophiles. Moreover, they make the A-A carbenes prone to side reactions (e.g., Wolff rearrangements, ylide formation and rearrangement, beta-lactam formation, dimerization, H-atom abstraction and radical polymerization, etc.) which create complex mixtures in reaction vessels preventing chemists from interpreting negative results.[10,14,15] For this reason, the majority of C-H functionalization reactions that feature acceptor-acceptor diazo compounds are performed intramolecularly.[16,17] Previous studies on their intramolecular C(sp^3)–H functionalization and cyclopropanation revealed that chemo- and regioselectivity of A-A carbene reactivity is highly sensitive to the identity of the acceptor groups.[16-19] However, understanding the roles of the steric bulkiness and nature of functional groups in the intramolecular reactions studied in the previous papers failed to offer generalizable rules for intermolecular systems.

3.1.2 Goals for this Study

By investigating the reactivity of acceptor-acceptor diazo compounds and their metal carbene complexes, we intend to develop generalized predictive rules for effective utilization of A-A carbenes in selective intermolecular C(sp^3)–H functionalization and cyclopropanation reactions. Previous intermolecular investigations have focused solely on carbenes derived from dimethyl diazomalonate and thus similarly lack comprehensiveness.[20,21] As such, little is known on the influence of the nature of the acceptor groups on A-A carbene C(sp^3)–H insertion in an intermolecular dirhodium catalyzed manifold.

3.1.3 Approach

Given the challenges regarding intermolecular synthetic investigations of A-A rhodium carbenes, we turned to density functional theory (DFT) studies where we could systematically probe acceptor group modifications and draw quantitative insights. To simplify the discussion and provide a reasonable starting point (with directly comparable parameters), the β-carbonyl ester class of A-A dirhodium carbenes will serve as the focus of this study. In a pioneering study, Nakamura et al. modeled, using DFT, the dirhodium tetraformate catalyzed C(sp^3)–H functionalization between alkanes and methyl diazoacetate or diazomethane (Scheme 23).[22]

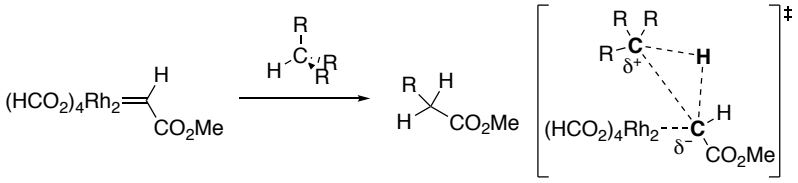

Scheme 23 – Transformation Previously Examined by Nakamura in 2002

This work demonstrated that, in a dirhodium carbene-mediated C-H insertion transition state, positive charge accumulates on the C-H bond donor while negative charge accumulates on the carbene unit. In this sense, C-H insertions are heuristically viewed as concerted hydride transfer and carbocation trapping processes. This view has been supported by experimental evidence showing that reaction rates are faster for benzylic and α-heteroatom C-H bond donors than for those containing only aliphatic C-H bonds.[23]

3.1.4 Hypothesis

Using Nakamura's study as a reference to guide our study, we hypothesized that the difference in C-H activation energies for various dirhodium carbenes of β-carbonyl esters could be explained by two factors. First, the ability of the carbonyl groups to stabilize negative charge accumulation at the carbene is anticipated to have a stabilizing effect on the C(sp^3)–H insertion transition state, thus, lowering the activation energy (Scheme 24). Second, allylic strain between the carbonyl substituent and the ester in the transition state would, in contrast, be a destabilizing interaction.

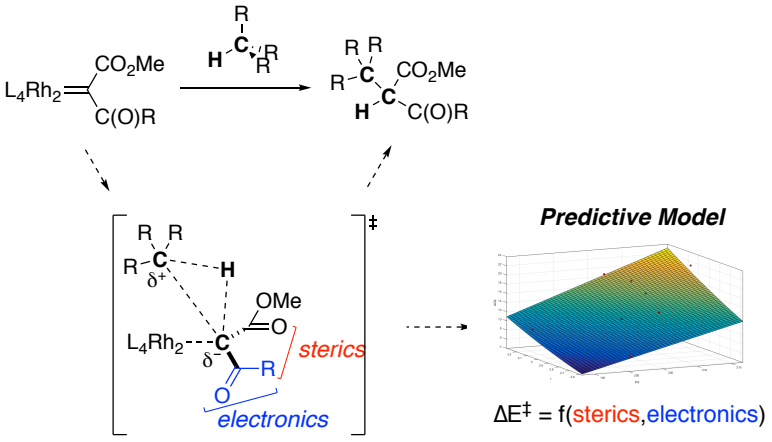

Scheme 24 – Hypothesizing a Predictive Model for Intermolecular C(sp^3)-H Insertion Activation Energies Generated from Steric and Electronic Parameters Obtained by a Broad DFT Investigation of A-A Carbenes

3.1.5 Summary

Herein, using DFT, we deconstruct the drivers of β-carbonyl ester carbene C(sp^3)–H activation energies into two orthogonal steric and electronic components. These components are directly related to the specific nature of the carbonyl substituent. Therefore, by changing the carbonyl substituent and examining effects on the stereoelectronic components, the reactivity of the dirhodium β-carbonyl ester carbene was

quantified. This acquired knowledge was then used to build a map of chemical space as a predictive model highlighting subcategories of this A-A carbene class in terms of their propensity for C(sp^3)–H insertion. Ultimately, this predictive model is validated through experimental evidence.

3.1.6 Computational Methods

Geometry optimizations and frequency calculations for all reported structures were performed at the M06L level of density functional theory in conjunction with 6-31G(d,p) basis sets for H, C, N, O, F and Cl atoms and Lanl2dz basis set and corresponding Hay-Wadt effective core potential for Rh.[24] Each reported minimum has zero imaginary frequencies and each transition state (TS) structure has only one imaginary frequency. Intrinsic reaction coordinate (IRC) calculations were performed for selected transition state structures to confirm their identity. Solvent effects are incorporated for all calculations using the self-consistent reaction field polarizable continuum model (IEF-PCM)[25] with dichloromethane as the solvent. The calculated Gibbs free energies are corrected to a solution standard state of 1M at room temperature (298.15K). To minimize redundant discussion, all energies discussed in this study will be in terms of enthalpy. Enthalpy values are generally more reliable than Gibbs free energies (which depends on concentration related parameters and more) and thus considered to be advantageous for establishing meaningful trends. Electronic energies (with and without zero-point-corrections), enthalpies, Gibbs free energies, and imaginary frequencies are provided in the Section 3.4.3.

3.2 Results and Discussion

3.2.1 An Instructive Model Study

As a suitable starting point for our investigation, we chose to model the metal carbene complex (**2g**) derived from α-diazo methyl acetoacetate (**1g**) and Rh_2esp_2 (Figure 10). We modeled the complex itself (Figure 10B) and compared it to the proposed transition state (**6g**) for C-H functionalization with propane (Figure 10C). Our initial calculations of **6g** demonstrate that positive charge accumulates on the carbon of the C-H bond donor while negative charge accumulates on the transferred carbene unit, C* (-0.1 for **2g** vs -0.45 for **6g**). Notably, second order perturbation analysis shows that, in a stabilizing fashion, the electron accumulation at the carbene center can be promoted by electron transfer from the adjacent carbonyls. This phenomenon is reflected in the shortening of the C*-C_α bond (1.469 vs 1.464 Å) and elongation of the C_α-O bond (1.228 vs 1.234 Å). In **6g**, the ester carbonyl assumed an anti-periplanar, or "down," conformation with respect to the incoming propane; meanwhile, the ketone carbonyl preferred a syn-periplanar, or "up," conformation. This orientation presumably allows for optimal dipole alignment as well as to eschew steric interactions between the ketone substituent and the propane due to increasing 1,2-allylic strain in the transition state.

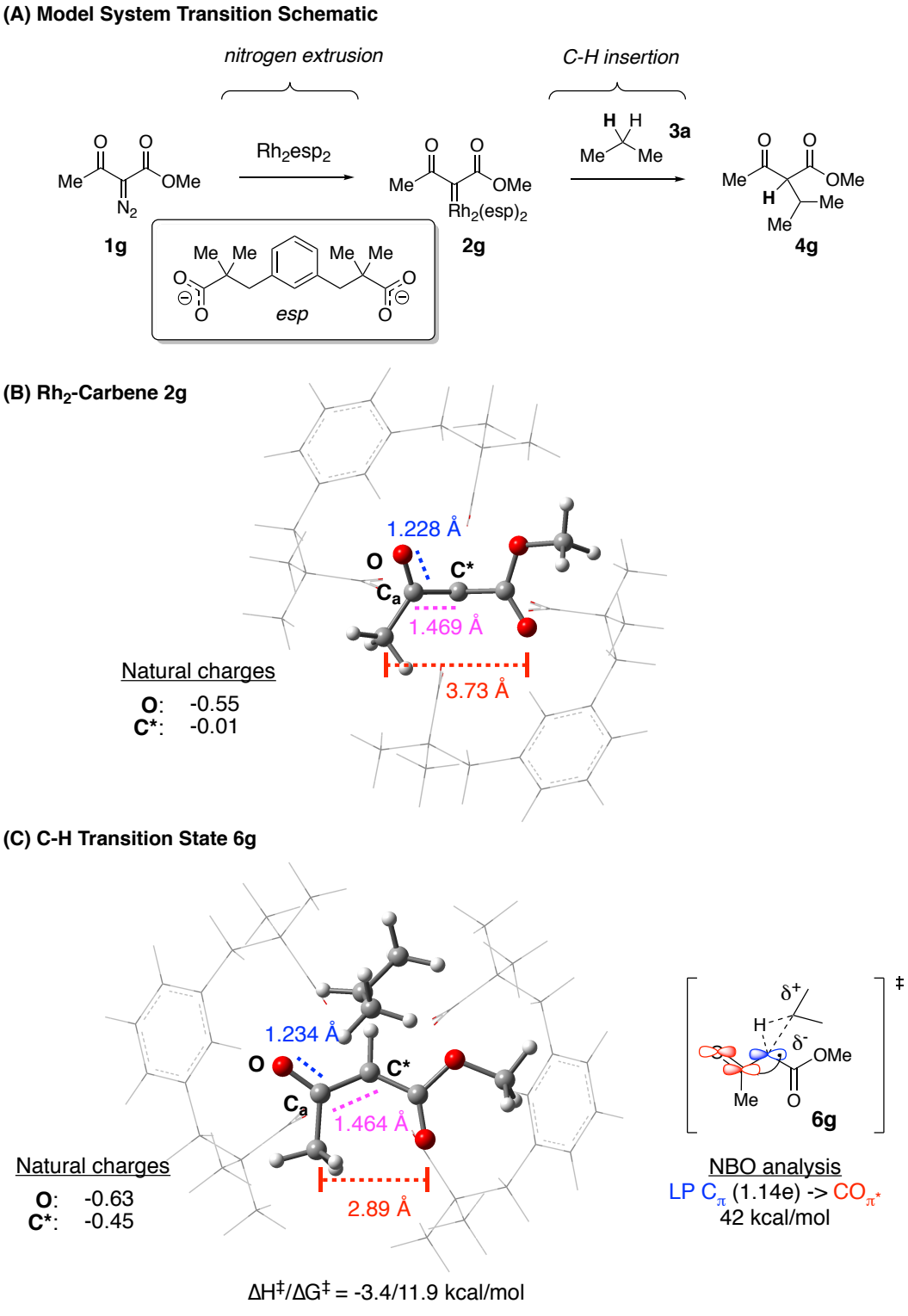

Figure 10 – The Model System

Intrigued by these results, we first hypothesized that the ability of the ketone substituent to modulate negative charge accumulation at the carbene would have a direct effect on the C(sp^3)–H bond insertion transition state and, consequently, the activation energy. We also hypothesized that the steric influence of the ketone substituent should similarly have a direct effect on the C(sp^3)-H bond insertion transition state by disrupting the preferred anti-periplanar orientation of the β-carbonyl ester carbene. To evaluate both hypotheses and any potential correlations, the electronic effects must be first be decoupled from any potential steric effects. Toward this end, we initially isolated electronic effects using Hammett substituent constants for *para*-substituted acetophenone-derived carbenes (Figure 11A) but, ultimately, settled on proton affinities as a general parameter for the electronics of carbonyl substituents. As the *p*-substituent is varied electronically, the steric differences remain negligible. Once the general electronic trends were understood, the relative steric influences were first quantified using well-established A-values for the carbonyl substituents.[26] This initial study led to the determination of new geometric parameters (**r** and **r'**) to generalize the steric effects across a range of carbonyl substituents (Figure 11B).

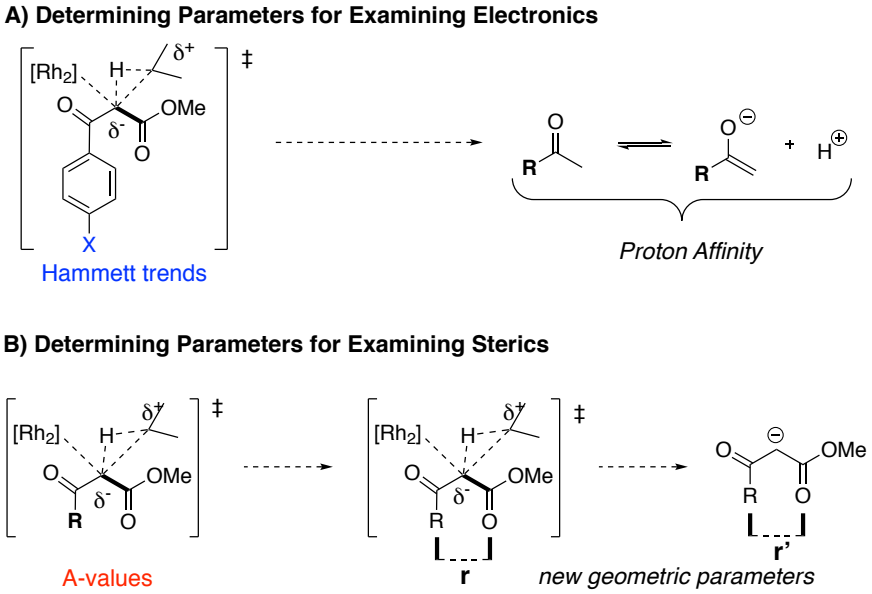

Figure 11 – Parameters for Examining C-H Insertion Transition States

3.2.2 Quantifying Electronic Effects

To understand and quantify electronic effects, steric differences were minimized by examining a series of β-ketoesters with *p*-substituted phenyl ketone groups (Figure 5). By modifying a position distal to the carbene, electronic effects become apparent as the steric effects are removed. Moreover, these *p*-substitued phenyl ketone substrates enable the use of the well-established Hammett coefficient, σ_p, to assess the effect of negative charge stabilization on the activation energy of the C-H insertion transition state.[27]

Table 5 – Para-Substituted Phenyl Ketone Series with Relevant Hammett Coefficients and Activation Enthalpies

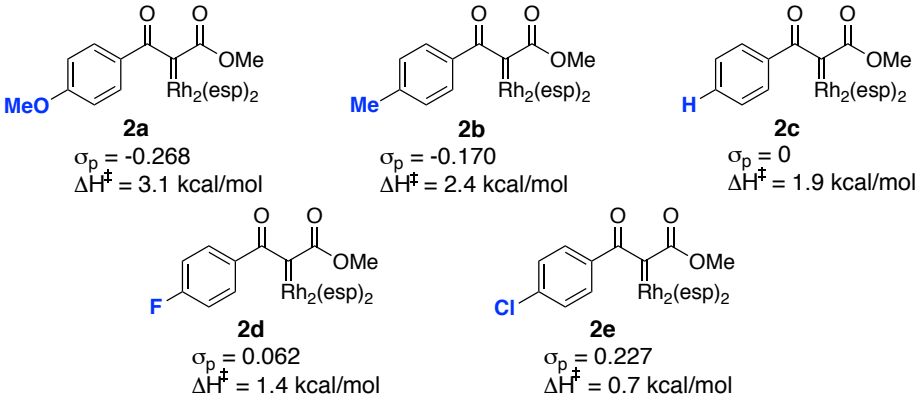

The calculations demonstrated a direct correlation between Hammett coefficient and activation energy for the series of *p*-substituted phenyl ketone substrates (Figure 6). For instance, with an activation energy of $\Delta H^{\ddagger}$ = 3.1 kcal/mol, the *p*-methoxyphenyl ketone **2a** is the least reactive carbene toward C(sp^3)–H bonds while, in contrast, the *p*-chlorophenyl ketone **2c** is significantly more reactive ($\Delta H^{\ddagger}$ = 0.5 kcal/mol). In general, as the phenyl ring becomes electron deficient, the C-H insertion activation energy decreases. Activation enthalpy ($\Delta H^{\ddagger}$) consistently drops 0.5 kcal/mol per 0.1 increase in σ_p for the range of compounds studied. Thus, the electronic nature of the carbonyl plays an important role in determining the barrier of C-H insertion.

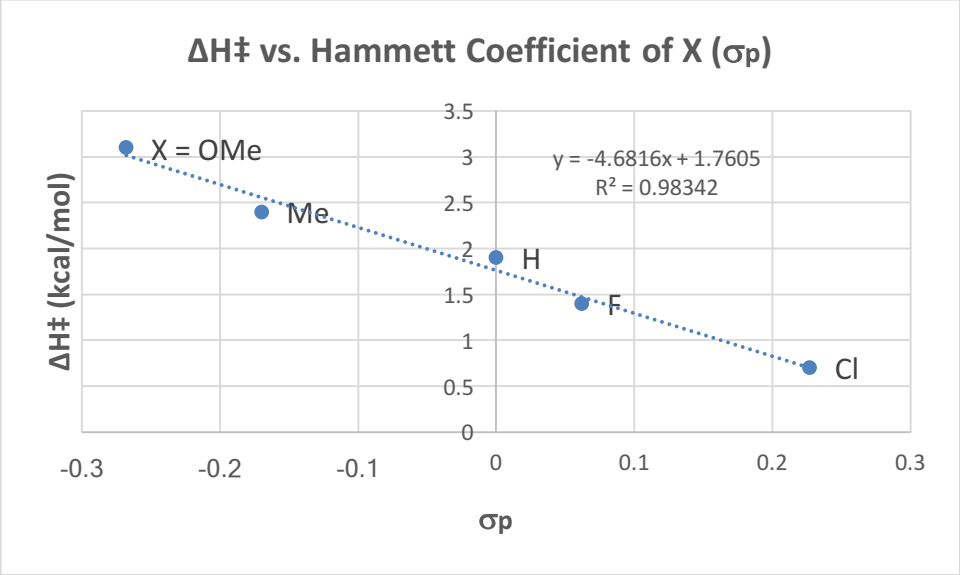

Figure 12 – Correlation Between Hammett Coefficients and C-H Insertion Activation Enthalpies

Since the Hammett coefficients only apply to substituted phenyl rings, other parameters had to be considered to quantify the general ability of a carbonyl substituent to stabilize negative charge accumulation on the carbene. A representative example is shown by comparing the dirhodium carbenes of the 4-chlorophenyl-containing β-ketoester **2e** and methyl acetoacetonate **2g**, the initial model system. Given that phenyl ketones are generally considered to be more electron poor than methyl ketones, one would expect the 4-chlorophenyl substrate **2e** to have a lower activation barrier to C-H insertion based on electronics. However, **2e** displayed a higher C-H insertion activation energy ($\Delta H^{\ddagger}/\Delta G^{\ddagger}$ = 0.5/13.5 kcal/mol) as compared to the methyl acetoacetate carbene complex **2g** ($\Delta H^{\ddagger}/\Delta G^{\ddagger}$ = -3.4/11.9 kcal/mol). This outcome can be explained by steric influences that seemingly raise the C-H insertion activation energy. Therefore, to address this issue, a more universal parameter was sought that could standardize the electronics across phenyl ketones as well as amides, esters, and alkyl ketones.

Given the buildup of negative charge on the carbene carbon of the β-carbonylester carbene complex in the C-H insertion transition state, one parameter that became very intriguing was proton affinity (PA, Table 6). PA is an intrinsic property and a well-established parameter for acetophenones and their corresponding enolates. When PA was plotted against Hammett coefficients for a series of *p*-substituted acetophenones, a strong correlation was observed (R^2=0.95). Thus, higher PA corresponds to the more electron-rich substrates (e.g., 4-methoxy and 4-methyl), while lower PAs represent the more electron-poor substrates. Given that PA is a readily determined parameter, we therefore hypothesized that PA would represent a more comprehensive measure of electronics than Hammett parameters. To validate this idea, PA was calculated for a variety of methyl-substituted carbonyls and used to construct a spectrum of electronic favorability of C(sp^3)–H insertion for the corresponding carbenes (Table 6). Based on R substituents, each methyl carbonyl was grouped by type – ketone, aldehyde, acid, ester, or amide – and further subdivided as needed.

Employing Nakamura's hydridic C-H insertion mechanistic framework, one would expect the more electron-poor carbene substrates to react faster. Thus, lower PAs would correspond to more electron-poor carbonyls with higher relative reactivity, while higher PAs represent more electron-rich carbonyls and less reactive substrates. Along these lines, acetaldehyde and the acetophenones were among the most electronically deficient carbonyl acceptor groups (PAs = 232.6–237.8 kcal/mol) while amides are among the most electron-rich (PAs = 238.3-250.2). Most of the simple alkyl ketones had PA ranges between 237.9 and 239.1, whereas higher PAs were observed for esters.

Table 6 – Electronic Spectrum of Carbene Carbonyl Groups

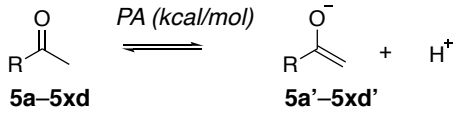

5a–5xd **5a'–5xd'**

Pheny ketones

R =

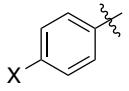

	5e (X = Cl)	232.6
	5d (X = F)	234.6
	5c (X = H)	234.9
*	5b (X = Me)	236.8
	5a (X = OMe)	**237.8**

Alkyl/vinyl ketones, aldehyde

5f (R = H)	234.0
5g (R = Me)	**239.1**
5h (R = Et)	**238.0**
5i (R = Np)	**237.9**
5j (R = iPr)	**238.1**
5k (R = Cy)	**238.1**
5l (R = tBu)	**237.9**
5m (R = Vinyl)	233.6

*Bold entries used to analyze sterics in Section 3.2.3

Esters, acid

5n (R = OH)	241.6
5o (R = OMe)	242.9
5p (R = OEt)	242.6
5q (R = OCH_2F)	234.4

Amides, acetamides

5r 248.5

5s 250.2

5t 246.8

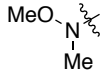

5u 242.8

5v 248.6

5w 250.3

5xa 242.1

5xd 238.3

Ar = 4-CF_3-Ph

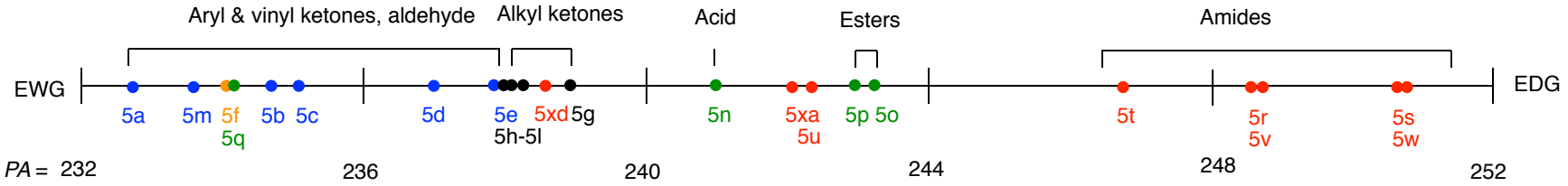

Representatives of each carbonyl type were selected to establish a heuristic hierarchy for interpreting β-carbonylester carbene electronics and C-H insertion favorability as a function of carbonyl substitution (Figure 13). For the selected molecules, the following trend was observed with decreasing PA: aldehyde (**5f**, 234.0 kcal/mol) < phenyl ketone (**5c**, 234.9 kcal/mol) < methyl ketone (**5g**, 239.1 kcal/mol) < methyl ester (**5o**, 242.9 kcal/mol) < dimethyl amide (**5r**, 248.5 kcal/mol).

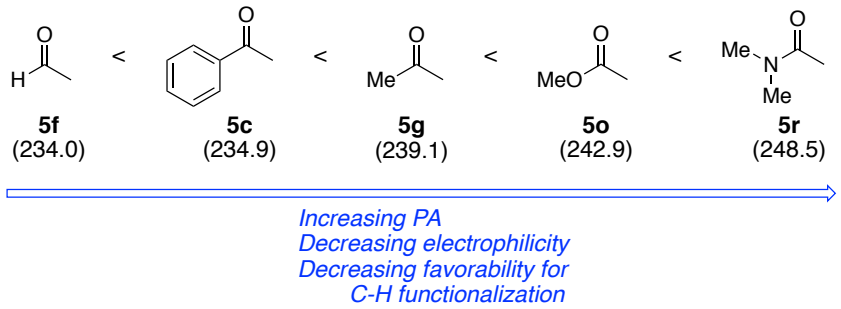

Figure 13 – Electronic Hierarchy for AA Carbenes as represented by Carbonyl Fragments

By no coincidence, this hierarchy matches that used to teach carbonyl electrophilicity to undergraduate chemistry students. Moreover, this hierarchy can be directly translated to C-H insertion transition state energy. For example, if sterics had no effect on C-H insertion transition state energy, aldehydes would be expected to have the lowest activation energies to C(sp^3)-H insertion and amides to have the highest. It should be noted that the true PA ranges of carbonyl types are broad, overlap significantly, and are limited only by one's ability to saturate the carbonyl substituent, R, with electron withdrawing/donating groups. For example, replacing a hydrogen with a fluorine on the methyl ester reduces PA by 8 kcal/mol, making it more reactive toward C-H insertion.

3.2.3 Quantifying Steric Effects

Steric effects have been widely studied and typically parameterized by A-values, which are derived from 1,3-diaxial interactions on cyclohexane rings.[26] Hypothesizing that the 1,5 R•••O steric interaction in the carbene complex was analogous to 1,3-diaxial strain, we examined the relationship between available literature A-values of alkyl groups and the C-H insertion activation energies of their associated β-carbonyl ester metal carbenes (Figure 14). To assess steric impact while eschewing convolution from electronic changes, a sterically diverse set of alkyl ketone carbene substrates with a narrow PA range (237.9 - 239.1 kcal/mol) was selected. To compare an aryl substituent with the alkyl ones while minimizing electronic influence, the 4-methoxyphenyl ketone carbene substrate **2a** (PA = 237.8 kcal/mol) was chosen. Given that literature A-values for individual 4-substituted phenyl groups are not readily available and are assumed to be sterically identical to the phenyl group, the phenyl A-value (3.0) was used instead.

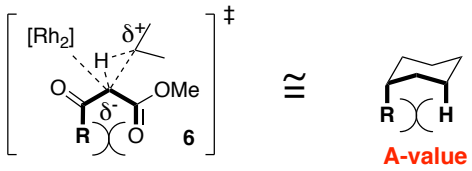

Figure 14 – Structural Similarity between 1,5-Sterics in The C-H Insertion Transition State and 1,3 Diaxial Interactions on Substituted Cyclohexanes

Table 7 displays a strong correlation between R group A-value and C-H activation energy for the series. Up to the 4-methoxyphenyl group (A = 3.0), C-H insertion activation enthalpies increased ~0.5 kcal/mol for every 0.1 increase in A-value of the R group. For example, comparing carbenes where R = neopentyl (Np) vs. methyl, the A-value difference (ΔA) was 0.3 while the difference in activation energies was 1.5 kcal/mol for $\Delta\Delta H^{\ddagger}$. Comparing the neopentyl group to the 4-OMe-phenyl group, a larger ΔA was observed

(1.0) along with a 5 kcal/mol difference in $\Delta\Delta H^{\ddagger}$. Attenuating this trend was the *t*-butyl group (A = 4.5). Despite having a higher A-value than the 4-OMe-phenyl group, the corresponding carbene is similarly reactive ($\Delta\Delta H^{\ddagger}$ = 0.5 kcal/mol). In this case, the relative destabilization of the C-H activation TS caused by the 1,5 R•••O repulsion is compensated by destabilizing interactions between the *t*-butyl group and the dirhodium catalyst in the carbene ground state.

Table 7 – Activation Enthalpies for a Series of Carbenes with Increasingly Bulky Ketone Acceptor Groups

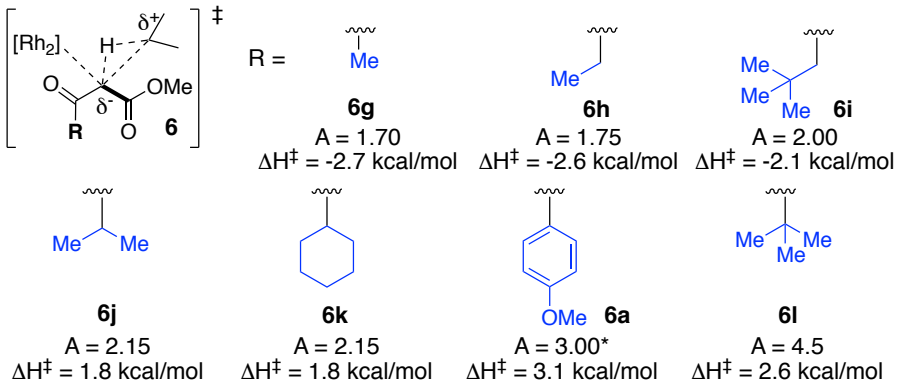

As was observed with Hammett coefficients in searching for generalizable electronic parameters, A-values are similarly limited given that not all R groups have reported values. To circumvent this issue, a new geometric parameter, **r**, was introduced, extracted from the transition state, and defined as the distance between the carbonyl substituent, R, and the ester carbonyl oxygen (Figure 15A). This parameter was highly correlated with the A-values from the set described above (Figure 15B) and thus envisioned as a proxy for assessing sterics in cases where A-values do not exist or conjugation between an R group and the carbonyl rigidifies the geometry rendering A-values inapplicable (e.g., an amide).

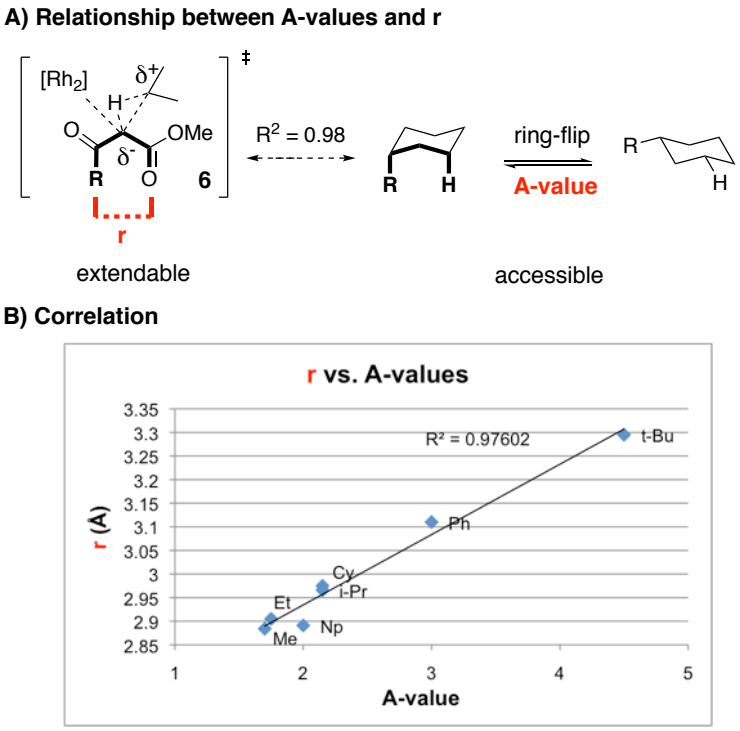

Figure 15 – The Steric Parameter, r

Using the same substrates as outlined in Table 6 for PA, **r** values were determined and grouped by type of carbonyl substituent. A steric hierarchy was then constructed to represent the severity of the 1,5 steric interactions in the C-H insertion transition state (Table 8). The hierarchy ranges from low sterics to high sterics. For instance, for the aliphatic ketones, the t-butyl ketone has the most 1,5-strain in the C-H insertion transition state with the largest **r** (3.25 Å), while the methyl ketone, with the lowest **r**, has the least. Comparatively, as expected, the aldehyde had even lower steric strain with **r** = 2.62 Å. Overall, the phenyl ketones had more steric strain when compared to the aliphatic ketones and their **r** values ranged between 3.02-3.13 Å. With the ability to rotate steric bulk away from the ester in the transition state, the aliphatic ketones are expected to lower strain that the phenyl groups, which prefer coplanarity with the carbonyl. The esters followed with **r** values between 2.79 and 2.85 Å. Steric bulk on the esters is distally located and thus has

little contribution to steric strain in the transition state. *tert*-Amides overlapped with this range with the dimethyl amide having an **r** value of 3.05 Å. Tethering the amide alkyl groups reduces the steric strain as evinced by the azetidine group (**r** = 2.96 Å), which had strain equal to the isopropyl ketone.

Table 8 – Steric Spectrum of Carbene Carbonyl Groups

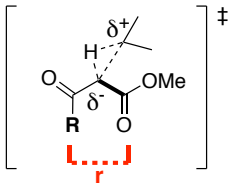

C-H insertion transition states **6a–6xd**

Pheny ketones

R =

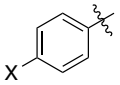

6e (X = Cl)	3.02
6d (X = F)	3.10
6c (X = H)	3.11
6b (X = Me)	3.13
6a (X = OMe)	3.08

Alkyl/vinyl ketones, aldehyde

6f (R = H)	2.62
6g (R = Me)	2.89
6h (R = Et)	2.90
6i (R = Np)	2.93
6j (R = iPr)	2.96
6k (R = Cy)	2.96
6l (R = tBu)	3.25
6m (R = Vinyl)	2.96

Esters, acid

6n (R = OH)	2.67
6o (R = OMe)	2.85
6p (R = OEt)	2.86
6q (R = OCH_2F)	2.79

Amides

R =

6r 3.05

6s 3.09

6t 2.96

6u 2.97

6v 2.78

6w 2.77

6xa 2.75

6xd 2.75

Ar = 4-CF_3-Ph

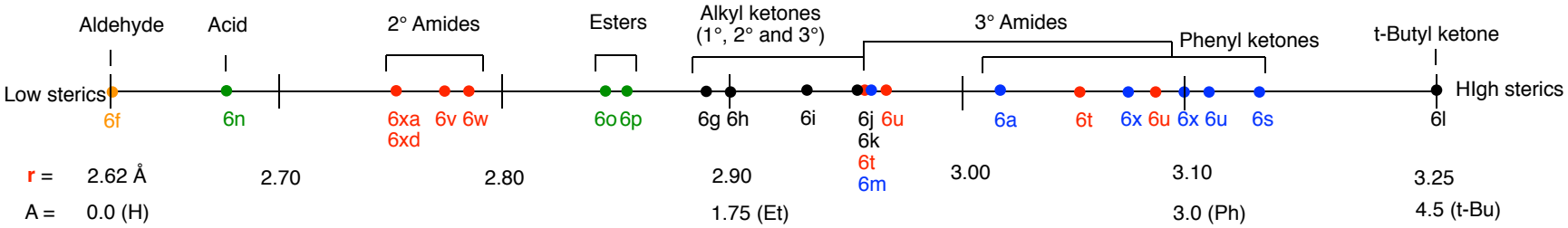

Interestingly, the **r** values (2.75-2.78 Å) for secondary acetamides were not only substantially lower (Δr = 0.2-0.3) than the tert-amides, but also similarly lower than the alkyl ketones. In one example, replacing a methyl group on **6r** with a hydrogen (as in **6w**) reduces **r** by 0.31 Å. This is due to the presence of a 1,6-hydrogen bonding interaction that pinches the transition state into a cyclic structure. Examining the carboxylic acid (**r** = 2.67 Å), which is capable of the 1,6-hydrogen bonding, a similar drop in **r** is also observed when compared to the corresponding esters (Δr = 0.1-0.2). Despite convoluting sterics and H-bonding in this instance, **r** succinctly captures both, predicting **6w** to be more reactive toward C-H insertion than **6r**. Indeed, the C-H insertion activation energy is 9.4 kcal/mol lower for **6w** despite both amides having similar PA (248.5 vs. 250.3).

3.2.4 Predictive Model

3.2.4.1 Mapping Chemical Space

Having successfully deconstructed the drivers of β-carbonyl ester carbene C(sp^3)-H activation into two orthogonal steric and electronic components, we next sought to draw a direct correlation between these components and activation energy. It is important to note that neither PA nor **r** can accurately predict the C-H insertion activation energy for a substrate. Instead, using both PA and **r** with DFT calculated C-H insertion activation energies, we fit an interpolating function to visually represent the change in C-H insertion activation energy as a function of sterics and electronics (Figure 16).

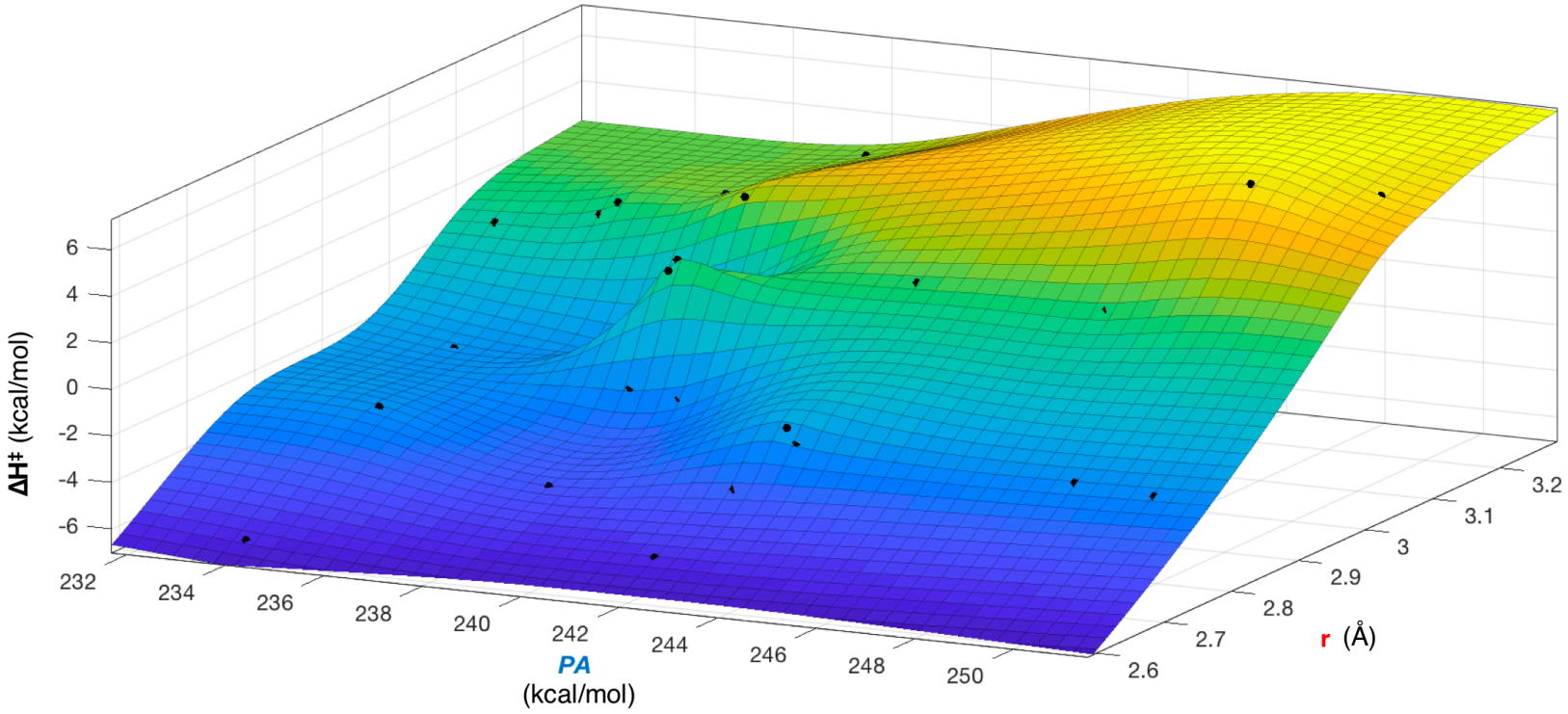

Figure 16 – Chemical Space 3D Plot

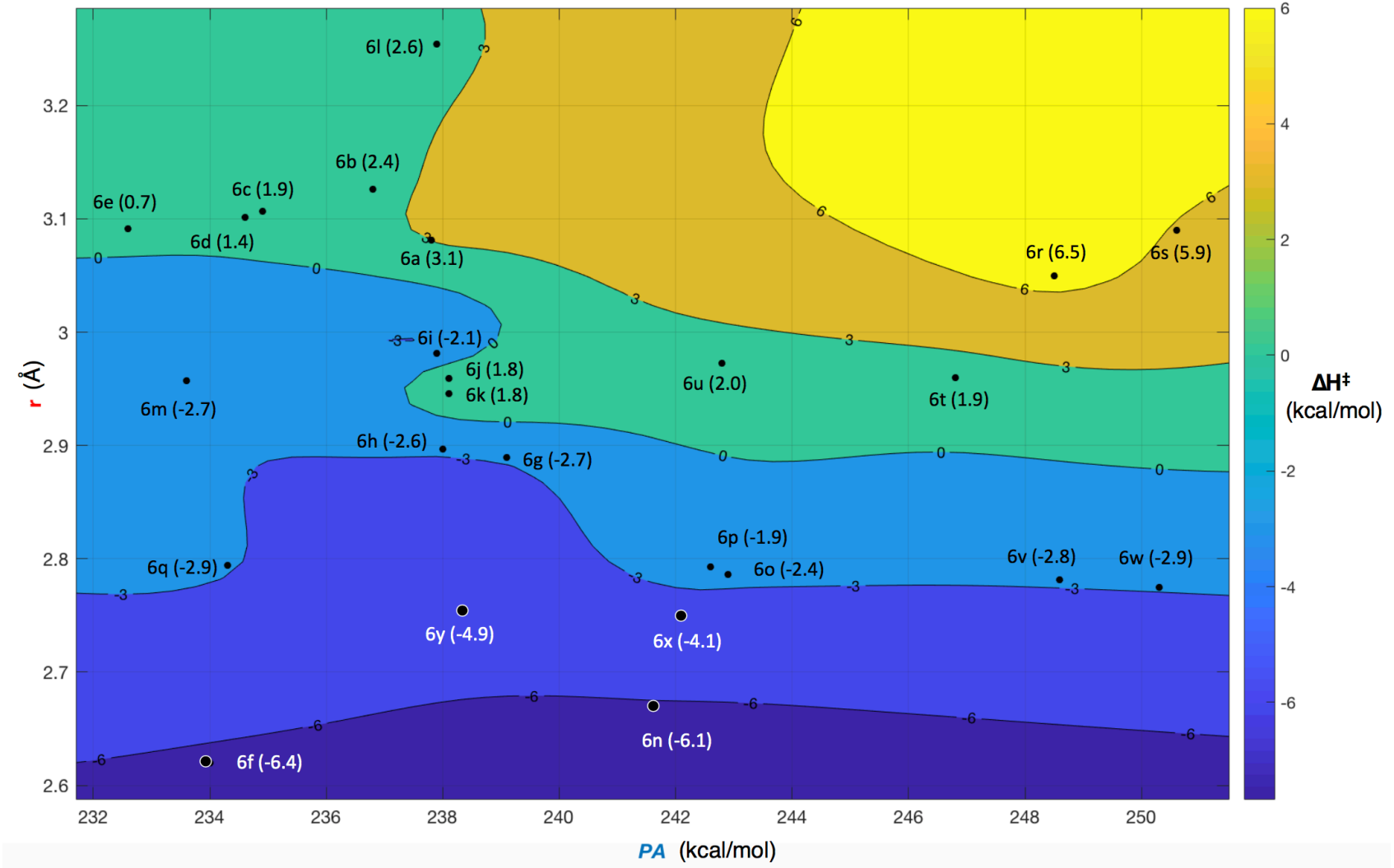

Figure 17 – Chemical Space Contour Plot

In terms of propensity for C-H insertion, favorable reactivity ($\Delta H<0$) is represented by the blue to violet color, while unfavorable reactivity ($\Delta H>0$) is represented by the yellow to green color. One apparent correlation from the map is the correlation between ΔH and **r** (steric component). As **r** gets shorter (less steric influence), the favorability for C-H insertion increases. In contrast, no general correlation between ΔH and PA can be observed across all the different substrate types.

Looking at a 2D representation of the map with each of the β-carbonyl ester substrates labeled (Figure 17), each carbonyl class is clustered as different places on the chemical map. For example, the aryl ketones (**6a-e**) are located in the upper left part of the map and have ΔH values > 0. The alkyl/vinyl ketones (**6f-m**) are spread across the left half of the map and have varied ΔH values which depend on **r**. Esters (**6o-q**) and carboxylic acid **6n** are located in the lower half of the map with ΔH values < 0. For the most part, the amides (**6r-y**) are clustered on the right half of the map and display varied ΔH values. Interestingly, the amides split into separate regions based on substitution with the tertiary amides (**6r-u**) in the upper right and the secondary ones (**6v-y**) in the bottom right.

From these observations, the existence of four major classes of carbenes becomes apparent. Each class is grouped together into specific locations on the surface, which allows the map to be divided into four sections or quadrants (Figure 18). *Quadrant 1* (**Q1**) represents the tertiary amides **6r-y**, the most electronically rich and sterically hindered carbenes, with $\Delta H^{\ddagger}_{C\text{-}H} > 0$. *Quadrant 2* (**Q2**) contains sterically hindered but electron poor carbenes such as phenyl ketones (**6a-e**) and alkyl ketones (**6i-l**) where the alkyl group is particularly bulky (e.g., R = neopentyl, *i*-Pr, Cy, *t*-Bu). Carbenes in **Q2** have $\Delta H^{\ddagger}_{C\text{-}H} > -1$ kcal/mol. *Quadrant 3* (**Q3**) contains electron poor and sterically unhindered carbenes such

as the aldehyde **6f** and simple alkyl ketones (**6g/h**, R= Me, Et). **Q3** has negative activation enthalpies (ΔH<0). *Quadrant 4* (**Q4**) houses esters **6o/p**, the secondary amides (**6v-x**), and carboxylic acid **6n**. These species have high PA due to lone pair donation into the carbonyl, but they have shorter **r** values due either to steric bulk being rotated away from the ester carbonyl oxygen in the transition state or the presence of 1,6-hydrogen bonding. By placing electron-withdrawing substituents on the ester (i.e., **6q**, where R = OCH_2F) or the secondary amide (i.e., **6y**, where R = 4-CF_3-Ph), the resulting carbenes, that would normally fall in **Q4**, are moved into **Q3**. This properly reflects the change to a more electron-poor system.

Q2 • **Aryl ketones, bulky alkyl ketones** • High sterics (longer **r**) • Low relative PA (less electron-rich carbonyl) • ΔH > -1 kcal/mol • Low C-H Functionalization Reactivity *r = 2.90 Å*	Q1 • ***tert*-Amides** • High sterics (longer **r**) • High relative PA (more electron-rich carbonyl) •ΔH > -1 kcal/mol • Low C-H Functionalization Reactivity
Q3 • **Small alkyl ketones, aldehyde, electron poor esters and 2° amides** • Low sterics (shorter **r**) • Low relative PA (less electron-rich carbonyl) • ΔH < -1 kcal/mol • High C-H Functionalization Reactivity	Q4 • **1° and 2° amides, esters, carboxylic acid** • Low sterics (shorter **r**) • High relative PA (More electron-rich carbonyl) • ΔH < -1 kcal/mol • High C-H Functionalization Reactivity

PA = 241 (kcal/mol)

Figure 18 – Quadrant Descriptions

3.2.4.2 Formulating a Predictive Model

This map of chemical space is envisioned to aid chemists by informing judgements concerning the process used to build molecules and to understand β-carbonyl ester dirhodium carbene reactivity. By knowing where a proposed carbene falls on the map (**Q1-Q4**), chemists can gauge the likely success of C-H insertion or recognize the potential for pitfalls and unexpected side reactions. For the chemical space map to have utility beyond rationalizing observable trends, it must become a predictive tool. For that transposition to occur, the ability to calculate PA and **r** must be straightforward so that a direct correlation with activation energy is accessible. While PA can be readily calculated using basic computational software, access to **r** values requires a great deal of computational resources to model the dirhodium carbene C-H insertion transition state. To address this limitation on potential broader use, another steric parameter, **r'**, was introduced (Figure 19).

Unlike **r**, the second parameter, **r'**, uses the R-O distance from the ground state hydridic carbene, or the anion of the corresponding β-carbonyl ester following C-H transfer. As shown for the *t*-butyl ketone, there is a similarity in space between A-value, **r**, and **r'**, with **r** and **r'** differing by ~0.04 Å (Figure 19).

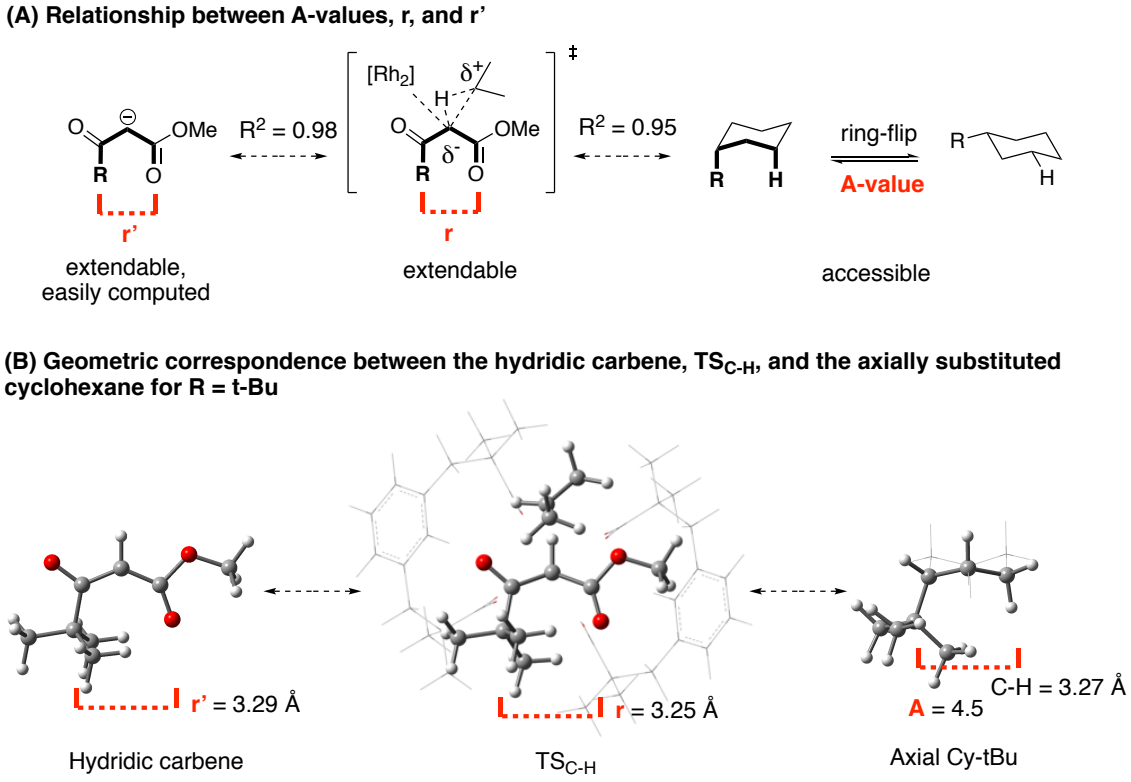

Figure 19 – Geometric Correspondence Between r', r, and A Parameter Origins

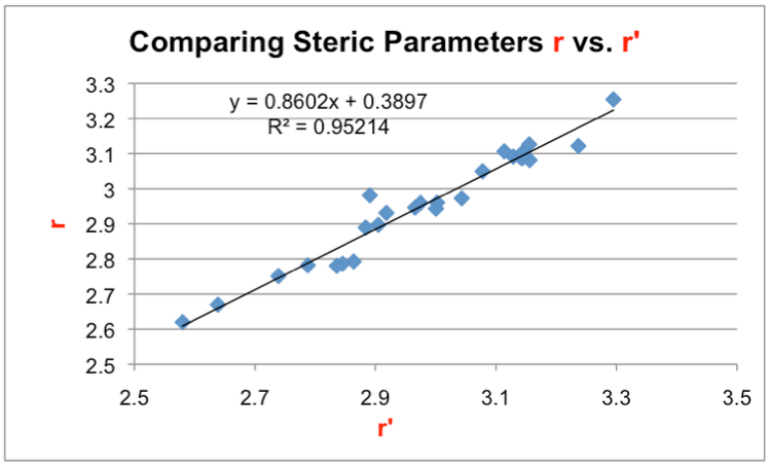

Figure 20 – Correlation between r and r'

Since **r** and **r'** are correlated (Figure 20), each can independently represent the steric impact of an R-group on the C-H insertion activation energy. Since the calculation for **r'** does not include the dirhodium catalyst or the complicated three-component transition state, minimal computational resources are necessary. This makes the model more broadly accessible. Interestingly, when **r'** is used in place of **r** in the generation of the map of chemical space, a slightly better correlation is obtained.

3.2.4.3 Testing the Model through Synthetic Experiments

To be a truly effective predictive model, the theoretical study must be consistent with experimental observations. For this reason, members of each class of β-carbonyl ester carbenes was selected to explore reactivity and to, ultimately, generalize carbene behavior. Experimentally, dirhodium carbenes were accessed from the corresponding α-diazo-β-carbonyl esters. Each diazo compound was then reacted with Rh_2esp_2 in neat, refluxing cyclohexane (Scheme 25). The reactions were quenched with methanol to trap any ketene intermediates resulting from Wolff rearrangements.

The aryl α-diazo-β-ketoesters were explored first. Interestingly, these substrates gave high conversions of diazo starting materials and the only products formed were either from C-H insertion or Wolff rearrangement. As suggested by the previous exploration of carbene electronics, the carbenes should become more selective for C-H insertion vs. Wolff rearrangement as the phenyl rings become more electron deficient. This trend plays out experimentally as the electron rich 4-MeO-phenyl substituted diazo **1a** reacted poorly and no C-H insertion product was detected. Instead, the Wolff product **9a** was isolated in 96% yield. Similarly, the tolyl ketone **1b** gave 21% yield of C-H insertion product **8b** and 71%

yield of Wolff rearrangement product **9b**. Phenyl ketone **1c** gave 34% of C-H insertion while 4-fluorophenyl ketone **1d** gave 49% C-H insertion. Notably, 4-chlorophenyl ketone **1e** afforded 63% yield of C-H insertion product **8e**.

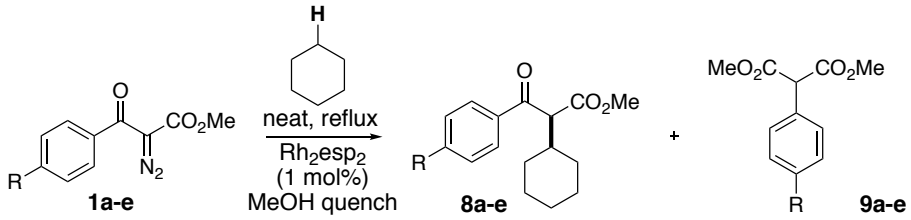

		% isolated yields		
R =	OMe (**a**):	0	:	96
	Me (**b**):	21	:	71
	H (**c**):	34	:	60
	F (**d**):	49	:	47
	Cl (**e**):	62	:	32

Scheme 25 – Electronically Tuning C-H Insertion vs. Wolff Rearrangement Reactivity

Next, the other carbonyl classes were evaluated (Scheme 26). In contrast to the clean reactions of the aryl ketones, the reactions with other carbonyl classes did not give appreciable amounts of Wolff rearrangement products and other degradation pathways are evident. In the case of the alkyl ketones, the results observed are consistent with the computational investigation of steric effects (Section 3.2). While methyl ketone **1g** reacted favorably to form C-H insertion product **8g** in 75% yield, no C-H insertion product was obtained with *t*-butyl ketone **1l**. Instead, cyclobutyl ketone **10l** was isolated as the major product resulting from intramolecular C-H insertion into one of the *t*-buyl methyl C-H bonds. A tipping point occurred between **1h** and **1j**. While the reaction tolerated the ethyl group (as in **1h**) to form **8h** in 34% yield, only trace amounts of **8j** (from isopropyl ketone **1j**) could be detected by NMR analysis of the crude reaction material. These results are fully consistent with our predictive quadrant model. Ketones **1j** and **1l** are both in Quadrant

2 (**Q2**) and were expected to have poor C-H insertion reactivity due to sterics, whereas ketones **1g** and **1h** are in Quadrant 3 (**Q3**) and were expected to have more favorable C-H insertion activity.

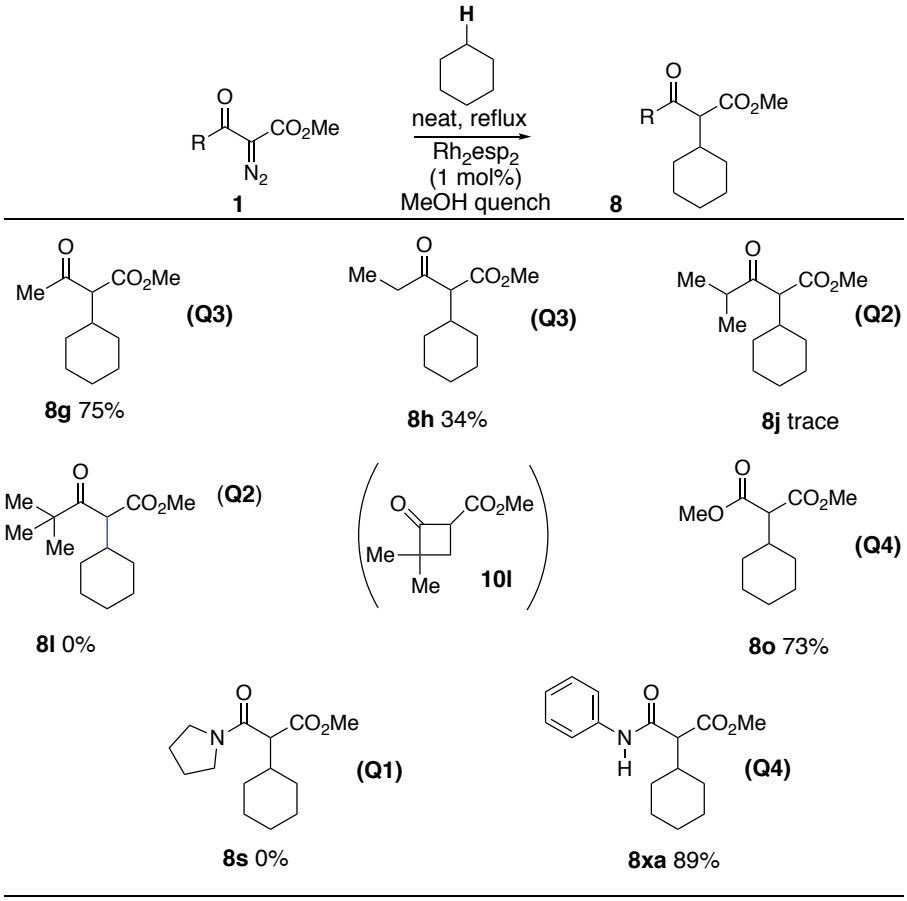

[a]Starting material was completely consumed; no desired product was observed.

Scheme 26 – Evaluation of Various Dicarbonyl-Based Carbenes for C-H Insertion Reactivity with Cyclohexane

Dimethyl diazomalonate **1o** is the most commonly studied β-carbonyl ester carbene precursor and its reactivity for intermolecular C-H functionalization has been established in the literature.[20] Consistent with the literature and for our own benchmarking purposes, **1o** formed C-H insertion product **8o** in 73% yield.

One tertiary and one secondary amide were subjected to the model reaction conditions. Unsurprisingly, the sterically-encumbered pyrrolidinyl amide **1s** yielded no C-H insertion product, which is expected for a **Q1** substrate. On the other hand, *N*-phenyl amide **1xa** (a **Q3** substrate), predicted to have a low barrier to C-H insertion due to 1,6-hydrogen-bonding in the transition state, furnished C-H insertion product in 89% yield. Without the theoretical model, the N-H bond-containing substrate would have been an unlikely candidate to be tested for intermolecular C-H insertion reactivity.

Combining the theoretical chemical map with the experimental results, the following generalizations can be established. (1) For the **aryl ketones**, selectivity for C-H insertion vs. Wolff rearrangement can be modified by tuning the electronics of the aryl ring. For instance, electron deficient rings favor C-H insertion. (2) For the **alkyl ketones**, linear alkyl groups tolerate intermolecular C-H insertion, whereas branched or other sterically-hindered alkyl groups do not. (3) Simple **esters** are both sterically and electronically amenable to intermolecular C-H insertion. (4) The steric bulk of the **tertiary amides** render them poor performers in intermolecular C-H insertion. This disadvantage is exacerbated by the availability of intramolecular β-lactam formation pathways. (5) **Secondary amides**, in contrast, have the highest selectivity for C-H insertion among the substrates studied. Their propensity is rationalized by a stabilizing H-bonding interaction in the C-H insertion transition state.

3.2.5 Revisiting H-Bonding Carbenes

Intrigued by the favorable C-H insertion reactions of the secondary amides, we sought to fully understand the unique nature of these carbenes. In Section 3.2.3, we

suggested that 1,6-hydrogen bonding interactions served as the key sterics-reducing factor that enabled C-H insertion reactivity to occur. To analyze the impact of these proposed 1,6-hydrogen bonding interactions, DFT was again employed to probe the system. As a starting point for establishing the influence of H-bonding, the tertiary N,N-dimethyl amide **2r** was directly compared to the secondary N-methyl amide **2w** (Figure 21). In the transition state, the tertiary amide **6r** has a long **r** (3.08 Å) and poor C-H insertion reactivity ($\Delta H^{\ddagger}$ = 6.5 kcal/mol) whereas the secondary amide **6w** has a short **r** (2.77 Å) and good C-H insertion reactivity ($\Delta H^{\ddagger}$ = -2.9 kcal/mol). For **6w**, the 1,6-hydrogen bond can be observed and confirmed by the 1.99 Å bond distance between the ester oxygen and the amide hydrogen.

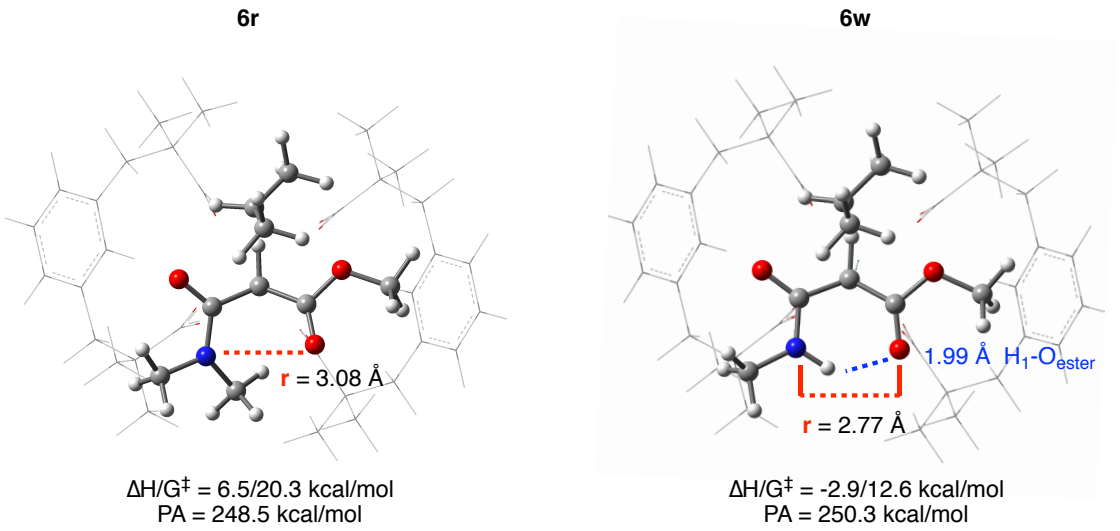

Figure 21 – Comparison of C-H Insertion Transition States of a Tert-Amide Carbene with an H-Bonding Secondary Amide

Interestingly, a second hydrogen bonding interaction is also evident between the amide hydrogen and the catalyst ligand in the metal carbene ground state. This interaction distorts the carbonyl into the plane of the Rh–carbene bond; the most pronounced example is **2x** shown in Figure 22.

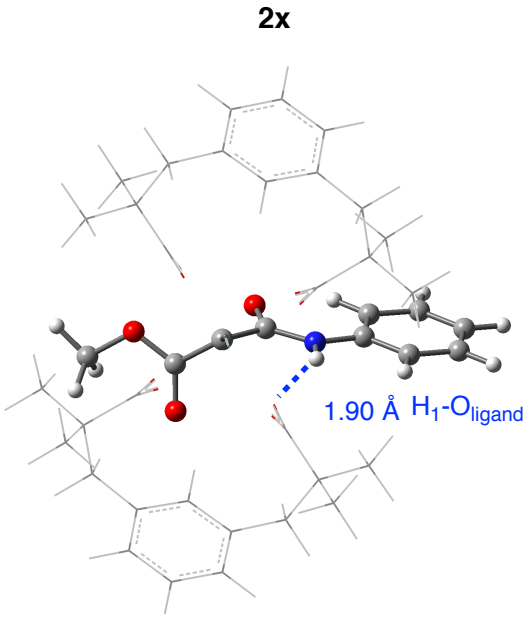

Figure 22 – H-Bonding Between a 2° Amide Carbene and the Catalyst Ligand

3.2.5.1 Carboxylic Acids

In hopes of utilizing these H-bonding interactions for selective metal carbene mediated transformations, we have begun to explore similar hydrogen bonding substrates beyond just secondary amides. As an initial foray into that realm, we chose the carboxylic acid carbene **2n** as the model system. Using DFT with this system, hydrogen bonding effects could be isolated by comparing *E* and *Z* conformers of the acid moiety (Figure 23, Figure 24). First, we calculated the free (not bound to the metal) singlet carbene energy difference between the acid's *E* and *Z* conformers (**FC-*Z*** and **FC-*E***). This energy difference (ΔH = 1.0 kcal/mol) indicates a conformational preference for the Z-conformer in the absence of an H-bonding environment. This value was then compared to the differences in energy of the conformers of the metal-bound carbene ground states (**2n-*Z*** and **2n-*E***) as well as the C-H insertion transition states (**6n-*Z*** and **6n-*E***). In the ground

state metal-bound carbene of the E isomer (**2n-*E***), intramolecular H-bonding was observed between carboxylic acid hydrogen and an oxygen atom on the dirhodium catalyst. No such stabilizing interaction was observed with the *Z* isomer. In the C-H insertion transition state (**6n-*E***), only the *E* isomer engaged in intramolecular 1,6-H-bonding (H-O_{ester} = 1.79 Å). Thus, despite an energetic preference for the *Z* conformer in the free singlet carbene where no H-bonding was available for either conformer, the *E* conformer was preferred by 2.6 kcal/mol and 5.6 kcal/mol in both the metal-bound carbene and C-H insertion transition state, respectively.

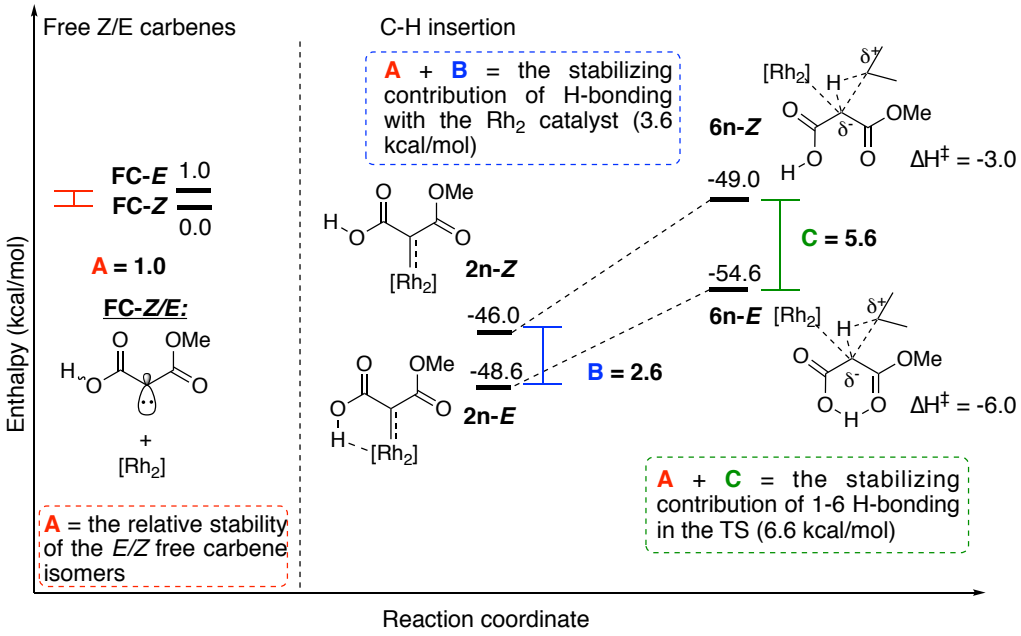

Figure 23 – Partial Reaction Coordinate for E and Z Carboxylic Acid Carbene Conformers Undergoing C-H insertion with Propane

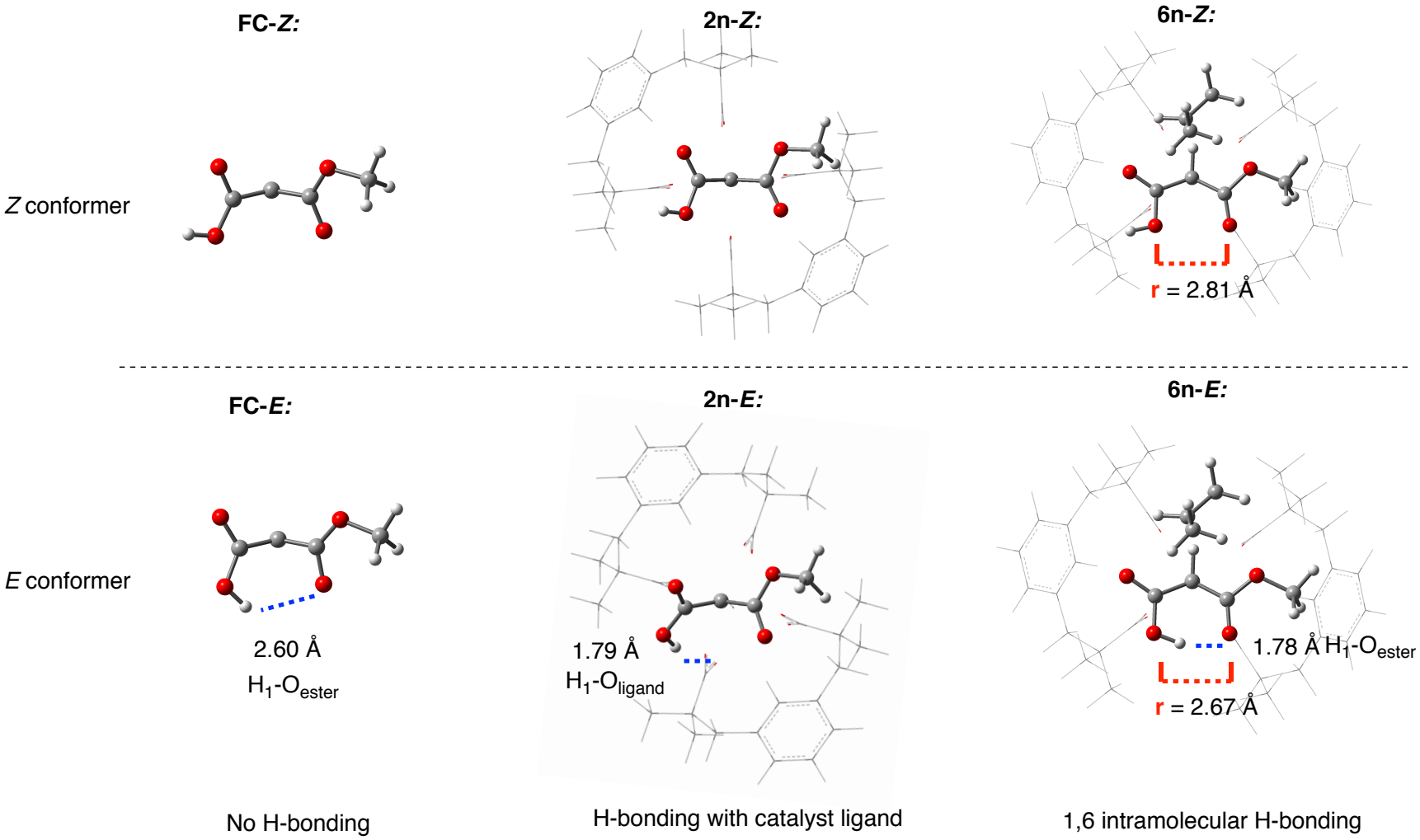

Figure 24 – Structures and Labels for the Carboxylic Acid Conformers

To quantify the impact of hydrogen-bonding in the metal carbene and transition state we added to each energetic difference (B and C), the energy difference inherent to E/Z stability absent H-bonding (A). Following this process, hydrogen bonding to the catalyst stabilizes **2n-*E*** by 3.6 kcal/mol. Meanwhile, 1,6-hydrogen bonding in the transition state reduces the activation enthalpy by 6.6 kcal/mol. This indicates that the hydrogen bonding interaction has surprisingly strong stabilizing influence on the C-H activation transition state – approximately the same effect as substituting a *t*-Bu group for a Me group. The computations suggest carbenes with the capacity for 1,6-hydrogen bonding, such as acids, primary, and secondary amides, to be relatively reactive toward C-H bonds as compared to the other β-carbonyl ester carbenes. Albeit, the synthetic utility may be compromised by deleterious intermolecular carbene insertion into heteroatom-H bond.

To probe this proposal experimentally, we attempted to synthesize the α-diazo-carboxylic acid **1n** (Scheme 27). Unfortunately, while saponification of dimethyl diazomalonate appeared to furnish the **1n**, we were unable to isolate pure material from unreacted dimethyl diazomalonate or doubly-saponified product. Using a reductive approach[28] from the benzylated diazoacetate **1z** was similarly unsuccessful due to over-reduction to the hydrazone **11**.

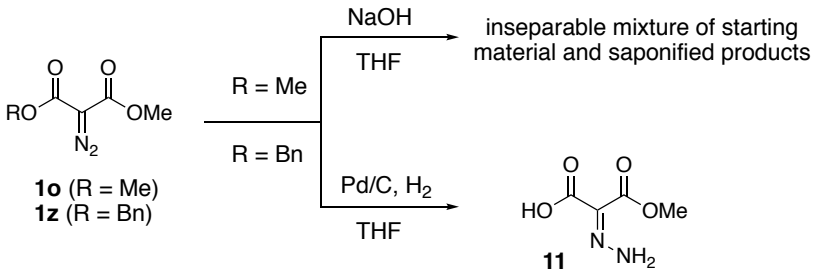

Scheme 27 – Unsuccessful Synthetic Approaches toward the Carboxylic Acid Diazo Compound

3.2.5.2 Secondary Amides

In the literature, carbenes derived from secondary α-diazo-β-amide esters have been shown to readily undergo X-H insertions. Surprisingly, examples of their utility for cyclopropanations (the standard carbene trapping reaction) and their capacity to perform C-H insertion reactions is extremely rare. Toward this end, we sought to probe the general reactivity potential of secondary α-diazo-β-amide esters. As a first step, we explored simple cyclopropanation with styrene. When alpha-diazoamide **1xa** was reacted with styrene (2 equiv) in the presence of catalytic Rh_2esp_2, cyclopropane **12** was cleanly furnished in 78% yield as a 3:1 mixture of diastereomers (Scheme 28).

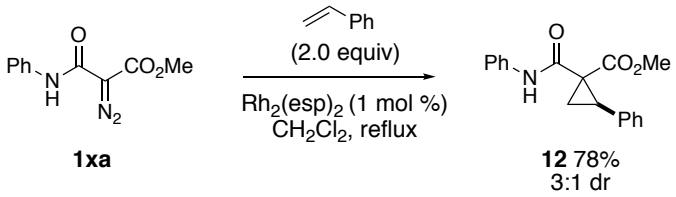

Scheme 28 – Cyclopropanation of the 2° Amide Diazo Compound with Styrene

Having established that α-diazoamide **1xa** cleanly provides the desired C-H insertion product in 89% yield when cyclohexane is used as the solvent, we sought to

explore the impact of having fewer equivalents of the alkane. When the five equivalents of cyclohexane are employed, the yield dramatically drops to 42% yield (Scheme 29). In hopes of improving the C-H insertion reaction, we looked to the predictive chemical space map as a starting point for optimization. For a series of N-aryl-substituted secondary α-diazo-β-amide esters **1xa-1xg**, PA and **r'** values were calculated (Table 9). Across the compounds, PAs varied between 238 and 244 kcal/mol while **r'** values remained fairly consistent (Δ**r'** < 0.03 Å).

Table 9 – Predicted Quadrants for Various 2° Amide Diazoacetates

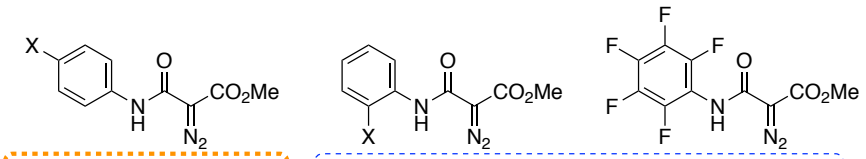

1xb: X = OMe — Q4
r' = 2.75 Å
PA = 244.0 kcal/mol
1xa: X = H
r' = 2.74 Å
PA = 241.1 kcal/mol

1xc: X = Cl — Q3
r' = 2.74 Å
PA = 240.0 kcal/mol
1xd: X = CF_3
r' = 2.74 Å
PA = 238.3 kcal/mol

1xe: X = Cl
r' = 2.75 Å
PA = 239.2 kcal/mol
1xf: X = CF_3
r' = 2.75 Å
PA = 238.1 kcal/mol

1xg
r' = 2.72 Å
PA = 238.0 kcal/mol

Q3

Each of the diazoamide compounds was subjected to the reaction conditions with 5 equivalents of cyclohexane (Scheme 29). The *p*-methoxyphenyl substrate **1xb** offered a lower yield (**8xb** 24%) than the parent phenyl compound. This result is consistent with the need for a more electron-poor carbene for better C-H insertion reactivity. In contrast, the *N*-(4-Cl-phenyl) and *N*-(4-CF_3-phenyl) substrates (**1xc** and **1xd**) gave their respective insertion products **8xc** and **8xd** in 55% and 63% yield. Higher yields were observed with

the *N*-(2-Cl-phenyl) and *N*-(2-CF_3-phenyl) substrates (**1xe** and **1xf**), respectively. Finally, with the lowest PA, the *N*-perfluoro-phenyl amide **1xg** was expected to have the lowest activation energy for sp^3 C-H insertion. Indeed, **1xg** afforded **8xg** in 82% yield. Considering the recent advancements in amide-based directing group C-H functionalization chemistry,[29] this series of results are highly auspicious and offer tremendous opportunity for orthogonal and/or tandem reactions.

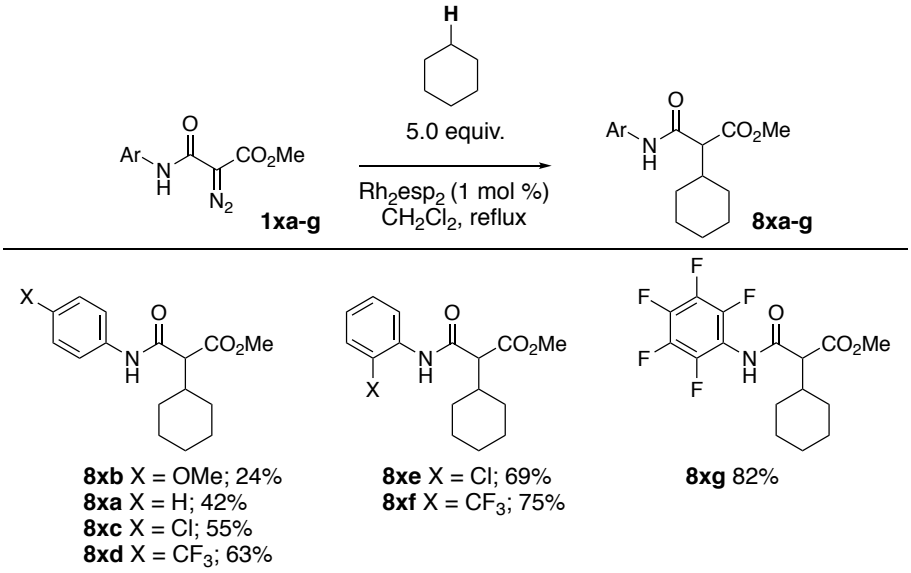

Scheme 29 – Performance of Each 2° Amide Diazoacetate Using Reduced Equivalents of Cyclohexane

To highlight the future potential of the reaction, we employed a chiral dirhodium catalyst complex in hopes of observing enantioselectivity (Scheme 30). When the C-H insertion reaction described above was performed with diazoamide **1xa** and cyclohexane in the presence of Rh_2(*S*-PTAD)$_4$ (1 mol %), the C-H alkylation product **8xa** was obtained in 26% ee (2:1 *er*), albeit with a lower yield (25%).

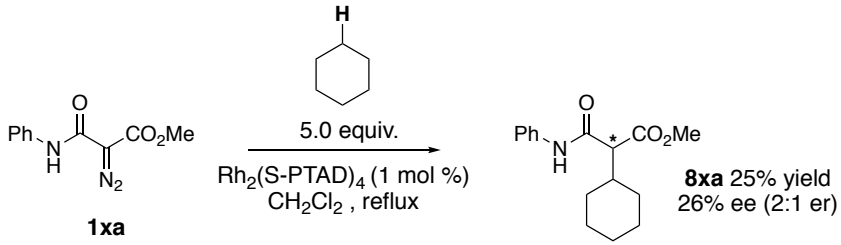

Scheme 30 – Enantioselective C-H Insertion Using a 2° Amide Diazoacetate

While modest, the enantiomeric excess represents a promising starting point for optimization and catalyst screening. Furthermore, in the reaction of diazo compound **1xf** with *n*-pentane, excellent site selectivity for the 2-position was demonstrated in 87% yield (**13** + **14**) (Scheme 31).

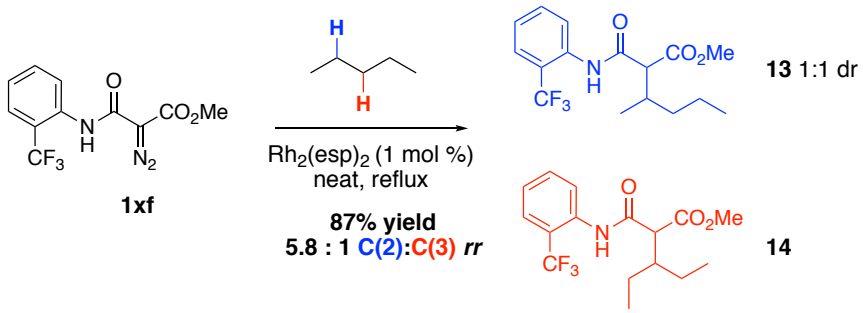

Scheme 31 – Site Selective C-H Insertion Using a 2° Amide Diazoacetate

3.3 Conclusion

In this study, density functional theory lead us on path to deconstruct, into steric and electronic drivers, the activation energies for intermolecular C(sp^3)-H insertions mediated by 1,3-dicarbonyl dirhodium carbenes. These drivers were then used to build a map of chemical space. As demonstrated through synthetic experiments, the information in this map can be leveraged to tune A-A carbenes to promote or suppress C-H insertion reactivity. This process lead us to posit N-aryl-substituted secondary α-diazo-β-amide

esters as a synthetically useful sub-class of A-A carbenes and, subsequently, report the first C-H insertion and cyclopropanation reactions with these species.

Understanding the drivers of intermolecular A-A C(sp^3)-H insertion activation energies and how to manipulate them provides synthetic practitioners with valuable information *en route* to target molecules. Moreover, the methodology community is now armed with unprecedented insight to be used in the design and development of new reactions involving A-A carbenes.

We expect this work to directly enable the development of site and enantioselective transformations for N-aryl-substituted secondary α-diazo-β-amide esters, development of subsequent electron-deficient amide coupling and auxiliary group directed C-H insertion transformations on the product space, rational design of catalysts that leverage H-bonding capabilities of carbenes, and the extension of this theoretical model to structurally analogous α-diazo-β-keto nitro carbenes.

3.4 Experimental

3.4.1 General Methods

All solvents used in the reported reactions were purchased anhydrous from commercial sources or freshly distilled.

Chromatographic purification was performed as flash chromatography with Dynamic Adsorbents silica gel (23-65 μm) and solvents indicated as eluent with 0.1-0.5 bar pressure. For quantitative flash chromatography, technical grade solvents were utilized.

Analytical thin-layer chromatography was performed on EMD silica gel 60 F254 TLC glass plates. Visualization was accomplished with UV light.

Proton and carbon nuclear magnetic resonance (^{1}H NMR and ^{13}C NMR) spectra were recorded on a Varian Mercury Vx 300 MHz spectrometer with solvent resonances as the internal standard (^{1}H NMR: $CHCl_3$ at 7.26 ppm; ^{13}C NMR: $CHCl_3$ at 77.0 ppm). ^{1}H NMR data are reported as follows: chemical shift (ppm), multiplicity (s = singlet, d = doublet, dd = doublet of doublets, dt = doublet of triplets, ddd = doublet of doublet of doublets, t = triplet, q = quartet, p = pentet, m = multiplet, br = broad), coupling constants (Hz), and integration. Mass spectra were obtained through EI on a Micromass AutoSpec Machine or through ESI on a Thermo Orbitrap XL. The accurate mass analyses run in EI mode were at a mass resolution of 10,000 and were calibrated using PFK (perfluorokerosene) as an internal standard. The accurate mass analyses run in EI mode were at a mass resolution of 30,000 using the calibration mixture supplied by Thermo.

3.4.2 Experimental Procedures

3.4.2.1 Diazo Compounds

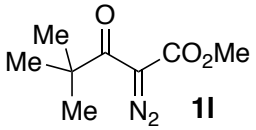

1l

Methyl 2-diazo-4,4-dimethyl-3-oxopentanoate (1l): To a dry round-bottom flask containing methyl 4,4-dimethyl-3-oxopentanoate (1 mL, 6 mmol), triethylamine (1 mL, 7.4 mmol), in acetonitrile (20 mL) at 0 °C was added 4-acetamindobenzenesulfonyl azide (1.7 g, 7.1 mmol). The ice bath was removed allowing the reaction to warm to room

temperature. The reaction mixture was stirred for 18 h. Upon completion of the reaction, solvents were removed via rotary evaporation. Cold dichloromethane (100 mL, 0 °C) was added to the crude material causing a white byproduct to precipitate. This precipitate was removed via vacuum filtration. The filtrate was purified via flash silica gel chromatography. **3l** was afforded as a yellow liquid (993 mg, 90% yield). **^{1}H NMR** (300 MHz, $CDCl_3$) δ = 3.79 (s, 3H), 1.27 (s, 9H). **^{13}C NMR** (75 MHz, $CDCl_3$) δ = 197.12, 161.26, 52.07, 44.28, 25.71. **HRMS-EI** (*m/z*): $[M+H]^+$ Calcd. for $C_8H_{13}O_3N_2$ 185.0921; Found 185.0916.

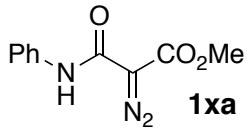

1xa

Methyl 2-diazo-3-oxo-3-(phenylamino)propanoate (1xa): ***To a dry round-bottom flask containing methyl 3-oxo-3-(phenylamino)propanoate (1.3 g, 6.7 mmol), triethylamine (1 mL, 7.4 mmol), in acetonitrile (30 mL) at 0 °C was added 4-acetamindobenzenesulfonyl azide (1.7 g, 7.1 mmol). The ice bath was removed allowing the reaction to warm to room temperature. The reaction mixture was stirred for 18 h. Upon completion of the reaction, solvents were removed via rotary evaporation. Cold dichloromethane (100 mL, 0 °C) was added to the crude material causing a white byproduct to precipitate. This precipitate was removed via vacuum filtration. The filtrate was then washed treated with 1 M HCl and extracted into dichloromethane. The filtrate was purified via flash silica gel chromatography **1xa was afforded as a yellow solid (1.1 g, 75% yield). **^{1}H NMR** (300 MHz, $CDCl_3$) δ = 9.57 (s, 1H), 7.56 (d, *J* = 8.4 Hz, 2H), 7.32 (dd, *J* = 8.4, 7.6 Hz, 2H),

7.10 (t, J = 7.4 Hz, 1H), 3.88 (s, 3H). **^{13}C NMR** (75 MHz, $CDCl_3$) δ = 164.90, 158.30, 137.83, 129.00, 124.28, 119.81, 52.63. **HRMS-EI** (*m/z*): $[M]^+$ Calcd. for $C_{10}H_9O_3N_3$ 219.0644; Found 219.0641.

*Note: compounds **1xb**-**1xg** were all prepared following the procedure used to synthesize **1xa**.

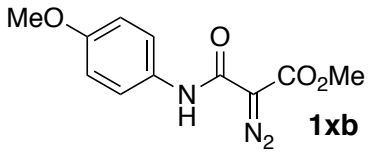

1xb

Methyl 2-diazo-3-((4-methoxyphenyl)amino)-3-oxopropanoate (1xb): 1xb was afforded as a yellow solid (2.83 g, 52% yield). **^{1}H NMR** (300 MHz, $CDCl_3$) δ = 9.41 (s, 1H), 7.46 (d, J = 9.0 Hz, 2H), 6.85 (d, J = 9.1 Hz, 2H), 3.86 (s, 3H), 3.77 (s, 3H). **^{13}C NMR** (75 MHz, $CDCl_3$) δ = ^{13}C NMR (75 MHz, Chloroform-*d*) δ 164.96, 158.02, 156.36, 130.99, 121.54, 114.10, 55.43, 52.57. **HRMS-EI** (*m/z*): $[M]^+$ Calcd. for $C_{10}H_9O_3N_3$ 219.0644; Found 219.0641.

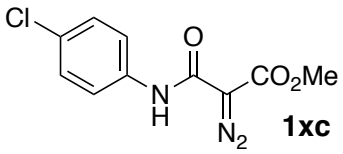

1xc

Methyl 3-((4-chlorophenyl)amino)-2-diazo-3-oxopropanoate (1xc): 1xc was afforded as an yellow solid (4.38 g, 78% yield). **^{1}H NMR** (300 MHz, $CDCl_3$) δ = 9.60 (s, 1H), 7.52

(d, J = 9.0 Hz, 2H), 7.28 (d, J = 11.8 Hz, 2H), 3.90 (s, 3H). **^{13}C NMR** (75 MHz, $CDCl_3$) δ = 164.82, 158.41, 136.38, 128.98, 128.95, 121.01, 52.72. **HRMS-EI** (*m/z*): $[M]^+$ Calcd. for $C_{10}H_8O_3N_3Cl$ 253.0254; Found 253.02.50.

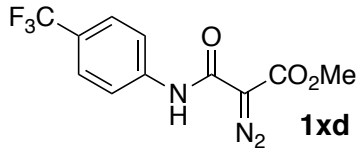

1xd

Methyl 2-diazo-3-oxo-3-((4-(trifluoromethyl)phenyl)amino)propanoate (1xd): 1xd was afforded as a white solid (1.62 g, 80% yield). **^{1}H NMR** (300 MHz, $CDCl_3$) δ = 9.59 (s, 1H), 7.50 (d, J = 8.7 Hz, 2H), 7.39 (d, J = 8.7 Hz, 2H), 3.72 (s, 3H). **^{13}C NMR** (75 MHz, $CDCl_3$) δ = 164.79, 158.73, 140.81, 126.25 (q, J = 3.8 Hz), 125.92 (q, J = 32.8 Hz), 124.06 (q, J = 271.6 Hz), 119.35, 52.77. **HRMS-EI** (*m/z*): $[M]^+$ Calcd. for $C_{11}H_8O_3N_3F_3$ 287.0518; Found 287.0507.

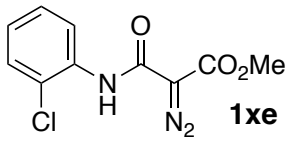

1xe

Methyl 3-((2-chlorophenyl)amino)-2-diazo-3-oxopropanoate (1xe): 1xe was afforded as a white solid (2.48 g, 76% yield). **^{1}H NMR** (300 MHz, $CDCl_3$) δ = 10.12 (s, 1H), 8.41 (d, J = 8.3 Hz, 1H), 7.37 (d, J = 8.0 Hz, 1H), 7.25 (t, J = 7.9 Hz, 1H), 7.02 (t, J = 7.7 Hz, 1H), 3.90 (s, 3H). **^{13}C NMR** (75 MHz, $CDCl_3$) δ = 164.60, 158.60, 135.08, 129.15, 127.54,

124.54, 123.12, 121.33, 52.77 . **HRMS-EI** (*m/z*): M]$^+$ Calcd. for $C_{10}H_8O_3N_3Cl$ 253.0254; Found 253.0249.

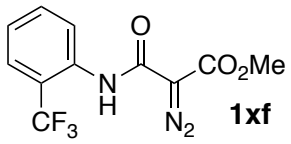

1xf

Methyl 2-diazo-3-oxo-3-((2-(trifluoromethyl)phenyl)amino)propanoate (1xf): 1xf was afforded as a white solid (1.35 g, 67% yield). **^{1}H NMR** (300 MHz, $CDCl_3$) δ = 9.99 (s, 1H), 8.26 (d, *J* = 8.3 Hz, 1H), 7.62 (d, *J* = 7.9 Hz, 1H), 7.55 (t, *J* = 7.9 Hz, 1H), 7.22 (t, *J* = 7.7 Hz, 1H), 3.92 (s, 3H). **^{13}C NMR** (75 MHz, $CDCl_3$) δ = 164.41, 159.13, 135.08, 132.71, 126.04 (q, *J* = 5.4 Hz), 124.31, 124.12, 123.80 (q, *J* = 272.9 Hz), 120.49 (q, *J* = 30.7 Hz), 52.80. **HRMS-EI** (*m/z*): [M]$^+$ Calcd. for $C_{11}H_8O_3N_3F_3$ 287.0518; Found 287.0511.

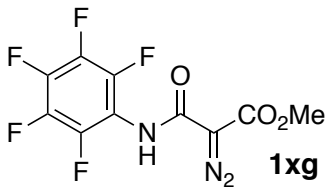

1xg

Methyl 2-diazo-3-oxo-3-((perfluorophenyl)amino)propanoate (1xg): 1xg was afforded as a white solid (1.10 g, 64% yield). **^{1}H NMR** (300 MHz, $CDCl_3$) δ = 9.15 (s, 1H), 3.91 (s, 3H). **^{13}C NMR** (75 MHz, $CDCl_3$) δ = 164.52, 159.23, 143.16 (d, *J* = 239.6 Hz), 140.16 (d,

J = 254.0 Hz), 137.76 (d, J = 253.8 Hz), 111.32, 52.90. **HRMS-EI** (m/z[M]$^+$ Calcd. for $C_{10}H_4O_3N_3F_5$ 309.0173; Found 309.0167.

3.4.2.2 C-H insertion products

For compounds **8b-8e**, **8g**, **8h**, **8o**, and **8xa**, Procedure A was used: To a dry round-bottom flask containing Rh_2esp_2 (1 mol %) and refluxing cyclohexane (7 mL, 81 °C) was added a solution of diazo compound **1** (0.5-0.7 mmol, 1 equiv.) in cyclohexane (3 mL) via syringe pump over 15 minutes. When the TLC showed complete consumption of the diazo compound, methanol (1 mL, 20 mmol) was added, and the temperature was reduced to 65 °C. The mixture continued to stir for 30 minutes. The crude material was purified via flash silica gel chromatography.

For compounds **8xf-8xg**, Procedure B was used: To a dry round-bottom flask containing Rh_2esp_2 (1 mol %) and cyclohexane (5 equiv.) in refluxing dichloromethane (3 mL, 40 °C) was added a solution of diazo compound **1** (0.28 mmol, 1 equiv.) in dichloromethane (2 mL) via syringe pump over 15 minutes.

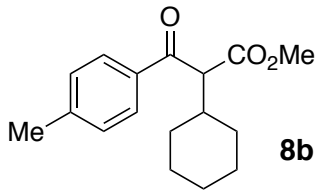

8b

Methyl 2-cyclohexyl-3-oxo-3-(*p*-tolyl)propanoate (8b): 127 mg (0.580 mmol) of methyl 2-diazo-3-oxo-3-(*p*-tolyl)propanoate **1b** was used. The crude material was purified via flash silica gel chromatography (25% EtOAc/Hexane, R_f = 0.78). **8b** was afforded as a clear

oil (33 mg, 21% yield). **^{1}H NMR** (300 MHz, $CDCl_3$) δ = 7.91 (d, *J* = 8.3 Hz, 2H), 7.26 (d, *J* = 8.5 Hz, 2H), 4.17 (d, *J* = 9.7 Hz, 1H), 3.65 (s, 3H), 2.41 (s, 3H), 2.42 – 2.30 (m, 1H), 1.80 – 1.57 (m, 5H), 1.42 – 1.20 (m, 2H), 1.19 – 1.04 (m, 2H), 0.97 – 0.85 (m, 1H). **^{13}C NMR** (75 MHz, $CDCl_3$) δ = 194.25, 169.60, 144.48, 134.61, 129.44, 128.71, 60.25, 52.28, 38.36, 31.36, 30.95, 26.14, 26.00, 25.95, 21.65. **HRMS-ESI** (*m/z*): $[M+H]^+$ Calcd. for $C_{17}H_{23}O_3$ 275.1642; Found 275.1638.

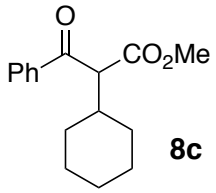

8c

Methyl 2-cyclohexyl-3-oxo-3-phenylpropanoate (8c): 118 mg (0.580 mmol) methyl 2-diazo-3-oxo-3-phenylpropanoate **1c** was used. The mixture continued to stir for 30 minutes. The crude material was purified via flash silica gel chromatography (25% EtOAc/Hexane, R_f = 0.56). **8c** was afforded as a clear oil (51 mg, 34% yield). **^{1}H NMR** (300 MHz, $CDCl_3$) δ = 8.04 (ddt, *J* = 8.01 (d, *J* = 7.1 Hz, 2H), 7.58 (t, *J* = 7.3 Hz, 1H), 7.47 (t, *J* = 7.4 Hz, 2H), 4.19 (d, *J* = 9.7 Hz, 1H), 3.66 (s, 3H), 2.44 – 2.29 (m, 1H), 1.79 – 1.59 (m, 5H), 1.43 – 1.02 (m, 4H), 1.00 – 0.84 (m, 1H) **^{13}C NMR** (75 MHz, $CDCl_3$) δ = 193.03, 169.34, 165.99 (d, *J* = 255.8 Hz), 133.44 (d, *J* = 3.1 Hz), 131.28 (d, *J* = 9.4 Hz), 115.91 (d, *J* = 21.9 Hz), 60.49, 52.41, 38.31, 31.37, 30.88, 26.09, 25.96, 25. **HRMS-ESI** (*m/z*): $[M+H]^+$ Calcd. for $C_{16}H_{21}O_3$ 216.1485; Found 216.1481.

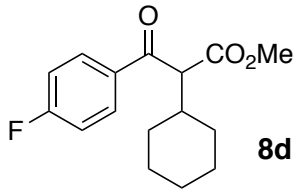

8d

Methyl 2-cyclohexyl-3-(4-fluorophenyl)-3-oxopropanoate (8d): 129 mg (0.58 mmol) of methyl 2-diazo-3-(4-fluorophenyl)-3-oxopropanoate **1d** was used. The crude material was purified via flash silica gel chromatography (25% EtOAc/Hexane, R_f = 0.59). **8d** was afforded as a clear oil (79 g, 49% yield). **^{1}H NMR** (300 MHz, $CDCl_3$) δ = 8.04 (ddt, *J* = 8.2, 5.0, 2.5 Hz, 2H), 7.21 – 7.07 (m, 2H), 4.13 (d, *J* = 9.8 Hz, 1H), 3.66 (s, 3H), 2.36 (qt, *J* = 9.6, 2.7 Hz, 1H), 1.80 – 1.58 (m, 5H) 1.33 (pt, *J* = 13.5, 3.4 Hz, 2H), 1.09 (pt, *J* = 11.7, 2.6 Hz, 5H), 0.90 (qd, *J* = 11.5, 2.3 Hz, 1H) **^{13}C NMR** (75 MHz, $CDCl_3$) δ = 193.03, 169.34, 165.99 (d, *J* = 255.8 Hz), 133.44 (d, *J* = 3.1 Hz), 131.28 (d, *J* = 9.4 Hz), 115.91 (d, *J* = 21.9 Hz), 60.49, 52.41, 38.31, 31.37, 30.88, 26.09, 25.96, 25.91. **HRMS-ESI** (*m/z*): $[M+H]^+$ Calcd. for $C_{16}H_{20}O_3F$ 279.1391; Found 279.1386.

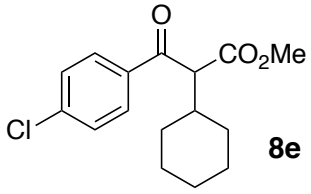

8e

Methyl 3-(4-chlorophenyl)-2-cyclohexyl-3-oxopropanoate (8e): 138 mg, (0.58 mmol) of methyl 3-(4-chlorophenyl)-2-cyclohexyl-3-oxopropanoate **1e** was used. The mixture continued to stir for 30 minutes. The crude material was purified via flash silica gel chromatography (25% EtOAc/Hexane, R_f = 0.66). **8e** was afforded as a clear oil (110 mg,

62% yield). **^{1}H NMR** (300 MHz, $CDCl_3$) δ = 7.94 (d, *J* = 8.8 Hz, 2H), 7.43 (d, *J* = 8.8 Hz, 2H), 4.11 (d, *J* = 9.7 Hz, 1H), 3.65 (s, 3H), 2.35 (qt, *J* = 11.5, 3.0 Hz, 1H), 1.79 – 1.55 (m, 5H), 1.30 (pt, *J* = 12.1, 3.0 Hz, 2H), 1.11 (pt, *J* = 11.8, 3.0 Hz, 2H), 0.90 (td, *J* = 11.8, 8.2 Hz, 1H) **^{13}C NMR** (75 MHz, $CDCl_3$) δ = 193.45, 169.23, 140.10, 135.30, 129.95, 129.08, 60.48, 52.42, 38.30, 31.35, 30.86, 26.07, 25.95, 25.91. **HRMS-EI** (*m/z*): $[M+H]^+$ Calcd. for $C_{16}H_{20}O_3Cl$ 295.1101; Found 295.1086.

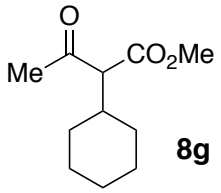

8g

Methyl 2-cyclohexyl-3-oxobutanoate (8g): 94 mg, (0.66 mmol) methyl 2-diazo-3-oxobutanoate **1g** was used. **8g** was afforded as a clear oil (99 mg, 75% yield). **^{1}H NMR** (300 MHz, $CDCl_3$) δ = 3.66 (s, 3H), 3.21 (d, *J* = 9.8 Hz, 1H), 2.17 (s, 3H), 2.14 – 2.00 (m, 1H), 1.73 – 1.49 (m, 5H), 1.33 – 1.05 (m, 3H), 1.04 – 0.84 (m, 2H). **^{13}C NMR** (75 MHz, CDCl3) δ = 203.16, 169.54, 66.61, 52.11, 37.97, 30.77, 30.71, 29.31, 25.93, 25.83. **HRMS-EI** (*m/z*): $[M+H]^+$ Calcd. for $C_{11}H_{19}O_3$ 199.1334; Found 199.1338.

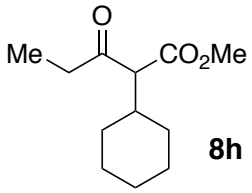

8h

Methyl 2-cyclohexyl-3-oxopentanoate (8h): 90 mg, (0.58 mmol) of methyl 2-diazo-3-oxopentanoate **1h** was used. **8h** was afforded as a clear oil (48 mg, 39% yield). **^{1}H NMR** (300 MHz, $CDCl_3$) δ = 3.67 (s, 3 H), 3.28 (d, *J* = 9.9 Hz, 1 H), 2.50 (m, 2 H), 2.13 (m, 1 H), 1.65 (m, 4 H), 1.53 (m, 1 H), 1.21 (m, 3 H), 1.02 (t, *J* = 7.2 Hz, 3 H), 0.92 (m, 2 H). **^{13}C NMR** (75 MHz, CDCl3) δ = 205.72, 169.54, 65.60, 52.13, 38.11, 36.12, 30.87, 30.85, 26.00, 25.87, 7.46. **HRMS-ESI** (*m/z*): $[M+H]^+$ Calcd. for $C_{12}H_{21}O_3$ 213.1485; Found 213.1481.

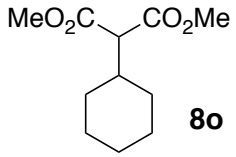

8o

Dimethyl 2-cyclohexylmalonate (8o): 104 mg, (0.66 mmol) of dimethyl diazomalonate **1o** was used. **8o** was afforded as a clear oil (103 mg, 73% yield). **^{1}H NMR** (300 MHz, $CDCl_3$) δ = 3.67 (s, 6H), 3.15 (d, *J* = 8.8 Hz, 1H), 2.05 (qt, *J* = 8.5, 2.9 Hz, 1H), 1.75 – 1.56 (m, 5H), 1.26 (pt, *J* = 12.3, 2.5 Hz, 2H), 1.16 – 0.94 (m, 3H). **^{13}C NMR** (75 MHz, $CDCl_3$) δ = 168.93, 57.98, 51.88, 37.94, 30.66, 25.94, 25.86.

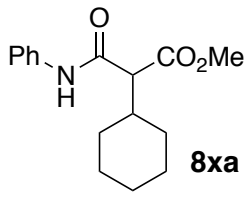

8xa

Methyl 2-cyclohexyl-3-oxo-3-(phenylamino)propanoate (8xa): 134 mg (0.62 mmol) of **1xa** was used. **8xa** was afforded as white solid (149 mg, 89% yield). **^{1}H NMR** (300 MHz, $CDCl_3$, 40 °C) δ = 8.66 (s, 1H), 7.54 (d, *J* = 8.4 Hz, 2H), 7.32 (t, *J* = 7.0 Hz, 2H), 7.10 (t, *J* = 7.4 Hz, 1H), 3.77 (s, 3H), 3.18 (d, *J* = 9.1 Hz, 1H), 2.14 – 1.95 (m, 1H), 1.87 – 1.60 (m, 5H), 1.39 – 1.01 (m, 5H). **^{13}C NMR** (75 MHz, $CDCl_3$, 40 °C) δ = 173.22, 165.53, 137.61, 128.91, 124.35, 119.87, 60.56, 52.27, 41.28, 31.00, 30.76, 25.90, 25.84. **IR**. **HRMS-ESI** (*m/z*): $[M+H]^+$ Calcd. for $C_{16}H_{22}O_3N$ 276.1594; Found 276.1588.

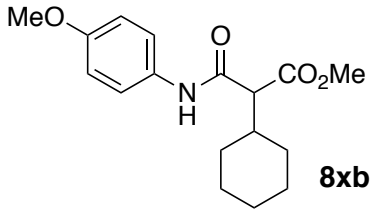

8xb

Methyl 2-cyclohexyl-3-((4-methoxyphenyl)amino)-3-oxopropanoate (8xb): 70 mg (0.28 mmol) of **1xb** was used. **8xb** was afforded as a white solid (21 mg, 24% yield). **^{1}H NMR** (300 MHz, $CDCl_3$, 40 °C) δ = 8.58 (s, 1H), 7.44 (d, *J* = 9.1 Hz, 2H), 6.84 (d, *J* = 9.1 Hz, 2H), 3.77 (s, 1H), 3.76 (s, 3H), 3.15 (d, *J* = 9.2 Hz, 1H), 2.12 – 1.92 (m, 1H), 1.90 – 1.55 (m, 5H), 1.16 (m, 5H). **^{13}C NMR** (75 MHz, $CDCl_3$, 40 °C) δ = 173.27, 165.41, 156.41, 130.73, 121.58, 114.07, 60.39, 55.46, 52.35, 41.23, 30.99, 30.75, 25.92, 25.90, 25.84. **HRMS-EI** (*m/z*): $[M]^+$ Calcd. for $C_{17}H_{23}O_4N$ 305.1627; Found 305.1627.

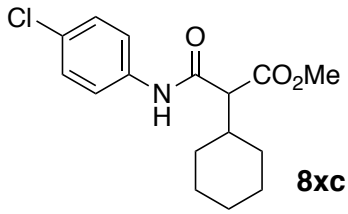

8xc

Methyl 3-((4-chlorophenyl)amino)-2-cyclohexyl-3-oxopropanoate (8xc): 110 mg (0.43 mmol) of **1xc** was used. **8xc** was afforded as a white solid (65 mg, 66% yield). **^{1}H NMR** (300 MHz, $CDCl_3$, 40 °C) δ = 8.80 (s, 1H), 7.51 (d, *J* = 8.7 Hz, 2H), 7.27 (d, *J* = 8.8 Hz, 2H), 3.77 (s, 3H), 3.17 (d, *J* = 8.7 Hz, 1H), 2.10 – 1.95 (m, 1H), 1.84 – 1.60 (m, 5H), 1.36 – 1.03 (m, 5H). **^{13}C NMR** (75 MHz, $CDCl_3$, 40 °C) δ = 173.40, 165.76, 136.12, 129.32, 128.94, 121.10, 60.37, 52.47, 41.47, 30.96, 30.78, 25.89, 25.88, 25.78.

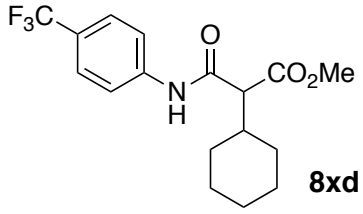

8xd

Methyl 2-cyclohexyl-3-oxo-3-((4-(trifluoromethyl)phenyl)amino)propanoate (8xd): 81 mg (0.28 mmol) of **1xd** was used. **8xd** was afforded as a white solid (61 mg, 63% yield). **^{1}H NMR** (300 MHz, $CDCl_3$) δ = 9.00 (s, 1H), 7.68 (d, *J* = 8.5 Hz, 2H), 7.57 (d, *J* = 8.6 Hz, 2H), 3.78 (s, 3H), 3.19 (d, *J* = 9.0 Hz, 1H), 2.03 (m, 1H), 1.82 – 1.63 (m, 5H), 1.38 – 1.06 (m, 5H). **^{13}C NMR** (75 MHz, $CDCl_3$, 40 °C) δ = 173.39, 166.03, 140.56 (d, *J* = 1.3 Hz), 126.21 (q, *J* = 3.8 Hz), 125.87 (d, *J* = 6.0 Hz), 129.58 – 119.46 (m), 119.47, 60.40, 52.54, 41.55, 30.96, 30.77, 25.86, 25.74.

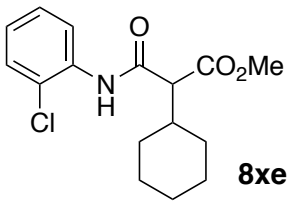

8xe

Methyl 2-cyclohexyl-3-oxo-3-(phenylamino)propanoate (8xe): 71 mg (0.28 mmol) of **1xe** was used. **8xe** was afforded as a white solid (60 mg, 69% yield). **^{1}H NMR** (300 MHz, $CDCl_3$, 40 °C) δ = 9.24 (s, 1H), 8.36 (d, *J* = 8.3 Hz, 1H), 7.37 (d, *J* = 8.0 Hz, 1H), 7.25 (t, *J* = 7.2 Hz, 1H), 7.11 – 6.98 (m, 1H), 3.79 (s, 3H), 3.21 (d, *J* = 9.1 Hz, 1H), 2.10 – 1.95 (m, 1H), 1.85 – 1.60 (m, 5H), 1.34 – 1.04 (m, 5H). **^{13}C NMR** (75 MHz, $CDCl_3$, 40 °C) δ = 172.83, 165.83, 134.51, 129.09, 127.56, 124.76, 123.29, 121.60, 60.86, 52.51, 41.50, 31.00, 30.75, 25.89, 25.87, 25.80. **HRMS-EI** (*m/z*): $[M]^+$ Calcd. for $C_{16}H_{20}O_3NCl$ 309.1132; Found 309.1140.

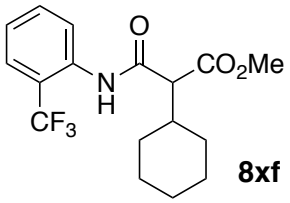

8xf

Methyl 2-cyclohexyl-3-oxo-3-((2-(trifluoromethyl)phenyl)amino)propanoate (8xf): 81 mg (0.28 mmol) of **1xf** was used. **8xf** was afforded as a white solid (72 mg, 75% yield). **^{1}H NMR** (300 MHz, $CDCl_3$, 40 °C) δ = 9.05 (s, 1H), 8.19 (d, *J* = 8.3 Hz, 1H), 7.61 (d, *J* = 9.3 Hz, 1H), 7.58 – 7.48 (m, 1H), 7.25 – 7.17 (m, 1H), 3.79 (s, 3H), 3.20 (d, *J* = 9.3 Hz, 1H),

2.08 – 1.96 (m, 1H), 1.83 – 1.61 (m, 5H), 1.37 – 1.01 (m, 5H). **^{13}C NMR** (75 MHz, $CDCl_3$) δ = 172.64, 166.03, 134.92 (q, *J* = 1.8 Hz), 132.93 – 132.17 (m), 126.01 (q, *J* = 5.4 Hz), 124.48, 124.32, 123.86 (q, *J* = 273.0 Hz), 120.49 (q, *J* = 29.8 Hz), 60.72, 52.50, 41.41, 30.98, 30.64, 25.84, 25.77.

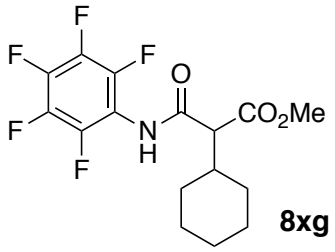

8xg

Methyl 2-cyclohexyl-3-oxo-3-((perfluorophenyl)amino)propanoate (8xg): 87 mg (0.28 mmol) of **1xag** was used. **8xg** was afforded as a white solid (84 mg, 82% yield). **^{1}H NMR** (300 MHz, $CDCl_3$, 40 °C) δ = 8.60 (s, 1H), 3.80 (s, 3H), 3.27 (d, *J* = 8.7 Hz, 1H), 2.12 – 1.94 (m, 1H), 1.86 – 1.58 (m, 5H), 1.36 – 1.02 (m, 5H). **^{13}C NMR** (75 MHz, $CDCl_3$, 40 °C) δ = 173.11, 166.33, 144.42, 141.97 – 138.96 (m), 136.09, 111.57, 59.31, 52.66, 41.72, 30.88, 30.55, 25.92, 25.90, 25.73. **HRMS-EI** (*m/z*): $[M]^+$ Calcd. for $C_{16}H_{16}O_3NF_5$ 365.1050; Found 365.1047.

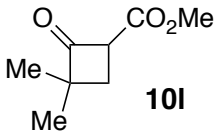

10l

Methyl 3,3-dimethyl-2-oxocyclobutane-1-carboxylate (10l): To a dry round-bottom flask containing Rh_2esp_2 (4.1 mg, 5.4 μmol) and refluxing cyclohexane (7 mL, 81 °C) was added a solution of methyl 2-diazo-4,4-dimethyl-3-oxopentanoate **1l** (100 mg, 0.54 mmol) in cyclohexane (3 mL) via syringe pump over 15 minutes. When the TLC showed complete consumption of the diazo compound, methanol (1 mL, 20 mmol) was added, and the temperature was reduced to 65 °C. The mixture continued to stir for 30 minutes. The crude material was purified via flash silica gel chromatography (25% EtOAc/Hexane, R_f = 0.36). **10l** was afforded as a clear oil (61 mg, 72% yield). **^{1}H NMR** (300 MHz, $CDCl_3$) δ = 4.20 (dd, *J* = 10.2, 7.7 Hz, 1H), 3.72 (s, 3H), 2.27 (dd, *J* = 11.6, 7.7 Hz, 1H), 2.04 (dd, *J* = 11.6, 10.3 Hz, 1H), 1.23 (d, *J* = 5.5 Hz, 6H). **^{13}C NMR** (75 MHz, CDCl3) δ = 206.62, 167.73, 60.24, 59.54, 52.44, 29.08, 23.22, 21.98. **HRMS-EI** (*m/z*): $[M+H]^+$ Calcd. for $C_8H_{13}O$ 157.0865; Found 157.0869.

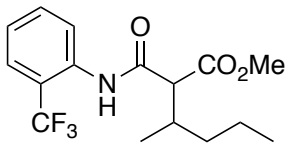

13

Methyl 3-methyl-2-((2-(trifluoromethyl)phenyl)carbamoyl)hexanoate (13): To a dry round-bottom flask containing Rh_2esp_2 (2.64 mg, 3.5 μmol) and refluxing n-pentane (5 mL, 38 °C) was added a solution of **1xf** (101 mg, 0.35 mmol) in DCM (0.5 mL) dropwise. The mixture continued to stir for 30 minutes. The crude material was purified via flash silica gel chromatography. **13** was afforded as a clear oil (101 mg, 87% yield). **^{1}H NMR** (300 MHz, $CDCl_3$, 40 °C) δ = 9.15 (s, 1H), 8.26 (d, *J* = 8.3 Hz, 1H), 7.61 (d, *J* = 8.3 Hz,

1H), 7.53 (t, J = 7.9 Hz, 1H), 7.21 (t, J = 7.6 Hz, 1H), 3.78 (s, 3H), 3.27 (t, J = 8.3 Hz, 1H), 2.35 – 2.14 (m, 1H), 1.49 – 1.17 (m, 4H), 1.02 (dd, J = 12.8, 6.7 Hz, 3H), 0.93 – 0.77 (m, 3H). **^{13}C NMR** (75 MHz, $CDCl_3$, 40 °C) δ =172.81, 172.64, 166.49, 166.21, 134.92 (q, J = 1.7 Hz), 132.77 – 132.63 (m), 126.01 (q, J = 5.4 Hz), 124.50, 124.35 (d, J = 1.8 Hz), 123.85 (q, J = 273.0 Hz), 120.54 (q, J = 29.7 Hz), 60.01, 59.84, 52.52, 52.45, 36.73, 36.68, 36.66, 36.32, 19.76, 19.75, 16.95, 16.78, 13.97, 13.92. **HRMS-EI** (*m/z*): $[M]^+$ Calcd. for $C_{16}H_{20}O_3NF_3$ 331.1395; Found 331.1386.

3.4.2.3 Wolff Rearrangement Products

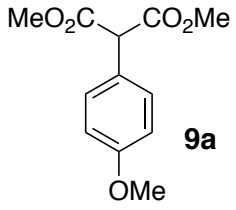

9a

Dimethyl 2-(4-methoxyphenyl)malonate (9a): To a dry round-bottom flask containing Rh_2esp_2 (4.4 mg, 5.8 μmol) and refluxing cyclohexane (7 mL, 81 °C) was added a solution of methyl 2-diazo-3-(4-methylphenyl)-3-oxopropanoaten **1a** (136 mg, 0.580 mmol) in cyclohexane (3 mL) via syringe pump over 15 minutes. The reaction was monitored by TLC. When the TLC showed complete consumption of the diazo compound, methanol (1 mL, 20 mmol) was added, and the temperature was reduced to 65 °C. The mixture continued to stir for 30 minutes. The crude material was purified via flash silica gel chromatography (25% EtOAc/Hexane, R_f = 0.39). **9a** was afforded as a clear liquid (134 mg, 97% yield). **^{1}H NMR** (300 MHz, $CDCl_3$) δ = 7.32 (d, J = 8.9 Hz, 2H), 6.89 (d, J = 8.9

Hz, 2H), 4.60 (s, 1H), 3.79 (s, 3H), 3.74 (s, 6H). **^{13}C NMR** (75 MHz, $CDCl_3$) δ = 168.82, 159.56, 130.34, 124.64, 114.07, 56.71, 55.23, 52.78. **HRMS-ESI** (*m/z*): $[M+H]^+$ Calcd. for $C_{12}H_{15}O_5$ 239.0914; Found 239.0911.

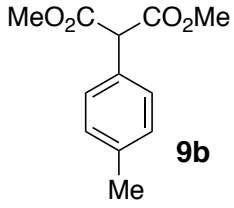

9b

Dimethyl 2-(*p*-tolyl)malonate (9b): (See procedure for **8b**) To a dry round-bottom flask containing Rh_2esp_2 (4.4 mg, 5.8 μmol) and refluxing cyclohexane (7 mL, 81 °C) was added a solution of methyl 2-diazo-3-(4-methylphenyl)-3-oxopropanoate **1b** (127 mg, 0.58 mmol) in cyclohexane (3 mL) via syringe pump over 15 minutes. The reaction was monitored by TLC. When the TLC showed complete consumption of the diazo compound, methanol (1 mL, 20 mmol) was added, and the temperature was reduced to 65 °C. The mixture continued to stir for 30 minutes. The crude material was purified via flash silica gel chromatography (25% EtOAc/Hexane, R_f = 0.63). **9b** was afforded as a clear oil (100 mg, 78% yield). **^{1}H NMR** (300 MHz, $CDCl_3$) δ = 7.29 (d, *J* = 8.3 Hz, 2H), 7.18 (d, *J* = 7.9 Hz, 2H), 4.63 (s, 1H), 3.75 (s, 6H), 2.35 (s, 3H). **^{13}C NMR** (75 MHz, $CDCl_3$) δ = 168.73, 138.16, 129.60, 129.39, 129.06, 57.20, 52.81, 21.13. **HRMS-EI** (*m/z*): $[M]^+$ Calcd. for $C_{12}H_{14}O_4$ 222.0892; Found 222.0892.

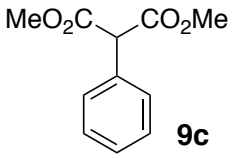

9c

Dimethyl 2-phenylmalonate (9c): (See procedure for **8c**) To a dry round-bottom flask containing Rh_2esp_2 (4.4 mg, 5.8 μmol) and refluxing cyclohexane (7 mL, 81 °C) was added a solution of methyl 2-diazo-3-oxo-3-phenylpropanoate **1c** (118 mg, 0.580 mmol) in cyclohexane (3 mL) via syringe pump over 15 minutes. The reaction was monitored by TLC. When the TLC showed complete consumption of the diazo compound, methanol (1 mL, 20 mmol) was added, and the temperature was reduced to 65 °C. The mixture continued to stir for 30 minutes. The crude material was purified via flash silica gel chromatography (25% EtOAc/Hexane, R_f = 0.41). **8c** was afforded as a clear oil (73 mg, 60% yield). **^{1}H NMR** (300 MHz, $CDCl_3$) δ = 7.43 – 7.33 (m, 5H), 4.66 (s, 1H), 3.75 (s, 6H). **^{13}C NMR** (75 MHz, $CDCl_3$) δ = 168.55, 132.55, 129.22, 128.67, 128.33, 57.56, 52.86. **HRMS-ESI** (*m/z*): $[M+H]^+$ Calcd. for $C_{11}H_{13}O_4$ 209.0808; Found 209.0805.

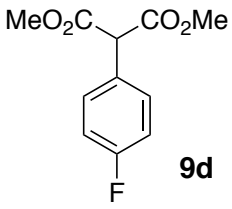

9d

dimethyl 2-(4-fluorophenyl)malonate (9d): (See procedure for **8d**) To a dry round-bottom flask containing Rh_2esp_2 (4.4 mg, 5.8 μmol) and refluxing cyclohexane (7 mL, 81 °C) was added a solution of methyl 2-diazo-3-(4-fluorophenyl)-3-oxopropanoate **1d** (129 mg, 0.580 mmol) in cyclohexane (3 mL) via syringe pump over 15 minutes. When the TLC

showed complete consumption of the diazo compound, methanol (1 mL, 20 mmol) was added, and the temperature was reduced to 65 °C. The mixture continued to stir for 30 minutes. The crude material was purified via flash silica gel chromatography (25% EtOAc/Hexane, R_f = 0.41). **9d** was afforded as a clear liquid (64 mg, 49% yield). **^{1}H NMR** (300 MHz, $CDCl_3$) δ = 7.38 (dd, *J* = 8.8, 5.1 Hz, 2H), 7.05 (t, *J* = 8.7 Hz, 2H), 4.63 (s, 1H), 3.76 (s, 6H). **^{13}C NMR** (75 MHz, $CDCl_3$) δ = 168.42, 162.70 (d, *J* = 247.5 Hz), 130.99 (d, *J* = 8.3 Hz), 128.31 (d, *J* = 3.3 Hz), 115.62 (d, *J* = 21.7 Hz), 56.68, 52.95. **HRMS-EI** (*m/z*): $[M]^+$ Calcd. for $C_{11}H_{11}O_4F$ 226.0641; Found 226.0644.

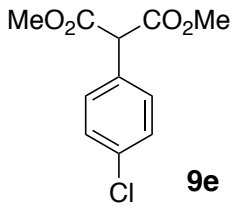

9e

Dimethyl 2-(4-chlorophenyl)malonate (9e): (See procedure for **8e**) To a dry round-bottom flask containing Rh_2esp_2 (4.4 mg, 5.8 μmol) and refluxing cyclohexane (7 mL, 81 °C) was added a solution of methyl 3-(4-chlorophenyl)-2-cyclohexyl-3-oxopropanoate **1e** (138 mg, 0.58 mmol) in cyclohexane (3 mL) via syringe pump over 15 minutes. When the TLC showed complete consumption of the diazo compound, methanol (1 mL, 20 mmol) was added, and the temperature was reduced to 65 °C. The mixture continued to stir for 30 minutes. The crude material was purified via flash silica gel chromatography (25% EtOAc/Hexane, R_f = 0.41). **9e** was afforded as a clear oil (44 mg, 31% yield). **^{1}H NMR** (300 MHz, $CDCl_3$) δ = 7.34 (s, 4H), 4.62 (s, 1H), 3.76 (s, 6H) **^{13}C NMR** (75 MHz, $CDCl_3$)

δ = 168.18, 134.46, 130.96, 130.63, 128.85, 56.83, 52.99. **HRMS-ESI** (*m/z*): $[M+H]^+$ Calcd. for $C_{11}H_{12}O_4Cl$ 243.0419; Found 243.0416.

3.4.2.4 Cyclopropanation products

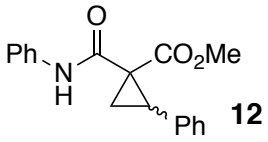

12

Methyl 2-phenyl-1-(phenylcarbamoyl)cyclopropane-1-carboxylate (12): To a dry round-bottom flask containing Rh_2esp_2 (2.7 mg, 3.5 μmol), dichloromethane (4 mL), and styrene (0.160 mL, 1.41 mmol) was added a solution of methyl 2-diazo-3-oxo-3-(phenylamino)propanoate **1xa** (155 mg, 0.707 mmol) in dichloromethane (3 mL) via syringe pump over 15 minutes. The reaction was monitored by TLC and stopped when the TLC showed complete consumption of the diazo compound. Two diasteromers were isolated via flash silica gel chromatography (25% EtOAc/Hexane, R_f = 0.71 and 0.36); **12-d1** (white solid; 131 mg, 63% yield) and **12-d2** (yellow liquid; 32 mg, 15% yield). **^{1}H NMR** (**12-d1**, 300 MHz, $CDCl_3$) δ = 9.81 (s, 1H), 7.34 – 7.16 (m, 9H), 7.09 – 6.97 (m, 1H), 3.83 (s, 3H), 3.17 (t, *J* = 9.0, 1H), 2.60 (dd, *J* = 8.4, 4.8 Hz, 1H), 2.14 (dd, *J* = 9.4, 4.8 Hz, 1H). **^{13}C NMR** (**12-d1**, 75 MHz, $CDCl_3$) δ = 172.91, 162.72, 137.83, 134.28, 129.12, 128.71, 128.14, 127.52, 124.05, 52.85, 37.91, 36.37, 18.72. **^{1}H NMR** (**12-d2**, 300 MHz, $CDCl_3$) δ = 10.63 (s, 1H), 7.63 (d, *J* = 7.5 Hz, 2H), 7.39 – 7.24 (m, 7H), 7.12 (t, *J* = 7.4 Hz, 1H), 3.30 (t, *J* = 8.8 Hz, 1H), 3.20 (s, 3H), 2.41 – 2.32 (m, 2H). **^{13}C NMR** (**12-d2**, 75 MHz, $CDCl_3$) δ = 171.75, 166.17, 138.07, 135.14, 129.21, 128.96, 128.11, 127.45, 124.18,

120.03, 51.63, 38.77, 35.59, 19.39. **HRMS-EI** (*m/z*): $[M]^+$ Calcd. for $C_{18}H_{17}O_3N$ 295.1208; Found 295.1206.

3.4.3 Computed Structure Energies and Imaginary Frequencies

Label	E	ZPE+E	H	G	Im. Freq. (cm-1)
2e	-3137.74575	-3136.92169	-3136.86523	-3137.00813	none
6e	-3256.87105	-3255.94383	-3255.88251	-3256.03338	-282.58
2d	-2777.39524	-2776.56862	-2776.51284	-2776.65277	none
6d	-2896.51880	-2895.59025	-2895.52912	-2895.68093	-204.97
2c	-2678.16901	-2677.33567	-2677.28039	-2677.41956	none
6c	-2797.29291	-2796.35590	-2796.29584	-2796.44425	-193.34
2b	-2717.48565	-2716.62388	-2716.56699	-2716.70991	none
6b	-2836.60814	-2835.64353	-2835.64353	-2835.64353	-242.02
2a	-2792.68590	-2791.81904	-2791.76149	-2791.90563	none
6a	-2911.80769	-2910.83702	-2910.77500	-2910.92614	-208.9
2f	-2447.11354	-2446.36125	-2446.31061	-2446.43953	none
6f	-2566.25031	-2565.39481	-2565.33923	-2565.47769	-315.39
2g	-2486.44148	-2485.66128	-2485.60975	-2485.74054	none
6g	-2605.57351	-2604.68937	-2604.63249	-2604.77313	-374.74
2h	-2525.75339	-2524.94518	-2524.89128	-2525.02786	none
6g	-2644.88463	-2643.97220	-2643.91382	-2644.05753	-339.87
2i	-2643.68500	-2642.79096	-2642.73357	-2642.87671	none
6i	-2762.81479	-2761.81693	-2761.75533	-2761.90418	-228.49
2j	-2565.06668	-2564.22996	-2564.17499	-2564.31292	none
6j	-2684.19028	-2683.24961	-2683.19002	-2683.33646	-358.8
2k	-2681.79534	-2680.89082	-2680.83457	-2680.97477	none
6k	-2800.92032	-2799.91059	-2799.85012	-2799.99740	-279.63
2l	-2604.37421	-2603.50906	-2603.45280	-2603.59331	none
6l	-2723.49758	-2722.52741	-2722.46702	-2722.61351	-183.48
2m	-2524.51816	-2523.73113	-2523.67859	-2523.81143	none
6m	-2643.64797	-2642.75883	-2642.70132	-2642.84332	-310.18
2n-Z	-2522.36619	-2521.60712	-2521.55580	-2521.68650	none
6n-Z	-2641.49680	-2640.63552	-2640.57900	-2640.71947	-196.62
2n-E	-2522.36940	-2521.61158	-2521.55993	-2521.69234	none
6n-E	-2641.50575	-2640.64426	-2640.58800	-2640.72756	-154.44
2o	-2561.66164	-2560.87534	-2560.82215	-2560.95750	none

6o	-2680.79193	-2679.90178	-2679.84439	-2679.98528	-280.99
2p	-2600.97736	-2600.16253	-2600.10820	-2600.24549	none
6p	-2720.10698	-2719.18863	-2719.12967	-2719.27480	-266.5
2q	-2660.88366	-2660.10372	-2660.05038	-2660.18548	none
6q	-2780.01403	-2779.13207	-2779.07346	-2779.21936	-140.46
2r	-2581.11599	-2580.28856	-2580.23417	-2580.36997	none
6r	-2700.23189	-2699.30148	-2699.24230	-2699.38720	-188.36
2s	-2658.53216	-2657.66830	-2657.61299	-2657.75213	none
6s	-2777.64864	-2776.68260	-2776.62202	-2776.77212	-187.45
2t	-2619.19049	-2618.35633	-2618.30179	-2618.43968	none
6t	-2738.31397	-2737.37621	-2737.31724	-2737.46212	-295.63
2u	-2656.25984	-2655.42937	-2655.37372	-2655.51266	none
6u	-2775.38169	-2774.44886	-2774.38890	-2774.53649	-182.41
2v	-2502.50800	-2501.73822	-2501.68611	-2501.81894	none
6v	-2621.63914	-2620.76572	-2620.70903	-2620.84902	-287.38
2w	-2541.81036	-2541.01216	-2540.95835	-2541.09561	none
6w	-2660.94114	-2660.039687	-2659.981345	-2660.125116	-331.11
2xa	-2733.53769	-2732.68439	-2732.62859	-2732.76901	none
6xa	-2852.66916	-2851.71514	-2851.65381	-2851.80516	-246.07
2xd	-3070.54246	-3069.68648	-3069.62645	-3069.77785	none
6xd	-3189.67653	-3188.71750	-3188.65276	-3188.81197	-207.94

3.4.4 ^{1}H and ^{12}C NMR Spectra

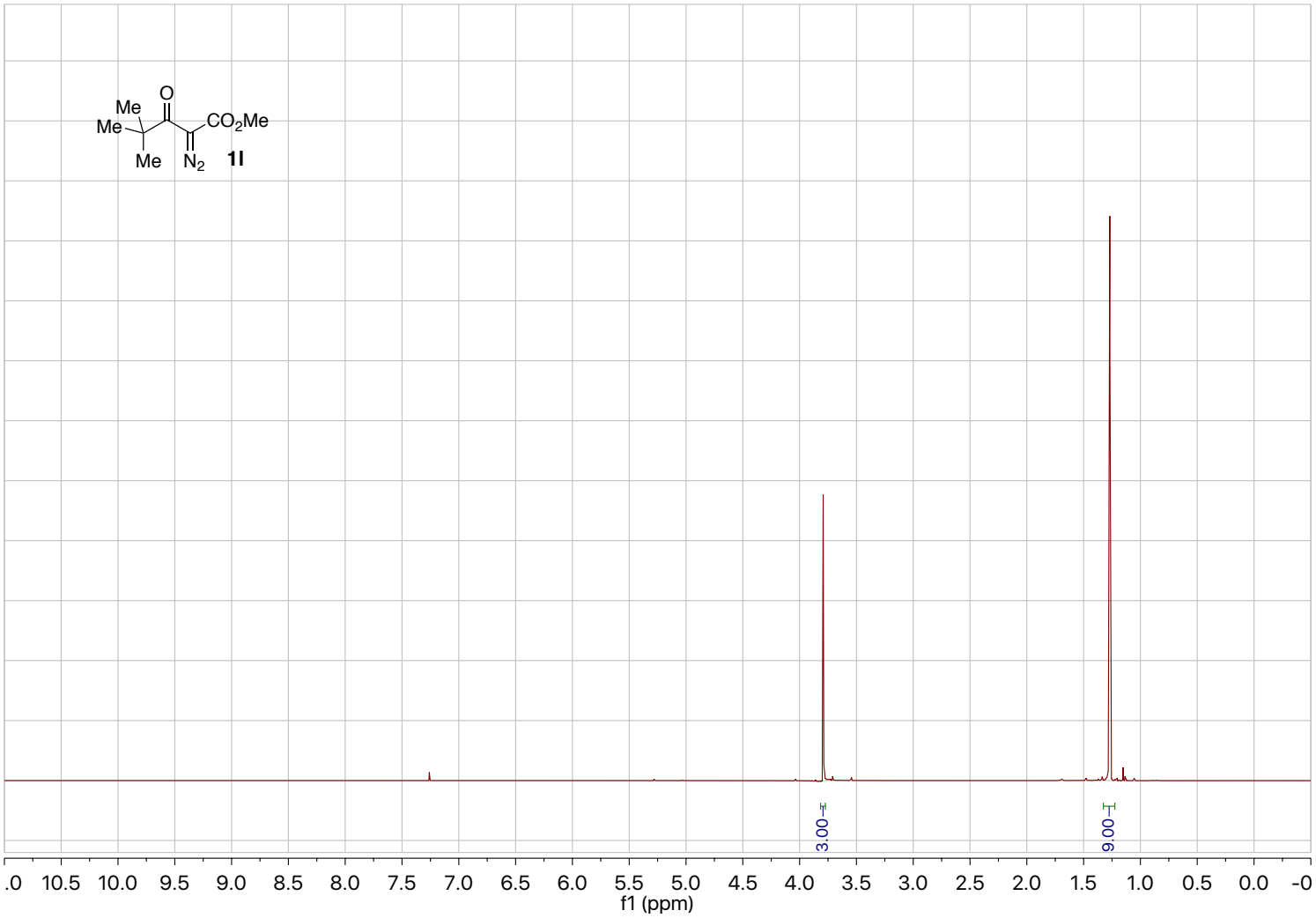
Me
Me
Me
O
CO2Me
N2
1l
3.00
9.00
.0 10.5 10.0 9.5 9.0 8.5 8.0 7.5 7.0 6.5 6.0 5.5 5.0 4.5 4.0 3.5 3.0 2.5 2.0 1.5 1.0 0.5 0.0 -0
f1 (ppm)

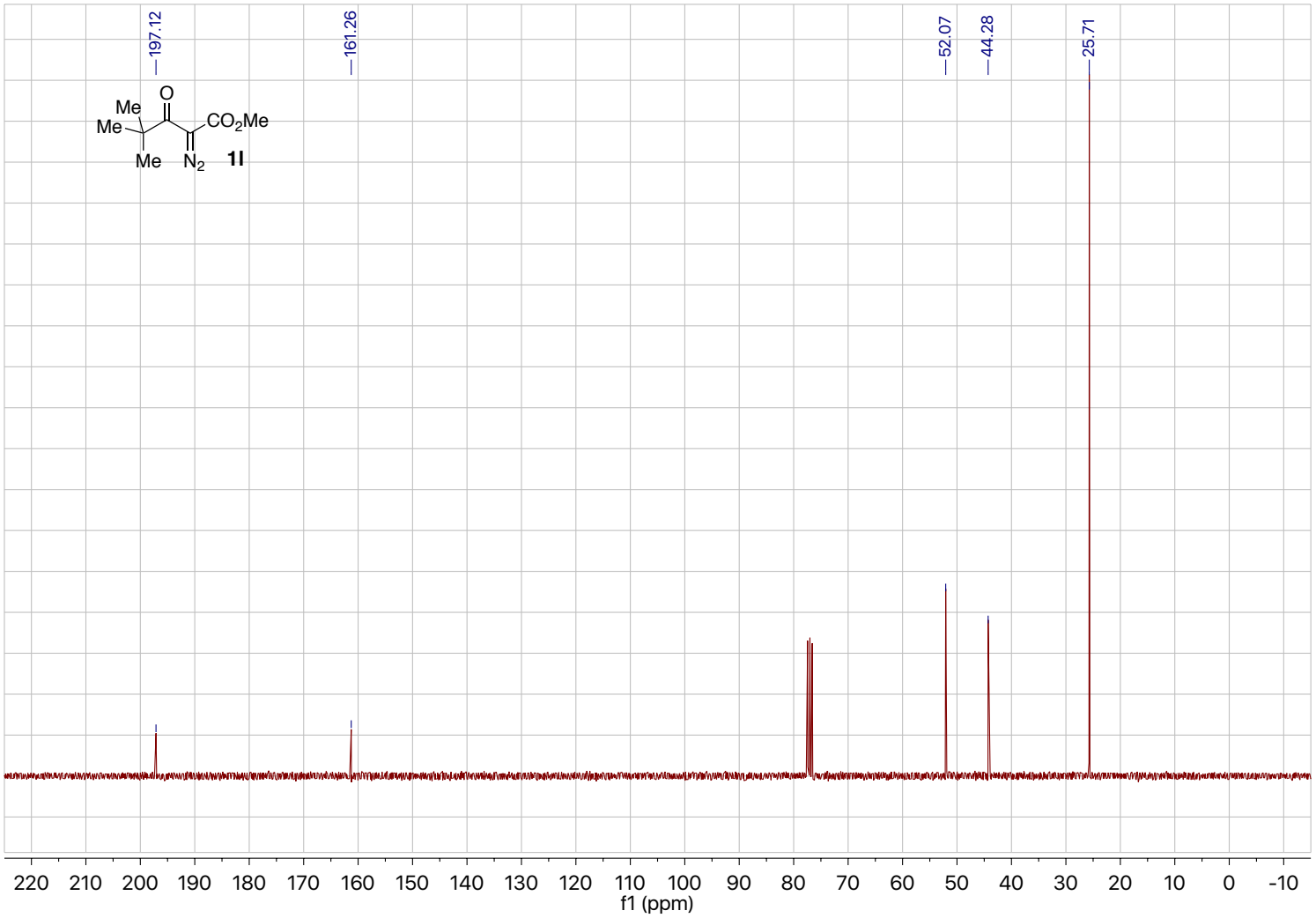
197.12
161.26
52.07
44.28
25.71
Me
Me
Me
O
CO2Me
N2
1l
220 210 200 190 180 170 160 150 140 130 120 110 100 90 80 70 60 50 40 30 20 10 0 -10
f1 (ppm)

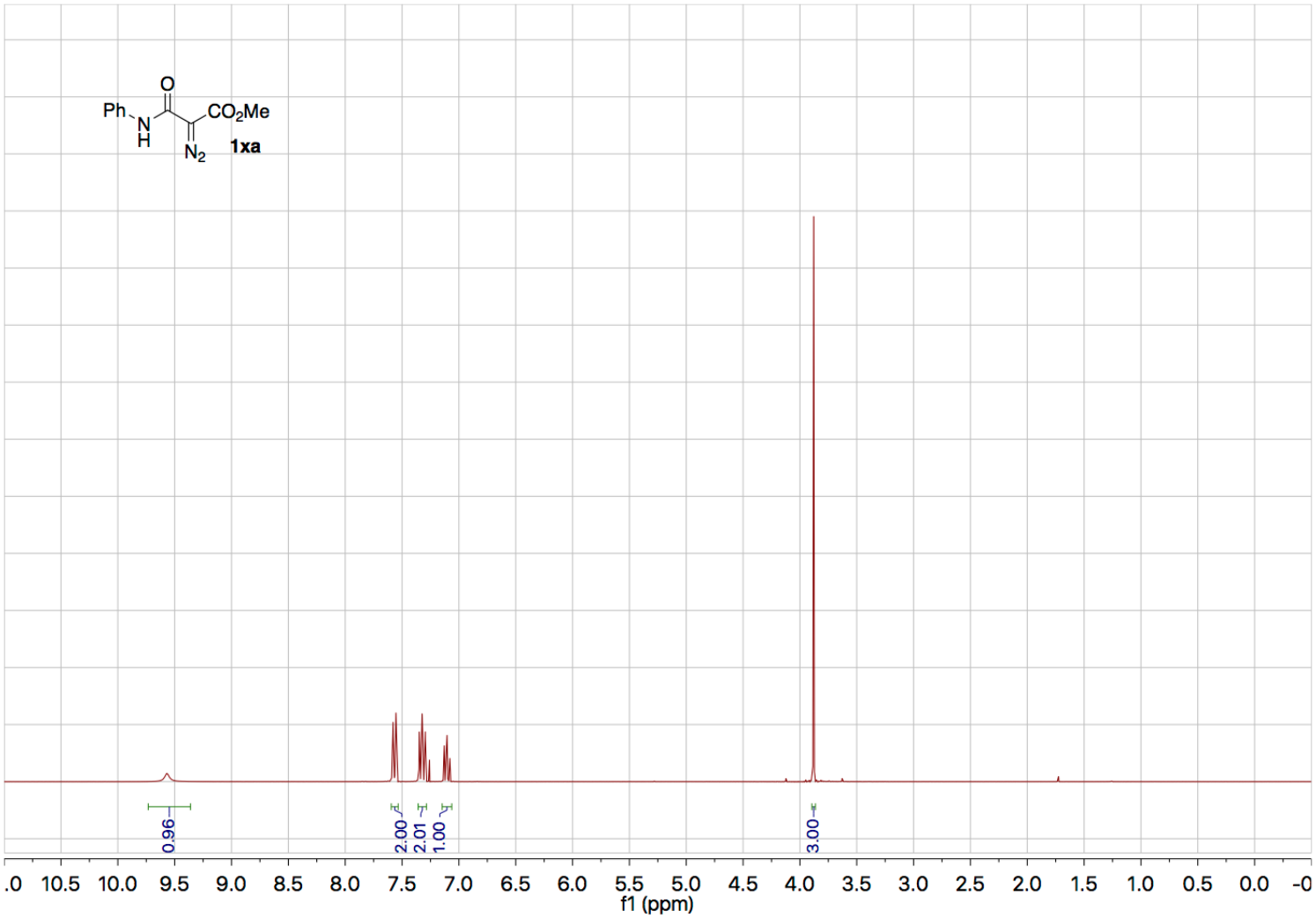
Ph
N
H
O
CO2Me
N2
1xa
0.96
2.00
2.01
1.00
3.00
.0 10.5 10.0 9.5 9.0 8.5 8.0 7.5 7.0 6.5 6.0 5.5 5.0 4.5 4.0 3.5 3.0 2.5 2.0 1.5 1.0 0.5 0.0 -0
f1 (ppm)

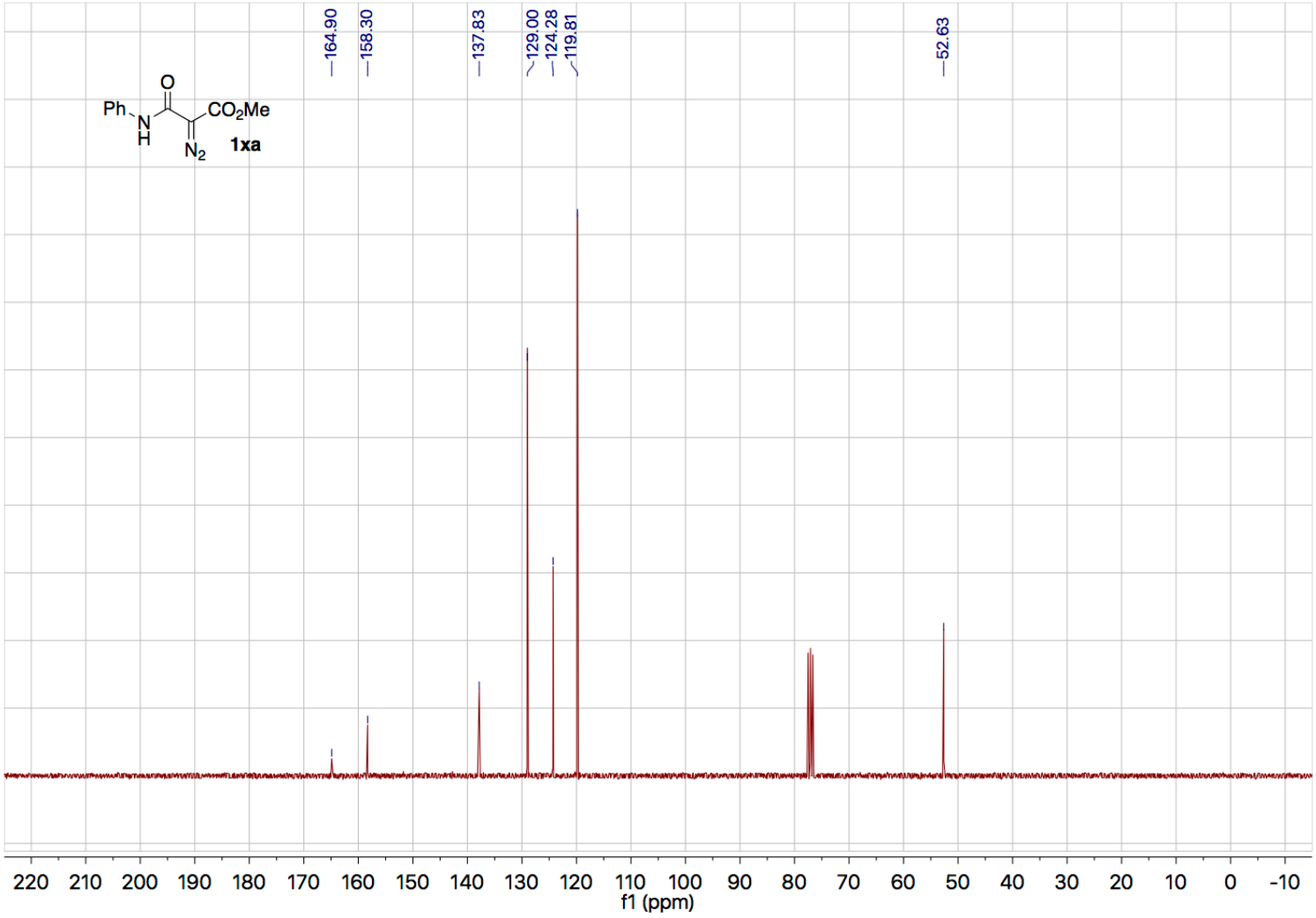
164.90
158.30
137.83
129.00
124.28
119.81
52.63
Ph
N
H
O
CO2Me
N2
1xa
220 210 200 190 180 170 160 150 140 130 120 110 100 90 80 70 60 50 40 30 20 10 0 -10
f1 (ppm)

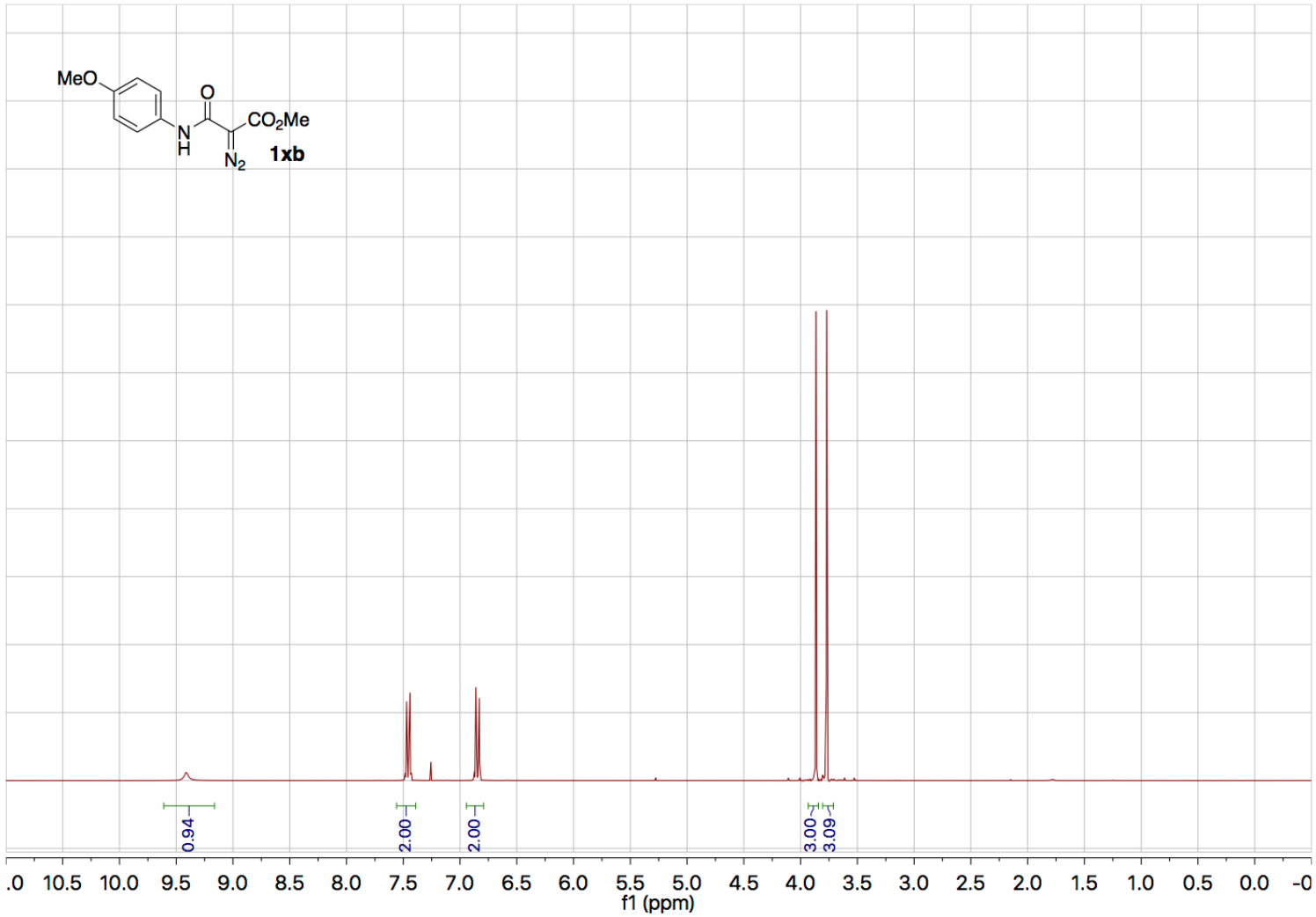
MeO
O
N
H
CO2Me
N2
1xb
0.94
2.00
2.00
3.00
3.09
.0 10.5 10.0 9.5 9.0 8.5 8.0 7.5 7.0 6.5 6.0 5.5 5.0 4.5 4.0 3.5 3.0 2.5 2.0 1.5 1.0 0.5 0.0 -0
f1 (ppm)

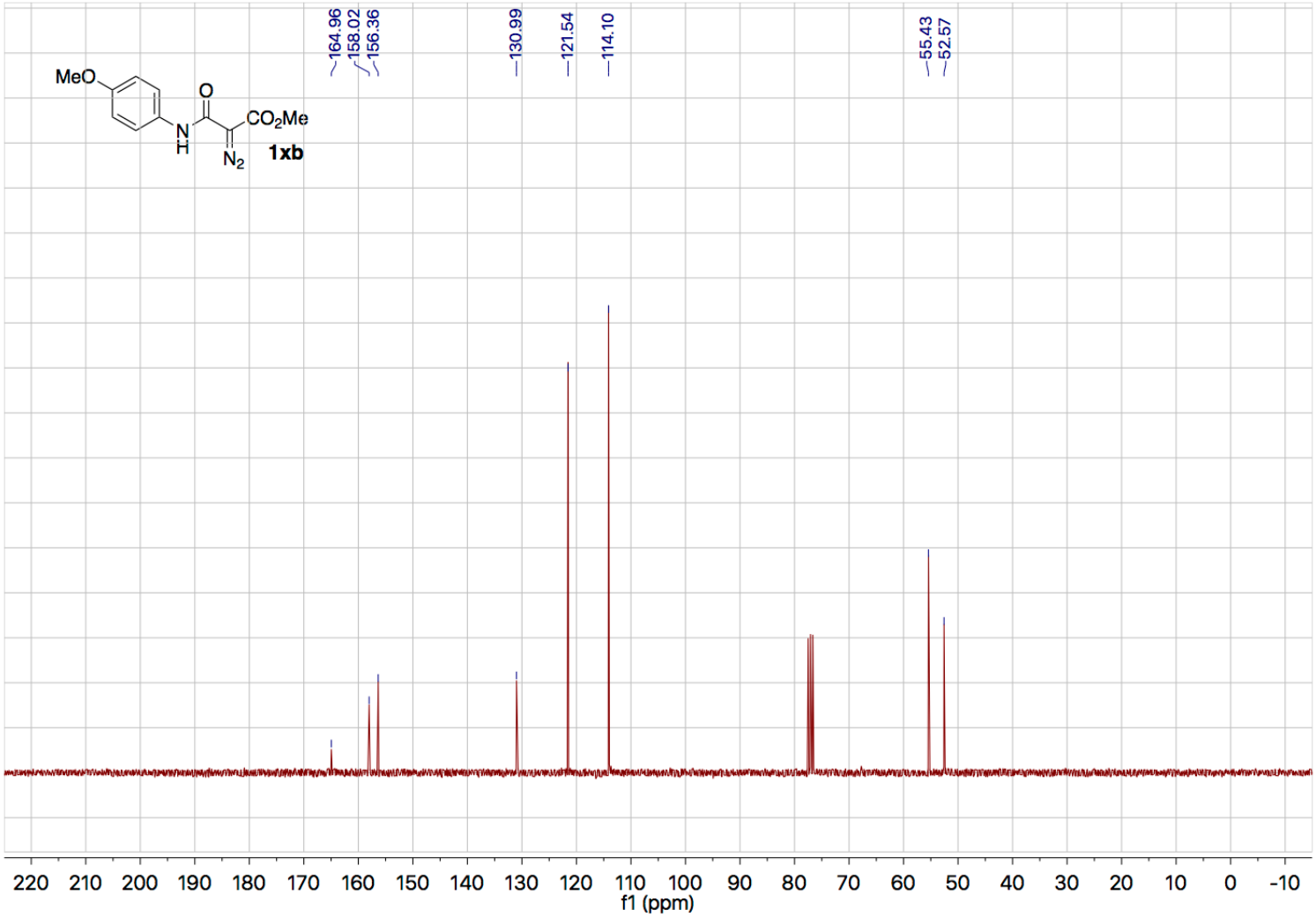
MeO
O
N
H
CO2Me
N2
1xb
164.96
158.02
156.36
130.99
121.54
114.10
55.43
52.57
220 210 200 190 180 170 160 150 140 130 120 110 100 90 80 70 60 50 40 30 20 10 0 -10
f1 (ppm)

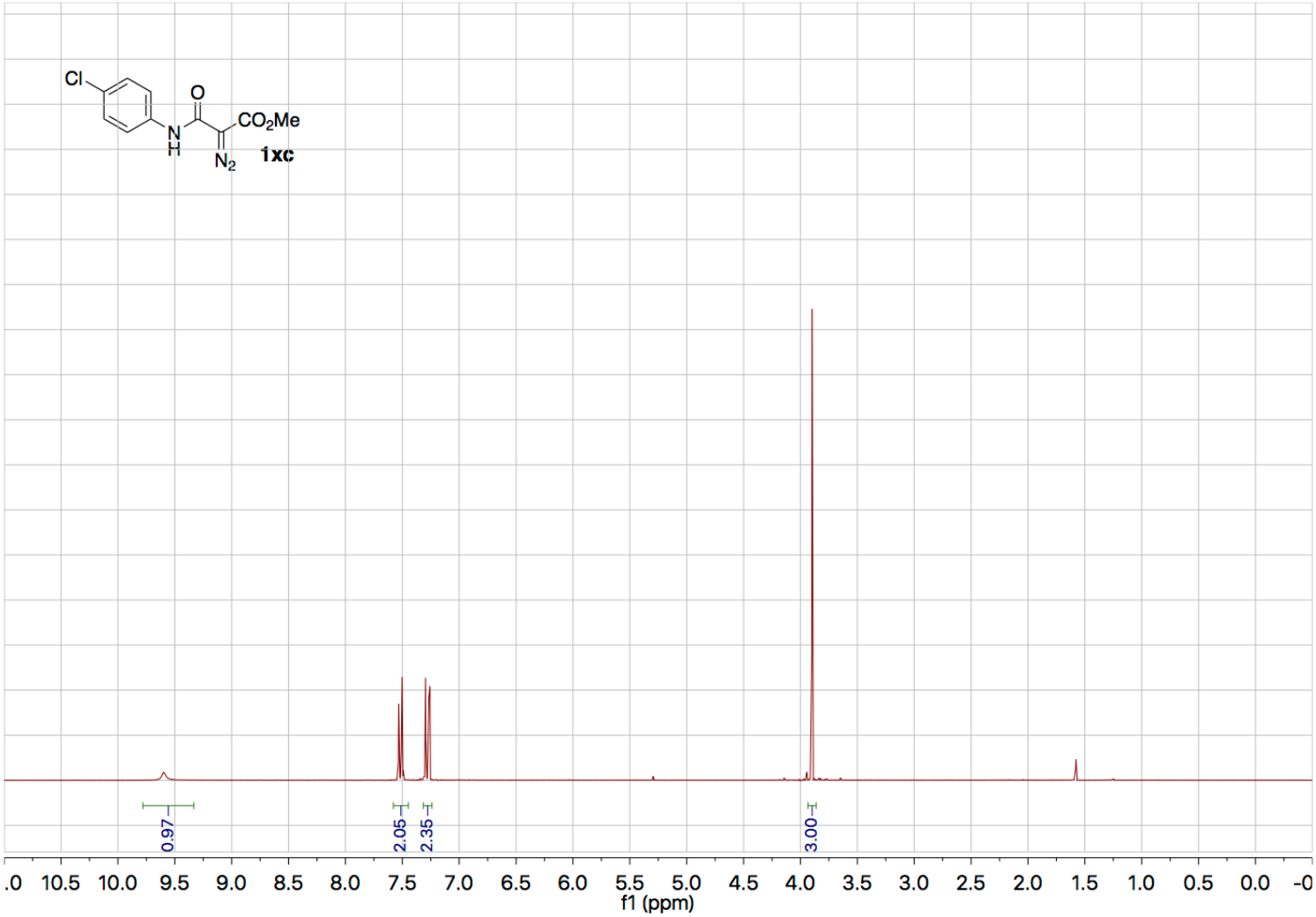
Cl
O
N
H
CO2Me
N2
1xc
0.97
2.05
2.35
3.00
.0 10.5 10.0 9.5 9.0 8.5 8.0 7.5 7.0 6.5 6.0 5.5 5.0 4.5 4.0 3.5 3.0 2.5 2.0 1.5 1.0 0.5 0.0 -0
f1 (ppm)

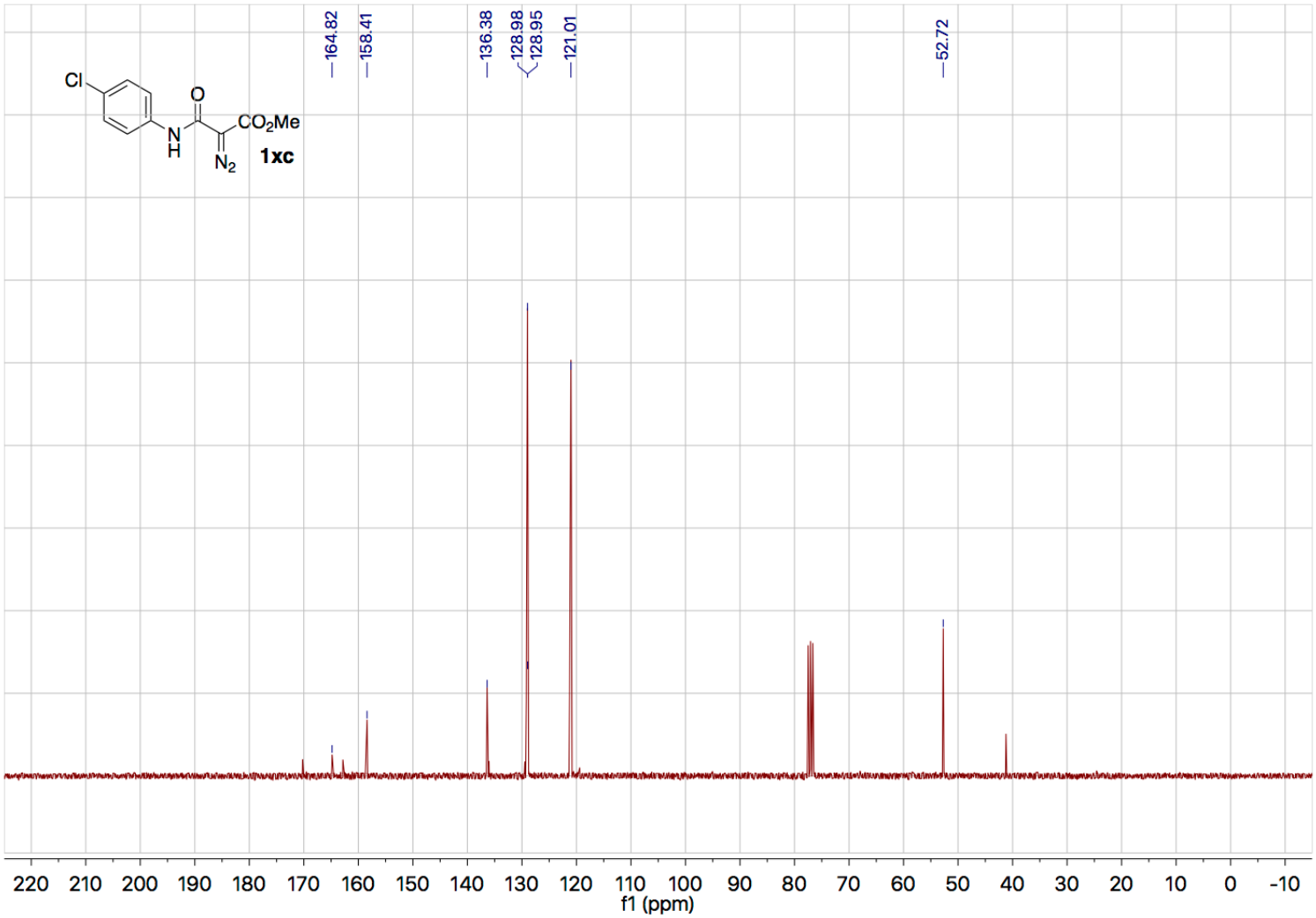
Cl
O
N
H
CO2Me
N2
1xc
164.82
158.41
136.38
128.98
128.95
121.01
52.72
220 210 200 190 180 170 160 150 140 130 120 110 100 90 80 70 60 50 40 30 20 10 0 -10
f1 (ppm)

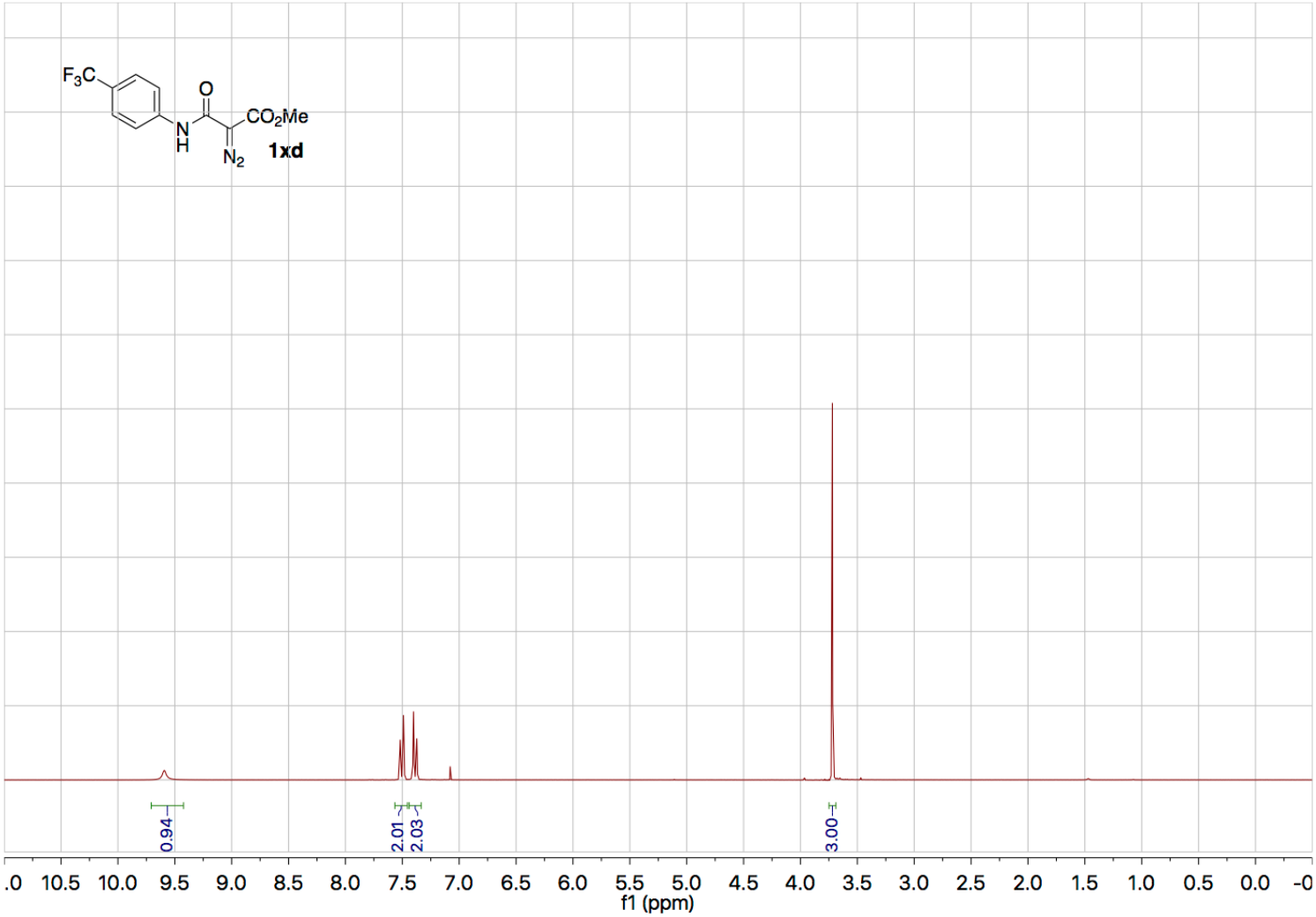
F3C
O
CO2Me
N
H
N2
1xd
0.94
2.01
2.03
3.00
.0 10.5 10.0 9.5 9.0 8.5 8.0 7.5 7.0 6.5 6.0 5.5 5.0 4.5 4.0 3.5 3.0 2.5 2.0 1.5 1.0 0.5 0.0 -0
f1 (ppm)

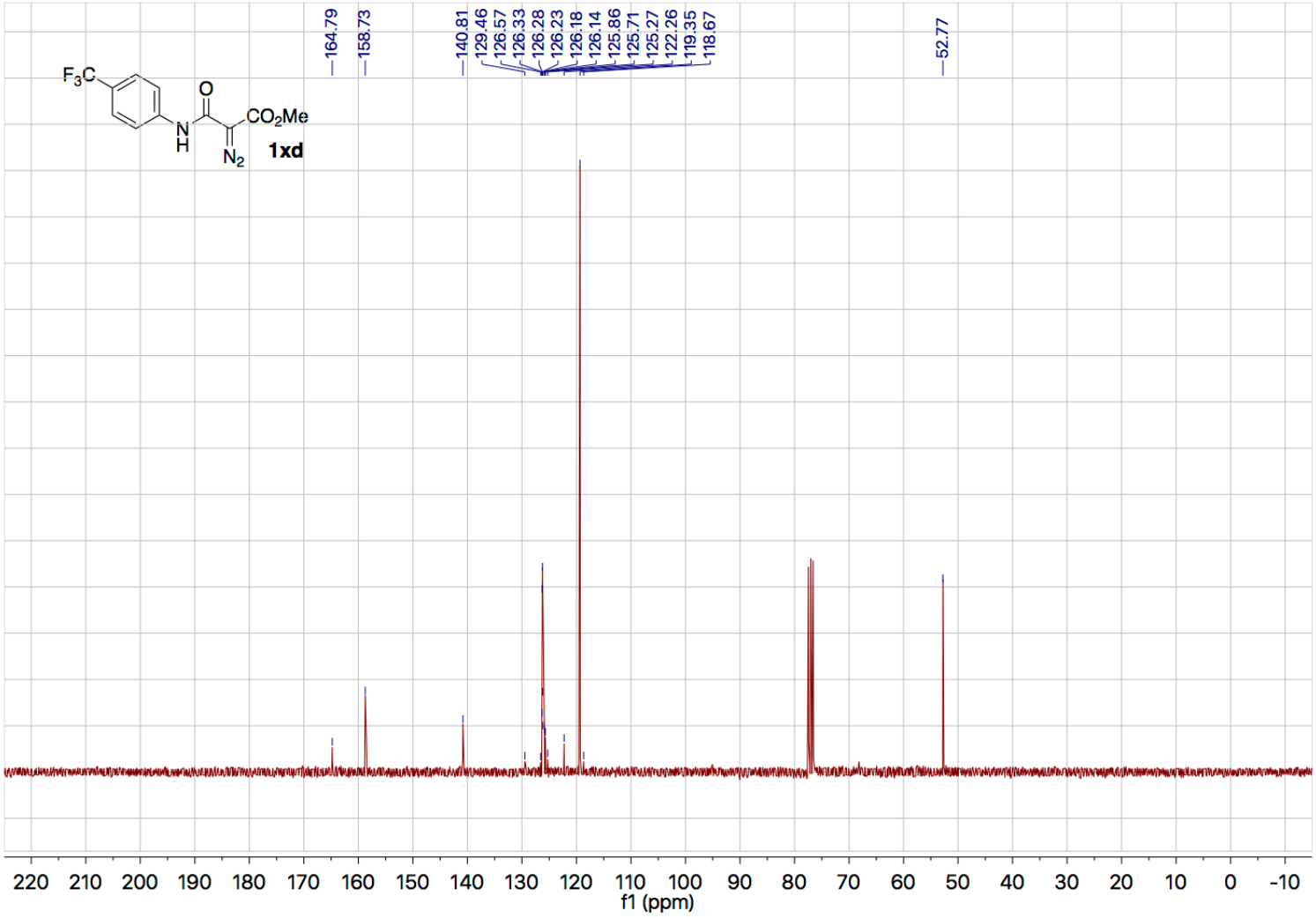
164.79
158.73
140.81
129.46
126.57
126.33
126.28
126.23
126.18
126.14
125.86
125.71
125.27
122.26
119.35
118.67
52.77
F3C
O
N
H
CO2Me
N2
1xd
220 210 200 190 180 170 160 150 140 130 120 110 100 90 80 70 60 50 40 30 20 10 0 -10
f1 (ppm)

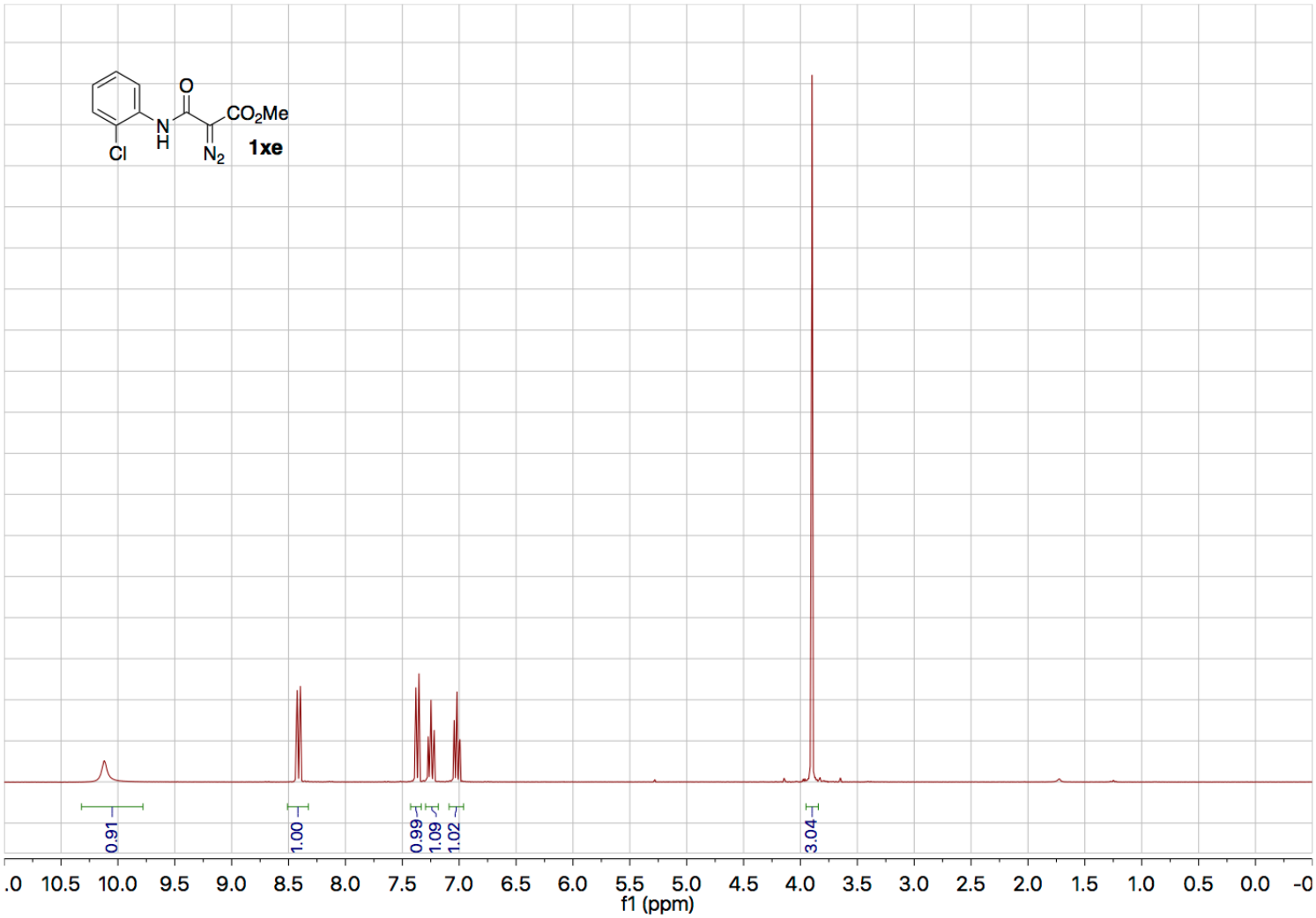
O
CO2Me
N
H
Cl
N2
1xe
0.91
1.00
0.99
1.09
1.02
3.04
.0 10.5 10.0 9.5 9.0 8.5 8.0 7.5 7.0 6.5 6.0 5.5 5.0 4.5 4.0 3.5 3.0 2.5 2.0 1.5 1.0 0.5 0.0 -0
f1 (ppm)

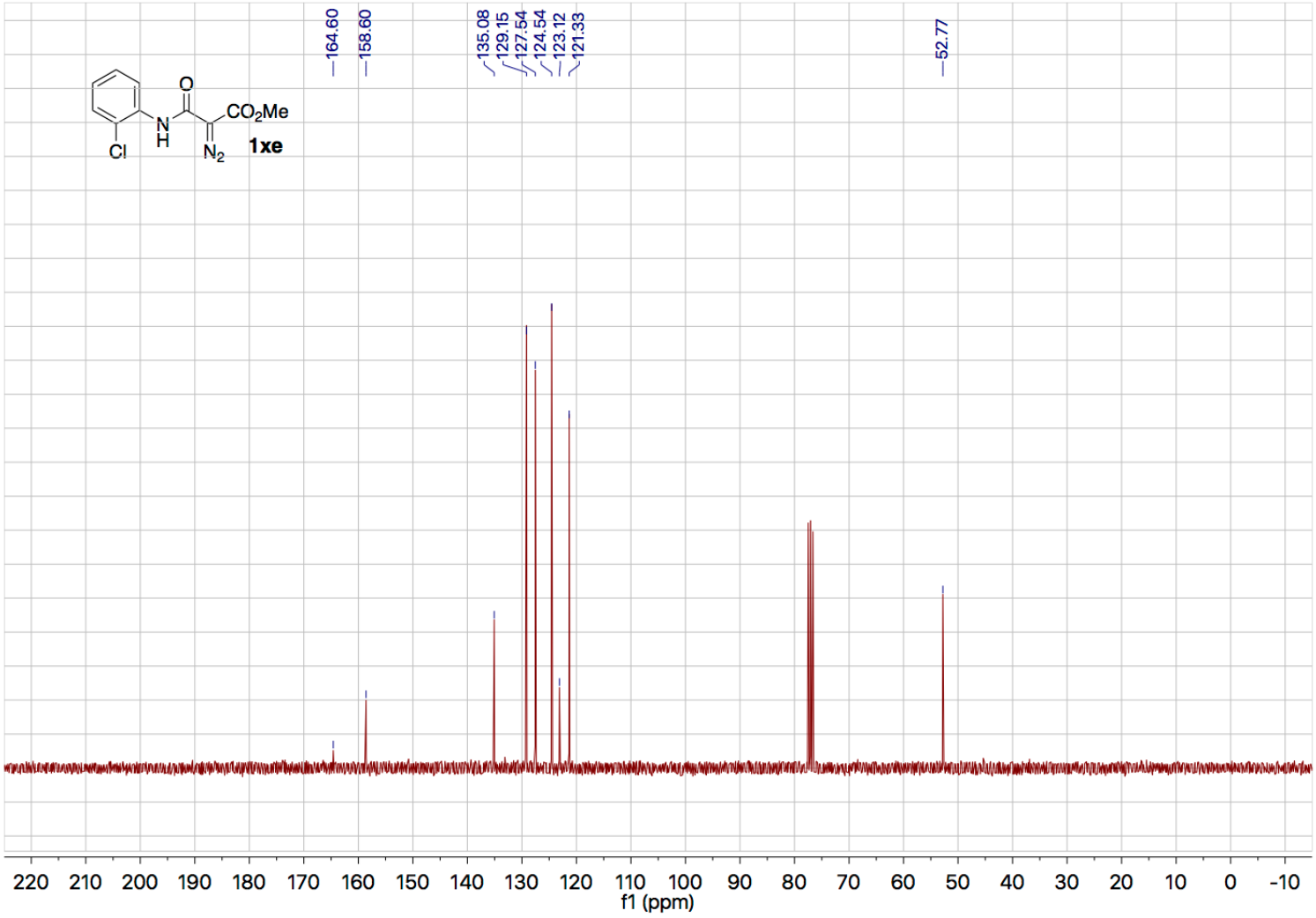
164.60
158.60
135.08
129.15
127.54
124.54
123.12
121.33
52.77
O
N
H
CO2Me
N2
Cl
1xe
220 210 200 190 180 170 160 150 140 130 120 110 100 90 80 70 60 50 40 30 20 10 0 -10
f1 (ppm)

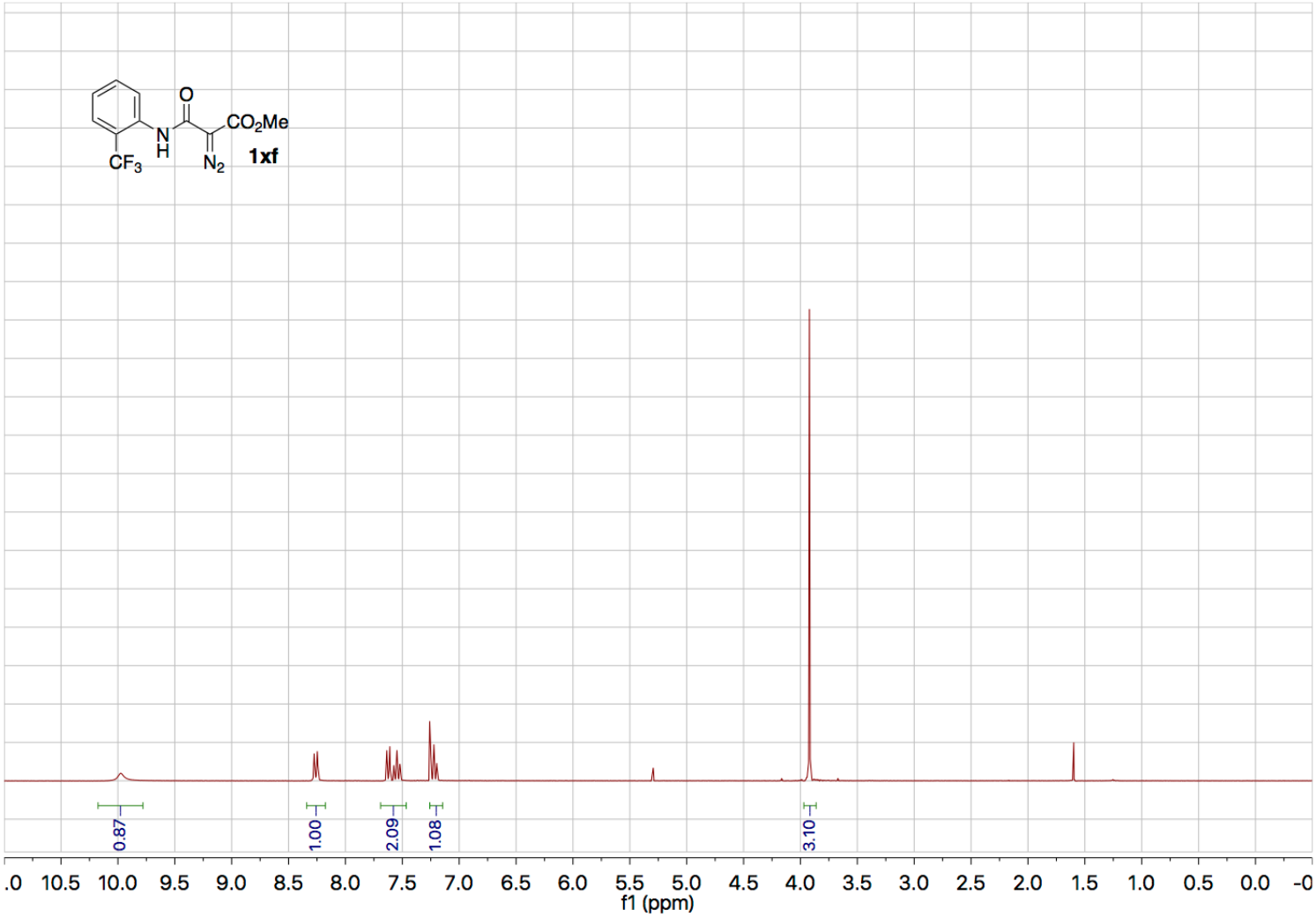
O
N
H
CO2Me
N2
CF3
1xf
0.87
1.00
2.09
1.08
3.10
.0 10.5 10.0 9.5 9.0 8.5 8.0 7.5 7.0 6.5 6.0 5.5 5.0 4.5 4.0 3.5 3.0 2.5 2.0 1.5 1.0 0.5 0.0 -0
f1 (ppm)

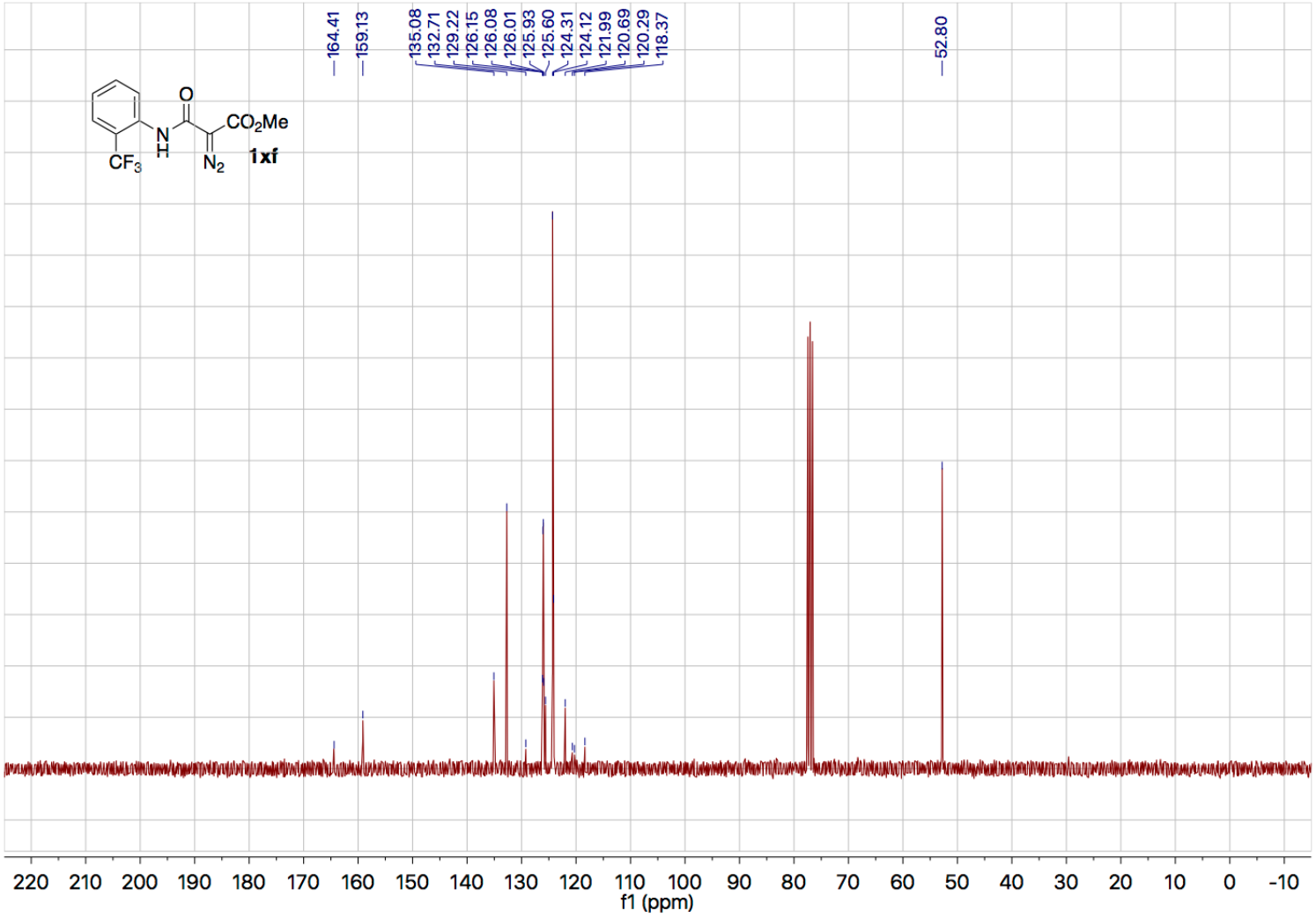
164.41
159.13
135.08
132.71
129.22
126.15
126.08
126.01
125.93
125.60
124.31
124.12
121.99
120.69
120.29
118.37
52.80
O
N
H
CO2Me
N2
CF3
1xf
220 210 200 190 180 170 160 150 140 130 120 110 100 90 80 70 60 50 40 30 20 10 0 -10
f1 (ppm)

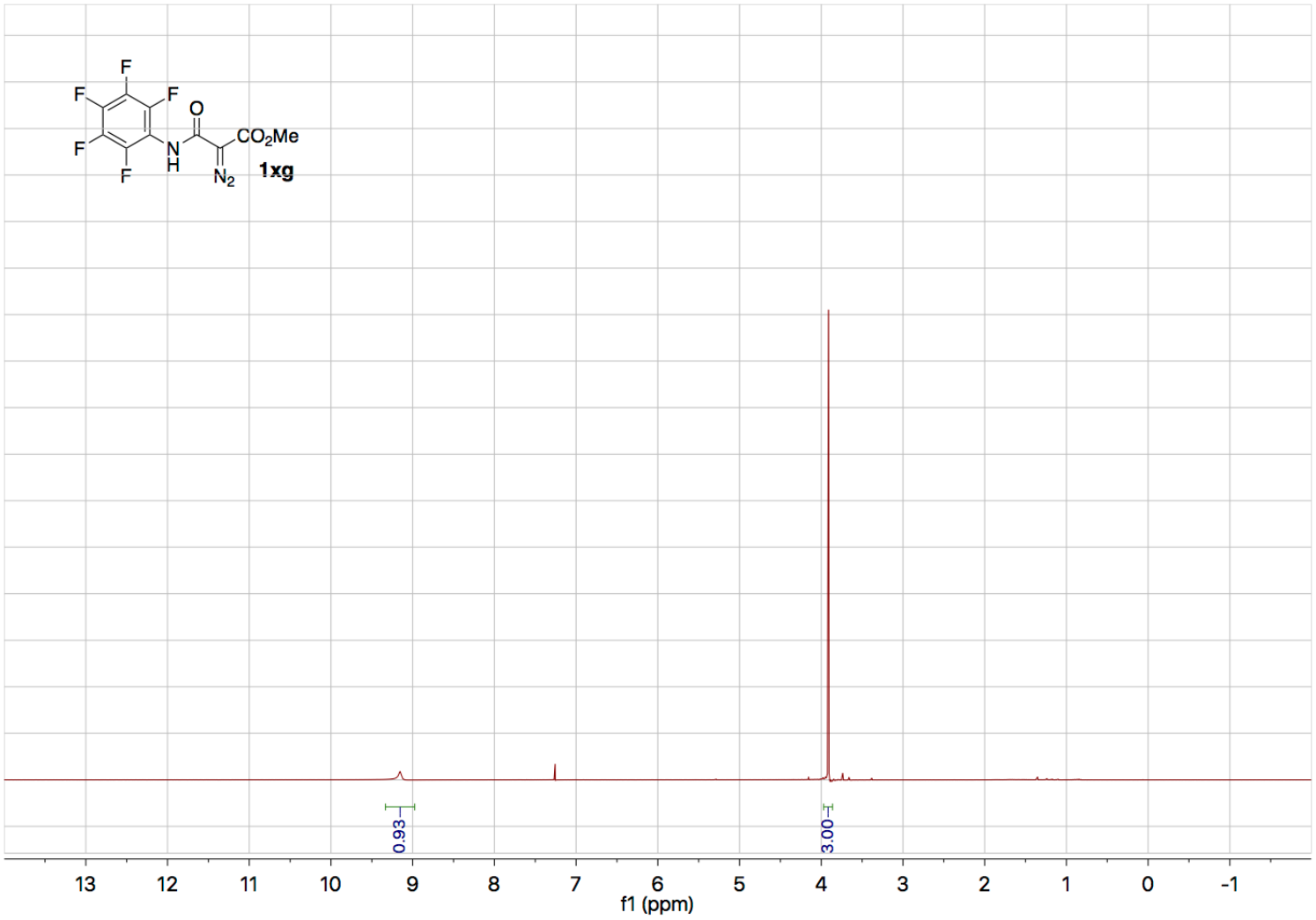
F
F
F
F
F
O
N
H
CO2Me
N2
1xg
0.93
3.00
13
12
11
10
9
8
7
6
5
4
3
2
1
0
-1
f1 (ppm)

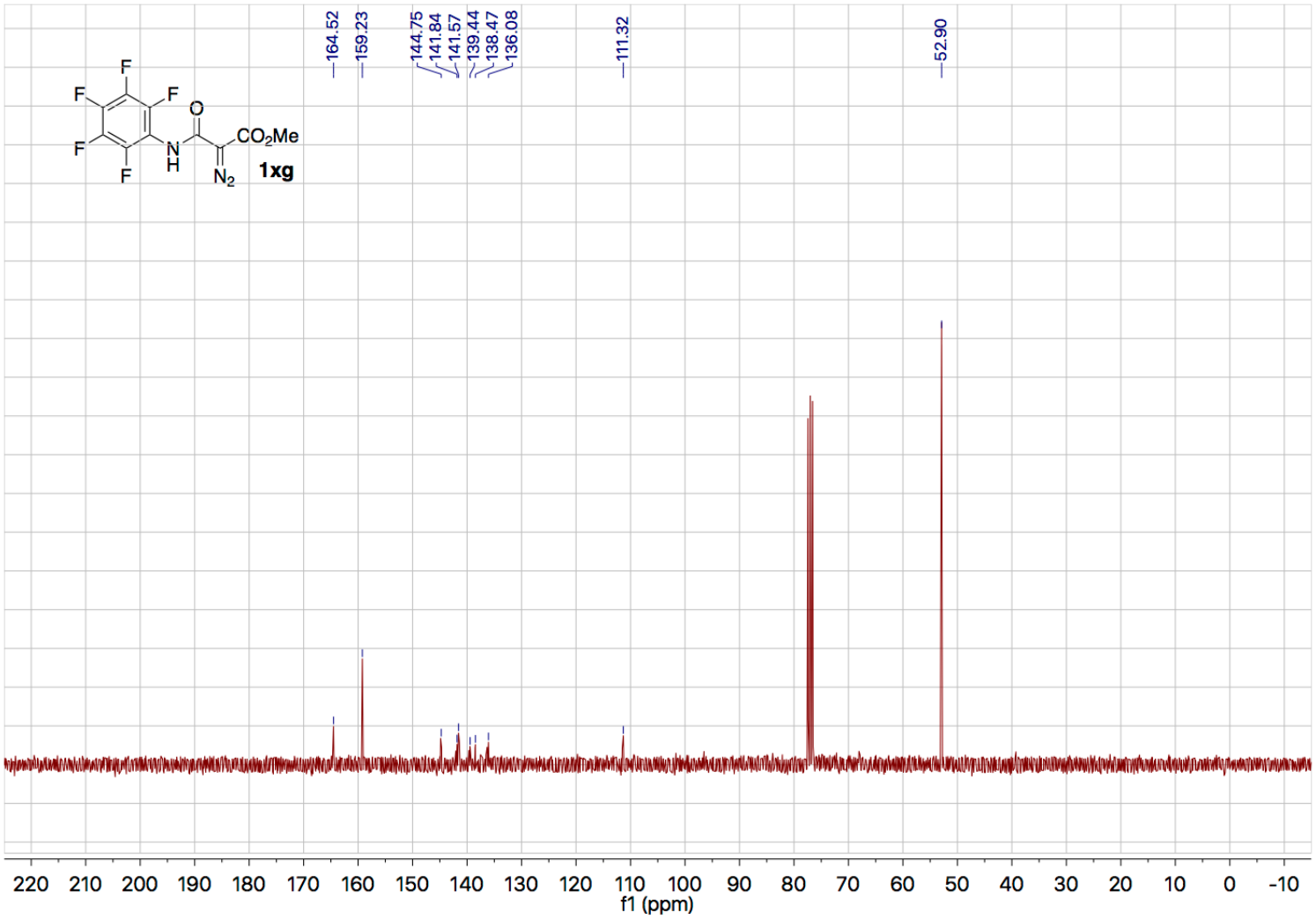
164.52
159.23
144.75
141.84
141.57
139.44
138.47
136.08
111.32
52.90
F
F
F
F
F
O
N
H
CO2Me
N2
1xg
220 210 200 190 180 170 160 150 140 130 120 110 100 90 80 70 60 50 40 30 20 10 0 -10
f1 (ppm)

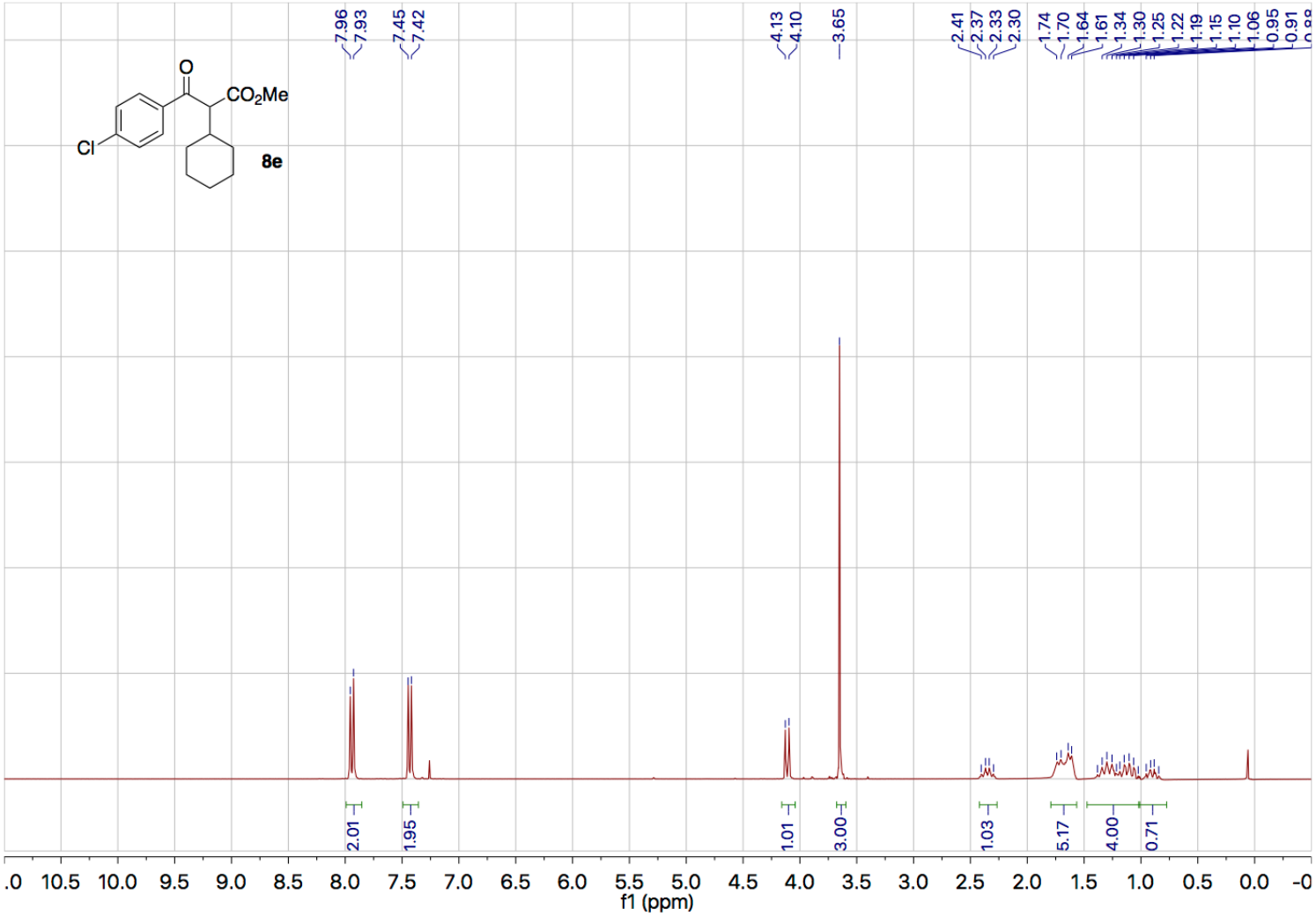
O
CO2Me
Cl
8e
7.96
7.93
7.45
7.42
4.13
4.10
3.65
2.41
2.37
2.33
2.30
1.74
1.70
1.64
1.61
1.34
1.30
1.25
1.22
1.19
1.15
1.10
1.06
0.95
0.91
2.01
1.95
1.01
3.00
1.03
5.17
4.00
0.71
f1 (ppm)

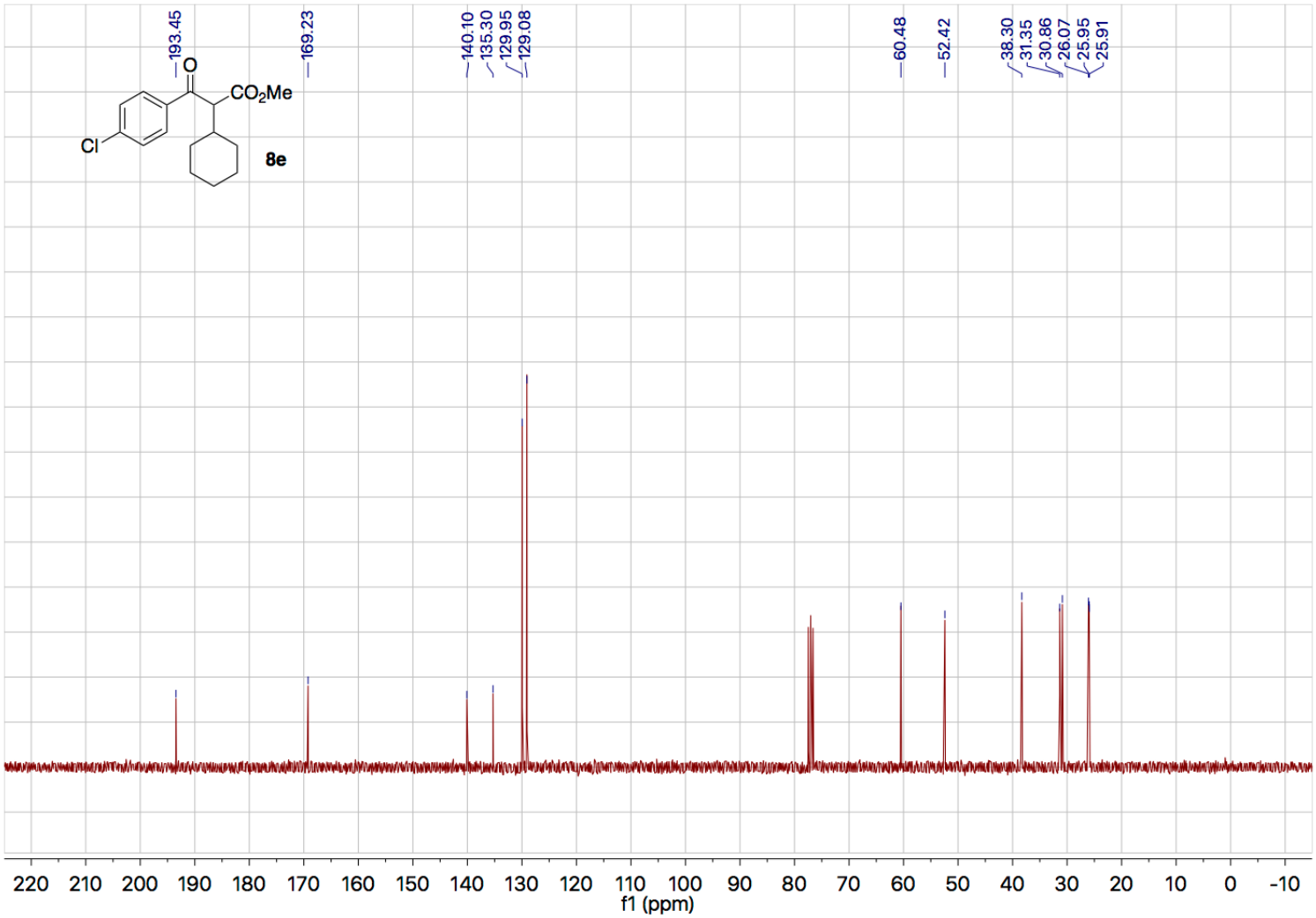
193.45
169.23
140.10
135.30
129.95
129.08
60.48
52.42
38.30
31.35
30.86
26.07
25.95
25.91
O
CO2Me
Cl
8e
220 210 200 190 180 170 160 150 140 130 120 110 100 90 80 70 60 50 40 30 20 10 0 -10
f1 (ppm)

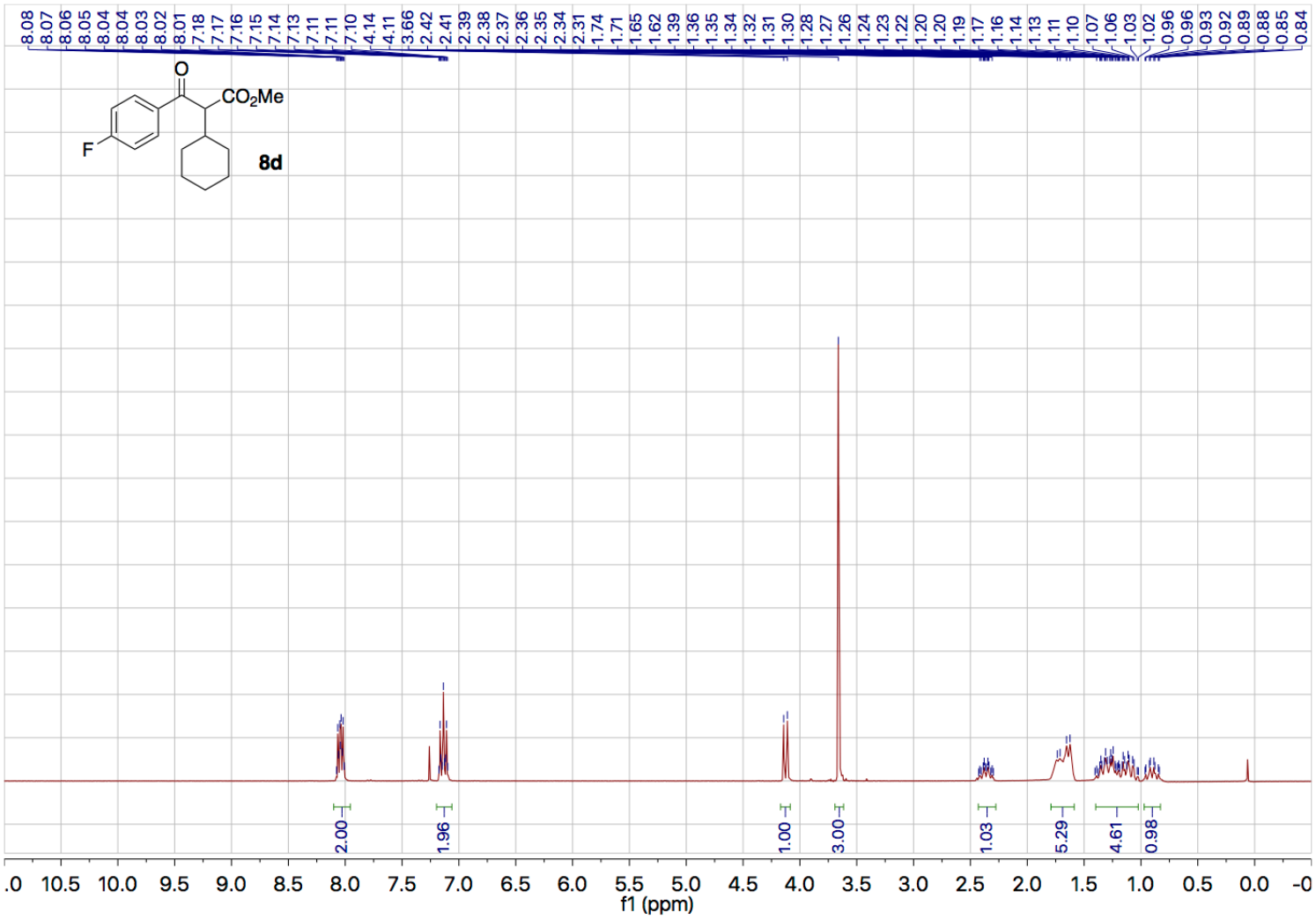
O
CO2Me
F
8d
f1 (ppm)

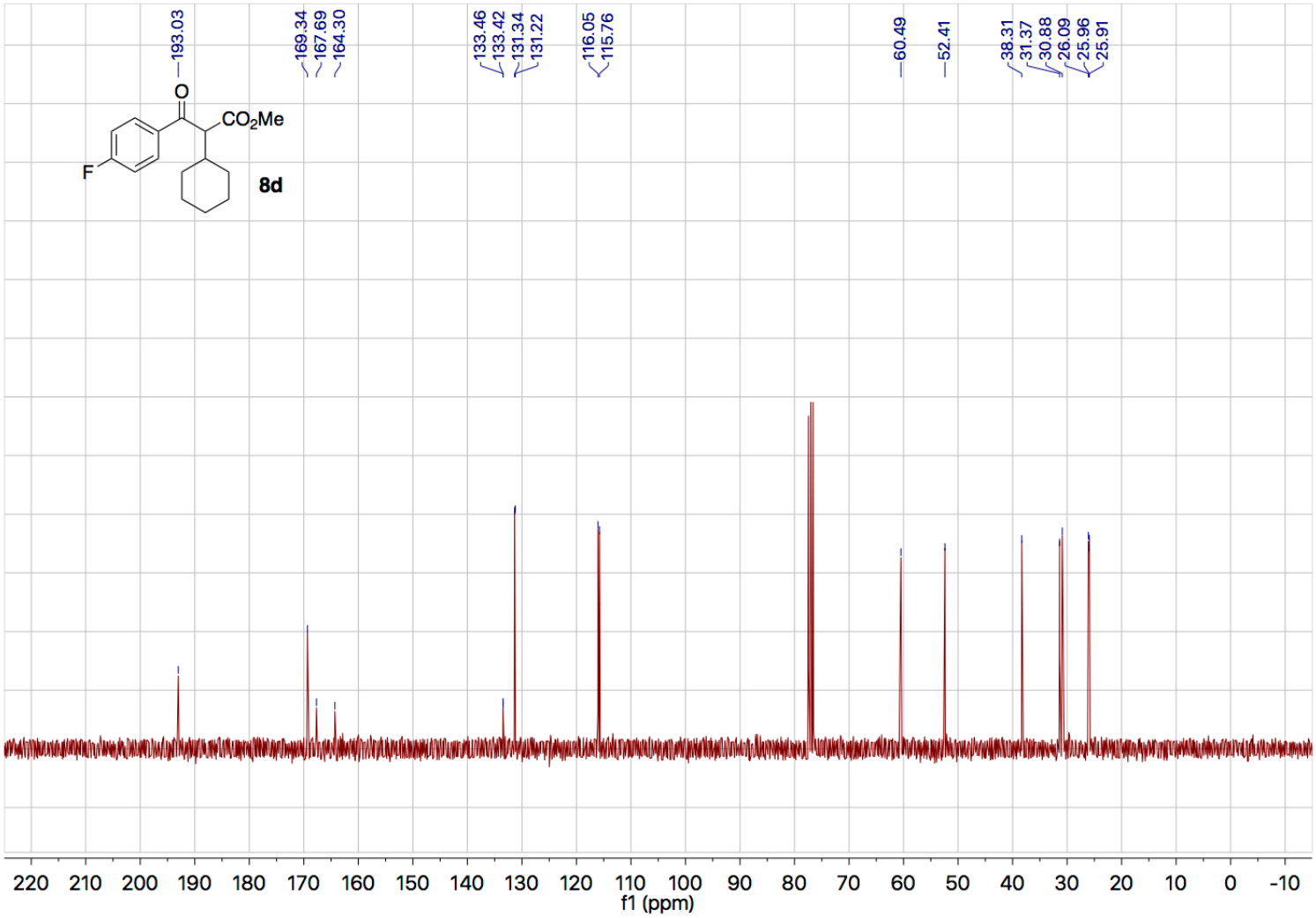
193.03
169.34
167.69
164.30
133.46
133.42
131.34
131.22
116.05
115.76
60.49
52.41
38.31
31.37
30.88
26.09
25.96
25.91
O
CO2Me
F
8d
220 210 200 190 180 170 160 150 140 130 120 110 100 90 80 70 60 50 40 30 20 10 0 -10
f1 (ppm)

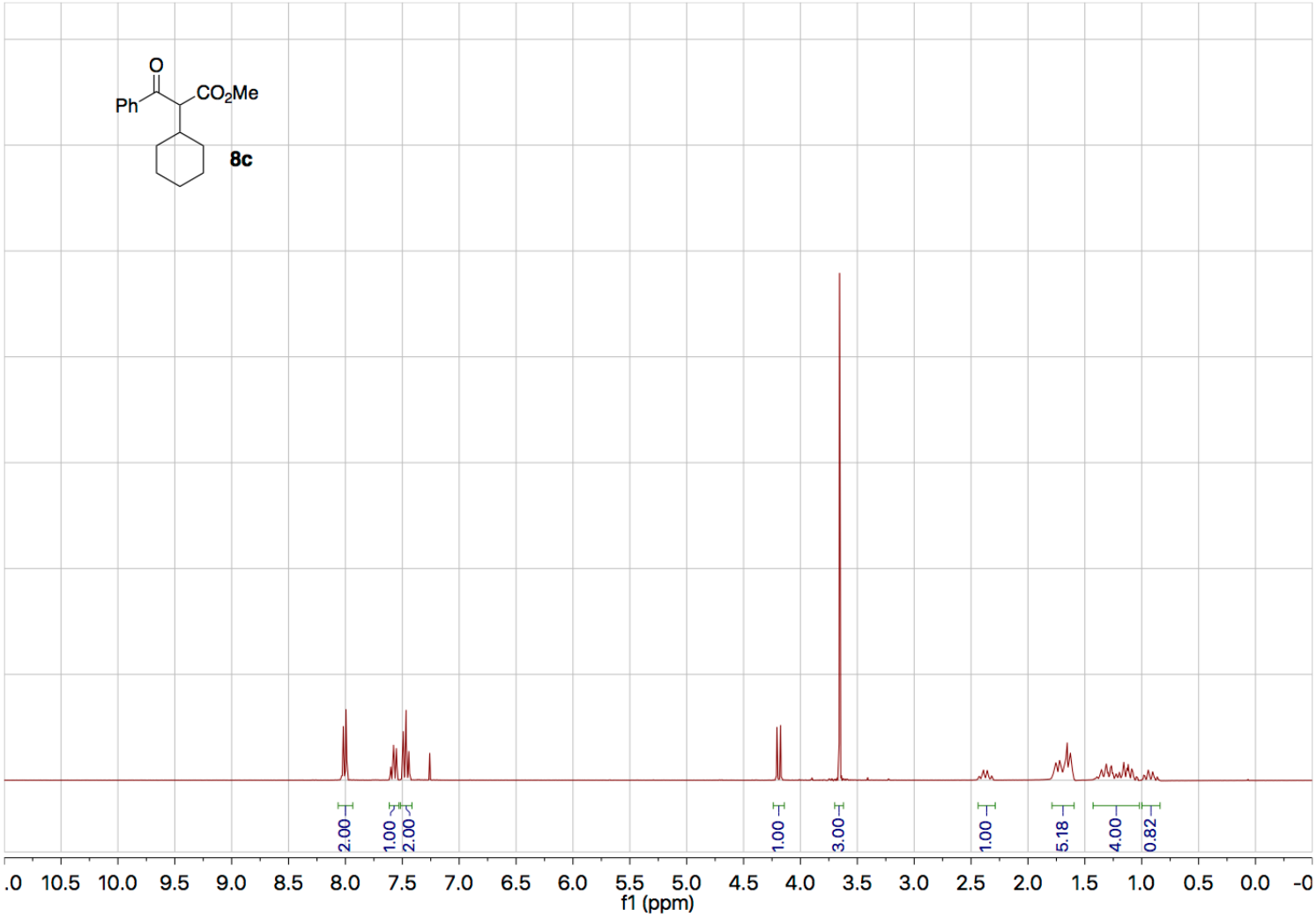
O
Ph
CO2Me
8c
2.00
1.00
2.00
1.00
3.00
1.00
5.18
4.00
0.82
.0 10.5 10.0 9.5 9.0 8.5 8.0 7.5 7.0 6.5 6.0 5.5 5.0 4.5 4.0 3.5 3.0 2.5 2.0 1.5 1.0 0.5 0.0 -0
f1 (ppm)

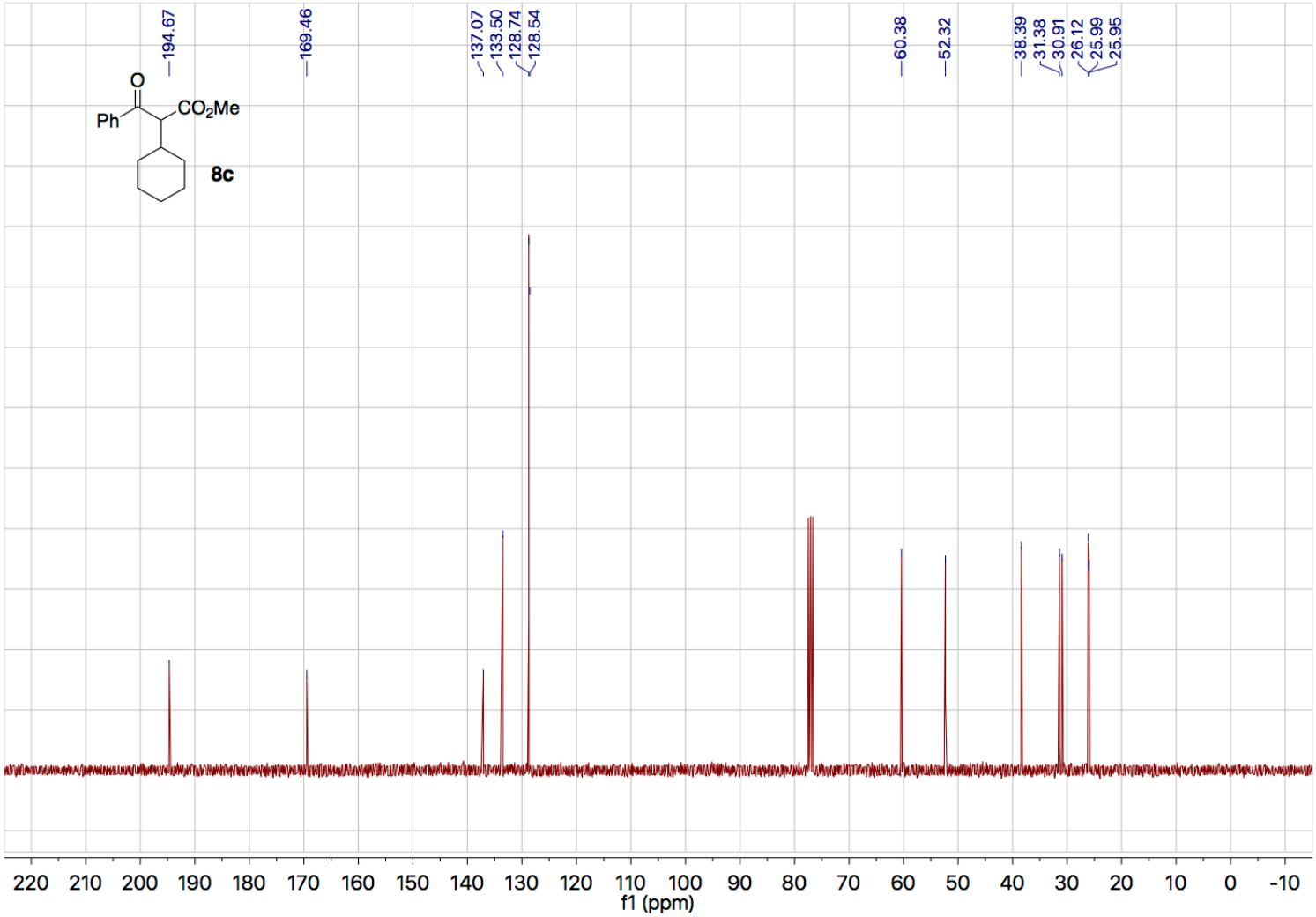
194.67
169.46
137.07
133.50
128.74
128.54
60.38
52.32
38.39
31.38
30.91
26.12
25.99
25.95
O
Ph
CO2Me
8c
220 210 200 190 180 170 160 150 140 130 120 110 100 90 80 70 60 50 40 30 20 10 0 -10
f1 (ppm)

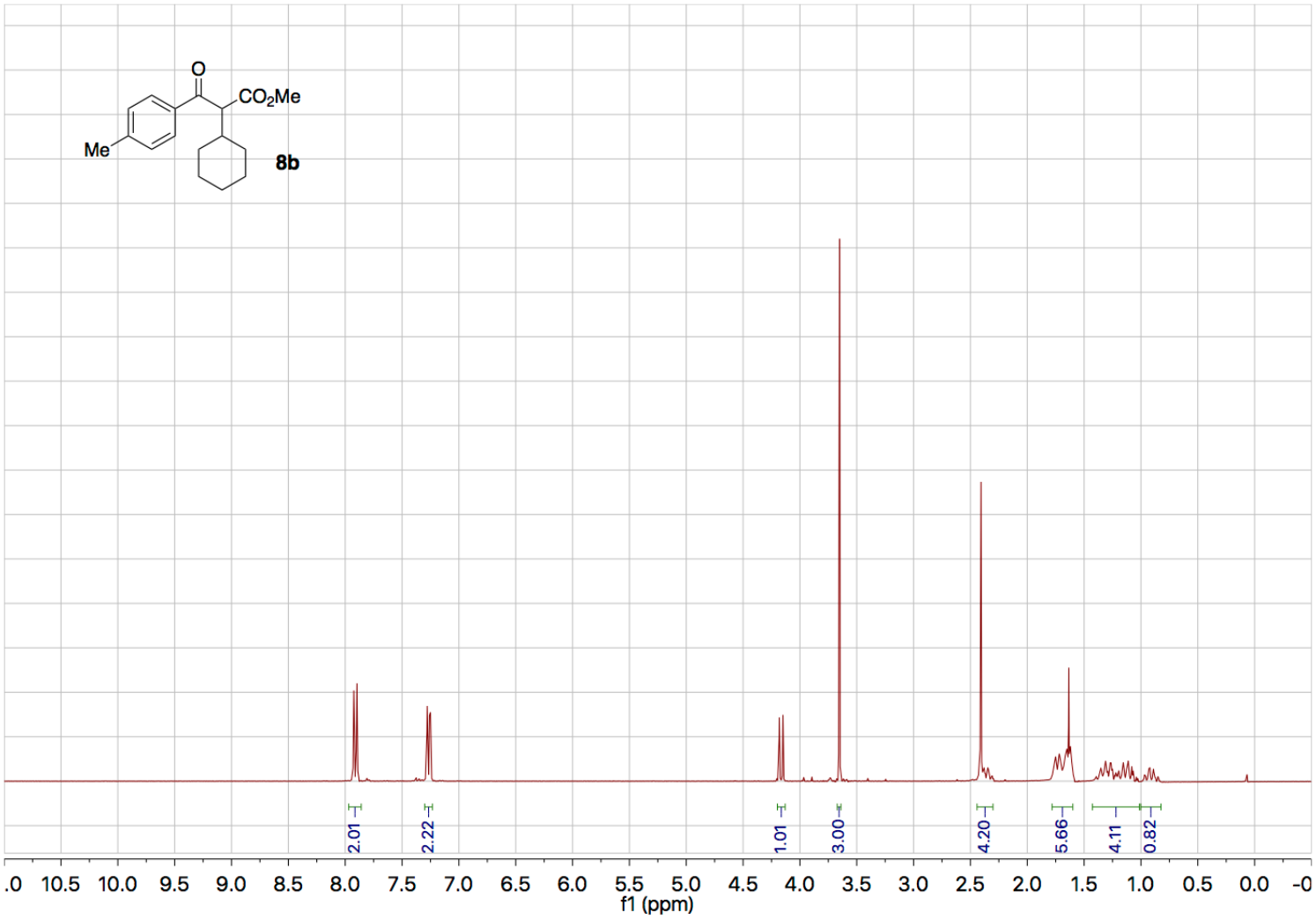
O
CO2Me
Me
8b
2.01
2.22
1.01
3.00
4.20
5.66
4.11
0.82
.0 10.5 10.0 9.5 9.0 8.5 8.0 7.5 7.0 6.5 6.0 5.5 5.0 4.5 4.0 3.5 3.0 2.5 2.0 1.5 1.0 0.5 0.0 -0
f1 (ppm)

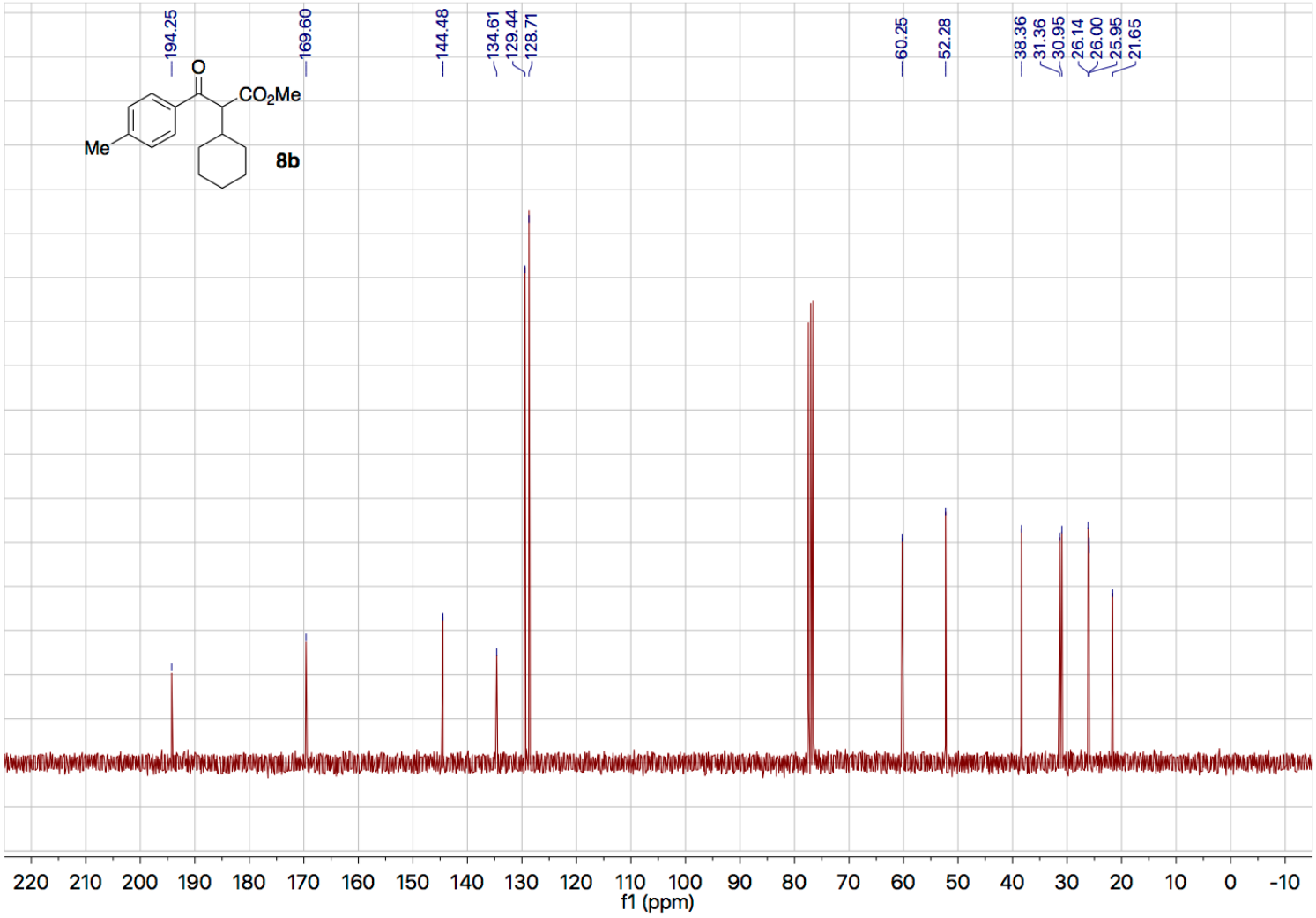
194.25
169.60
144.48
134.61
129.44
128.71
60.25
52.28
38.36
31.36
30.95
26.14
26.00
25.95
21.65
O
CO2Me
Me
8b
220 210 200 190 180 170 160 150 140 130 120 110 100 90 80 70 60 50 40 30 20 10 0 -10
f1 (ppm)

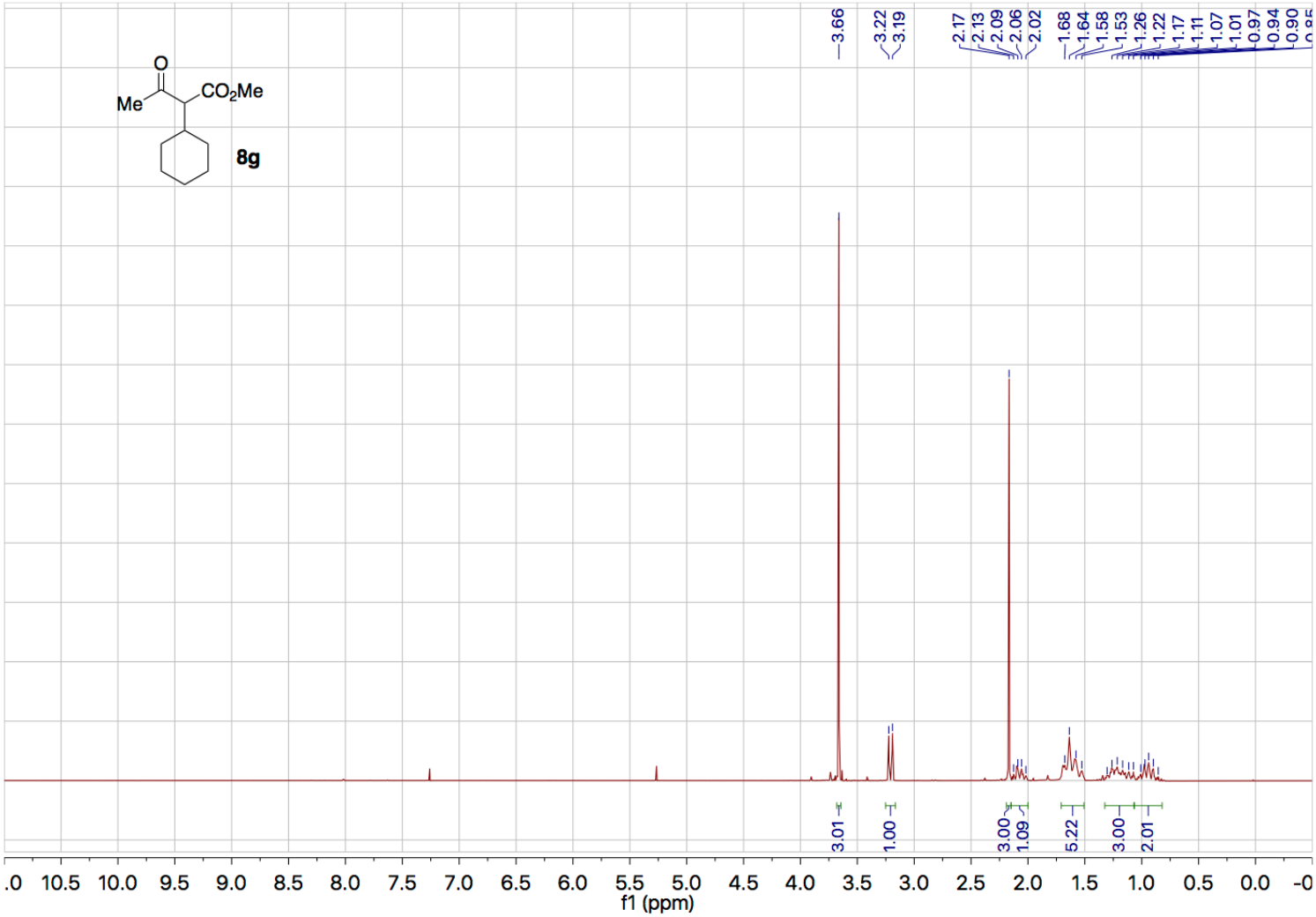
Me
O
CO2Me
8g
3.66
3.22
3.19
2.17
2.13
2.09
2.06
2.02
1.68
1.64
1.58
1.53
1.26
1.22
1.17
1.11
1.07
1.01
0.97
0.94
0.90
3.01
1.00
3.00
1.09
5.22
3.00
2.01
f1 (ppm)

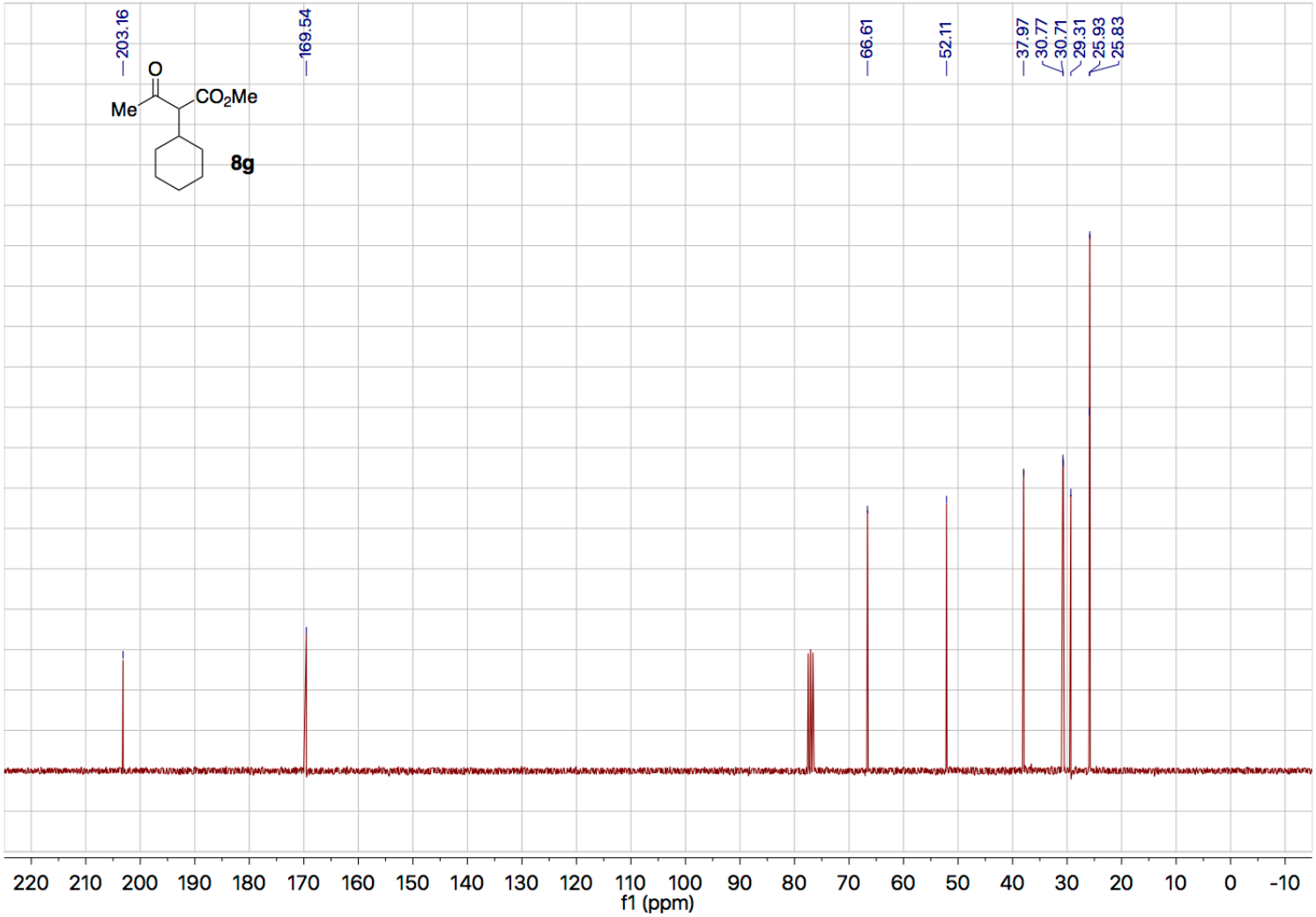
203.16
169.54
66.61
52.11
37.97
30.77
30.71
29.31
25.93
25.83
O
Me
CO2Me
8g
220 210 200 190 180 170 160 150 140 130 120 110 100 90 80 70 60 50 40 30 20 10 0 -10
f1 (ppm)

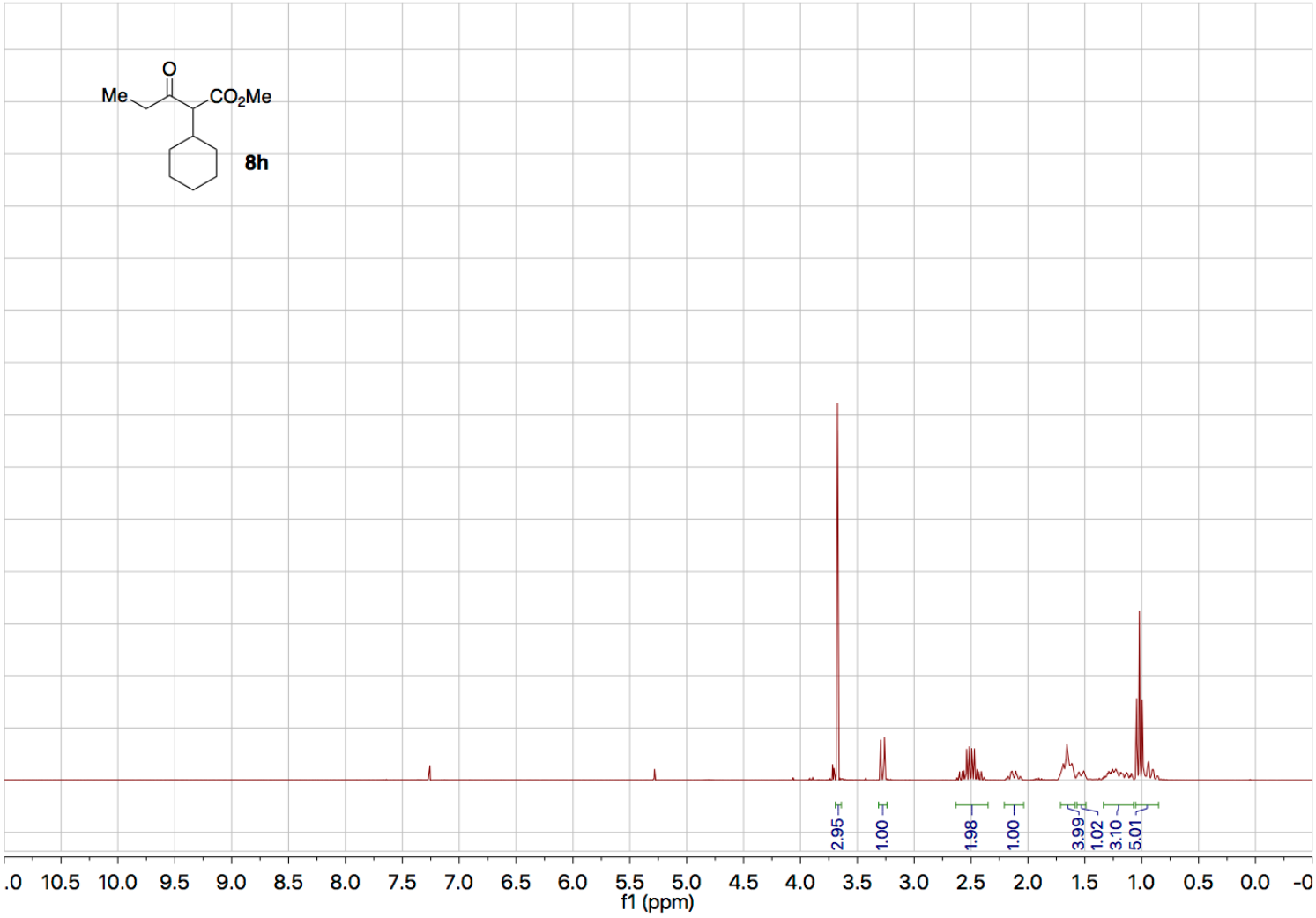
O
Me
CO2Me
8h
2.95
1.00
1.98
1.00
3.99
1.02
3.10
5.01
.0 10.5 10.0 9.5 9.0 8.5 8.0 7.5 7.0 6.5 6.0 5.5 5.0 4.5 4.0 3.5 3.0 2.5 2.0 1.5 1.0 0.5 0.0 -0
f1 (ppm)

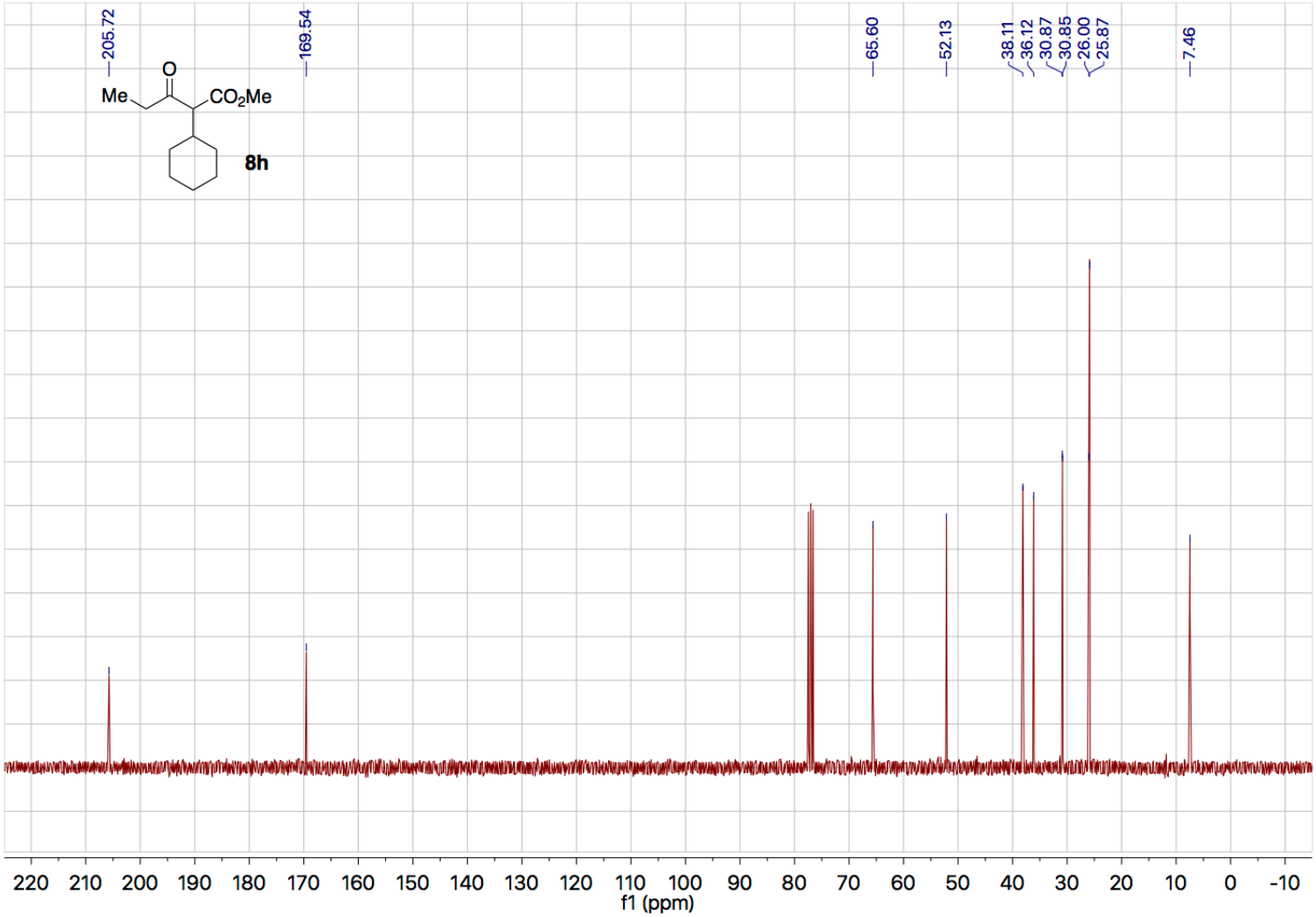
205.72
169.54
65.60
52.13
38.11
36.12
30.87
30.85
26.00
25.87
7.46
O
Me
CO2Me
8h
220 210 200 190 180 170 160 150 140 130 120 110 100 90 80 70 60 50 40 30 20 10 0 -10
f1 (ppm)

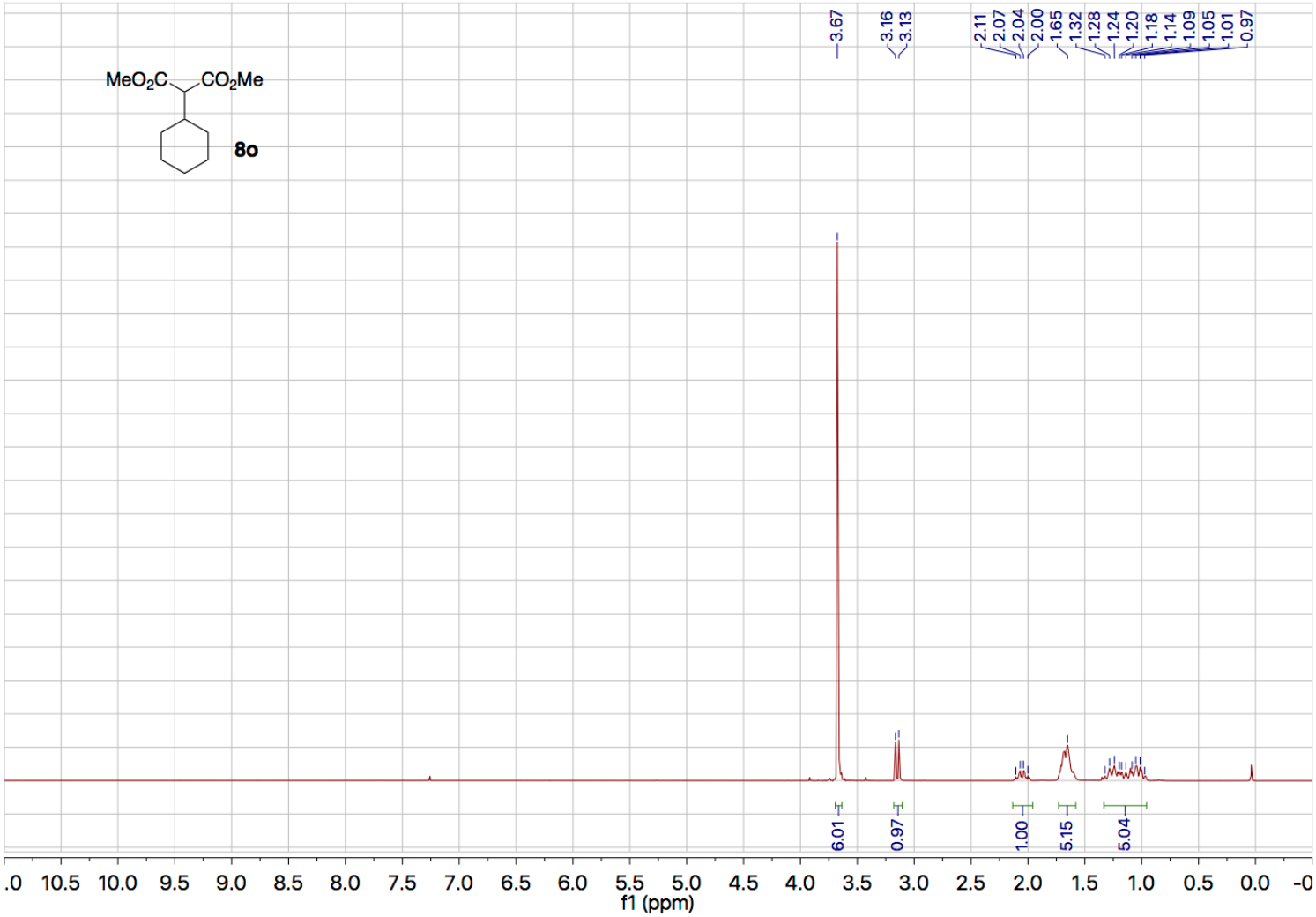
MeO2C
CO2Me
8o
3.67
3.16
3.13
2.11
2.07
2.04
2.00
1.65
1.32
1.28
1.24
1.20
1.18
1.14
1.09
1.05
1.01
0.97
6.01
0.97
1.00
5.15
5.04
f1 (ppm)

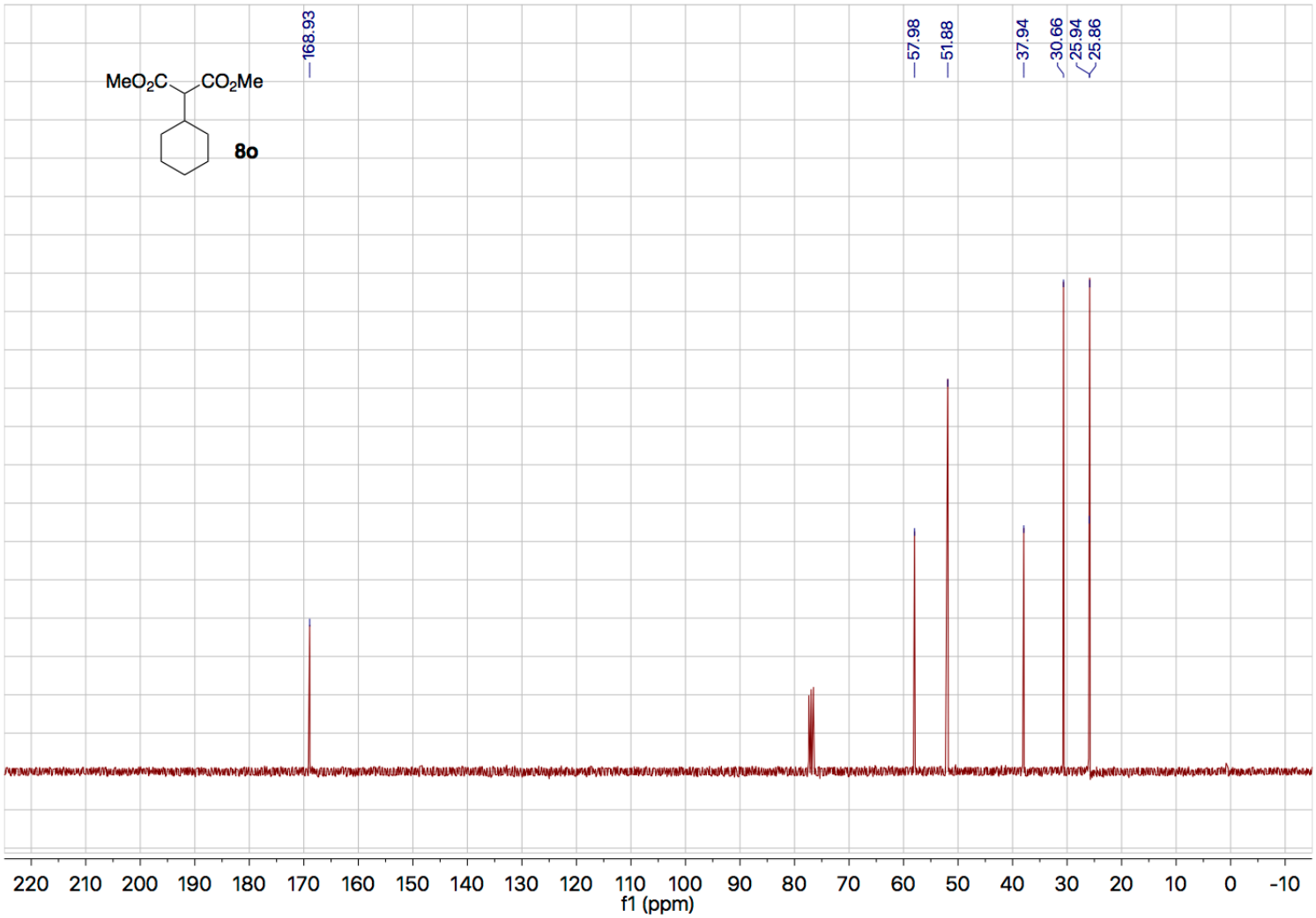
MeO2C
CO2Me
8o
168.93
57.98
51.88
37.94
30.66
25.94
25.86
220 210 200 190 180 170 160 150 140 130 120 110 100 90 80 70 60 50 40 30 20 10 0 -10
f1 (ppm)

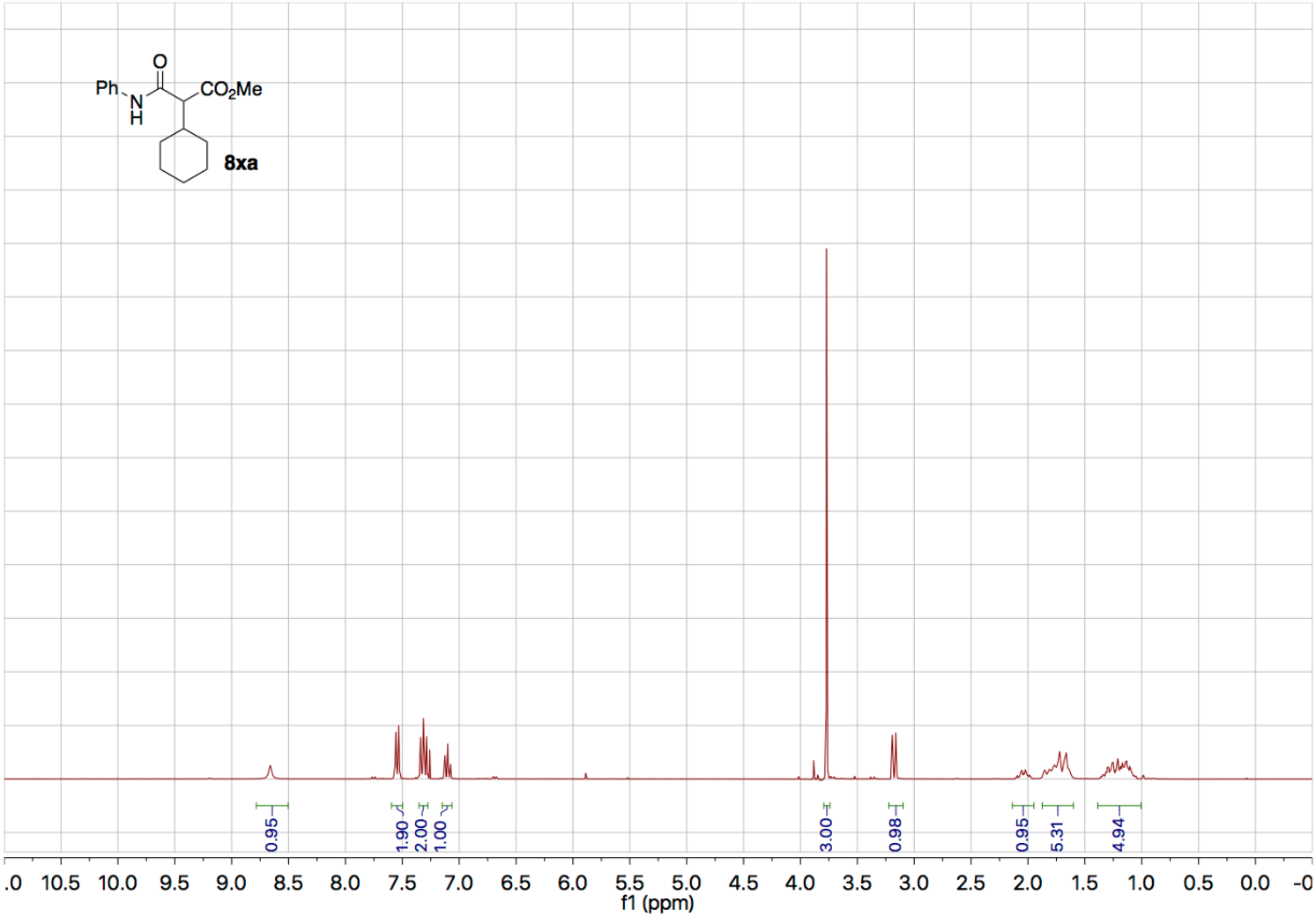
Ph
N
H
O
CO2Me
8xa
0.95
1.90
2.00
1.00
3.00
0.98
0.95
5.31
4.94
.0 10.5 10.0 9.5 9.0 8.5 8.0 7.5 7.0 6.5 6.0 5.5 5.0 4.5 4.0 3.5 3.0 2.5 2.0 1.5 1.0 0.5 0.0 -0
f1 (ppm)

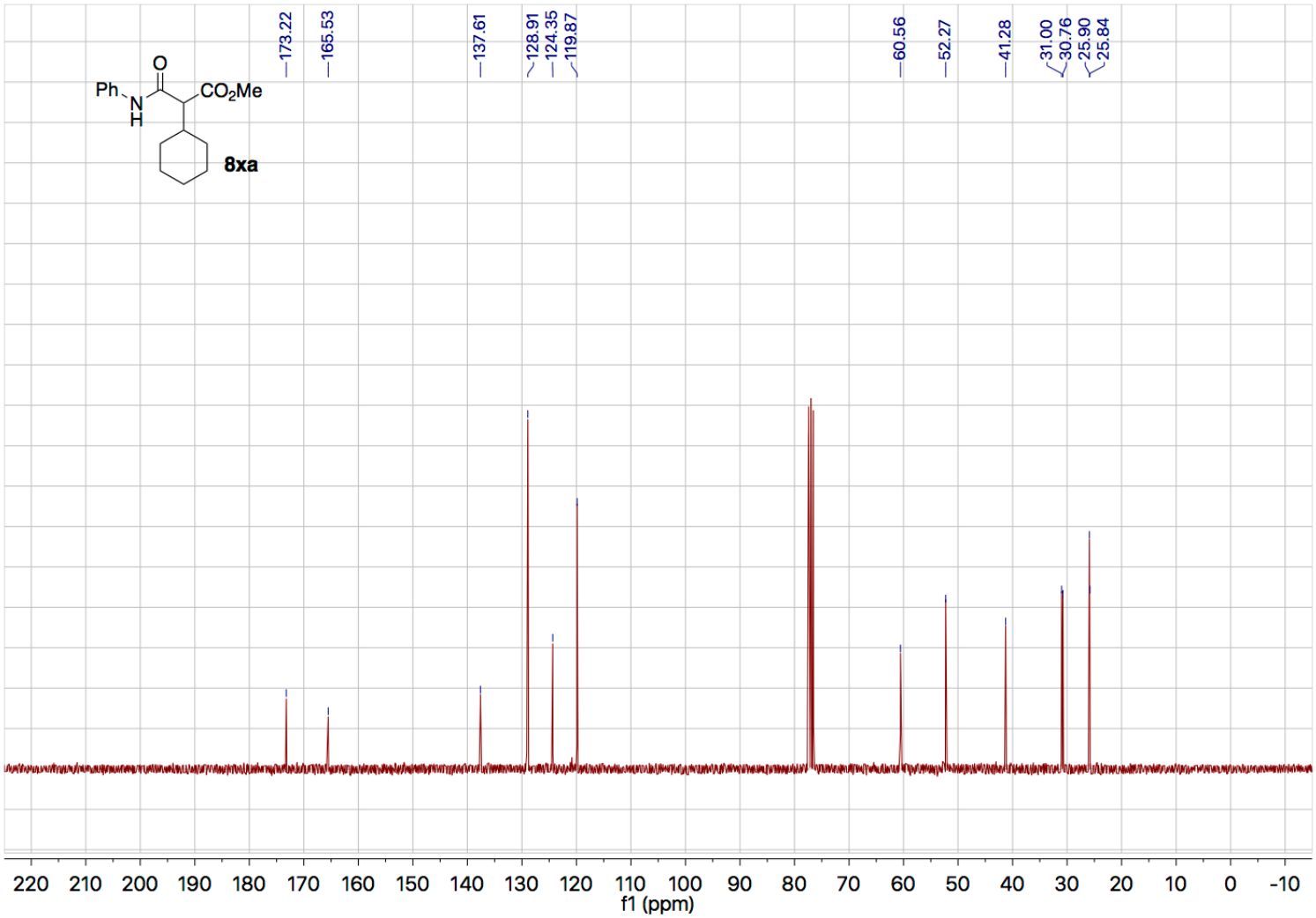
173.22
165.53
137.61
128.91
124.35
119.87
60.56
52.27
41.28
31.00
30.76
25.90
25.84
Ph
N
H
O
CO2Me
8xa
220 210 200 190 180 170 160 150 140 130 120 110 100 90 80 70 60 50 40 30 20 10 0 -10
f1 (ppm)

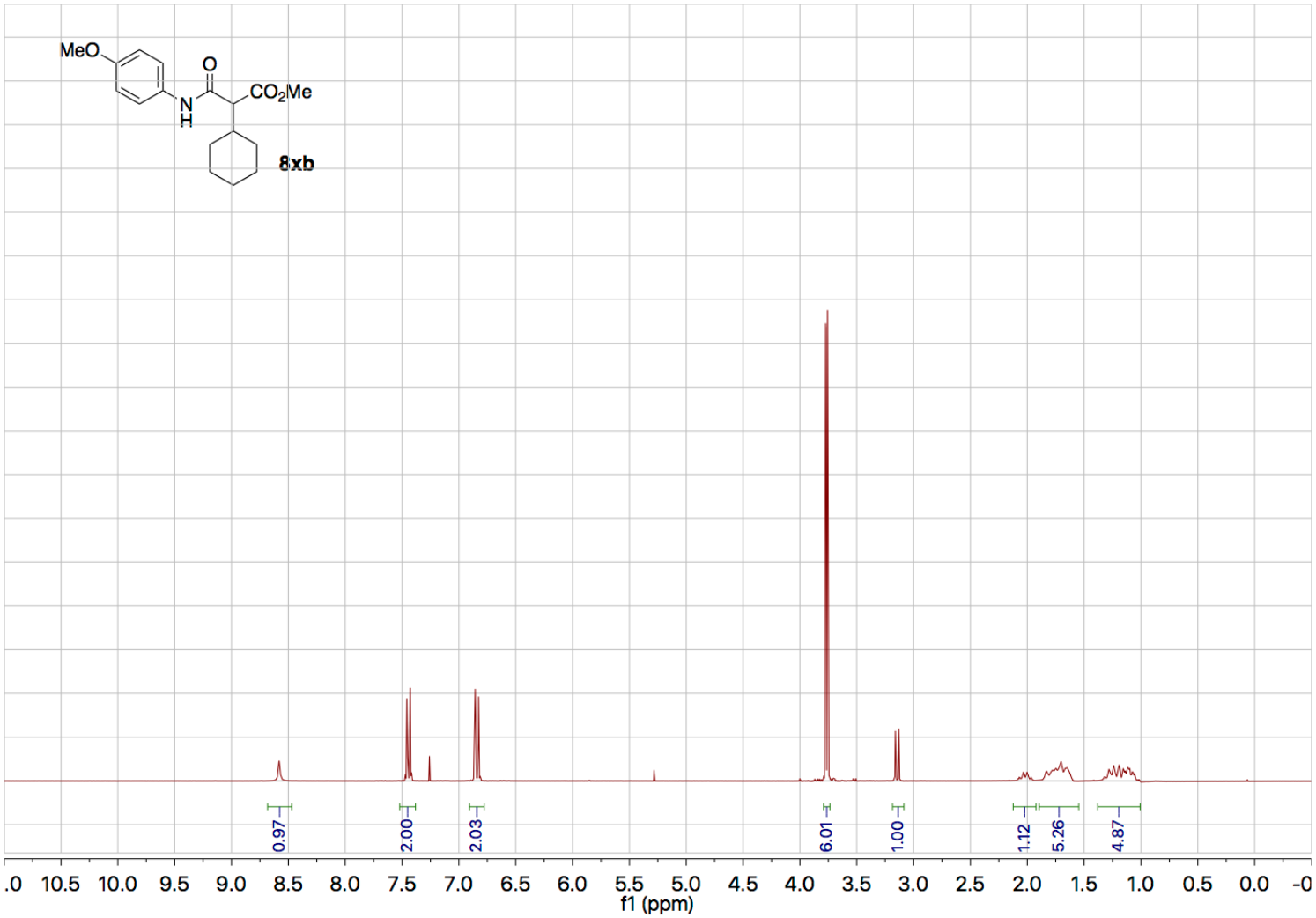
MeO
O
N
H
CO2Me
8xb
0.97
2.00
2.03
6.01
1.00
1.12
5.26
4.87
.0 10.5 10.0 9.5 9.0 8.5 8.0 7.5 7.0 6.5 6.0 5.5 5.0 4.5 4.0 3.5 3.0 2.5 2.0 1.5 1.0 0.5 0.0 -0
f1 (ppm)

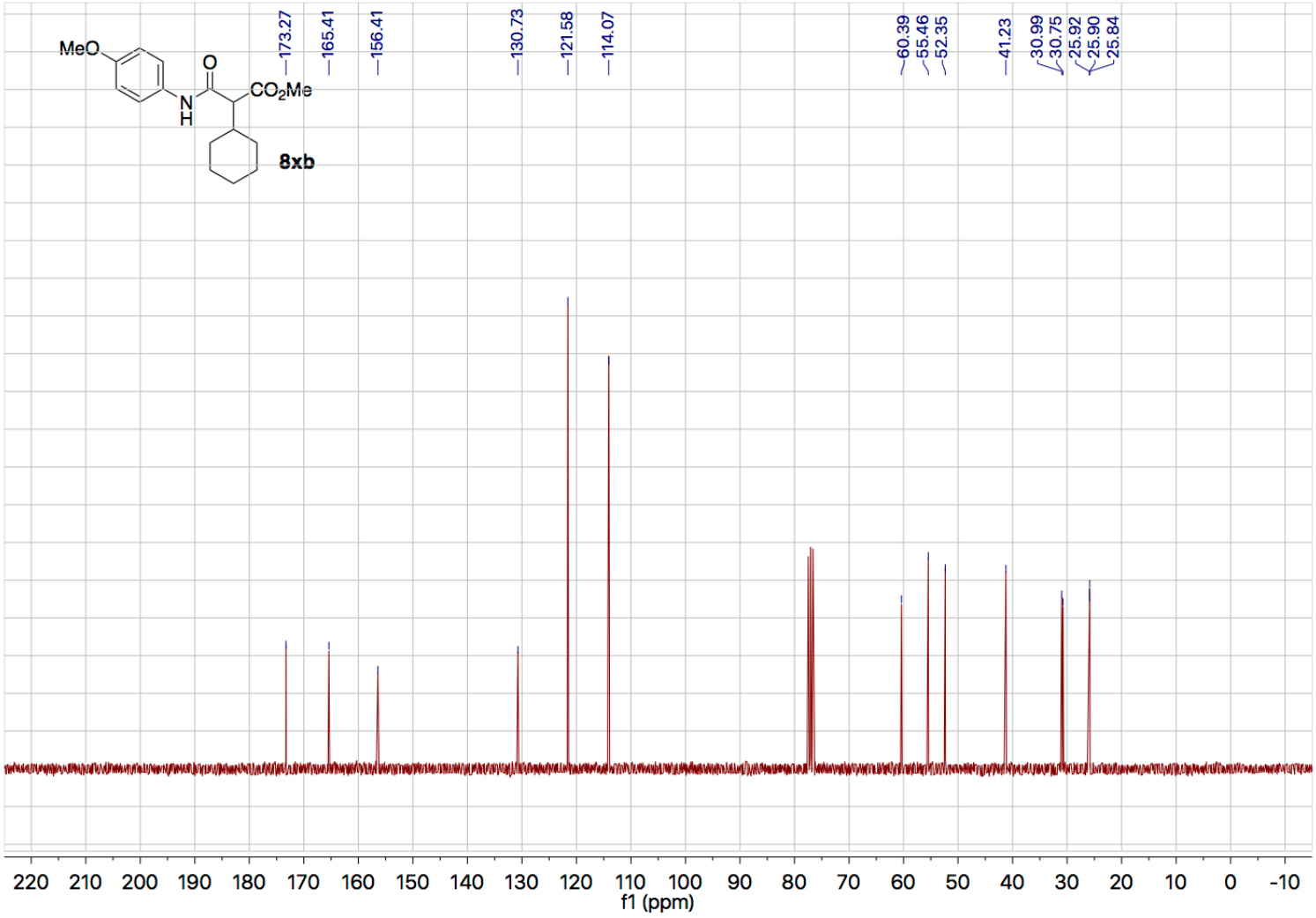
MeO
O
N
H
CO2Me
8xb
173.27
165.41
156.41
130.73
121.58
114.07
60.39
55.46
52.35
41.23
30.99
30.75
25.92
25.90
25.84
220 210 200 190 180 170 160 150 140 130 120 110 100 90 80 70 60 50 40 30 20 10 0 -10
f1 (ppm)

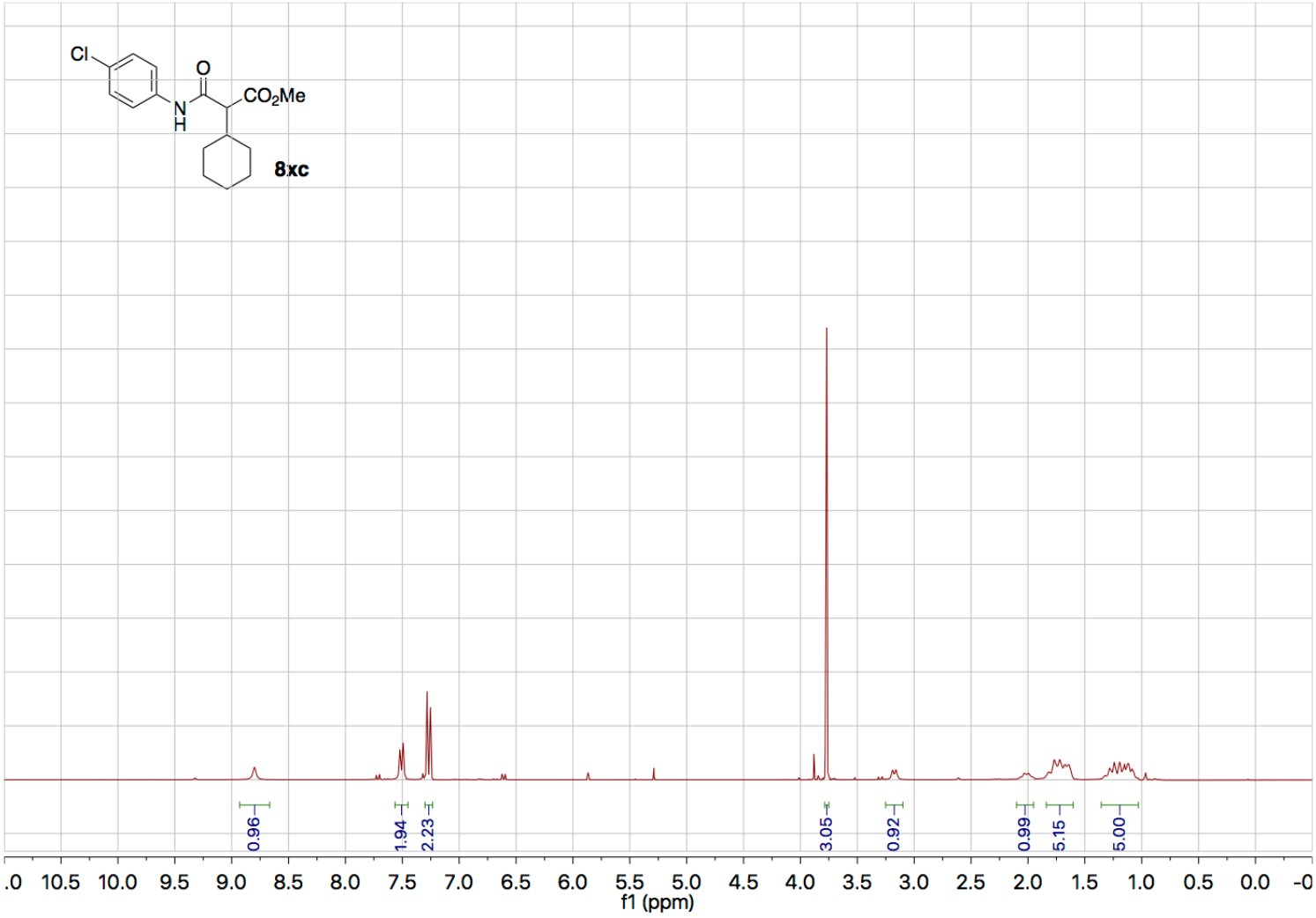
Cl
O
N
H
CO2Me
8xc
0.96
1.94
2.23
3.05
0.92
0.99
5.15
5.00
.0 10.5 10.0 9.5 9.0 8.5 8.0 7.5 7.0 6.5 6.0 5.5 5.0 4.5 4.0 3.5 3.0 2.5 2.0 1.5 1.0 0.5 0.0 -0
f1 (ppm)

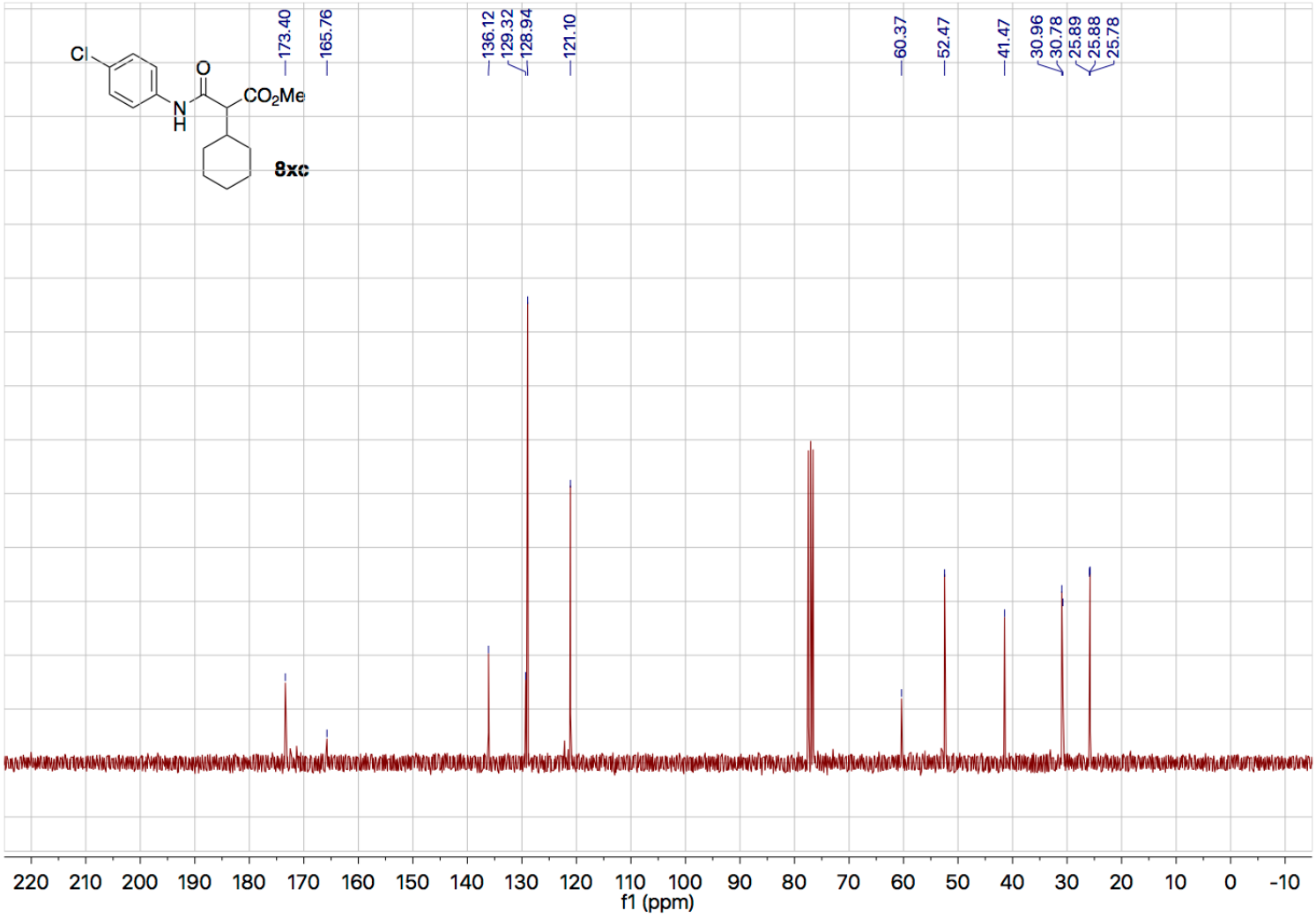
Cl
O
N
H
CO2Me
8xc
173.40
165.76
136.12
129.32
128.94
121.10
60.37
52.47
41.47
30.96
30.78
25.89
25.88
25.78
220 210 200 190 180 170 160 150 140 130 120 110 100 90 80 70 60 50 40 30 20 10 0 -10
f1 (ppm)

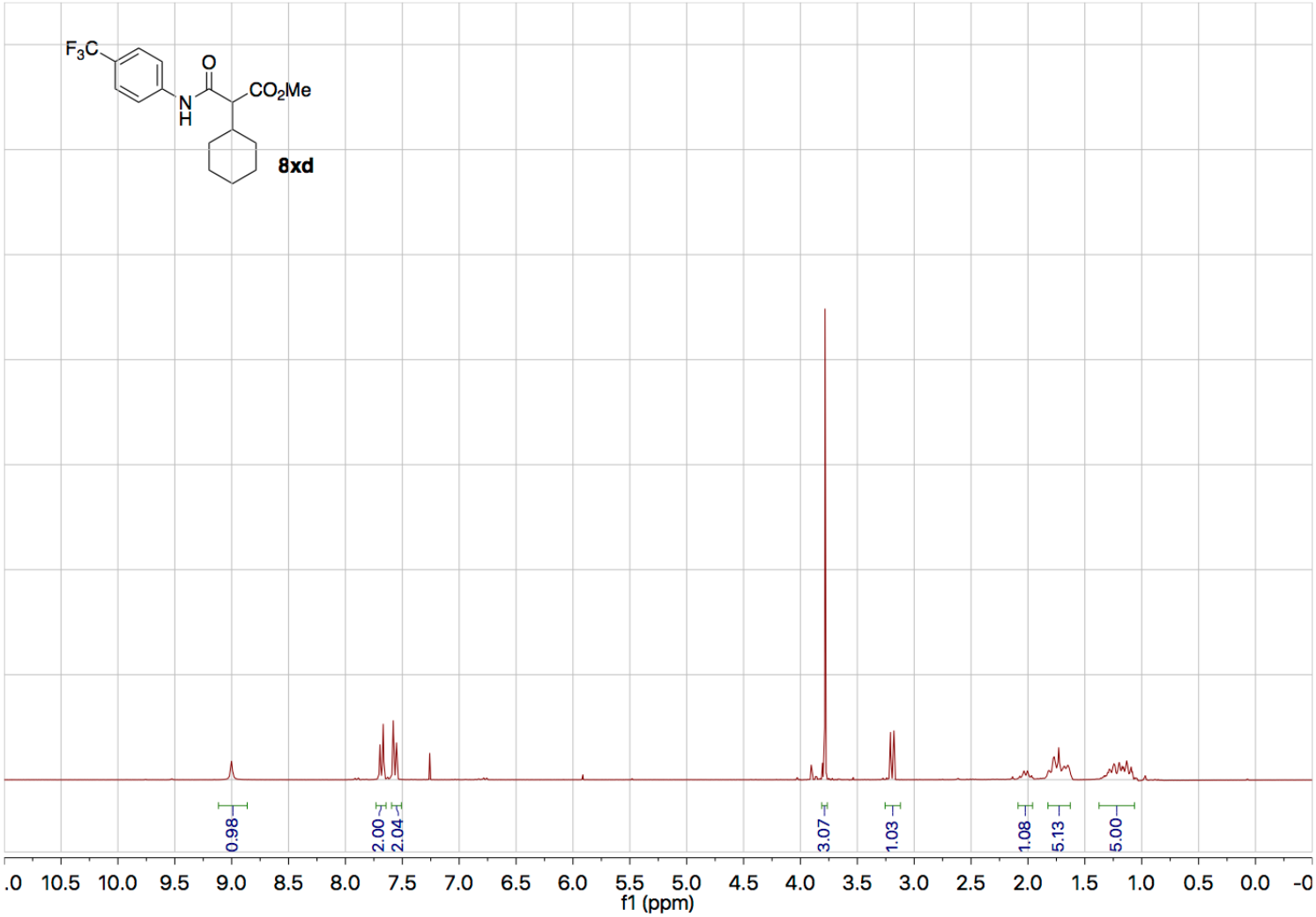
F3C
O
N
H
CO2Me
8xd
0.98
2.00
2.04
3.07
1.03
1.08
5.13
5.00
.0 10.5 10.0 9.5 9.0 8.5 8.0 7.5 7.0 6.5 6.0 5.5 5.0 4.5 4.0 3.5 3.0 2.5 2.0 1.5 1.0 0.5 0.0 -0
f1 (ppm)

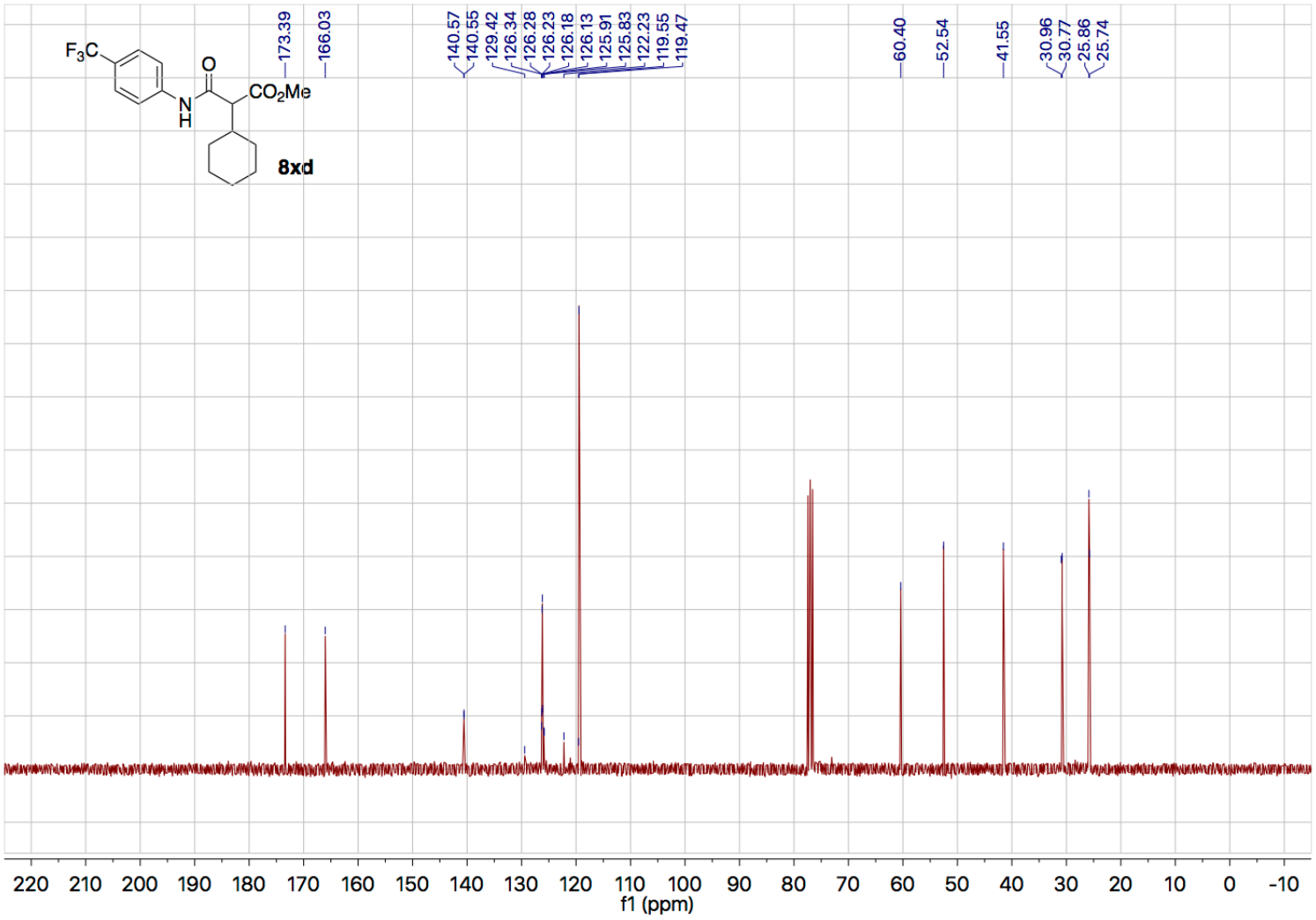
F3C
O
N
H
CO2Me
8xd
173.39
166.03
140.57
140.55
129.42
126.34
126.28
126.23
126.18
126.13
125.91
125.83
122.23
119.55
119.47
60.40
52.54
41.55
30.96
30.77
25.86
25.74
220 210 200 190 180 170 160 150 140 130 120 110 100 90 80 70 60 50 40 30 20 10 0 -10
f1 (ppm)

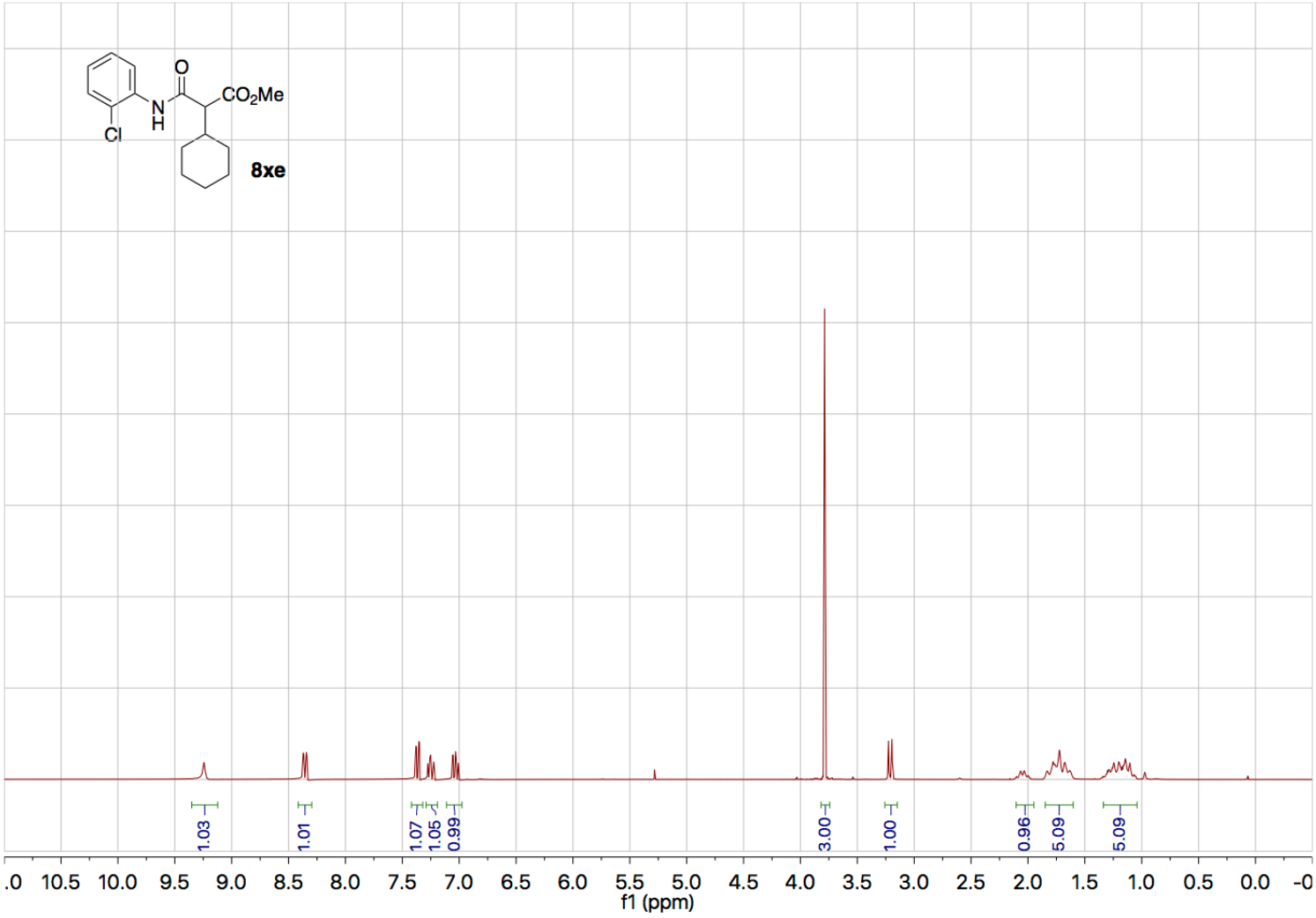
O
N
H
Cl
CO2Me
8xe
1.03
1.01
1.07
1.05
0.99
3.00
1.00
0.96
5.09
5.09
.0 10.5 10.0 9.5 9.0 8.5 8.0 7.5 7.0 6.5 6.0 5.5 5.0 4.5 4.0 3.5 3.0 2.5 2.0 1.5 1.0 0.5 0.0 -0
f1 (ppm)

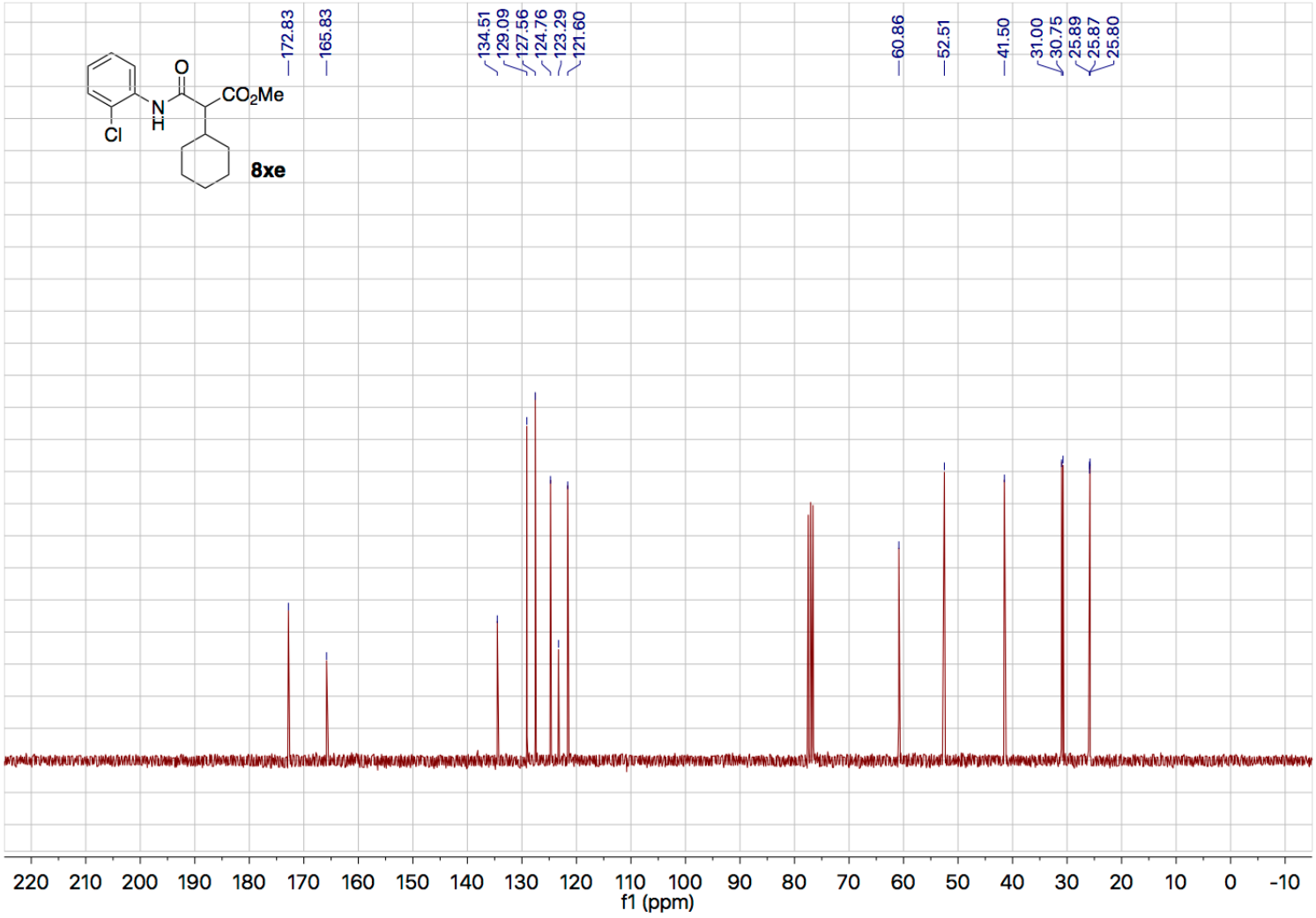
172.83
165.83
134.51
129.09
127.56
124.76
123.29
121.60
60.86
52.51
41.50
31.00
30.75
25.89
25.87
25.80
O
N
H
Cl
CO2Me
8xe
220 210 200 190 180 170 160 150 140 130 120 110 100 90 80 70 60 50 40 30 20 10 0 -10
f1 (ppm)

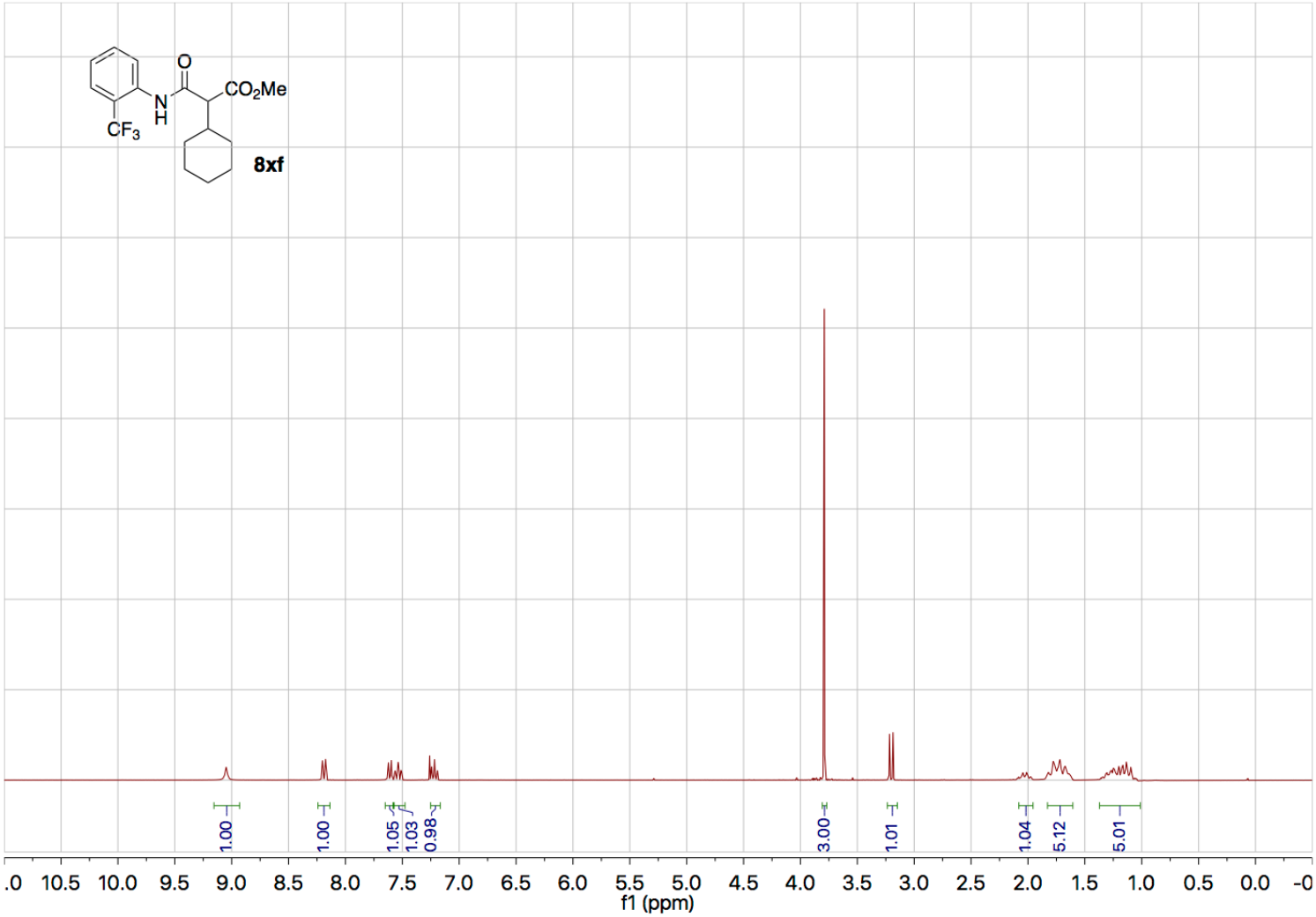
O
N
H
CO2Me
CF3
8xf
1.00
1.00
1.05
1.03
0.98
3.00
1.01
1.04
5.12
5.01
.0 10.5 10.0 9.5 9.0 8.5 8.0 7.5 7.0 6.5 6.0 5.5 5.0 4.5 4.0 3.5 3.0 2.5 2.0 1.5 1.0 0.5 0.0 -0
f1 (ppm)

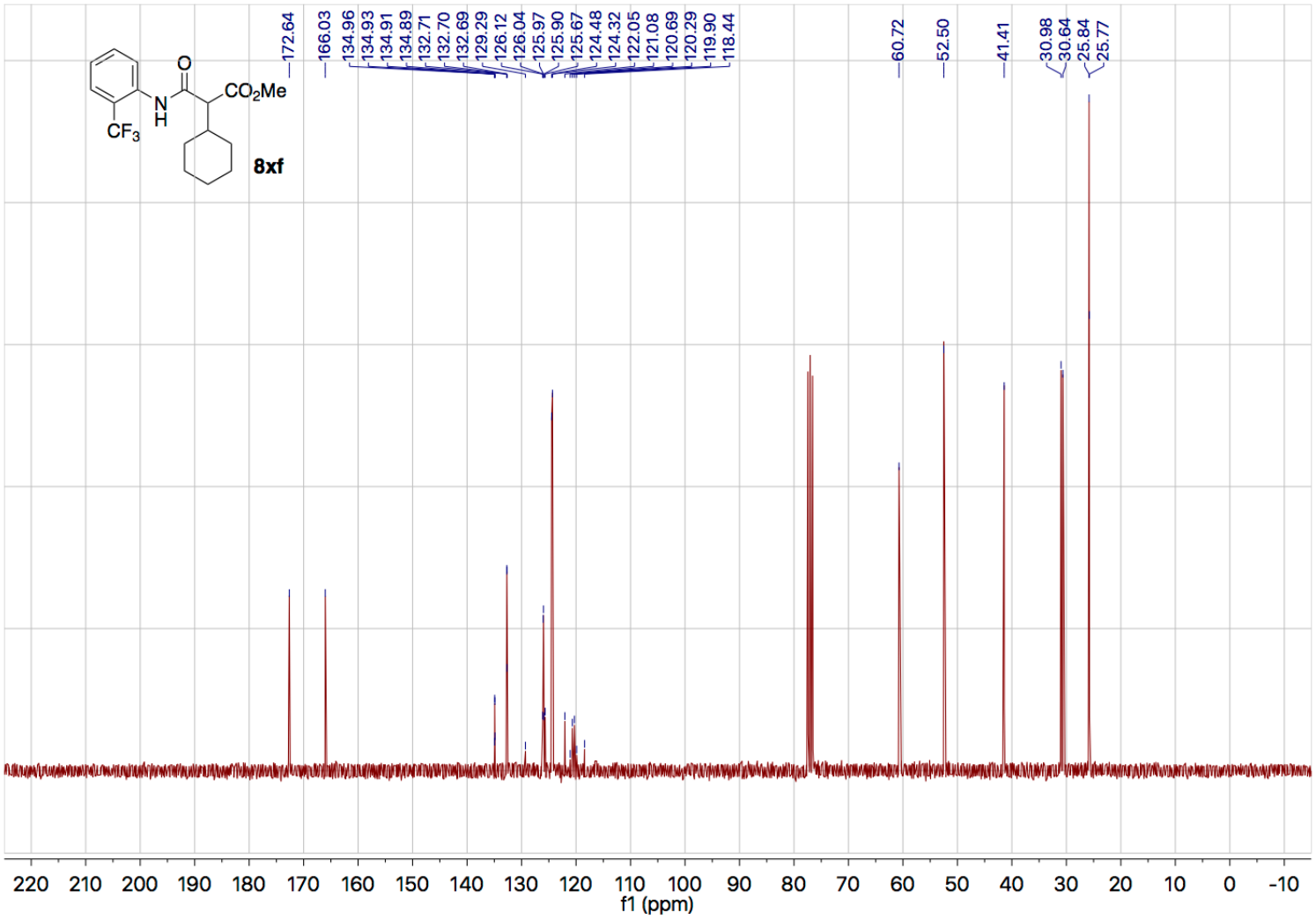
172.64
166.03
134.96
134.93
134.91
134.89
132.71
132.70
132.69
129.29
126.12
126.04
125.97
125.90
125.67
124.48
124.32
122.05
121.08
120.69
120.29
119.90
118.44
60.72
52.50
41.41
30.98
30.64
25.84
25.77
O
N
H
CO2Me
CF3
8xf
220 210 200 190 180 170 160 150 140 130 120 110 100 90 80 70 60 50 40 30 20 10 0 -10
f1 (ppm)

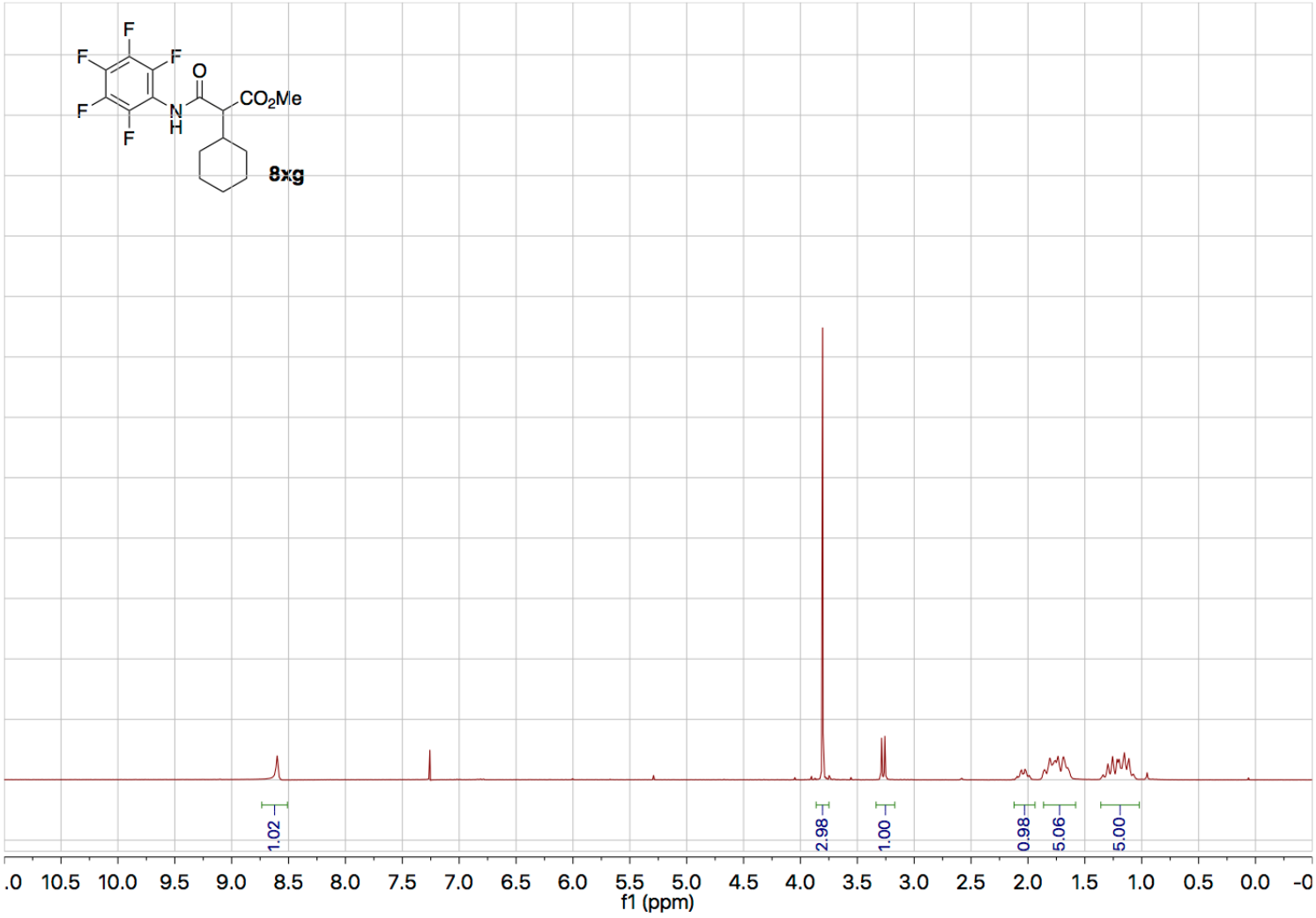
F
F
F
F
F
O
N
H
CO2Me
8xg
1.02
2.98
1.00
0.98
5.06
5.00
.0 10.5 10.0 9.5 9.0 8.5 8.0 7.5 7.0 6.5 6.0 5.5 5.0 4.5 4.0 3.5 3.0 2.5 2.0 1.5 1.0 0.5 0.0 -0
f1 (ppm)

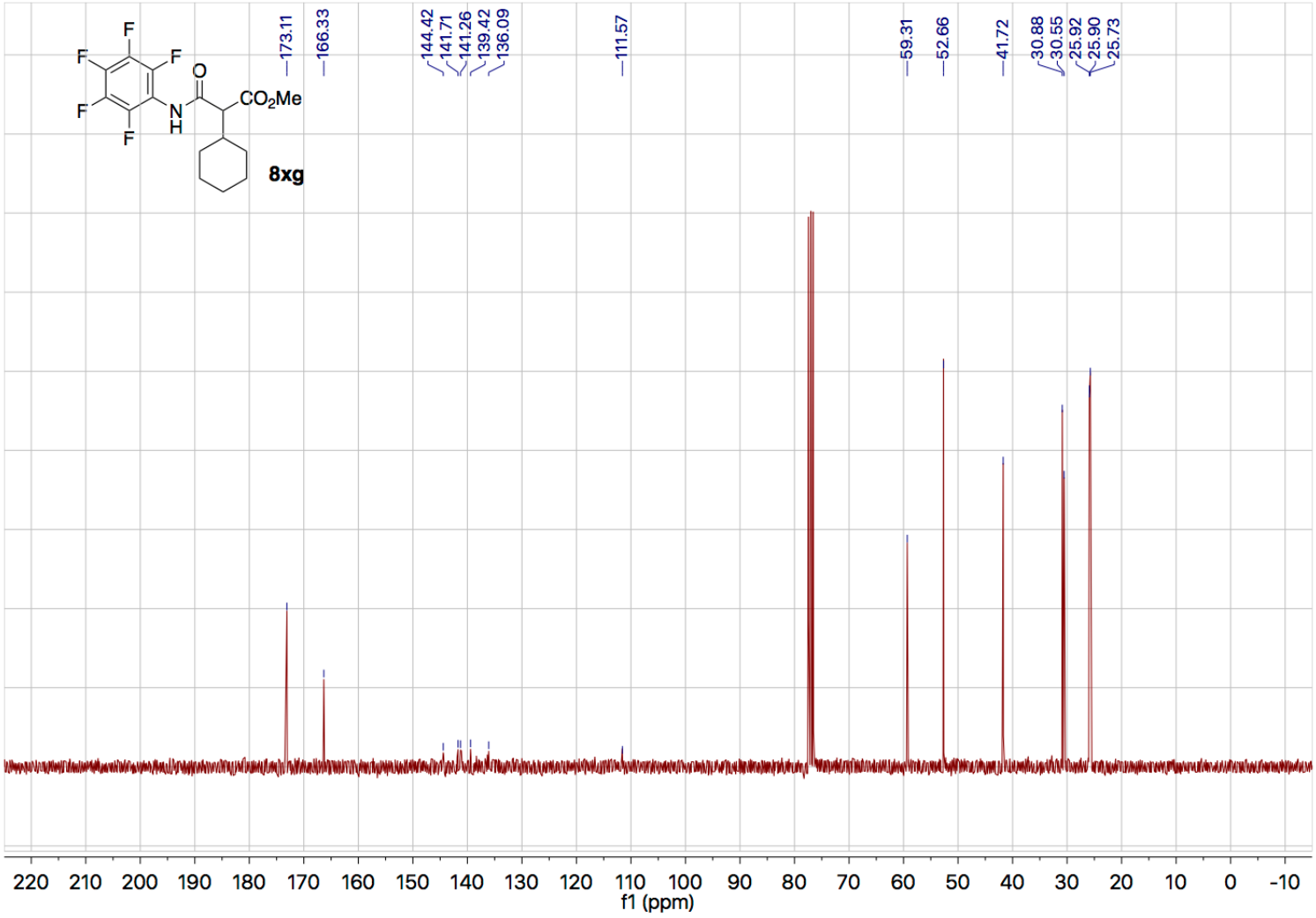
F
F
F
F
F
O
N
H
CO2Me
8xg
173.11
166.33
144.42
141.71
141.26
139.42
136.09
111.57
59.31
52.66
41.72
30.88
30.55
25.92
25.90
25.73
220 210 200 190 180 170 160 150 140 130 120 110 100 90 80 70 60 50 40 30 20 10 0 -10
f1 (ppm)

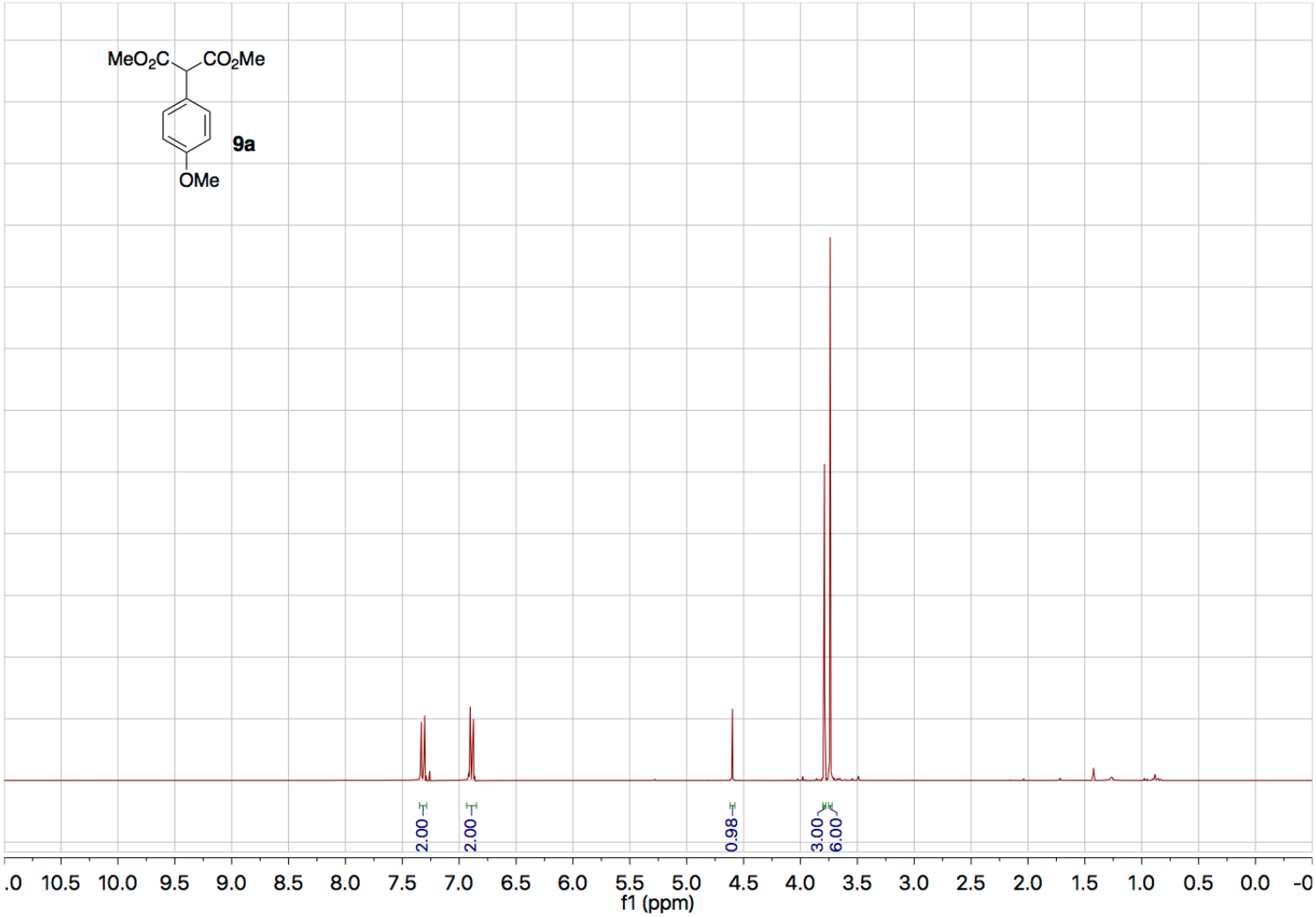
MeO2C
CO2Me
OMe
9a
2.00
2.00
0.98
3.00
6.00
.0 10.5 10.0 9.5 9.0 8.5 8.0 7.5 7.0 6.5 6.0 5.5 5.0 4.5 4.0 3.5 3.0 2.5 2.0 1.5 1.0 0.5 0.0 -0
f1 (ppm)

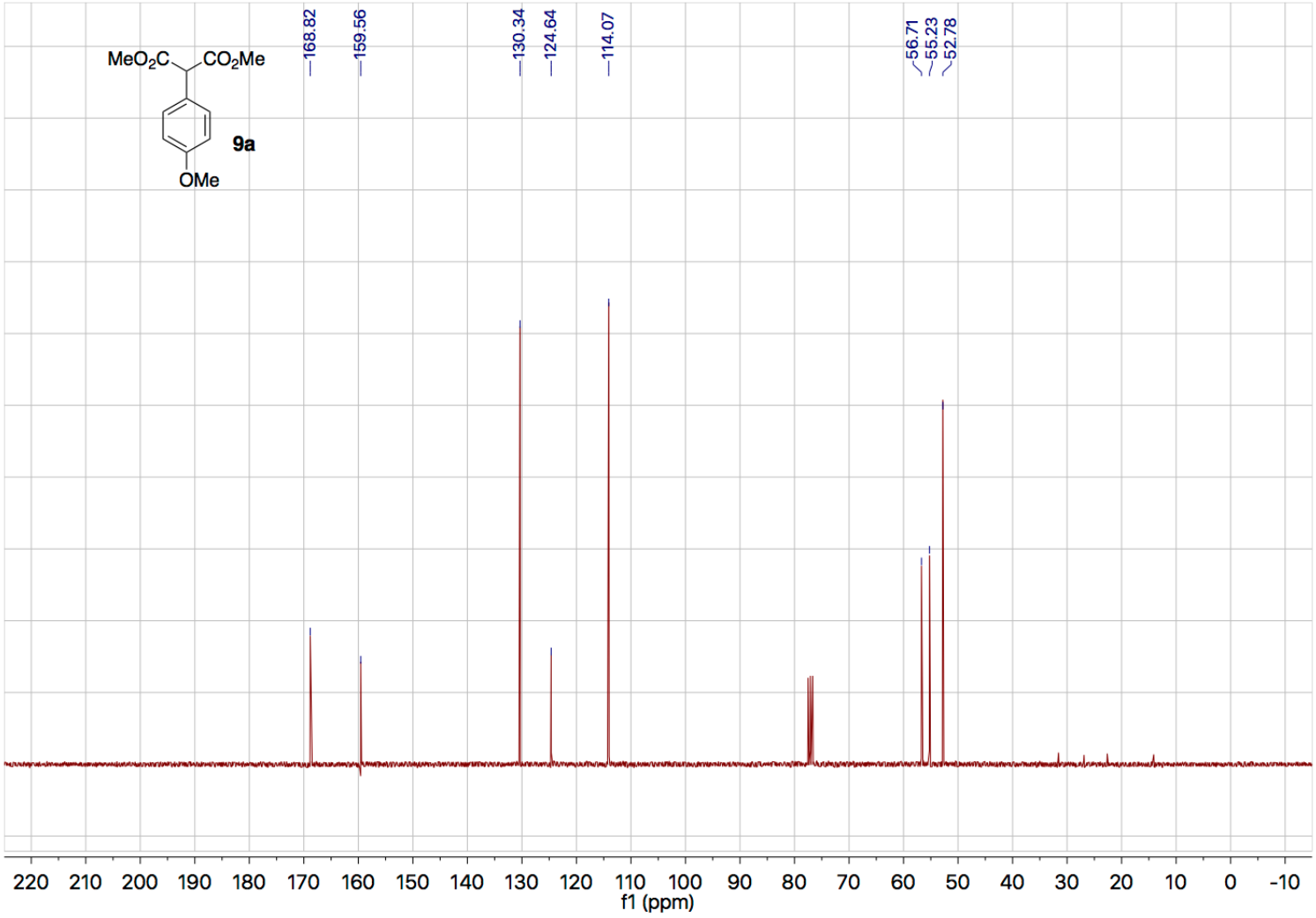
MeO2C
CO2Me
OMe
9a
168.82
159.56
130.34
124.64
114.07
56.71
55.23
52.78
220 210 200 190 180 170 160 150 140 130 120 110 100 90 80 70 60 50 40 30 20 10 0 -10
f1 (ppm)

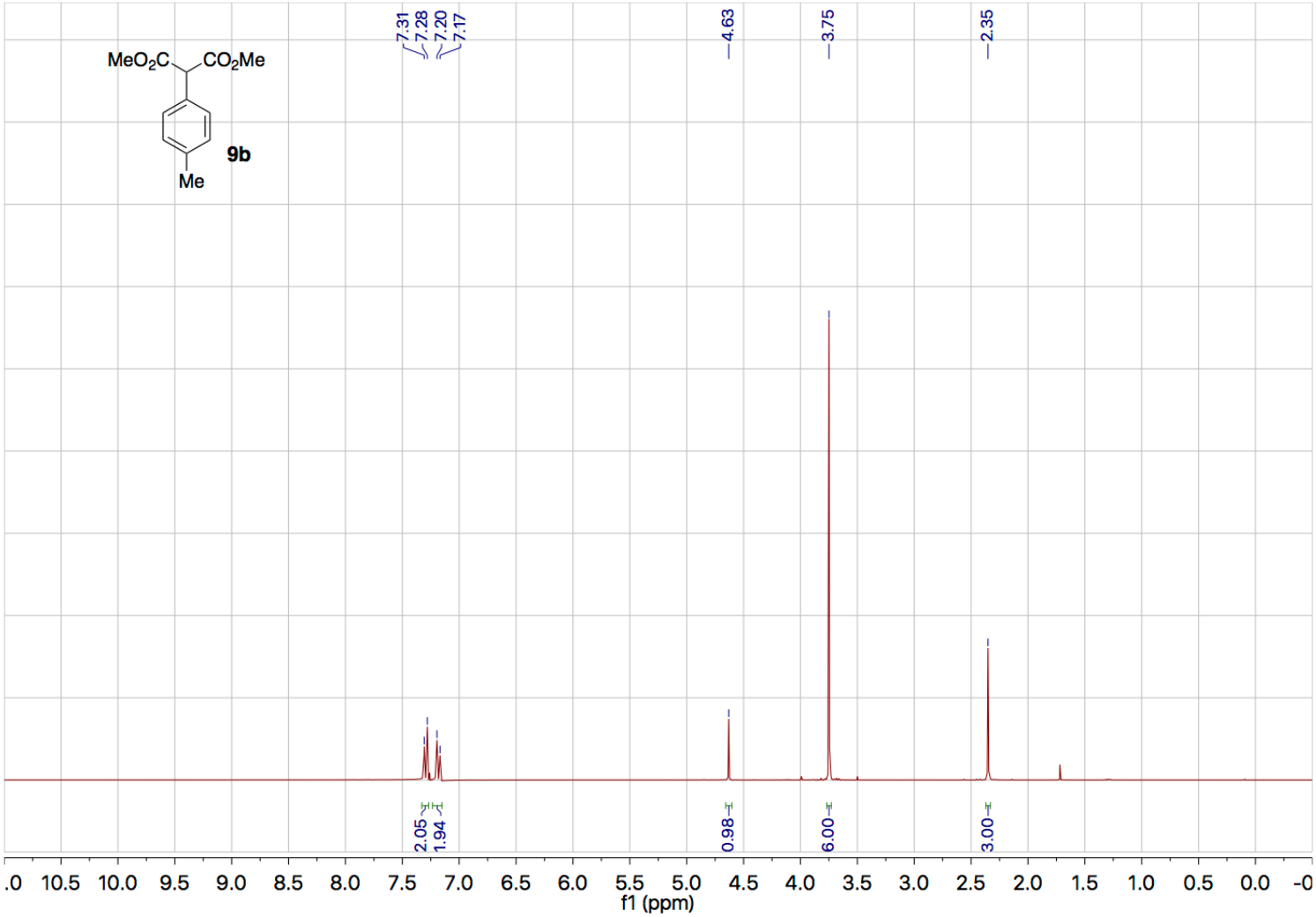
MeO2C
CO2Me
Me
9b
7.31
7.28
7.20
7.17
4.63
3.75
2.35
2.05
1.94
0.98
6.00
3.00
f1 (ppm)

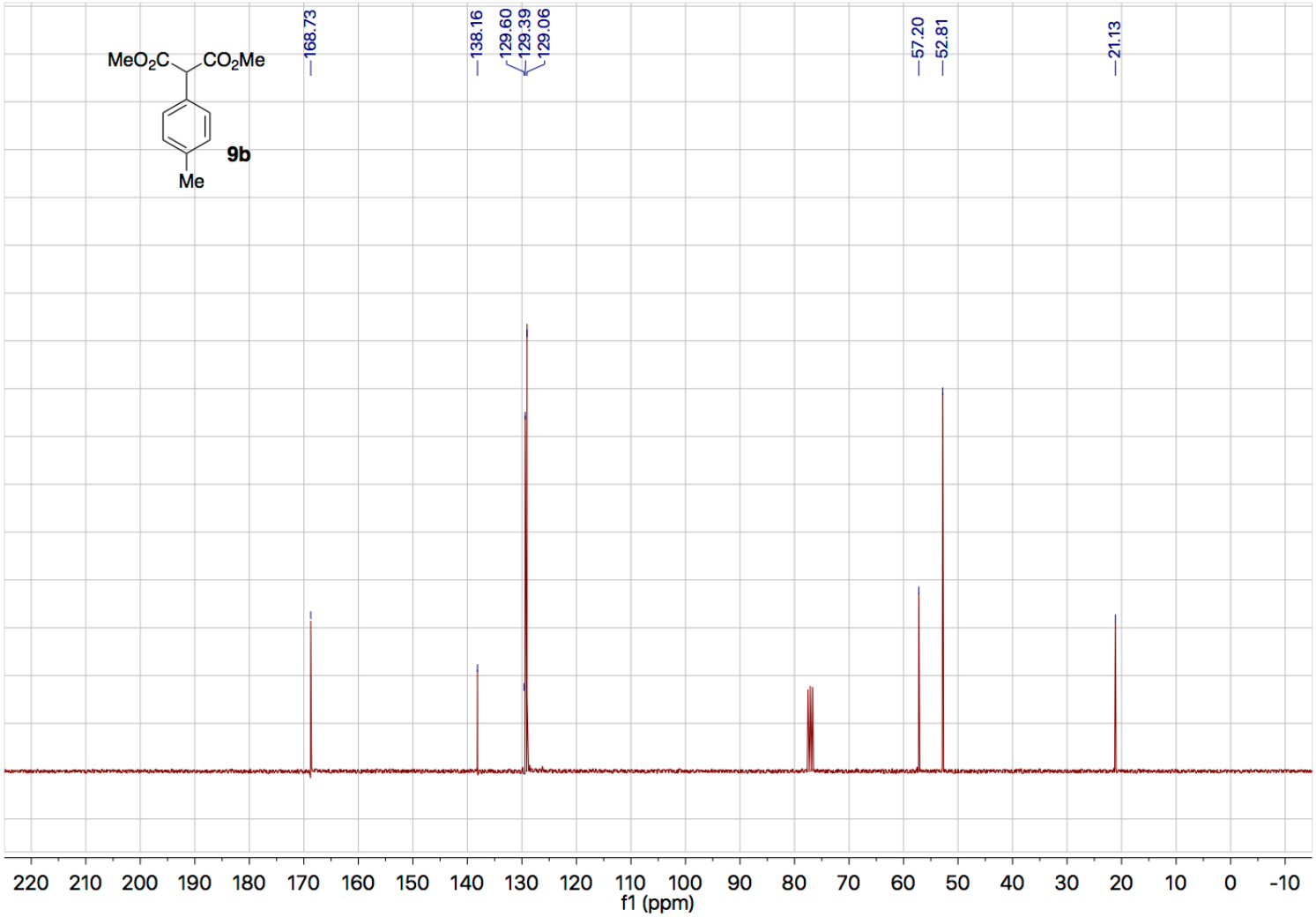
MeO2C
CO2Me
Me
9b
168.73
138.16
129.60
129.39
129.06
57.20
52.81
21.13
220 210 200 190 180 170 160 150 140 130 120 110 100 90 80 70 60 50 40 30 20 10 0 -10
f1 (ppm)

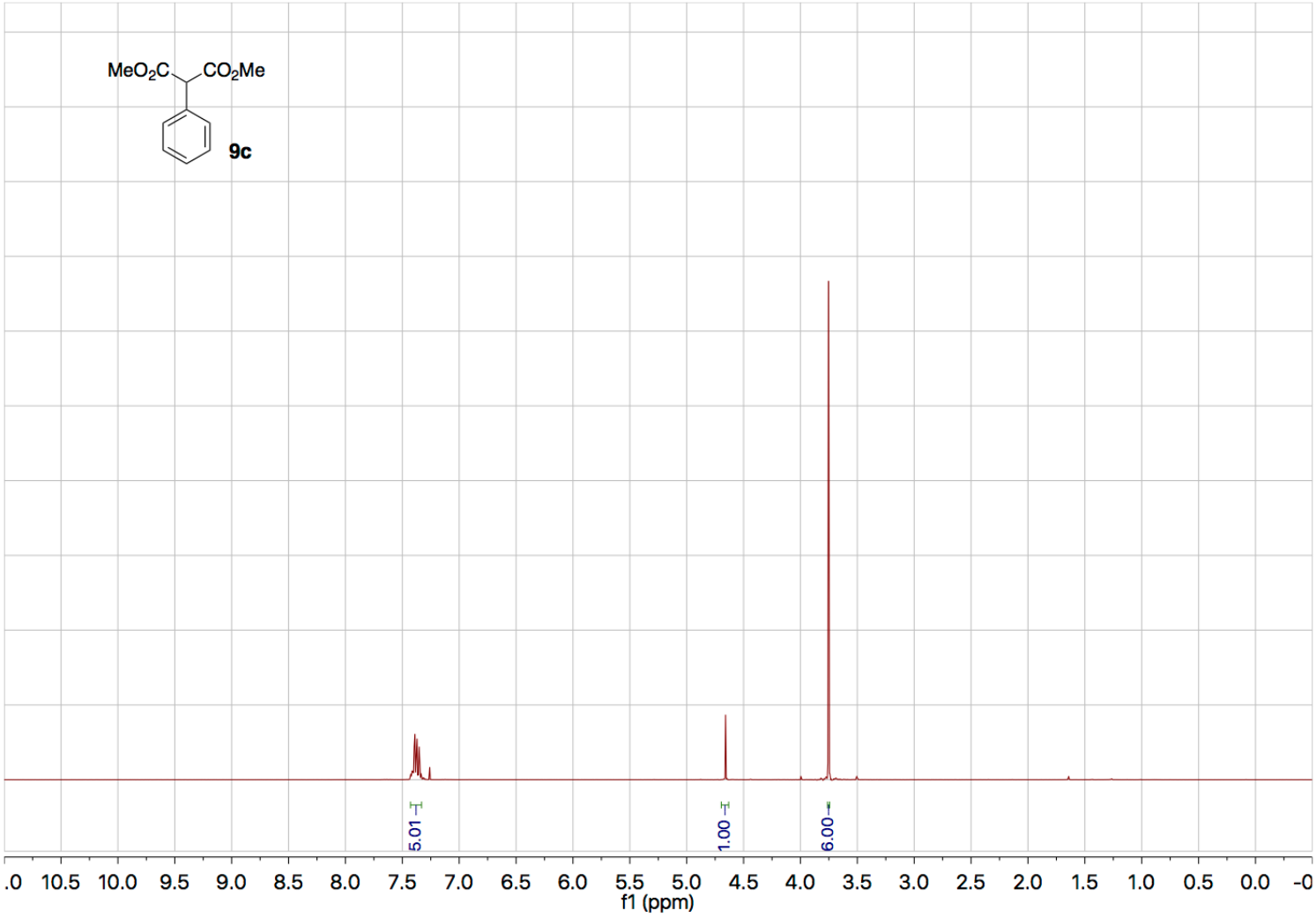
MeO2C
CO2Me
9c
5.01
1.00
6.00
.0 10.5 10.0 9.5 9.0 8.5 8.0 7.5 7.0 6.5 6.0 5.5 5.0 4.5 4.0 3.5 3.0 2.5 2.0 1.5 1.0 0.5 0.0 -0
f1 (ppm)

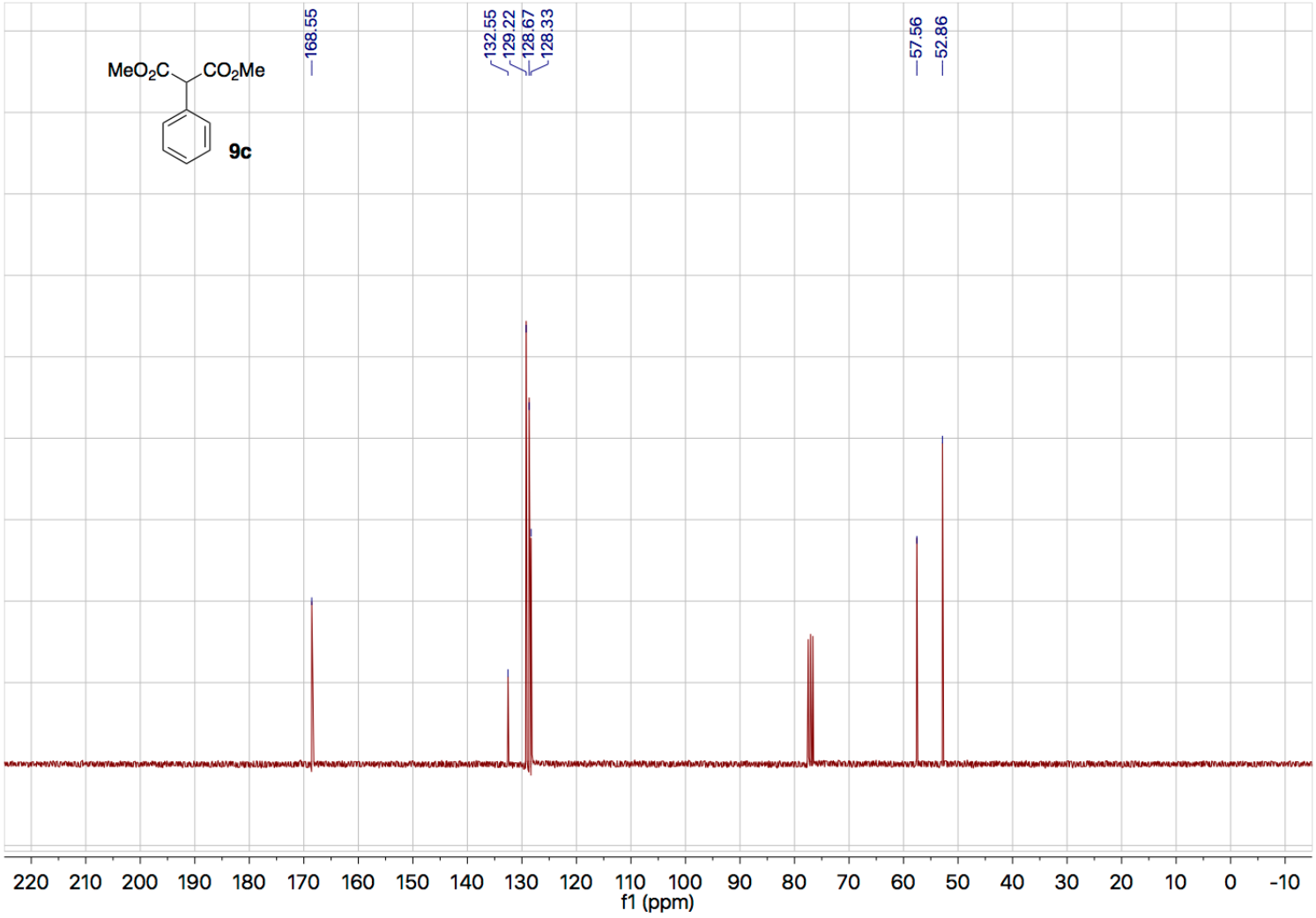
MeO2C
CO2Me
9c
168.55
132.55
129.22
128.67
128.33
57.56
52.86
220 210 200 190 180 170 160 150 140 130 120 110 100 90 80 70 60 50 40 30 20 10 0 -10
f1 (ppm)

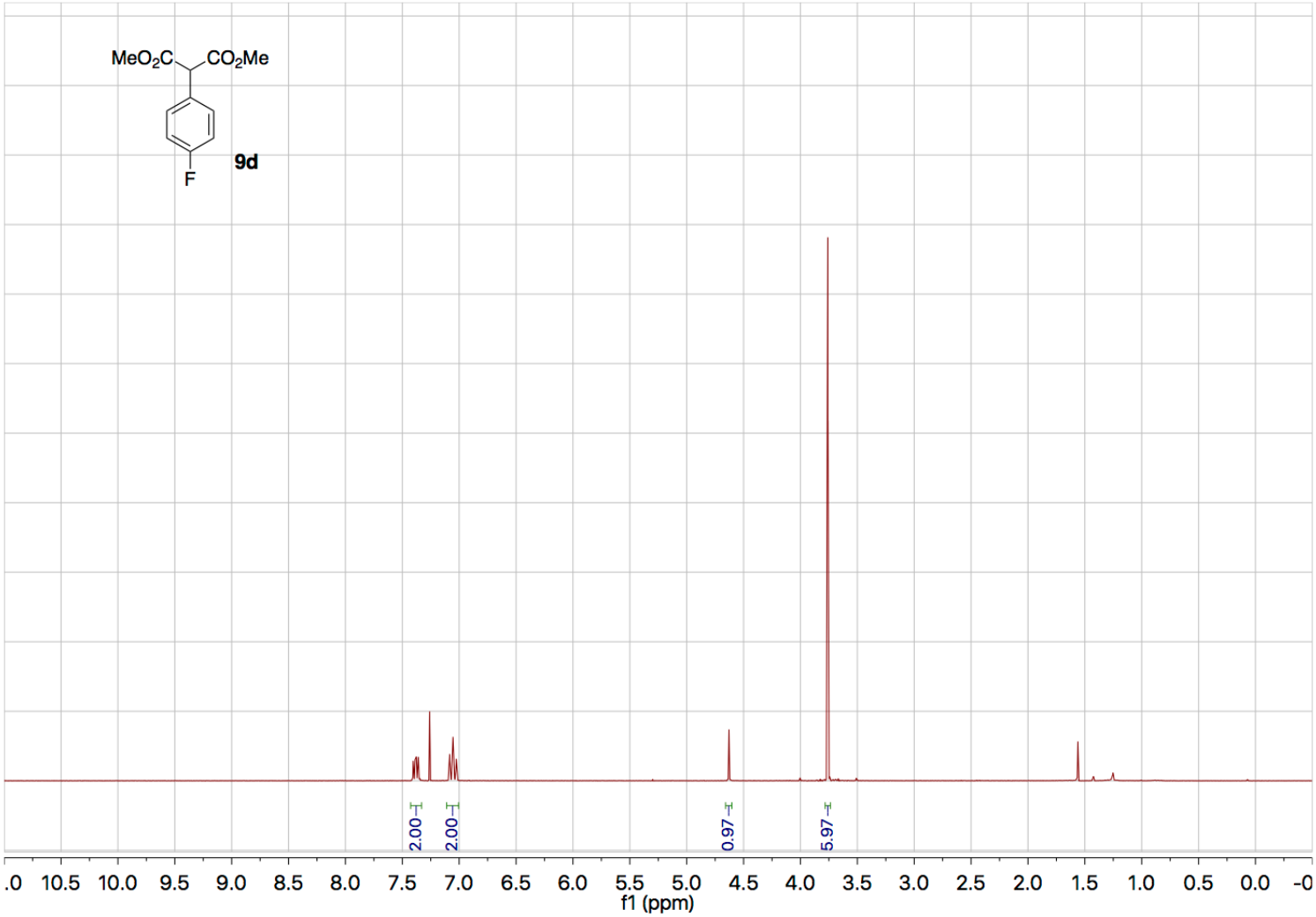
MeO2C
CO2Me
F
9d
2.00
2.00
0.97
5.97
.0 10.5 10.0 9.5 9.0 8.5 8.0 7.5 7.0 6.5 6.0 5.5 5.0 4.5 4.0 3.5 3.0 2.5 2.0 1.5 1.0 0.5 0.0 -0
f1 (ppm)

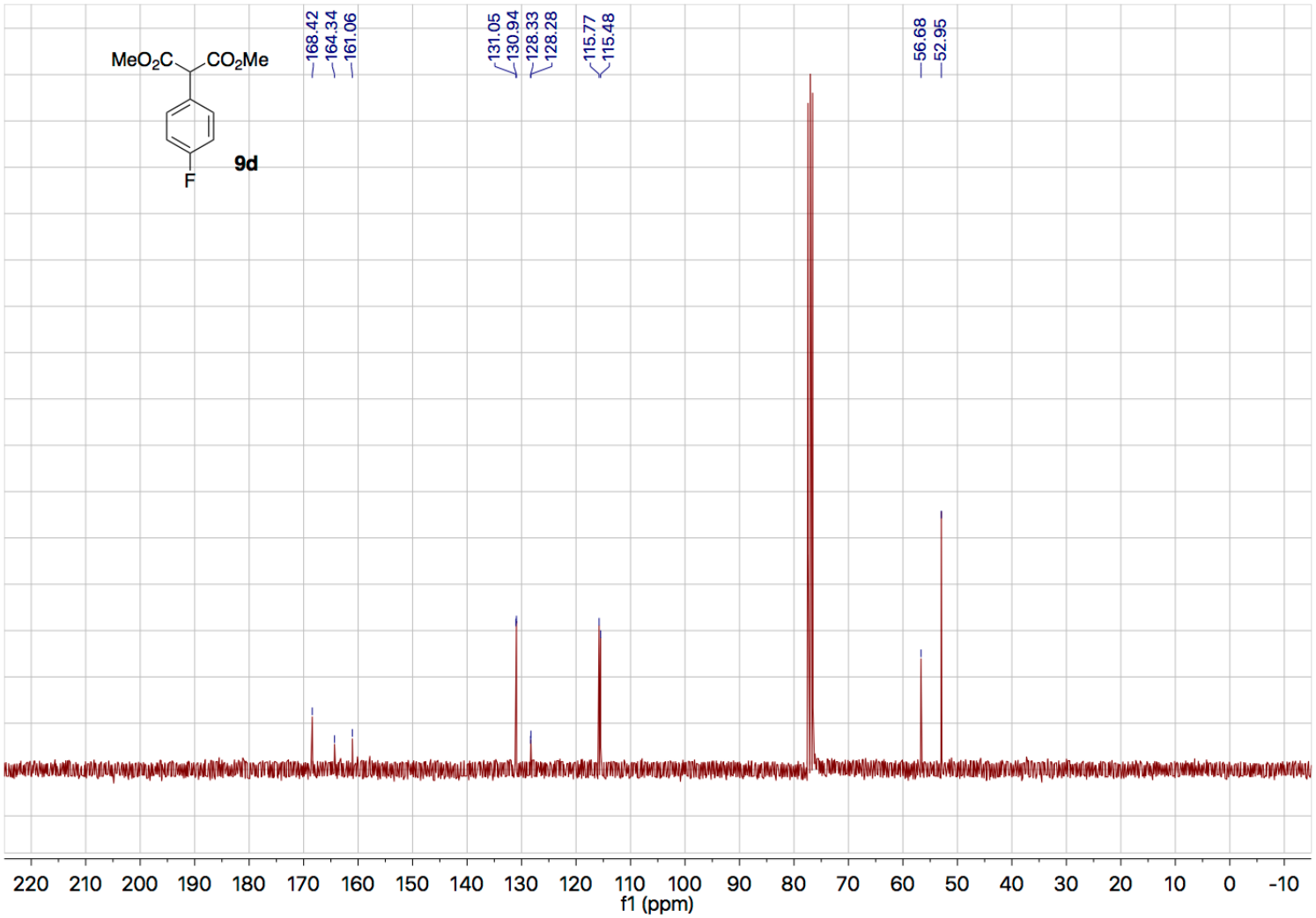
MeO2C
CO2Me
F
9d
168.42
164.34
161.06
131.05
130.94
128.33
128.28
115.77
115.48
56.68
52.95
220 210 200 190 180 170 160 150 140 130 120 110 100 90 80 70 60 50 40 30 20 10 0 -10
f1 (ppm)

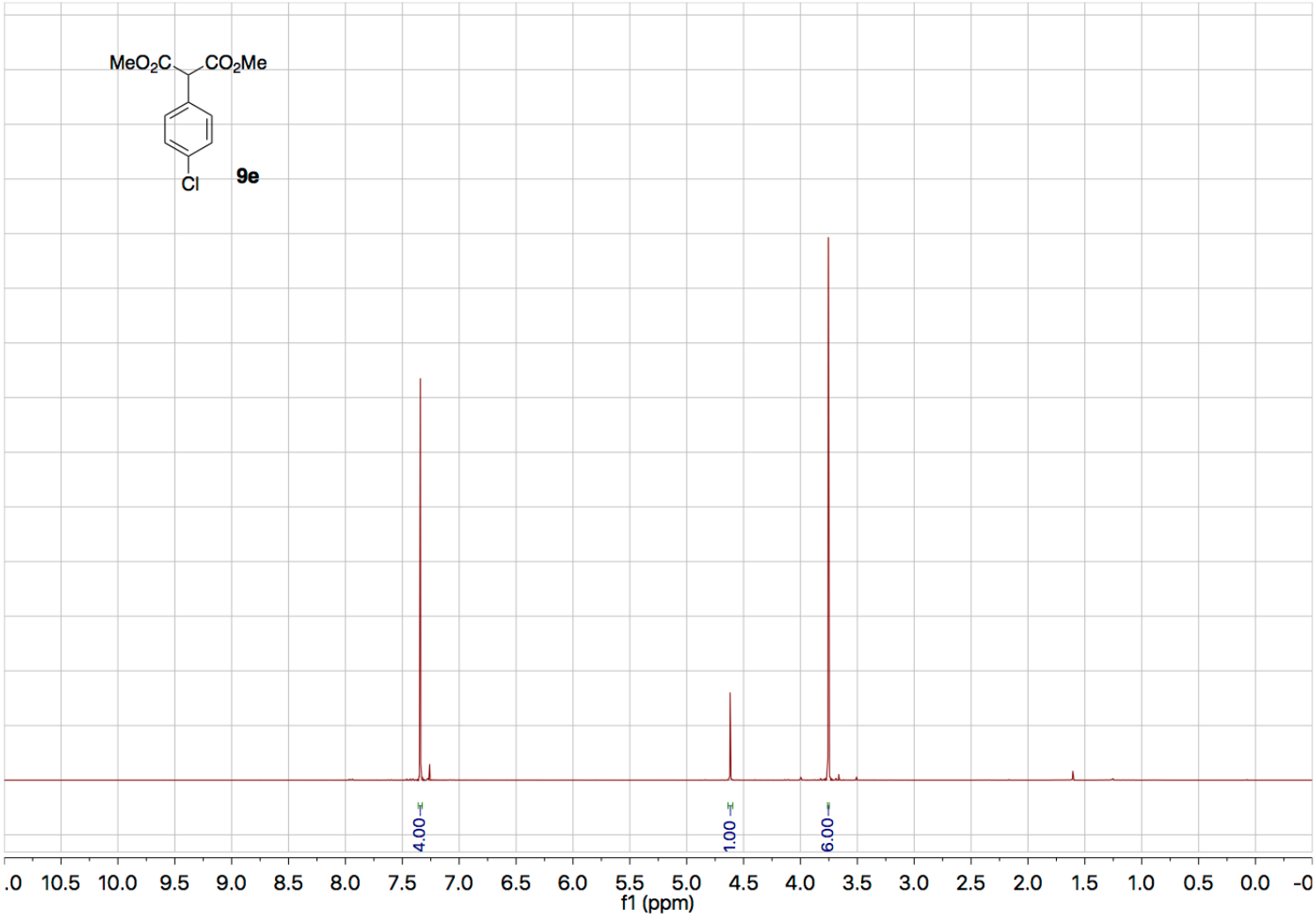
MeO2C
CO2Me
Cl
9e
4.00
1.00
6.00
.0 10.5 10.0 9.5 9.0 8.5 8.0 7.5 7.0 6.5 6.0 5.5 5.0 4.5 4.0 3.5 3.0 2.5 2.0 1.5 1.0 0.5 0.0 -0
f1 (ppm)

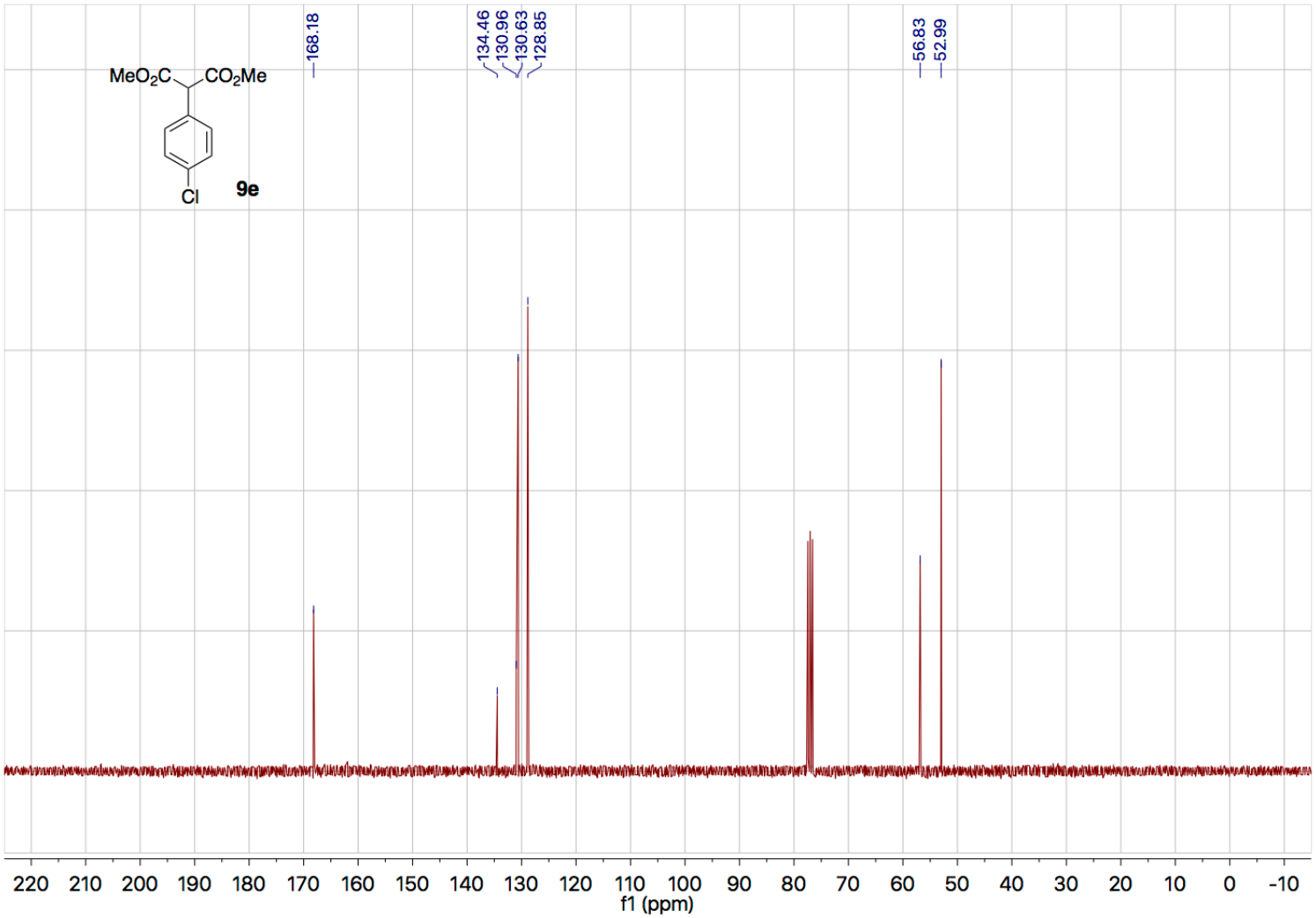
MeO2C
CO2Me
Cl
9e
168.18
134.46
130.96
130.63
128.85
56.83
52.99
220 210 200 190 180 170 160 150 140 130 120 110 100 90 80 70 60 50 40 30 20 10 0 -10
f1 (ppm)

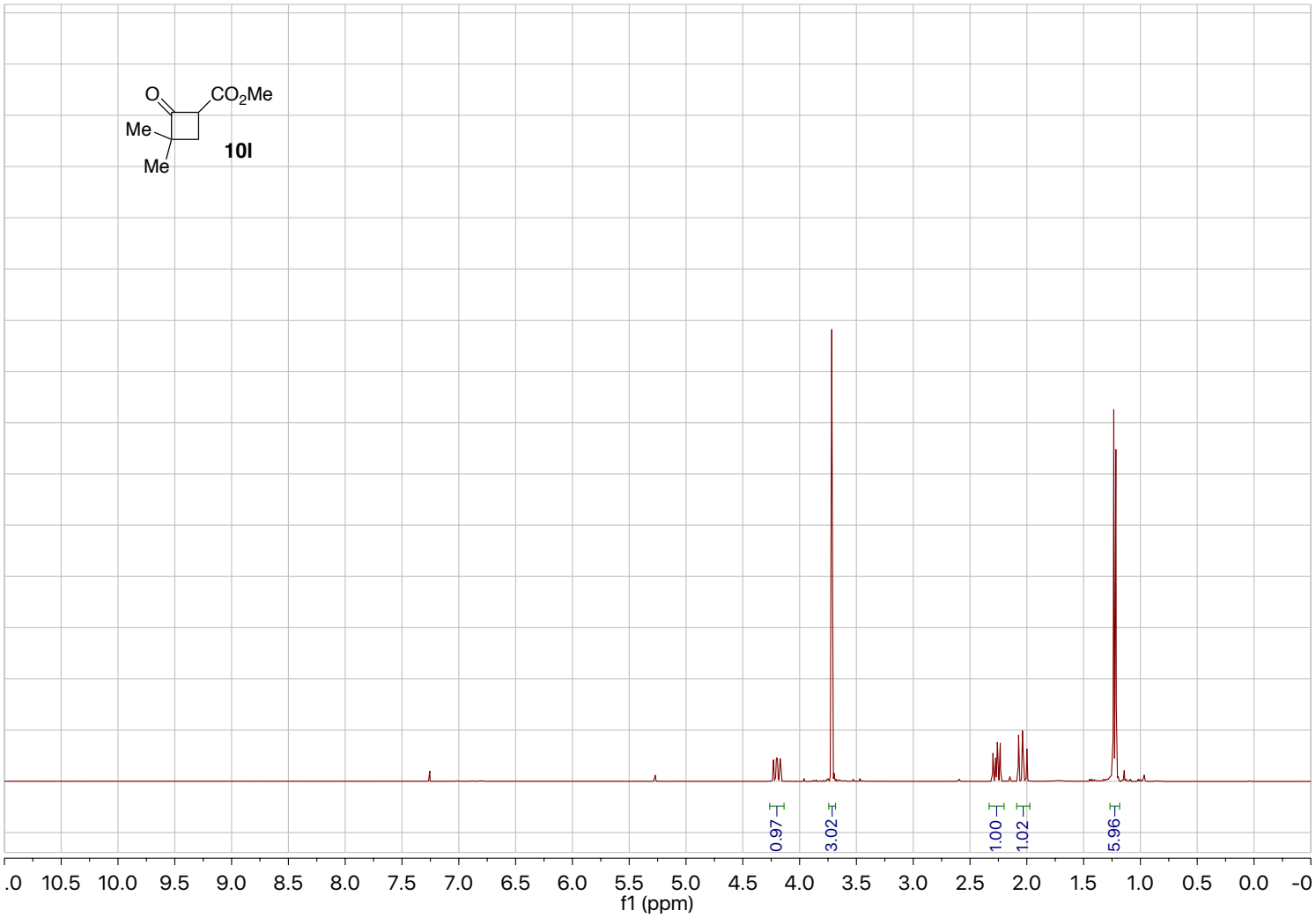
O
CO2Me
Me
Me
10l
0.97
3.02
1.00
1.02
5.96
.0 10.5 10.0 9.5 9.0 8.5 8.0 7.5 7.0 6.5 6.0 5.5 5.0 4.5 4.0 3.5 3.0 2.5 2.0 1.5 1.0 0.5 0.0 -0
f1 (ppm)

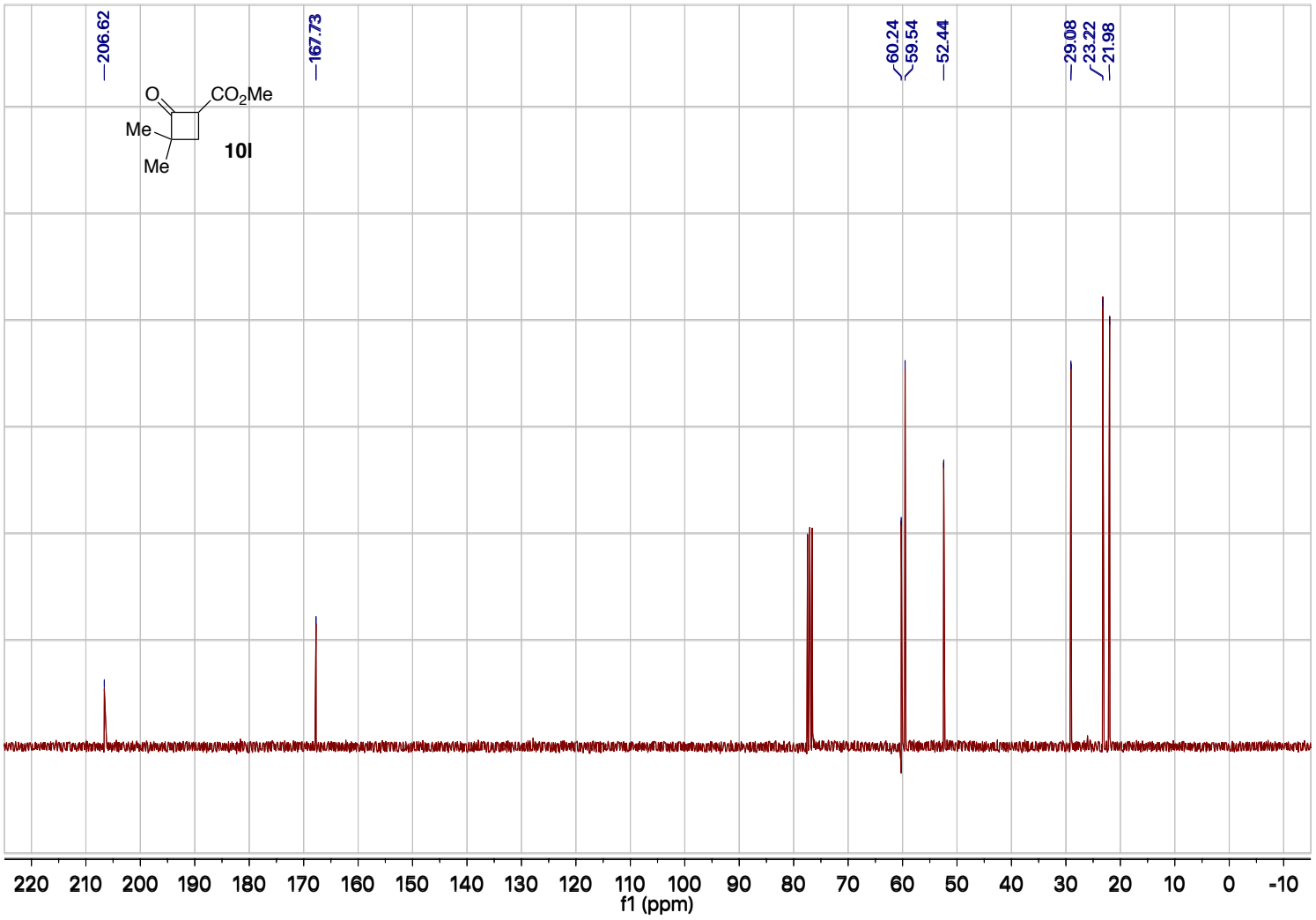
206.62
167.73
60.24
59.54
52.44
29.08
23.22
21.98
O
CO2Me
Me
Me
10l
220 210 200 190 180 170 160 150 140 130 120 110 100 90 80 70 60 50 40 30 20 10 0 -10
f1 (ppm)

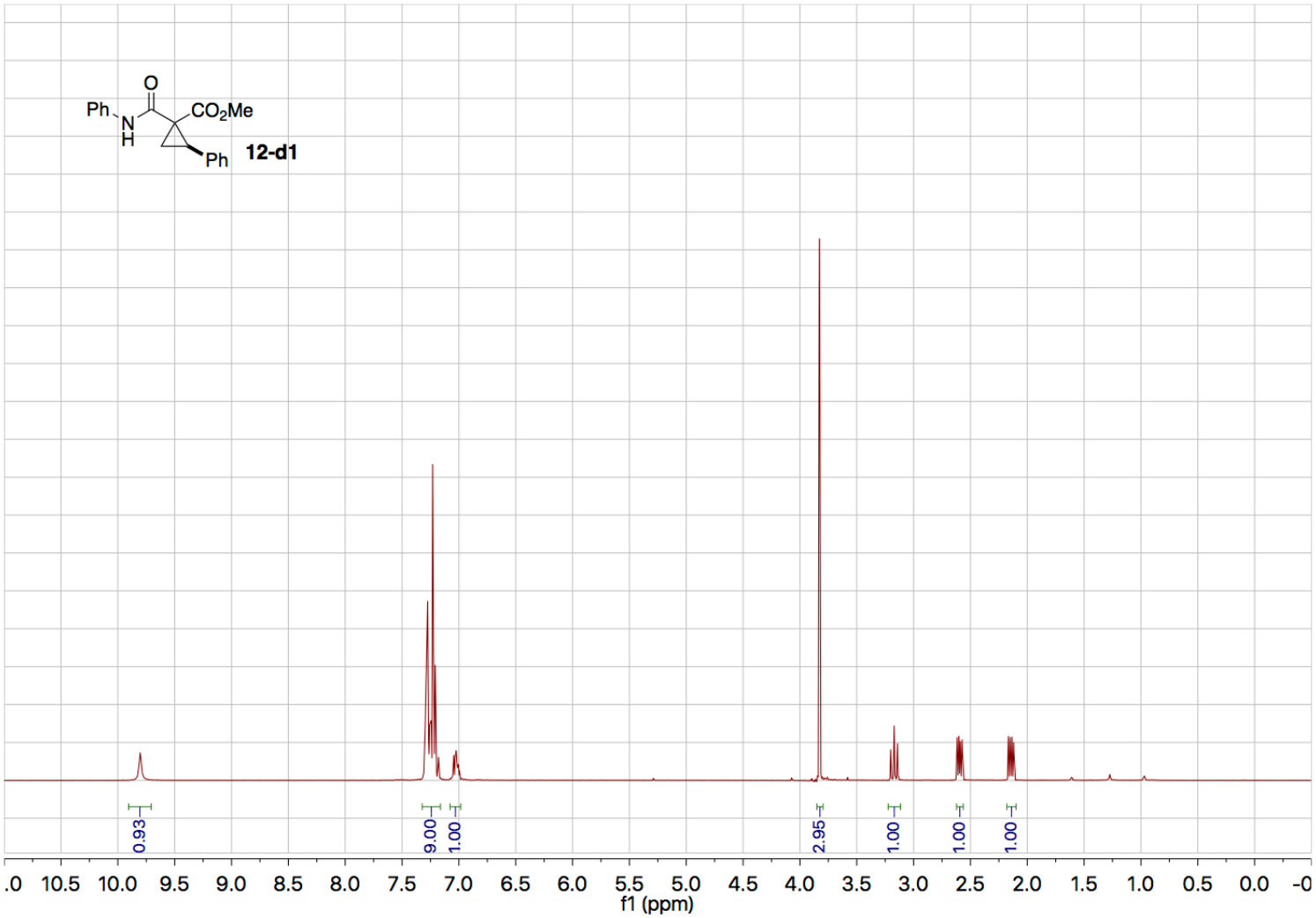
O
Ph
N
H
CO2Me
Ph
12-d1
0.93
9.00
1.00
2.95
1.00
1.00
1.00
.0 10.5 10.0 9.5 9.0 8.5 8.0 7.5 7.0 6.5 6.0 5.5 5.0 4.5 4.0 3.5 3.0 2.5 2.0 1.5 1.0 0.5 0.0 -0
f1 (ppm)

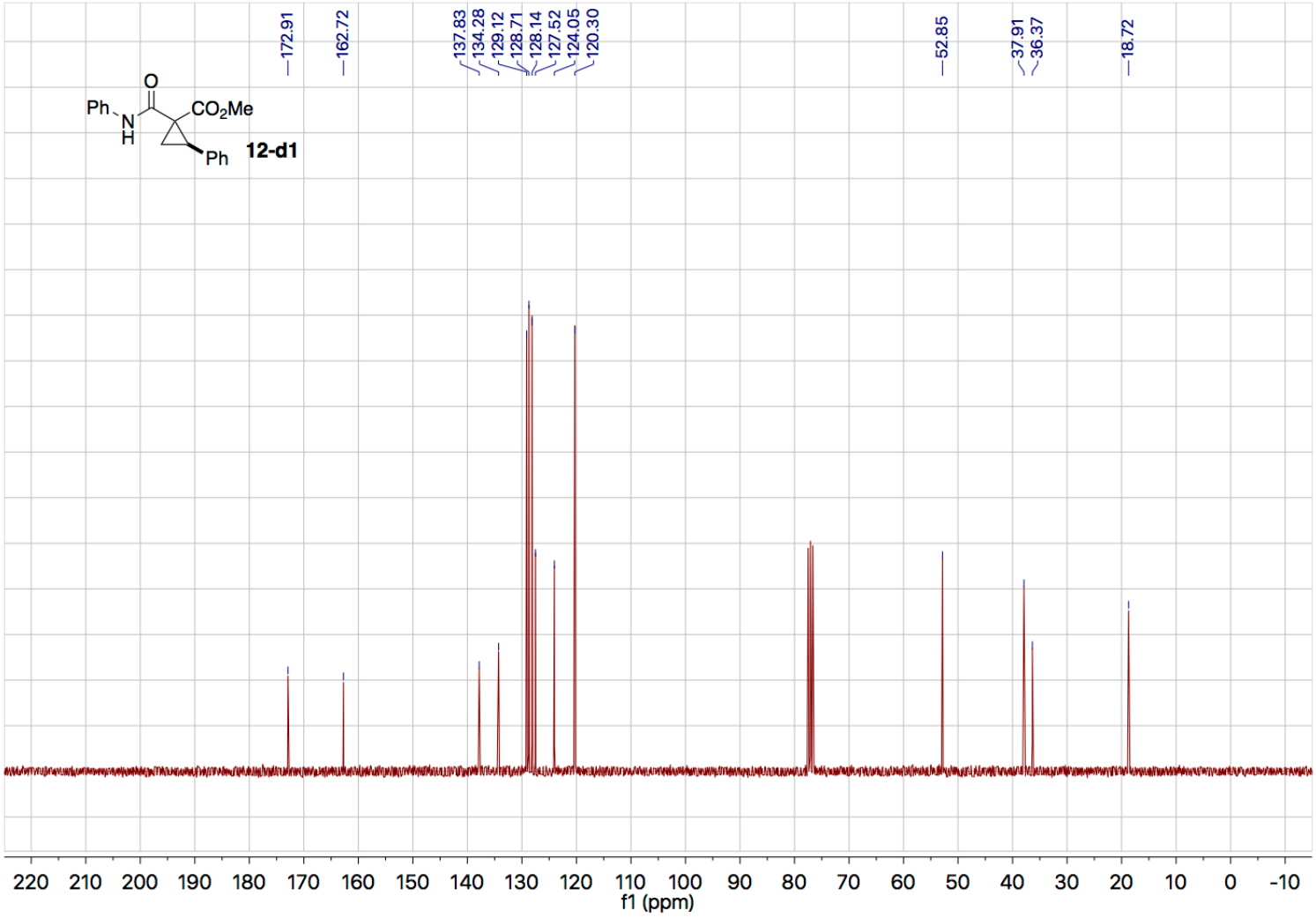
172.91
162.72
137.83
134.28
129.12
128.71
128.14
127.52
124.05
120.30
52.85
37.91
36.37
18.72
Ph
N
H
O
CO2Me
Ph
12-d1
220 210 200 190 180 170 160 150 140 130 120 110 100 90 80 70 60 50 40 30 20 10 0 -10
f1 (ppm)

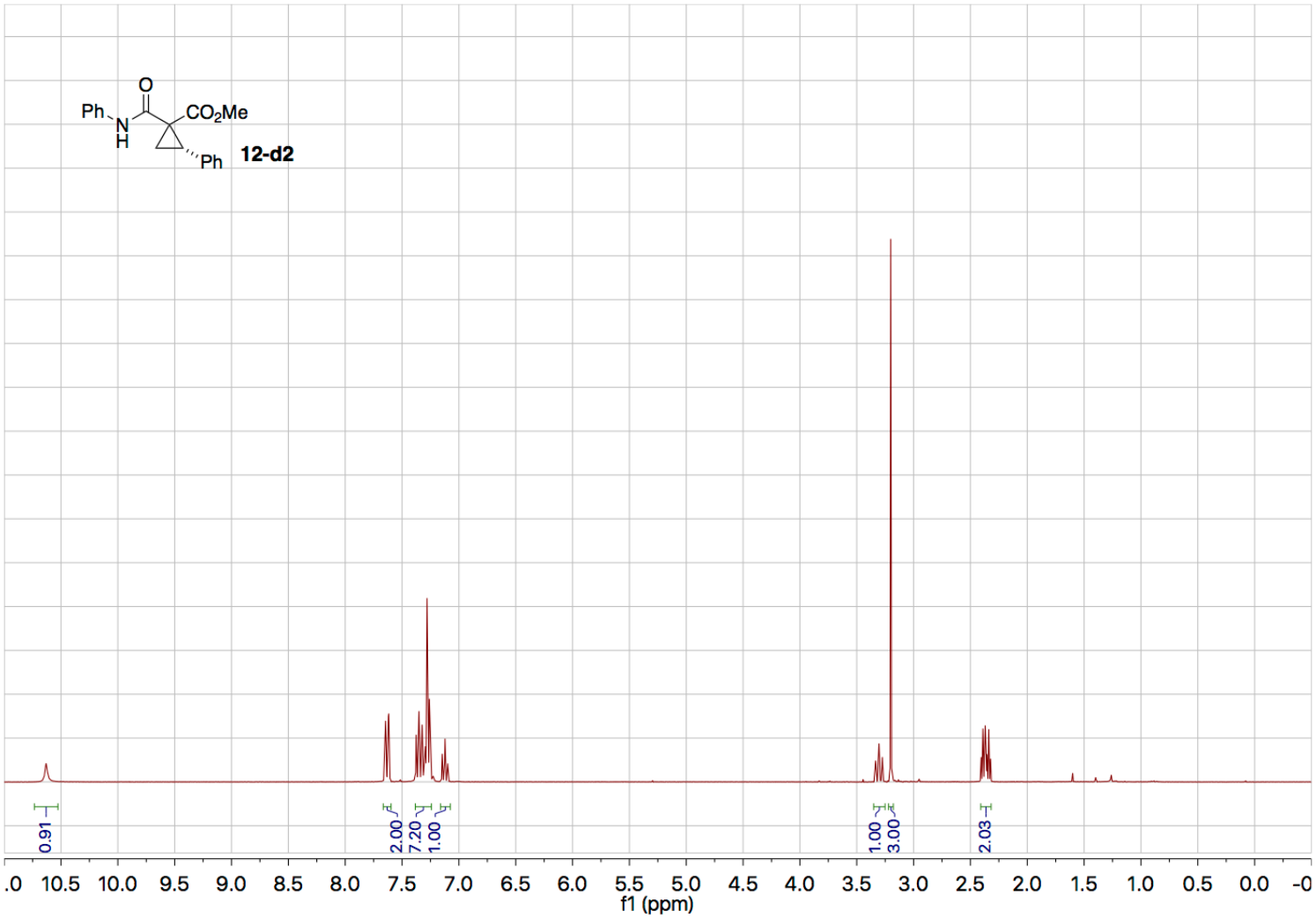
O
Ph
N
H
CO2Me
Ph
12-d2
0.91
2.00
7.20
1.00
1.00
3.00
2.03
.0 10.5 10.0 9.5 9.0 8.5 8.0 7.5 7.0 6.5 6.0 5.5 5.0 4.5 4.0 3.5 3.0 2.5 2.0 1.5 1.0 0.5 0.0 -0
f1 (ppm)

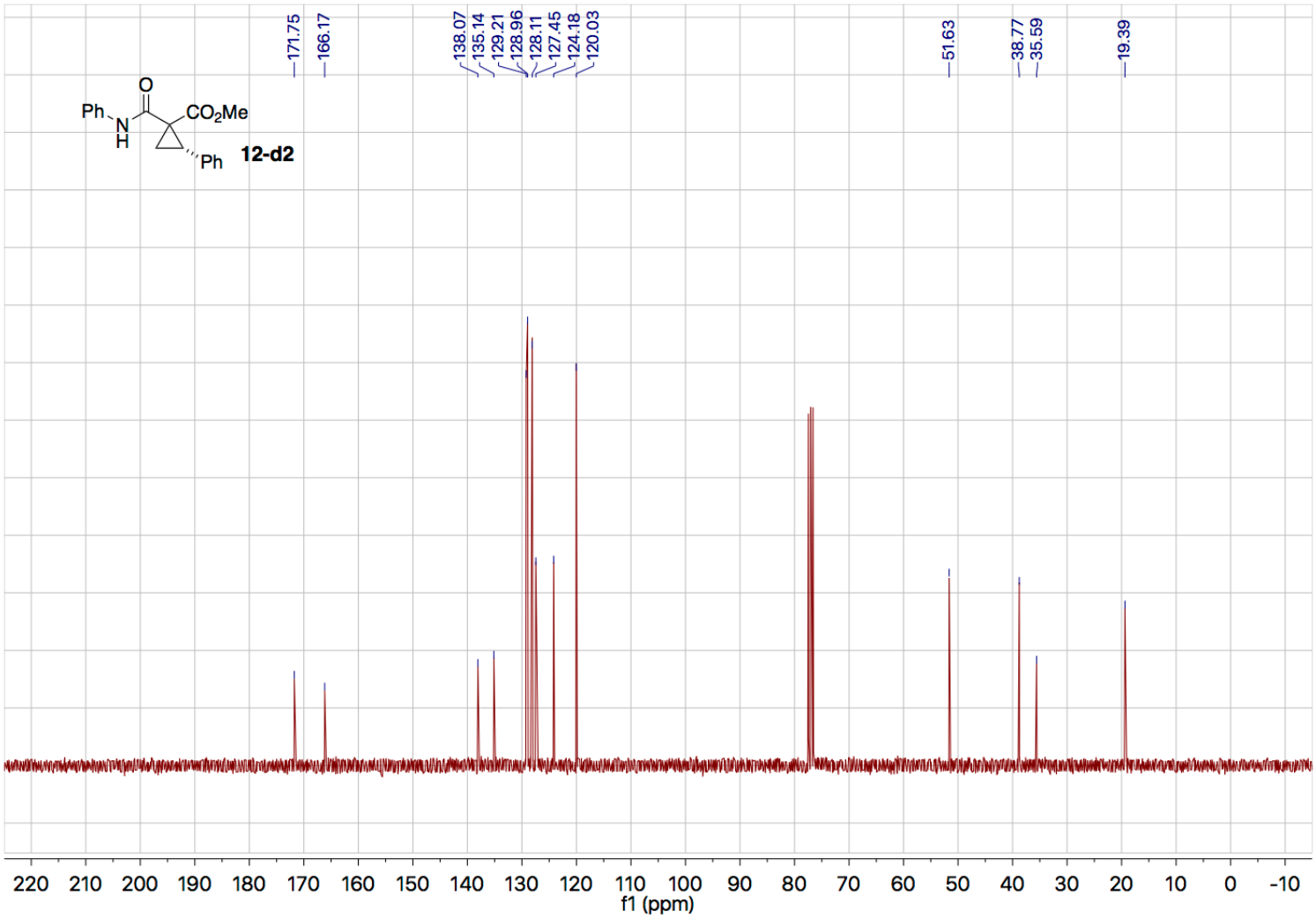
171.75
166.17
138.07
135.14
129.21
128.96
128.11
127.45
124.18
120.03
51.63
38.77
35.59
19.39
Ph
N
H
O
CO2Me
Ph
12-d2
220 210 200 190 180 170 160 150 140 130 120 110 100 90 80 70 60 50 40 30 20 10 0 -10
f1 (ppm)

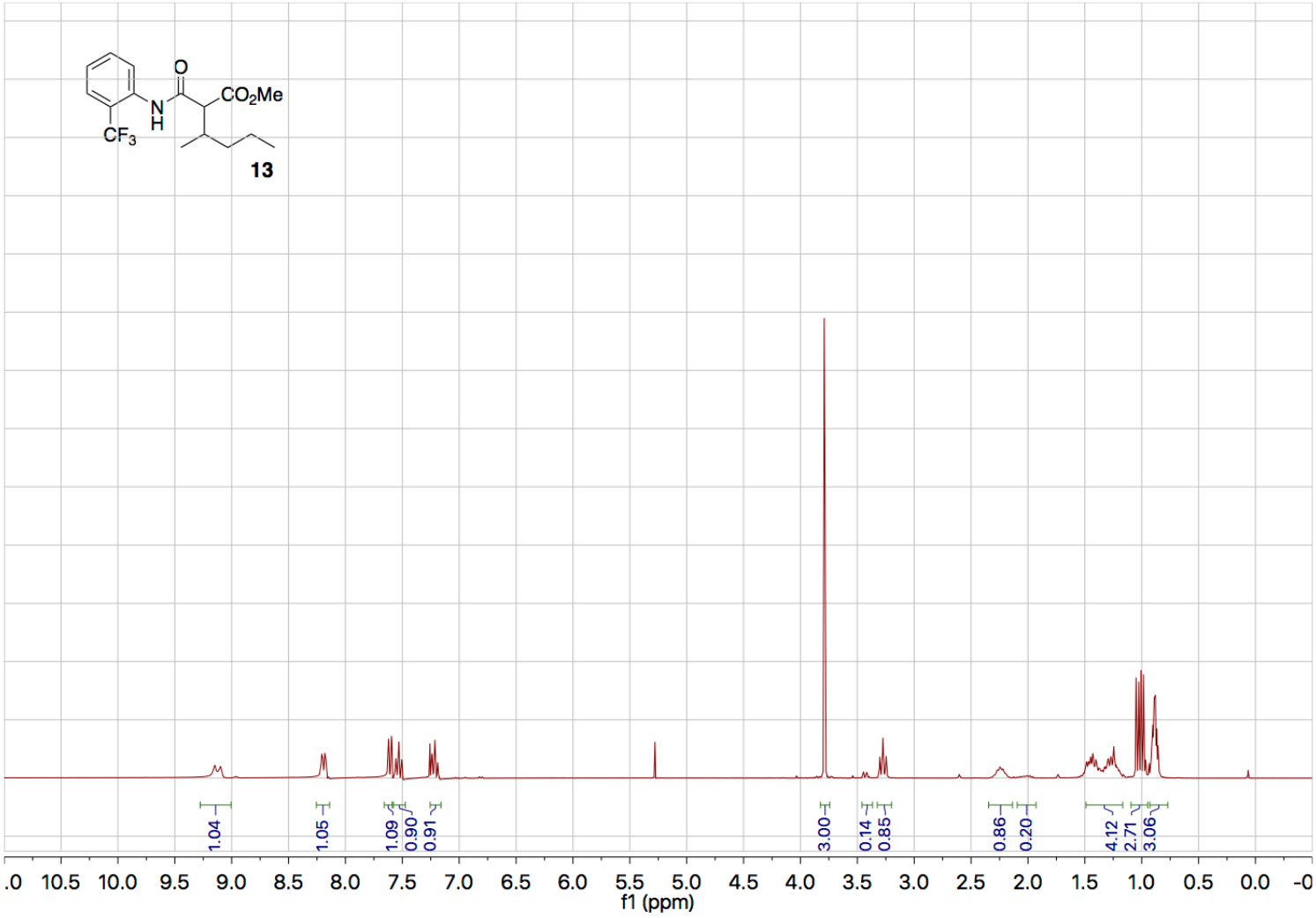
O
N
H
CO2Me
CF3
13
1.04
1.05
1.09
0.90
0.91
3.00
0.14
0.85
0.86
0.20
4.12
2.71
3.06
.0 10.5 10.0 9.5 9.0 8.5 8.0 7.5 7.0 6.5 6.0 5.5 5.0 4.5 4.0 3.5 3.0 2.5 2.0 1.5 1.0 0.5 0.0 -0
f1 (ppm)

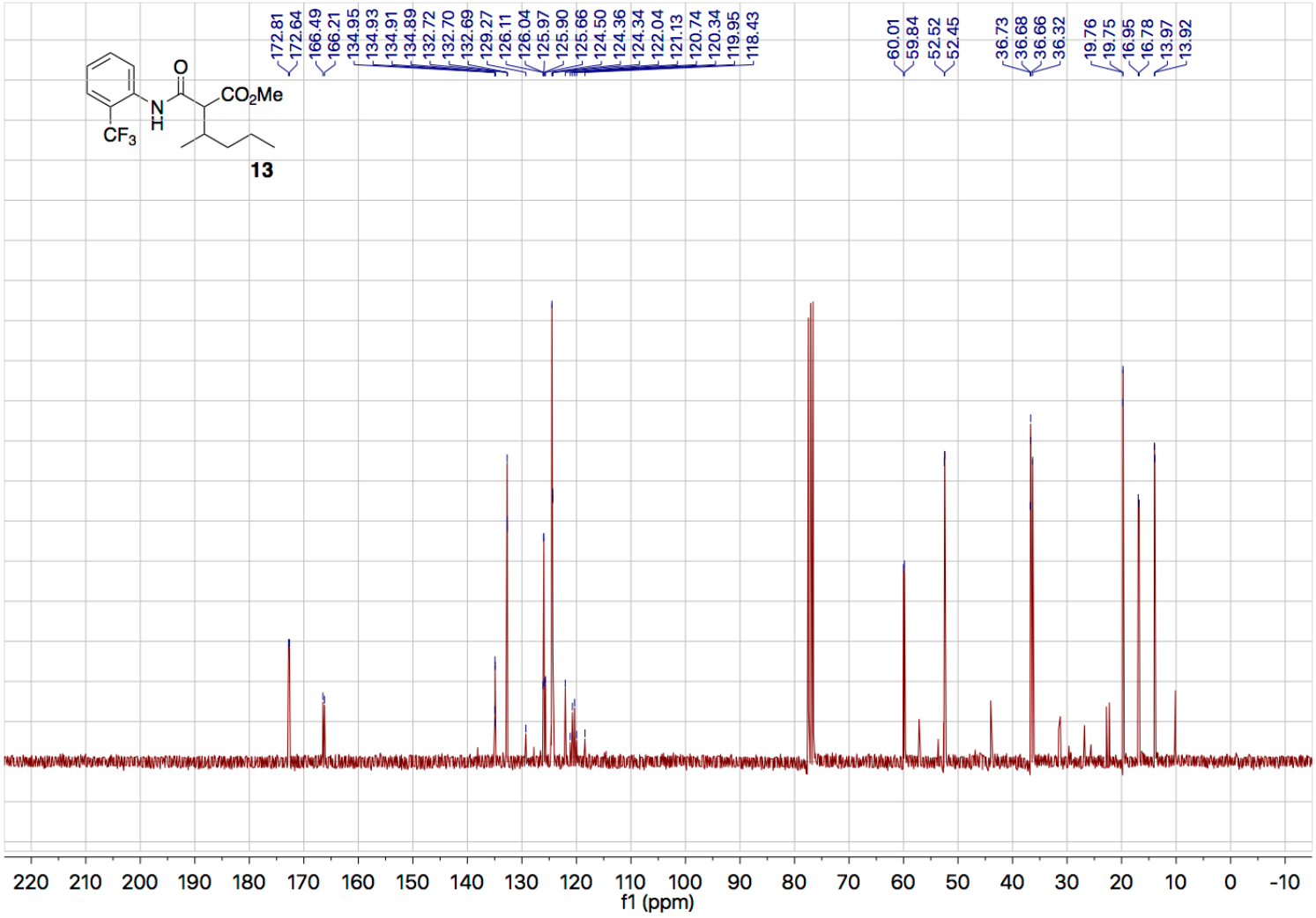
172.81
172.64
166.49
166.21
134.95
134.93
134.91
134.89
132.72
132.70
132.69
129.27
126.11
126.04
125.97
125.90
125.66
124.50
124.36
124.34
122.04
121.13
120.74
120.34
119.95
118.43
60.01
59.84
52.52
52.45
36.73
36.68
36.66
36.32
19.76
19.75
16.95
16.78
13.97
13.92
O
N
H
CO2Me
CF3
13
220 210 200 190 180 170 160 150 140 130 120 110 100 90 80 70 60 50 40 30 20 10 0 -10
f1 (ppm)

3.5 References

[1] Davies, H. M. L. and B. T. Parr (2013). "Rhodium Carbenes." Contemporary Carbene Chemistry, John Wiley & Sons, Inc.**:** 363-403.

[2] Guy Bertrand. Carbene Chemistry: From Fleeting Intermediates to Powerful Reagents. CRC Press. 2002.

[3] Audia, J. E.; Droste J. J.; Gevorgyan, V.; Rubin, M.; Chan, W.; Yu, W.; McLarney, B.; France, S. (2016) "Dimethyl Diazomalonate." Encyclopedia of Reagents for Organic Synthesis. John Wiley & Sons, Ltd.

[4] Lindsay, V. N. G.; Nicolas, C.; Charette, A. B. *Journal of the American Chemical Society* **2011**, *133*, 8972.

[5] Mclarney, B.D.; Cavitt, M.A.; Donnell, T.M.; Musaev, D.G.; France, S.A. *Chemistry – A European Journal* **2017**, *23*, 1129.

[6] England, D. B.; Eagan, J. M.; Merey, G.; Anac, O.; Padwa, A. *Tetrahedron* **2008**, *64*, 988.

[7] Morton, D.; Blakey, S. B. *ChemCatChem* **2015**, *7*, 577.

[8] Davies, H. M. L.; Morton, D. *Chemical Society Reviews* **2011**, *40*, 1857.

[9] Doyle, M. P.; Duffy, R.; Ratnikov, M.; Zhou, L. *Chemical Reviews* **2010**, *110*, 704.

[10] Kirmse, W. *European Journal of Organic Chemistry* **2002**, *2002*, 2193.

[11] Scott, A. P.; Platz, M. S.; Radom, L. *Journal of the American Chemical Society* **2001**, *123*, 6069.

[12] Gronert, S.; Keeffe, J. R.; More O'Ferrall, R. A. *Journal of the American Chemical Society* **2011**, *133*, 3381.

[13] Nemirowski, A.; Schreiner, P. R. *The Journal of Organic Chemistry* **2007**, *72*, 9533.

[14] Alonso, M. E.; Fernandez, R.; *Tetrahedron* **1989**, *45*, 3313.

[15] Alonso, M. E.; Del Carmen Garcia, M. *Journal of Organic Chemistry* **1985**, *50*, 988.

[16] Nani, R. R.; Reisman, S. E. *Journal of the American Chemical Society* **2013**, *135*, 7304.

[17] (a) Watanabe, N.; Masashio, A.; Hashimoto, S.-I.; Ikegami, S. *Synlett* **1994**, *12*, 1031; (b) Anada, M.; Hashimoto, S.-i. *Tetrahedron Letters* **1998**, *39*, 79; (c) Anada, M.; Hashimoto, S.-i. *Tetrahedron Letters* **1998**, *39*, 9063; (d) Anada, M.; Watanabe, N. *Chemical Communications* **1998**, 1517.

[18] Doyle, M. P.; Hu, W.; Wee, A. G. H.; Wang, Z.; Duncan, S. C. *Organic Letters* **2003**, *5*, 407.

[19] Zhang, B.; Wee, A. G. H. *Organic & Biomolecular Chemistry* **2012**, *10*, 4597.

[20] Muller, P.; Tohill, S. *Tetrahedron* **2000**, 56, 1725.

[21] Davies, H. M. L.; Hansen, T. *Journal of the American Chemical Society* **1997**, *119*, 9075.

[22] Nakamura, E.; Yoshikai, N.; Yamanaka, M. *Journal of the American Chemical Society* **2002**, *124*, 7181.

[23] (a) Taber, D. F.; Ruckle, R. E., Jr. *J. Am. Chem. Soc.* **1986**, *108*, 7686; (b) Doyle, M. P.; Westrum, L. J.; Wolthuis, W. N. E.; See, M. M.; Boone, W. P.; Bagheri, V.; Pearson, M. M. *Journal of the American Chemical Society* **1993**, *115*, 958; (c) Davies, H. M. L.; Ren, P.; Jin, Q. *Organic Letters.* **2001**, *3*, 3587.

[24] (a) Gaussian 09, Revision D.01, M. J. Frisch, G. W. Trucks, H. B. Schlegel, G. E. Scuseria, M. A. Robb, J. R. Cheeseman, G. Scalmani, V. Barone, B. Mennucci, G. A. Petersson, H. Nakatsuji, M. Caricato, X. Li, H. P. Hratchian, A. F. Izmaylov, J. Bloino, G. Zheng, J. L. Sonnenberg, M. Hada, M. Ehara, K. Toyota, R. Fukuda, J. Hasegawa, M. Ishida, T. Nakajima, Y. Honda, O. Kitao, H. Nakai, T. Vreven, J. A. Montgomery, Jr., J. E. Peralta, F. Ogliaro, M. Bearpark, J. J. Heyd, E. Brothers, K. N. Kudin, V. N. Staroverov, R. Kobayashi, J. Normand, K. Raghavachari, A. Rendell, J.C. Burant, S.S. Iyengar, J. Tomasi, M. Cossi, N. Rega, J. M. Millam, M. Klene, J. E. Knox, J. B. Cross, V. Bakken, C. Adamo, J. Jaramillo, R. Gomperts, R. E. Stratmann, O. Yazyev, A. J. Austin, R. Cammi, C. Pomelli, J. W. Ochterski, R. L. Martin, K. Morokuma, V. G. Zakrzewski, G. A. Voth, P. Salvador, J. J. Dannenberg, S. Dapprich, A. D. Daniels, Ö. Farkas, J. B. Foresman, J. V. Ortiz, J. Cioslowski, and D. J. Fox, Gaussian, Inc., Wallingford CT, **2013**; (b) Chai, J.-D.; Head-Gordon, M. *Physical Chemistry Chemical Physics* **2008**, *10*, 6615; (c) Wadt, W. R.; Hay, P. J. *Journal of Chemical Physics* **1985**, *82*, 284; (d) Hay, P. J.; Wadt, W. R. *Journal of Chemical Physics* **1985**, *82*, 270.

[25] (a) Tomasi, J.; Mennucci, B.; Cammi, R. *Chemical Reviews* **2005**, *105*, 2999 and references cited therein; (b) Tomasi, J.; Mennucci, B. Cances, E. *THEOCHEM* **1999**, *464*, 211; (c) Pascal-Ahuir, J.L.; Silla, E.; Tuñoń, I. *Journal of Computational Chemistry* **1994**, *15*, 1127.

[26] Anslyn, E. V.; Dougherty, D. A. (2006). Modern Physical Organic Chemistry. Sausalito, CA: University Science Books: 104–105.

[27] Hammett, L. P. *Journal of the American Chemical Society* **1937**, *59*, 96.

[28] Meyer, M. E.; Ferreira, E. M.; Stoltz, B. M. *Chemical Communications* **2006**, 1316.

[29] (a) Wu, Q.-F.; Wang, X.-B.; Shen, P.-X.; Yu, J.-Q. *ACS Catalysis* **2018**, *8*, 2577; (b) Zhu, R.-Y.; Saint-Denis, T. G.; Shao, Y.; He, J.; Sieber, J. D.; Senanayake, C. H.; Yu, J.-Q. *Journal of the American Chemical Society* **2017**, *139*, 5724.

CHAPTER 4. DESIGNING CARBENES

4.1 Introduction

4.1.1 The Indole Core

4.1.1.1 Biological Importance of the Indole Core

Indole **1**, a bicyclic heteroaromatic with the formula C_8H_7N, represents a very important core structure in biological systems (Figure 25).[1] Indole itself is naturally produced by bacteria and plays several important roles in intercellular bacterial communication, but its diverse and nearly limitless set of derivatives are found in key roles in nearly every corner of life.[1] Tryptophan, the indole-containing amino acid, is one of the fundamental building blocks of life and thus widely manifested in nature via proteins (Figure 26). Other naturally occurring indole derivatives, such as serotonin and melatonin play critical roles in psychological functioning of many mammals. Strychnine causes powerful muscle contractions, and toxiferines can serve as muscle relaxants.

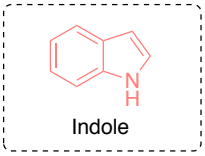

Figure 25 – The Structure of Indole

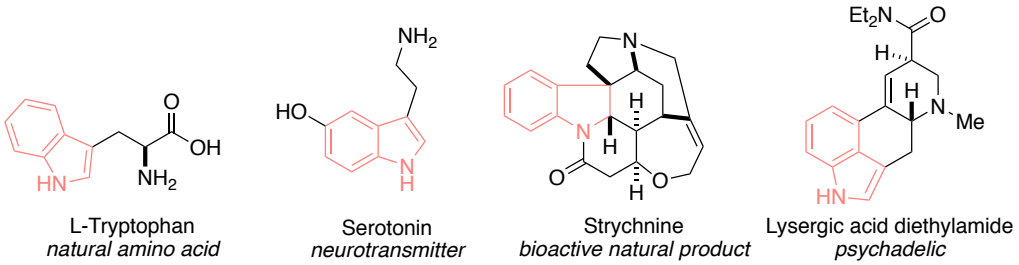

Figure 26 – Notable Examples of Biologically Relevant Indole Alkaloids

Many indole alkaloids have earned fame as anticancer therapeutics, and others, notoriety as DEA Schedule 1 narcotics (e.g. psilocybin and lysergic acid diethylamide). The family of indoles is a fountain of biological activity and, as such, a well of inspiration for medicinal chemists.

4.1.1.2 Current Synthetic Methods for Construction of the Indole Core

Many approaches to indole synthesis currently exist; a 2011 review by Taber and Tirunahari presented a classification system for the infamous heterocycle's construction resulting in nine, fundamentally different approaches to the core structure (Figure 27).[2] Albeit the authors admit their aim was "to be illustrative, not exhaustively inclusive" as the latter would be a daunting task.

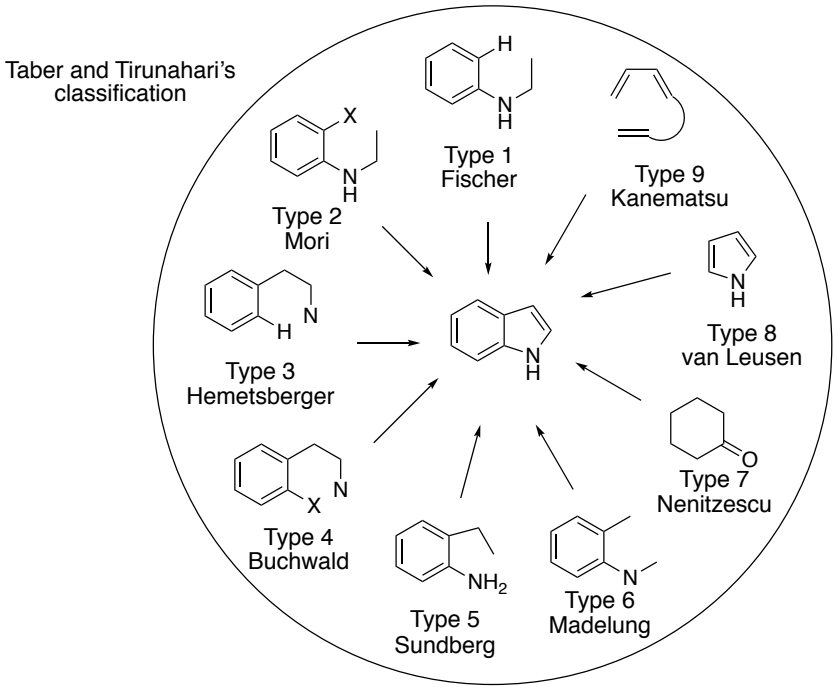

Figure 27 – Taber and Tirunahari's Nine-Type Classification of Indole Syntheses

Types 1-6 are the most widely used approaches and rely on constructing the pyrrole unit from an existing benzene or aniline derivative. The Fischer indole synthesis (Scheme 32), first performed in 1883 by Herman Emil Fischer, is the oldest, most robust representative and considered the "gold standard" among these approaches.[3] Mechanistically, it occurs by the elimination of ammonia from a cyclic aminal intermediate obtained from an aryl hydrazone.

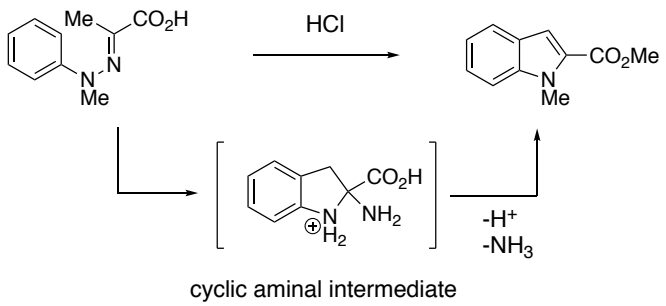

Scheme 32 – Original Fischer Indole Synthesis (1883)

The Fischer indole synthesis continues to be developed today. In 2004, Buchwald synthesized a highly-substituted indole with a variation of the Fischer's original conditions (Scheme 33).[4] Meanwhile contributions made by Mori,[5] MacLeod,[6] Fukuyama,[7] Larock,[8] and Jones[9] serves as representative examples of Types 2-6 respectively.

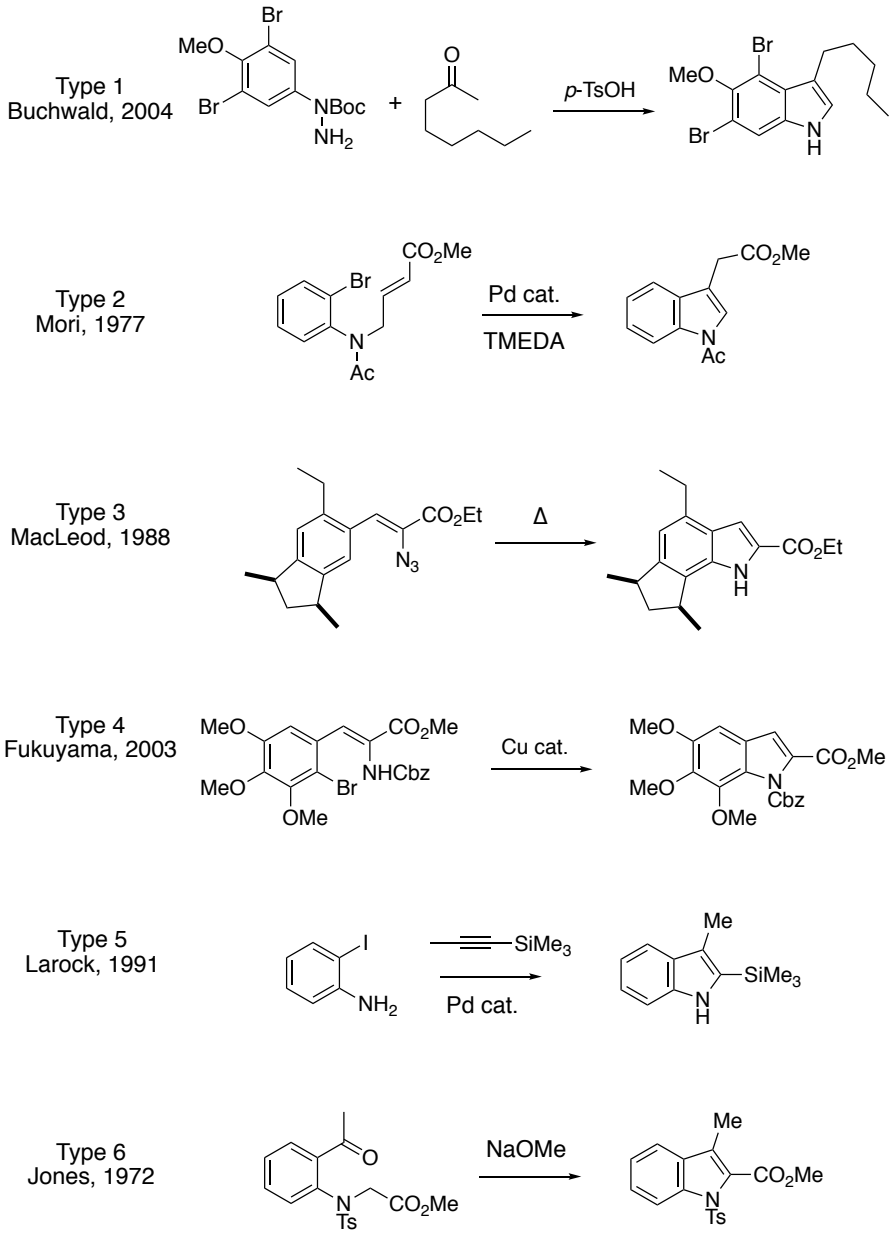

Scheme 33 – Illustrative Examples of Indole Syntheses Types 1-6

Type 8 relies on building the benzene portion from a functionalized pyrrole side chain, a strategy pioneered by van Leusen in 1986 (Scheme 34).[10] Unlike Types 1-6 and 8, neither Types 7 nor 9 rely on aromatic starting materials. Instead, Type 7 first builds the heterocyclic scaffold, typically using a cyclohexanone derivative, and then oxidizes the system to the indole.[11] Type 9 reverses this process, constructing the indole from a cascade

cyclization on an unsaturated nitrogen-containing chain.[12] A tenth approach has emerged which was not mentioned in Taber and Tirunahari's 2011 review. This approach constructs substituted indoles via C(sp^2)-H functionalization indole itself; a transformation by Shi (2017),[13] selective for the 5-position, is shown in Scheme 34, but many others have contributed to the popularization of C-H functionalization approaches.[14]

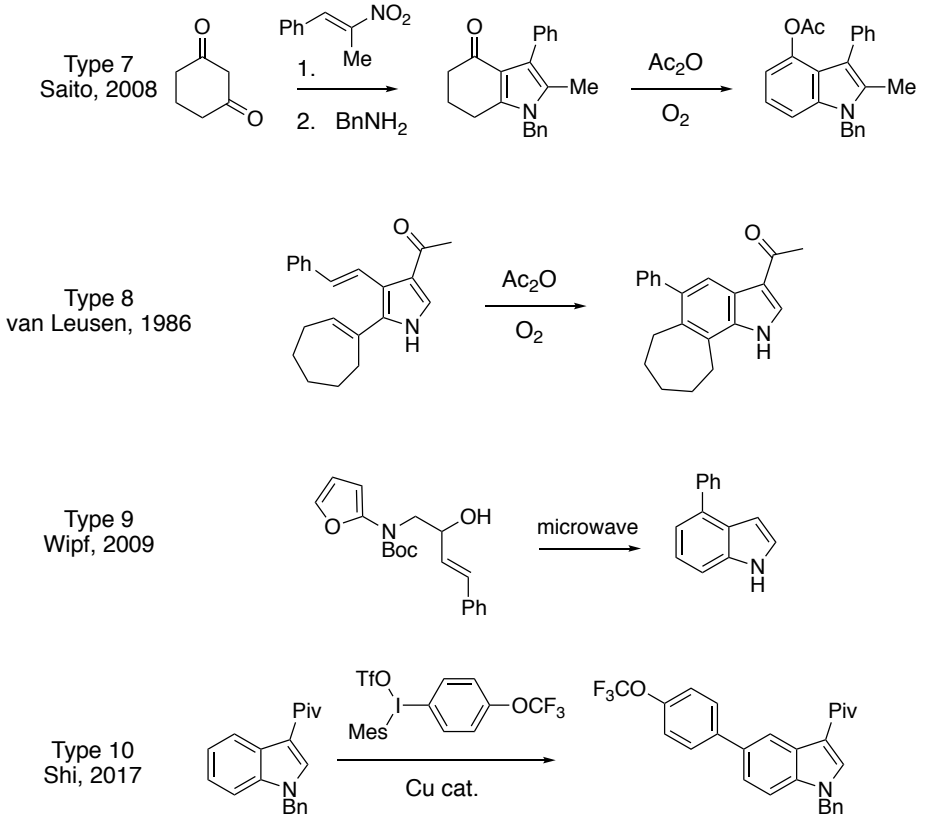

Scheme 34 – Illustrative Examples of Indole Syntheses Types 7-10

It can be heuristically useful to reduce Taber and Tirunahari's classification to only five types of indole syntheses by conflating Types 1-6 into a single class and then dividing the approaches into two subcategories: **I**) approaches that rely on aromatic starting materials and **II**) those that do not (Figure 28).

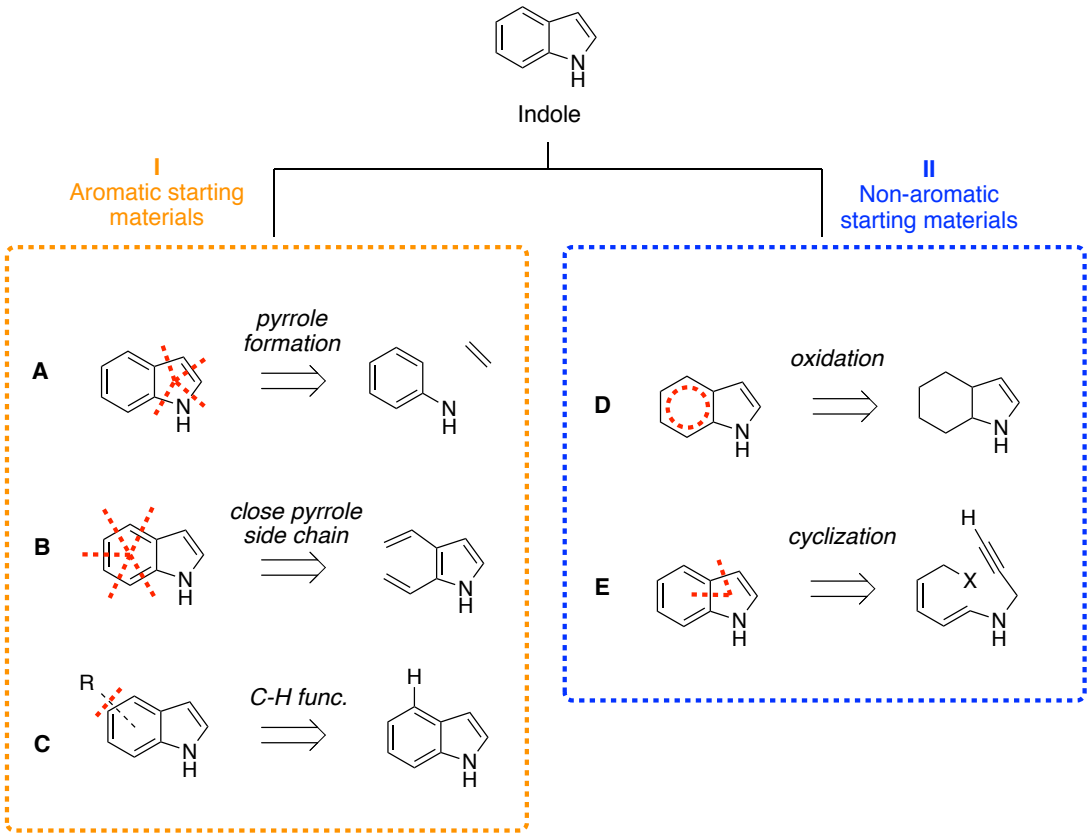

Figure 28 – Five Approaches to Indole Core Construction

We can then subdivide **I** into three categories based on which aromatic building block is used and how it is elaborated into the indole core: (**A**) a pyrrole ring is constructed from a benzene (or aniline) derivative; (**B**) a pyrrole side chain is cyclized to form the benzene portion of indole; (**C**) an indole core is modified through a C-H functionalization to obtain a core with desirable substitution. Class **II** contains approaches to indole cores from non-aromatic systems. These systems are non-aromatic either because they lack the requisite 10 π-electrons (**D**) or the π-electrons are not yet arranged in a cyclic array (**E**).

4.1.1.3 Limitations and Opportunities

Modular methods for indole construction are in demand. In a world where time, not money or waste, is the enemy of medicinal chemists, the primary limitation in the field of substituted indole synthesis is the linearity of approaches which cannot be carried out in parallel work streams.[15] To efficiently enable drug discovery strategies, medicinal chemists require convergent syntheses for complex building blocks. In this sense, a useful method would be one that offers access to uncharted areas of substituted indole chemical space while offering modularity for construction of the benzene portion of the indole ring. This is because, for highly substituted indoles made by the most popular approaches (Types 1-6), the benzene fragment typically requires the most linear synthetic steps and fixes substitution on the benzene early in the sequence. Recent developments in the France Lab inspired us toward solving this problem using a C-H functionalization approach from an acceptor-acceptor diazo compound **1** (Scheme 35).

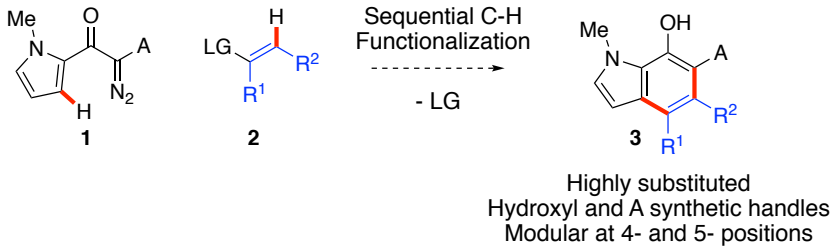

Scheme 35 – France Lab Approach towards Highly Substituted Indoles with Modular Functionality at 4- and 5-Positions

4.1.2 Methodology Development Strategy

4.1.2.1 Aponte-Guzman's Ring-Opening Benzannulation of 2,3-Dihydrofuran Acetals

In 2016, Joel Aponte-Guzman, a graduate student in our lab, reported a cascade ring-opening benzannulation of O,O- and N,O-2,3-dihydrofuran acetals that generated

naphthalenes, benzofurans, and benzothiophenes with multiple substitutions, among them a carboxylate at the 7-position (6-position for the benzofurans and benzothiophenes) (Scheme 36).[16] In the study, the dihydrofuran acetal starting materials were prepared from diazoacetates and enol ethers in the presence of a dimeric Rh(II) catalyst (Scheme 36).

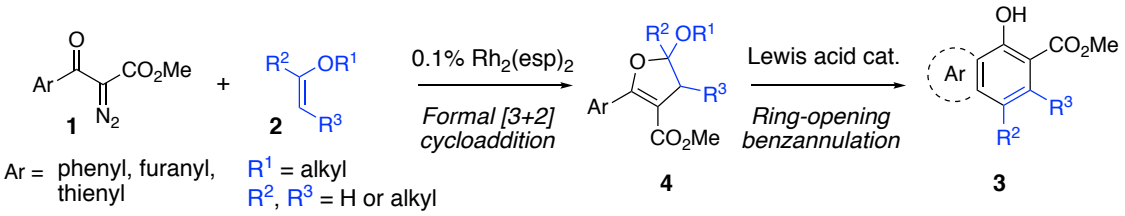

Scheme 36 – Inspiring Benzannulation Method from the France Lab (J. Aponte-Guzman)

The proposed mechanism of the benzannulation step involved Lewis acid coordination to and opening of the acetal moiety (Scheme 37).

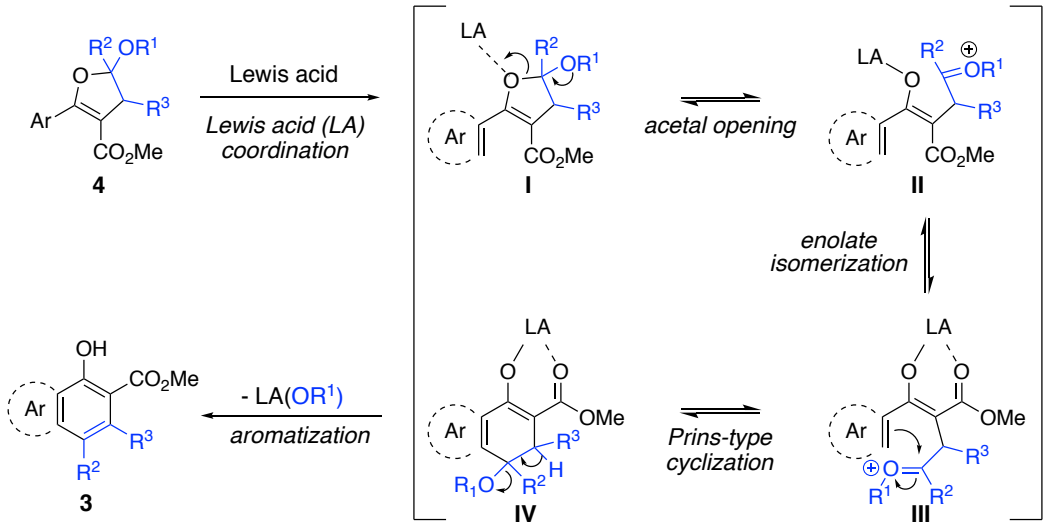

Scheme 37 – Proposed Mechanism for the Benzannulation Reaction

Opening of the acetal is followed by a conformational enolate isomerization that aligns the oxonium and aryl ring for a Prins-type cyclization. Aromatization occurs upon

loss of a proton and the alkoxy moiety; reprotonation would promote dissociation of the Lewis acid generating the benzannulated product and completing the catalytic cycle.

Aponte-Guzman recognized that his transformation could, hypothetically, be applied to the generation of a highly-substituted 7-hydroxy-indole 6-carboxylates by using a pyrrole aryl group instead of a phenyl ring, furan, or thiophene. However, his attempts translating the benzannulation chemistry to the indole manifold presented unexpected challenges (Scheme 38). Specifically, the DHF acetal intermediates could not be observed in attempts to react the diazo **1a** with enol ether **2a**. A trace amount of the cyclized 6-carboxylate indole **3aa** was observed, but attempts to optimize results toward formation of either product **3a** or **4aa** were unsuccessful.[17]

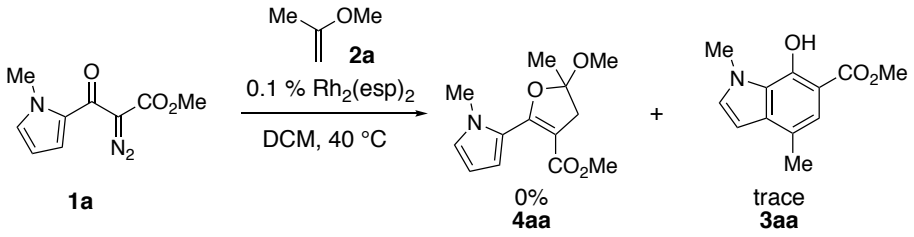

Scheme 38 – Unsuccessful Attempts to Adapt the Benzannulation Chemistry to the Formation of Indole-6-Carboxylates

4.1.2.2 Hypothesizing the Use of a Diazonitrile

Metal carbenes generated from diazonitriles are considered more electrophilic than those from diazoacetates due to their decreased steric bulk. Furthermore, addition products of nitrile-substituted metal carbenes are, historically, less prone to rearrangement chemistry than their ester counterparts.[18] In fact, in Chapter 2 we demonstrated the selectivity of diazonitriles for dihydrofuran acetal products in the presence of enol ethers and a dimeric

Rh(II) catalyst. For these reasons, it was hypothesized that a diazonitrile, such as **1b**, could be used in place of the diazoacetates to promote DHF acetal formation and persistence (Scheme 39).

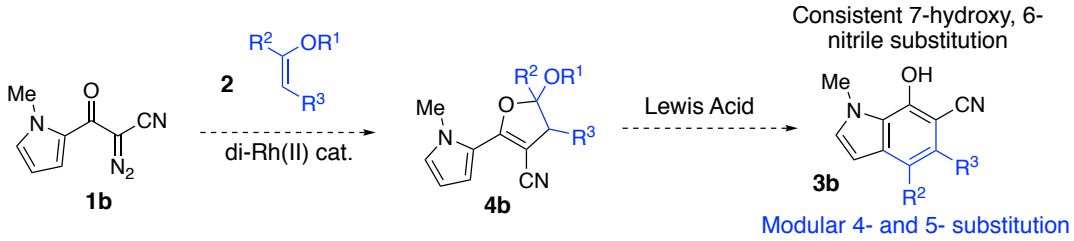

Scheme 39 – Hypothesizing the Use of a Diazonitrile

Given the distal relationship between the acceptor group-of-choice and the reactive acetal center, the switch from ester to nitrile was expected to leave the ring-opening benzannulation step unaffected, and, thus, enable the route to 6-nitrile indoles **3b**. The 6-nitrile indoles could be readily converted to indole-6-carboxylates via oxidation to access the ester's product space, but they have the added benefit of an auspiciously situated nitrogen atom that could be leveraged for chemistry not available from the carboxylates. Not only could this method provide access to indoles with a highly-substituted benzene fragment, but two of those substitutions, the hydroxyl and nitrile, will be versatile synthetic handles. Moreover, the enol ether provides modularity at positions where substitution is otherwise fixed early in the synthetic sequence.

4.2 Results and Discussion

4.2.1 Testing the Diazonitrile

The diazonitrile **1b** was prepared from 3-(1-methyl-1*H*-pyrrol-2-yl)-3-oxopropanenitrile **5b** and 1H-imidazole-1-sulfonyl azide hydrochloride **6** (Scheme 40).

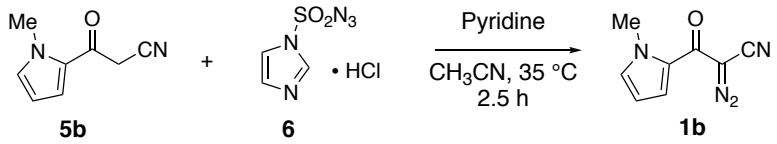

Scheme 40 – Preparation of the Diazonitrile Starting Material

Gratifyingly, reacting diazonitrile **1b** with enol ether **2a** in the presence of Rh_2esp_2 furnished DHF **4ba** in 40% yield. Treating **4ba** with conditions reported by Aponte-Guzman generated the 6-cyanoindole **3ba** in 63% yield (Scheme 41).[16] Encouraged by these results, we commenced independent optimizations of the two steps.

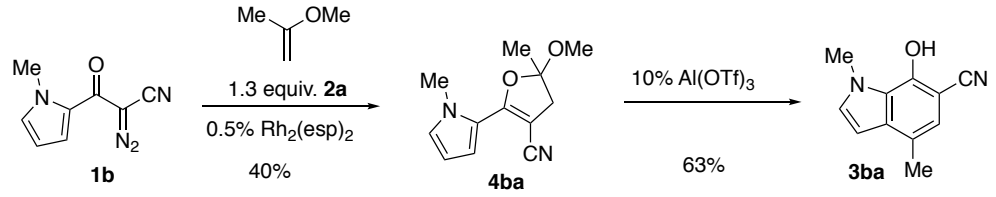

Scheme 41 – Initial Results Using the Diazonitrile to Generate a 7-Hydroxy-Indole-6-Carbonitrile

4.2.2 Optimizing the Formation of the 2,3-Dihydrofuran

Optimization of 2,3-dihydrofuran acetal formation proceeded through two stages: (1) identifying the best performing catalyst, and (2) optimizing the reaction conditions.

4.2.2.1 Identifying the Best Performing Catalyst

A variety of rhodium and copper catalysts were explored for the catalytic decomposition of diazonitrile **1b** in the presence of 1.3 equivalents of enol ether **2a**. These

reactions were performed at 40 °C in dichloromethane using 0.5% (2.5%) of the rhodium (copper) catalyst (Table 10).

Table 10 – Catalyst Optimization for Dihydrofuran Acetal Formation

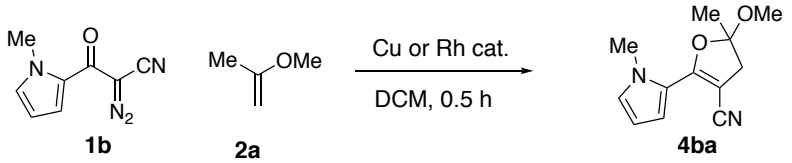

1b **2a** **4ba**

Entry	Cat.	Mol %	Equiv. **2a**	[M]	Temp. (°C)	% Yield[b]
1	$Cu(OTf)_2$	2.5	1.3	0.15	40	0[c]
2	$Cu(acac)_2$	2.5	1.3	0.15	40	18
3	$Cu(F_3acac)_2$	2.5	1.3	0.15	40	21
4	$Rh(Cp^*Cl_2)_2$	0.5	1.3	0.15	40	0
5	$Rh_2(OAc)_4$	0.5	1.3	0.15	40	25
6	$Rh_2(TFA)_4$	0.5	1.3	0.15	40	0
7	$Rh_2(PTAD)_4$	0.5	1.3	0.15	40	50
8	$Rh_2(PTTL)_4$	0.5	1.3	0.15	40	61
9	$Rh_2(NTTL)_4$	0.5	1.3	0.15	40	49
10	$Rh_2(DOSP)_4$	0.5	1.3	0.15	40	28
11	$Rh_2(esp)_2$	0.5	1.3	0.15	40	40

[a]Reactions were run in dichloromethane (0.15 M, 40 °C) with the addition of the diazo compound to the reaction mixture occurring via syringe pump over 1 hour. [b]Isolated yields. [c]Complete consumption of the diazo compound was observed, but no desired product was observed via ^1H NMR analysis of the crude reaction material.

Yields for the copper catalyzed reactions peaked at 21% with $Cu(F_3acac)_2$ (entry 3). Catalytic $Cu(acac)_2$ demonstrated good selectivity for the desired product but was sluggish, only converting a fifth of the starting material (entry 2). Catalytic $Cu(OTf)_2$ fully decomposed the starting material, but failed to generate any of the DHF acetal **4ba** (entry 1). Yields above 25% were not observed until second generation dirhodium catalysts were employed in the reaction. Of these, $Rh_2(PTTL)_4$ performed the best, yielding 61% of **4ba**

(entry 8), followed closely by its structural analogues, $Rh_2(PTAD)_4$ and $Rh_2(NTTL)_4$, which furnished **4ba** in 50% and 49%, respectively (entries 7 and 9). Given the scarcity of these exotic second generation catalysts, we proceeded to optimize reaction conditions employing the cheaper and more abundant Rh_2esp_2 catalyst, which yielded a modest 40% **4ba** with the unoptimized conditions (entry 11).

4.2.2.2 Optimizing the Reaction Conditions

Using Rh_2esp_2, we first explored the temperature dependence of the reaction. At room temperature, the reaction proceeded satisfactorily yielding 34% **4ba**, so we continued the optimizations at room temperature for convenience (Table 11)

Table 11 – Optimization of Conditions for Dihydrofuran Acetal Formation

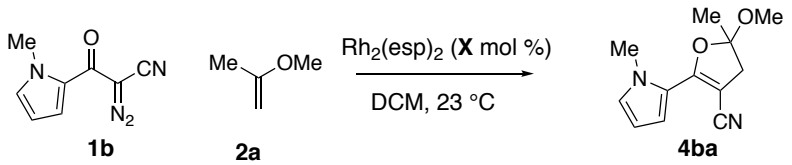

1b **2a** **4ba**

Entry[a]	**X** Mol %	Equiv. **2a**	Slow-Add. Time (h)	% Yield[b]
1	0.5	1.3	1	34
2	1.0	1.3	1	25
3	2.0	1.3	1	trace[c]
4	0.1	1.3	1	43
5	0.05	1.3	1	43
6	0.1	1.3	2	38
7	0.1	1.3	0.5	40
8	0.1	1.3	0.25	45
9	0.1	1.3	1 shot	42
10	0.1	2.5	0.25	65
11	0.1	5.0	0.25	81

[a]Reactions were run using $Rh_2(esp)_2$ at **X** mol % loading in dichloromethane (0.15 M, 23 °C) with the addition of the diazo compound to the reaction mixture occurring via syringe pump over the specified time. After addition, the mixture was allowed to stire for 0.5 hour. [b]Isolated yields. [c]Complete consumption of the diazo compound was observed, no desired product was isolated, and trace amounts of desired product were observed via ^{1}H NMR analysis of the crude reaction material.

While exploring the effect of catalyst loading, we discovered an inverse relationship between catalyst loading and yield. Yields plateaued at 43% for loadings at or below 0.1 mol% Rh_2esp_2. Next, we explored the effect of syringe pump-mediated slow-addition of the diazo compound. Our experiments revealed little dependence of yield on slow-addition time, so we proceeded with a convenient 0.25 h slow-addition which yielded 45% **4ba** (entry 8). Lastly, we examined the effects of enol ether stoichiometry. Yields increased along with the equivalents of **2a** used; 65% and 81% yields of **4ba** were obtained for 2.5 and 5.0 equivalents of **2a** used, respectively (entries 10 and 11).

With reaction parameters nearly optimized, we returned to the high performance $Rh_2(PTTL)_4$ catalyst (Table 12). The reaction failed to proceed at room temperature using $Rh_2(PTTL)_4$ (entry 1), but at 40 °C and 1.3 equivalents of **2a**, 61% **4ba** was obtained (entry 2). At 5.0 equivalents of enol ether, 91% yield **4ba** was obtained (entries 3 and 5). Entries 3, 4, and 5, showed that concentrations of 0.15 M or higher were ideal; meanwhile, lower concentrations resulted a slight drop in yield. The conditions chosen to generate the substrate scope in the next section are represented in entry 3: 0.1% $Rh_2(PTTL)_4$, with 5.0 equivalents of **2a**, 0.15 M in refluxing dichloromethane (40 °C), with the diazo compounds added via syringe pump over 15 minutes.

Table 12 – Continued Optimization of Conditions for Dihydrofuran Acetal Formation

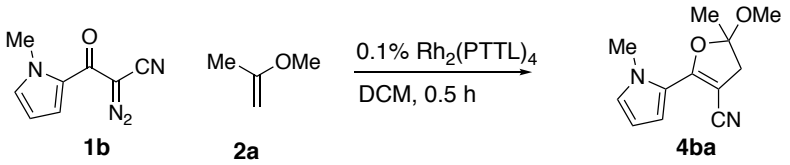

1b **2a** **4ba**

Entry	Equiv. **2a**	[M]	Temp. (°C)	% Yield[b]
1	1.3	0.15	23	0[c]
2	1.3	0.15	40	61
3	5.0	0.15	40	91
4	5.0	0.08	40	85
5	5.0	0.30	40	91

[a]Reactions were run using $Rh_2(PTTL)_2$ at 0.1 mol % loading in CH_2Cl_2 with the addition of the diazo compound to the reaction mixture occurring via syringe pump over 15 minutes. After addition, the mixture was allowed to stire for 0.5 hours. [b]Isolated yields. [c]Starting material was recovered.

4.2.3 Preliminary 2,3-Dihyrdofuran Substrate Scope

Using the optimized conditions, we generated a preliminary substrate scope by reacting diazonitrile **1b** or **1c** with various enol ether units **2a-2e** (Table 13).

Encouragingly, the method afforded DHF acetal products from mono- and di-substituted enol ethers in high yields as represented by **4bb** (83%), **4ba** (91%), and **4bc** (88%) (entries 1-3). When tri-substituted enol ether **2d** was employed, **4bd** was obtained in 19% yield. Given the importance and synthetic challenge of generating 5,6,7,8-substituted indoles and the potential for **2d** to afford such a compound, we developed separate optimal conditions for **4bd** formation which yielded the DHF acetal from the tri-substituted enol ether **2d** in 61% yield (entry 4). Formation of **4ca** from the 3-acyl-indole diazonitrile **1c** suggests tolerance in the diazonitrile scope as well as the potential of this method to be applied toward the synthesis of 6-cyano-carbazoles (entry 6).

Table 13 – Substrate Scope for Dihydrofuran Acetal Formation

Entry[a]	Diazo Compound	Enol Ether	Product	**Product**, Yield[b]
1	**1b**	 **2b**	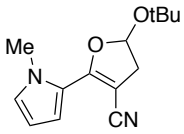	**4bb**, 83%
2	**1b**	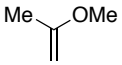 **2a**	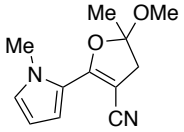	**4ba**, 91%
3	**1b**	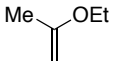 **2c**	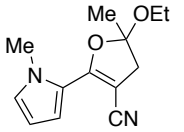	**4bc**, 88%
4	**1b**	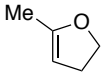 **2d**	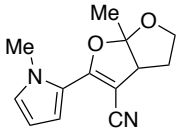	**4bd**, 61%[c]
5	**1b**	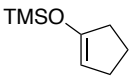 **2e**	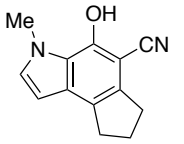	**3be**, 32%
6	**1c**	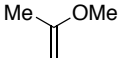 **2a**	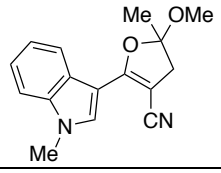	**4ca**, 70%[d]

[a]Reactions were performed using the optimized conditions (**Table 12**, Entry 3) . [b]Isolated yields. [c]This result was independently optimized and obtained using the following conditions: 0.1% $Rh_2(PTTL)_4$, 2.5 equiv. **2d**, dichloromethane (0.08 M, 40 °C), slow-add. over 15 minutes, reaction time of 18 hours. [d]3-acyl-indole diazo nitrile **1c** was used instead of **1b**.

Interestingly, when tri-substituted enol silane **2e** was employed in the reaction, 32% of the cyclopentane[e]indole label was obtained (entry 5). Based on crude ^{1}H NMR analysis, we suspect that an approximately 1:1 ratio of **4be** to **3be** is formed in the reaction vessel and purification conditions effect an isomerization to **3be**.

4.2.4 Optimizing the Benzannulation Reaction

Confident that DHF acetal starting materials could be generated in sufficient quantity and diversity to substantiate the hypothesized benzannulation reaction, we commenced optimization of this transformation. First, we tested the reaction of **4ba** in a variety of solvents at 40 °C using 10 mol% $Al(OTf)_3$, the optimal catalyst in Aponte-Guzman's 2016 study (Table 14).

Table 14 – Initial Solvent Optimization of the Ring-Opening Benzannulation Reaction to Form 7-Hydroxy-Indole-6-Carbonitriles

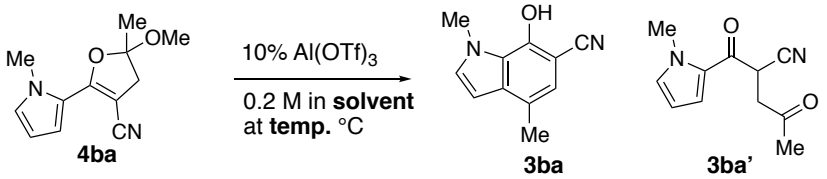

4ba **3ba** **3ba'**

Entry[a]	**Solvent**	**Temp.** (°C)	Time (h)	% Yield **3ba**[b]	**3ba** : **3ba'**[c]
1	Toluene	40	2.5	0[d]	0 : 1
2	1,2-DCE	40	12	23	1 : 3
3	Chloroform	40	12	24	1 : 3
4	Cyclohexane	40	12	23	1 : 2
5	DCM	40	2.5	38	1 : 1

[a]Reactions were run in **solvent** (0.2 M, **Temp** °C) for the specified time using 10% $Al(OTf)_3$. [b]Isolated yields. [c]Determined by ^1H NMR analysis of the crude reaction material. [d]Complete degredation of **4ba** was observed; no **3ba** was isolated or observed during the ^1H NMR analysis of the crude reaction matarial.

Overall yields of the transformation were generally very good, but, when performed in toluene, 1,2-dichloroethane, chloroform, or cyclohexane, the reaction was preferentially selective for the diketone **3ba'** resulting in yields in the mid-20s% of the indole-6-carbonitrile **3ba**. Dichloromethane showed 1:1 **3ba**:**3ba'** selectivity, yielding **3ba** in 38%.

Unsatisfied with the 38% yield and 1:1 **3ba**:**3ba'** selectivity achieved with $Al(OTf)_3$ after solvent optimization, we performed a catalyst screen to determine if a better performing Lewis acid catalyst could be identified (Table 15).

Table 15 – Lewis Acid Optimization for the Ring-Opening Benzannulation Reaction to Form 7-Hydroxy-Indole-6-Carbonitriles

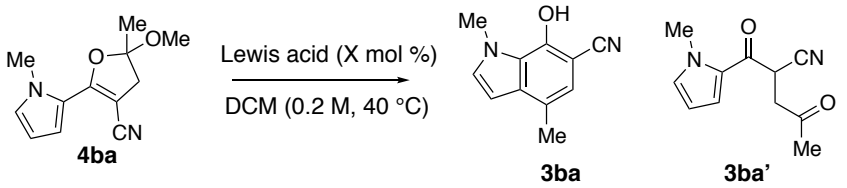

Entry[a]	**Catalyst**	**Mol %**	% Yield **3ba**[b]	**3ba** : **3ba'**[c]
1	$Al(OTf)_3$	10	38	1 : 1
2	$In(OTf)_3$	10	17	1 : 4
3	$Sc(OTf)_3$	10	24	1 : 3
4	$MADNTf_2$	10	0[d]	–
5	$Ca(NTf_2)_2$ / NBu_4PF_6	10 / 5	30	2 : 1

[a]Reactions were run in CH_2Cl_2 (0.2 M, 40 °C) for 2.5 hours using the specified Lewis acid catalyst and loading. [b]Isolated yields. [c]Determined by ^1H NMR analysis of the crude reaction material. [d]Starting material was recovered.

Other triflate-ligated Lewis acids did not outperform $Al(OTf)_3$ in either yield or selectivity; use of $Al(OTf)_3$ resulted in a 17% yields of **3ba**, while use of $Al(OTf)_3$ only achieved 24% yield of **3ba** with 1:3 **3ba**:**3ba'** selectivity. Given the success of $MADNTf_2$ to catalyze ring-opening cyclizations in the literature,[19] we applied the aluminum-based Lewis acid to our system but observed no conversion of the starting material. Using the 10 mol% $Ca(NTf_2)_2$ and 5 mol% NBu_4PF_6 system, **4ba** was converted into **3ba** and **3ba'** in 45% yield with 2:1 selectivity in favor of **3ba** (30% **3ba** was obtained). Encouraged by the preferential formation of the indole-6-carbonitrile, we advanced the $Ca(NTf_2)_2$ / NBu_4PF_6 system forward for further optimization (Table 16).

Table 16 – Optimization of Reaction Conditions for the Benzannulation Reaction to Form 7-Hydroxy-Indole-6-Carbonitriles

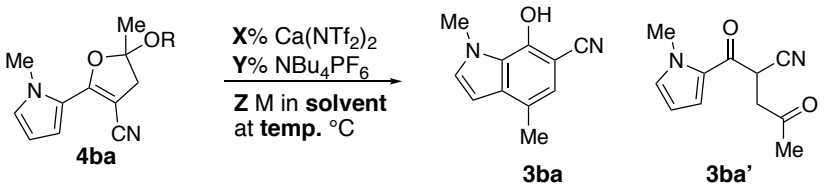

Entry[a]	**Solvent**	**X**	**Y**	**Temp.** (°C)	**Z** [M]	% Yield **3ba**[b]	**3ba** : **3ba'**[c]
1	DCM	10	5	40	0.2	30	2 : 1
2	DCM	10	5	80[d]	0.2	82	17 : 1
3	Toluene	10	5	80	0.2	77	50 : 1
4	Toluene	5	2.5	80	0.2	74	3 : 1
5	Toluene	2.5	1.3	80	0.2	73	3 : 1
6	Toluene	10	5	100	0.2	65	7 : 1
7	Toluene	10	10	80	0.2	67	10 : 1
8[e]	Toluene	10	10	80	0.2	65	99 : 1
9	Toluene	10	10	80	0.3	72	99 :1
10	Toluene	10	10	80	0.1	trace[f]	5 : 1
11	Toluene	10	10	80	0.4	49	7 : 1
12	Toluene	10	0	80	0.2	trace[f]	1: 4
13	Toluene	10	15	80	0.3	79	20 : 1

[a]Reactions were run in **solvent** (**Z** M, **Temp.** °C) for 1 hours using the $Ca(NTf_2)_2$ / NBu_4PF_6 Lewis acid system at the specified loading; R = Me . [b]Isolated yields. [c]Determined by ^1H NMR analysis of the crude reaction material. [d]Reaction was carried out in a pressure tube. [e]R = Et for this reaction. [f]Starting material consumed, but no benzannulation product was observed by ^1H NMR analysis of the crude reaction material.

Performing the reaction with 10 mol% $Ca(NTf_2)_2$ and 5 mol% NBu_4PF_6 in DCM at 80 °C (using a pressure tube) and obtaining 82% yield of **3ba** with 17:1 **3ba**:**3ba'** selectivity was a promising result demonstrating the importance of high temperatures to obtain favorable selectivity. Since the application of a pressure tube fails the method design principle of scalability, we returned to the original solvent of choice, toluene, to achieve the desired 80 °C temperature in a standard round-bottom flask. This change resulted in similar yield of 77% (entry 3). In entries 4 and 5, the transformation is demonstrated to be robust toward decreased catalyst loadings; 73% yield of **3ba** is obtained even with only 2.5

mol% $Ca(NTf_2)_2$ and 1.3 mol% NBu_4PF_6. Entry 6 demonstrates that increasing the temperature beyond 80 °C has a negative impact on both yield and selectivity; at 100 °C, **3ba** is formed in only 65% yield. Changing the $Ca(NTf_2)_2$ / NBu_4PF_6 loading ratio to 1:1 similarly decreases yield as represented in entry 7, and entry 12 demonstrates the necessity of the NBu_4PF_6 additive. Use of the OEt-derived starting material **4bc** resulted in no appreciable difference in yield (entry 8). The effect of concentration is explored in entries 9, 10, and 11; the reaction proceeded best at 0.3 M. Interestingly, changing the $Ca(NTf_2)_2$ / NBu_4PF_6 loading to 10/15 mol% increases yield slightly to 79% at 0.3 M (entry 13).

In summary, the benzannulation reaction is best performed at 80 °C and 0.2-0.3 M. Yields were not consistent enough to make a secure claim about the optimal catalyst loading and $Ca(NTf_2)_2$: NBu_4PF_6 ratio; however, the NBu_4PF_6 is necessary for the reaction to procced and the highest yields were obtained with 10/5 mol% and 10/15 mol% ($Ca(NTf_2)_2$ / NBu_4PF_6) systems.

4.2.5 Scope of the Benzannulation

Outside **4ba**, **4bc**, and **4bd**, the treatment of DHF acetals with the $Ca(NTf_2)_2$ / NBu_4PF_6 catalyst system to generate indole-6-carbonitriles was not explored. Compounds **4ba** and **4bc** both afforded the indole-6-carbonitrile **3ba** in good yields (Table 16, entries 3 and 8, respectively). When **4bd** was subjected to the optimized conditions, the benzannulation failed to proceed suggesting that the $Ca(NTf_2)_2$ / NBu_4PF_6 catalyst system could not accommodate the DHF acetal products formed from tri-substituted enol ethers such as **3bd**. However, treating **4bd** with 1 equivalent of boron trifluoride etherate in dichloromethane overnight afforded **3bd** in 50% yield (Scheme 42).

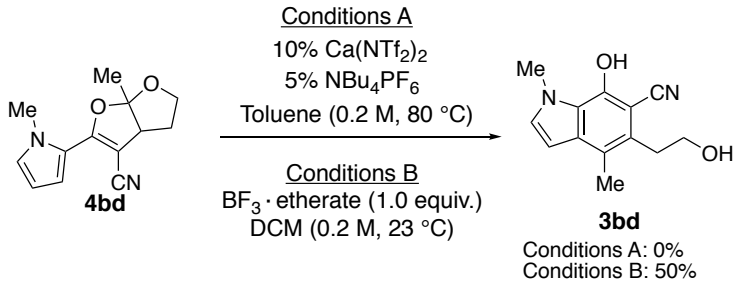

Scheme 42 – Benzannulation Conditions for Compound 4bd

4.3 Conclusion

Subjecting DHF acetal carbonitriles with Lewis acidic conditions to affect ring-opening benzannulations represents a promising strategy to generate functionally-substituted indole building blocks relevant to natural product and pharmaceutical synthesis. Our efforts optimizing the formation of both the DHF acetal carbonitriles intermediates and the indole-6-carbonitriles has forged a path to the completion of this methodology. These efforts resulted in the synthesis of DHF acetal carbonitriles from mono-, di-, and tri-substituted enol ethers and indole-6-caronitriles with optional alkyl substation at both the 4- and 5-positions. Table 17 displays the range of dihydrofuran acetal and 7-hydroxy-indole-6-carbonitrile products synthesized thus far.

Table 17 – Dihydrofuran Acetal and 7-Hydroxy-Indole-6-Carbonitrile Products Synthesized in this Study

a. Dihydrofuran acetal products

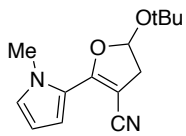

4bb 83%

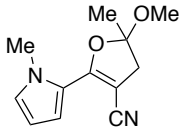

4ba 91%

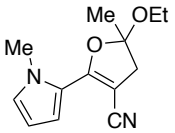

4bc 88%

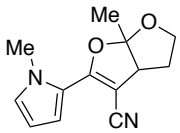

4bd 61%

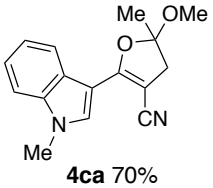

4ca 70%

b. 7-Hydroxy-indole-6-carbonitrile products

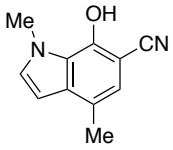

3ba 77%

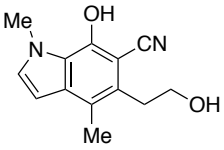

3bd 50%

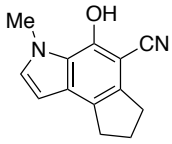

3be 32%

Generating a substrate scope for the ring-opening benzannulation reaction and demonstrating the utility of the transformation via the synthesis of a biologically relevant indole alkaloid would complete the development of this methodology.

4.4 Experimental

4.4.1 General Methods

All solvents used in the reported reactions were purchased anhydrous from commercial sources or freshly distilled. All enol ether starting materials were purchased from commercial sources as well.

Chromatographic purification was performed as flash chromatography with Dynamic Adsorbents silica gel (23-65 μm) and solvents indicated as eluent with 0.1-0.5

bar pressure. For quantitative flash chromatography, technical grade solvents were utilized. Analytical thin-layer chromatography was performed on EMD silica gel 60 F254 TLC glass plates. Visualization was accomplished with UV light.

Proton and carbon nuclear magnetic resonance (^{1}H NMR and ^{13}C NMR) spectra were recorded on a Varian Mercury Vx 300 MHz spectrometer with solvent resonances as the internal standard (^{1}H NMR: $CHCl_3$ at 7.26 ppm; ^{13}C NMR: $CHCl_3$ at 77.0 ppm). ^{1}H NMR data are reported as follows: chemical shift (ppm), multiplicity (s = singlet, d = doublet, dd = doublet of doublets, dt = doublet of triplets, ddd = doublet of doublet of doublets, t = triplet, q = quartet, p = pentet, m = multiplet, br = broad), coupling constants (Hz), and integration. In most cases, deuterated chloroform was the solvent used for obtaining NMR spectra, but in some cases, when solubility was an issue, deuterated acetonitrile or deuterated pyridine was used. Mass spectra were obtained through EI on a Micromass AutoSpec Machine or through ESI on a Thermo Orbitrap XL. The accurate mass analyses run in EI mode were at a mass resolution of 10,000 and were calibrated using PFK (perfluorokerosene) as an internal standard. The accurate mass analyses run in EI mode were at a mass resolution of 30,000 using the calibration mixture supplied by Thermo.

4.4.2 Experimental Procedures

4.4.2.1 Diazo Compounds

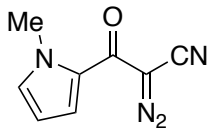

1b

2-Diazo-3-(1-methyl-1*H*-pyrrol-2-yl)-3-oxopropanenitrile (1b) To a dry round-bottom flask containing 3-(1-methyl-1H-pyrrol-2-yl)-3-oxopropanenitrile (4.85 g, 32.7 mmol), pyridine (13 ml, 164 mmol) in acetonitrile (100 mL) was added 1H-imidazole-1-sulfonyl azide hydrochloride (10.3 g, 49.1 mmol). The reaction was heated to 35 °C and stirred for 2.5 hours. The crude material was concentrated onto silica purified via flash silica gel chromatography. **1b** was afforded as a yellow solid (4.16 mg, 73% yield). **^{1}H NMR** (300 MHz, $CDCl_3$) δ = 7.29 (dd, *J* = 4.3, 1.6 Hz, 1H), 6.95 – 6.87 (m, 1H), 6.18 (dd, *J* = 4.3, 2.5 Hz, 1H), 3.93 (s, 3H). **^{13}C NMR** (75 MHz, $CDCl_3$) δ = 171.00, 132.34, 126.69, 119.99, 110.11, 109.08, 37.73.

4.4.2.2 Dihydrofuran Acetal Products

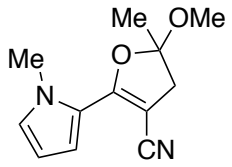

4ba

5-methoxy-5-methyl-2-(1-methyl-1*H*-pyrrol-2-yl)-4,5-dihydrofuran-3-carbonitrile (4ba): To a dry round-bottom flask containing $Rh_2(PTTL)_4$ (4 mg, 2.5 μmol) and 2-methoxyprop-1-ene (280 μl, 2.9 mmol) in refluxing dichloromethane (2 mL, 40 °C) was added a solution of **1b** (100 mg, 0.57 mmol) in dichloromethane (2 mL) via syringe pump over 15 minutes. The reaction was monitored by TLC and stopped when the TLC showed complete consumption of the diazo compound. The crude material was purified via flash silica gel chromatography (30% EtOAc/Hexane, R_f = 0.40). **4ba** was afforded as a yellow oil (114 mg, 91% yield). **^{1}H NMR** (300 MHz, $CDCl_3$) δ = 7.12 (dd, *J* = 4.0, 1.7 Hz, 1H),

6.74 – 6.66 (m, 1H), 6.18 (dd, J = 4.0, 2.6 Hz, 1H), 3.80 (s, 3H), 3.36 (s, 3H), 3.00 (d, J = 15.8 Hz, 1H), 2.89 (d, J = 15.8 Hz, 1H), 1.66 (s, 3H). **^{13}C NMR** (75 MHz, $CDCl_3$) δ = 159.78, 127.72, 120.75, 117.84, 116.18, 112.82, 109.09, 75.50, 50.41, 39.88, 37.16, 24.88. **HRMS (EI)** *m/z*: $[M]^+$ Calcd. for $C_{12}H_{14}O_2N_2$ 218.1055; Found 218.1050.

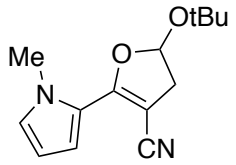

4bb

5-(*tert*-butoxy)-2-(1-methyl-1*H*-pyrrol-2-yl)-4,5-dihydrofuran-3-carbonitrile (4bb) To a dry round-bottom flask containing $Rh_2(PTTL)_4$ (4 mg, 2.5 μmol) and 2-methyl-2-(vinyloxy)propane (380 μl, 2.9 mmol) in dichloromethane (2 mL) was added a solution of 2-diazo-3-(1-methyl-1H-pyrrol-2-yl)-3-oxopropanenitrileoxopropanoate **1b** (100 mg, 0.57 mmol) in dichloromethane (2 mL) via syringe pump over 15 minutes. The reaction was monitored by TLC and stopped when the TLC showed complete consumption of the diazo compound. The crude material was purified via flash silica gel chromatography (30% EtOAc/Hexane, R_f = 0.17). **4bb** was afforded as a white solid (118 mg, 83% yield). **^{1}H NMR** (300 MHz, $CDCl_3$) δ = 7.11 (dd, J = 4.0, 1.6 Hz, 1H), 6.71 – 6.63 (m, 1H), 6.16 (dd, J = 4.0, 2.6 Hz, 1H), 6.00 (dd, J = 7.7, 3.8 Hz, 1H), 3.78 (s, 3H), 3.14 (dd, J = 15.4, 7.7 Hz, 1H), 2.75 (dd, J = 15.4, 3.8 Hz, 1H), 1.31 (s, 9H). **^{13}C NMR** (75 MHz, $CDCl_3$) δ = 159.81, 127.45, 121.16, 118.23, 115.95, 108.94, 101.71, 75.10, 37.87, 37.24, 28.59. **HRMS (EI)** *m/z*: $[M]^+$ Calcd. for $C_{14}H_{18}O_2N_2$ 246.1368; Found 246.1361**.**

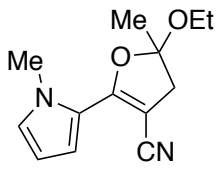

4bc

5-ethoxy-5-methyl-2-(1-methyl-1*H*-pyrrol-2-yl)-4,5-dihydrofuran-3-carbonitrile (4bc): To a dry round-bottom flask containing $Rh_2(PTTL)_4$ (8 mg, 5 μmol) and 2-ethoxyprop-1-ene (650 μl, 5.7 mmol) in refluxing dichloromethane (4 mL, 40 °C) was added a solution of **1b** (200 mg, 1.15 mmol) in dichloromethane (4 mL) via syringe pump over 15 minutes. The reaction was monitored by TLC and stopped when the TLC showed complete consumption of the diazo compound. The crude material was purified via flash silica gel chromatography (30% EtOAc/Hexane, R_f = 0.50). **4bc** was afforded as a yellow oil (235 mg, 88% yield). **^{1}H NMR** (300 MHz, $CDCl_3$) δ = 7.11 (dd, *J* = 4.0, 1.7 Hz, 1H), 6.73 – 6.65 (m, 1H), 6.17 (dd, *J* = 4.0, 2.6 Hz, 1H), 3.78 (s, 3H), 3.60 (qd, *J* = 7.0, 1.4 Hz, 2H), 2.99 (d, *J* = 15.7 Hz, 1H), 2.88 (d, *J* = 15.7 Hz, 1H), 1.66 (s, 9H), 1.21 (t, *J* = 7.0 Hz, 3H). **^{13}C NMR** (75 MHz, $CDCl_3$) δ = 159.78, 127.66, 120.84, 117.96, 116.05, 112.71, 109.03, 75.42, 58.59, 40.38, 37.13, 25.40, 15.36. **HRMS (EI)** *m/z*: $[M]^+$ Calcd. for $C_{13}H_{16}O_2N_2$ 232.1213; Found 232.1212.

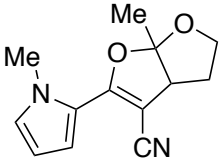

4bd

6a-methyl-2-(1-methyl-1*H*-pyrrol-2-yl)-3a,4,5,6a-tetrahydrofuro[2,3-*b*]furan-3-carbonitrile (4bd): To a dry round-bottom flask containing $Rh_2(PTTL)_4$ (4 mg, 2.5 μmol) and 5-methyl-2,3-dihydrofuran (105 μl, 1.15 mmol) in dichloromethane (2 mL) was added a solution of 2-diazo-3-(1-methyl-1H-pyrrol-2-yl)-3-oxopropanenitrileoxopropanoate **1b** (100 mg, 0.57 mmol) in dichloromethane (2 mL) via syringe pump over 15 minutes. The reaction was left to reflux for approximately 18 hours. The crude material was purified via flash silica gel chromatography (30% EtOAc/Hexane, R_f = 0.41). **4bd** was afforded as a white solid (68 mg, 51% yield. **^{1}H NMR** (300 MHz, $CDCl_3$) δ = 7.14 (dd, *J* = 4.1, 1.7 Hz, 1H), 6.74 – 6.66 (m, 1H), 6.18 (dd, *J* = 4.1, 2.6 Hz, 1H), 4.12 (dd, *J* = 8.8, 7.3 Hz, 1H), 3.91 – 3.81 (m, 1H), 3.79 (s, 3H), 3.47 (d, *J* = 7.5 Hz, 1H), 2.23 – 2.04 (m, 2H), 1.70 (s, 3H). **^{13}C NMR** (75 MHz, $CDCl_3$) δ = 160.92, 128.03, 120.37, 120.35, 117.96, 116.28, 109.10, 78.04, 67.94, 51.14, 37.33, 32.14, 23.97. **HRMS (EI)** *m/z*: $[M]^+$ Calcd. for $C_{13}H_{14}O_2N_2$ 230.1055; Found 230.1047.

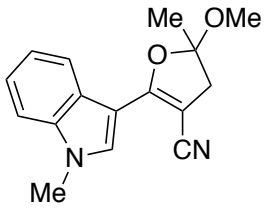

4ca

5-methoxy-5-methyl-2-(1-methyl-1*H*-indol-3-yl)-4,5-dihydrofuran-3-carbonitrile (4ca): To a dry round-bottom flask containing $Rh_2(PTTL)_4$ (3 mg, 2 μmol) and 2-methoxyprop-1-ene (210 μl, 2.2 mmol) in refluxing dichloromethane (1.5 mL, 40 °C) was added a solution of 2-diazo-3-(1-methyl-1H-indol-3-yl)-3-oxopropanenitrile **1c** (100 mg,

0.45 mmol) in dichloromethane (1.5 mL) via syringe pump over 15 minutes. The reaction was monitored by TLC and stopped when the TLC showed complete consumption of the diazo compound. The crude material was purified via flash silica gel chromatography (30% EtOAc/Hexane, R_f = 0.40). **4ca** was afforded as a white solid (84 mg, 70% yield. **^{1}H NMR** (300 MHz, $CDCl_3$) δ = 8.08 (d, *J* = 7.2 Hz, 1H), 8.04 (s, 1H), 7.39 – 7.21 (m, 3H), 3.84 (s, 3H), 3.41 (s, 3H), 3.05 (d, *J* = 15.5 Hz, 1H), 2.96 (d, *J* = 15.5 Hz, 1H), 1.74 (s, 3H). **^{13}C NMR** (75 MHz, $CDCl_3$) δ = 164.71, 136.52, 132.01, 125.59, 122.98, 122.01, 121.54, 119.06, 112.27, 109.81, 104.24, 72.55, 50.30, 39.90, 33.50, 24.99. **HRMS (EI)** *m/z*: $[M]^+$ Calcd. for $C_{16}H_{16}O_2N_2$ 268.1212; Found 268.1212.

4.4.2.3 Indole-6-Carbonitriles

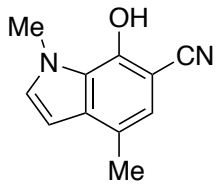

3ba

7-hydroxy-1,4-dimethyl-1*H*-indole-6-carbonitrile (3ba): To a dry round-bottom flask containing $Ca(NTf_2)_2$ (23 mg, 38 μmol), NBu_4PF_6 (22 mg, 56 μmol), and refluxing toluene (0.6 mL, 81 °C) was added a solution of 5-methoxy-5-methyl-2-(1-methyl-1H-pyrrol-2-yl)-4,5-dihydrofuran-3-carbonitrile **4ba** (82 mg, 0.38 mmol) in toluene (0.6 mL). The reaction was allowed to proceed for 30 minutes at reflux. The crude material was purified via flash silica gel chromatography (30% EtOAc/Hexane, R_f = 0.48). **3ba** was afforded as a white solid (77 mg, 79% yield). **^{1}H NMR** (300 MHz, $CDCl_3$) δ = 6.92 – 6.86 (m, 1H), 6.78 – 6.66 (m, 1H), 6.25 – 6.15 (m, 2H), 3.83 (s, 3H), 2.34 (s, 3H). **^{13}C NMR** (75 MHz,

$CDCl_3$) δ = 153.83, 151.03, 126.33, 121.51, 115.34, 112.66, 108.84, 107.83, 90.69, 36.47, 13.36. **HRMS (EI)** *m/z*: $[M]^+$ Calcd. for $C_{11}H_{10}ON_2$ 186.0793; Found 186.0787.

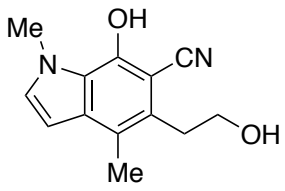

3bd

7-hydroxy-5-(2-hydroxyethyl)-1,4-dimethyl-1*H*-indole-6-carbonitrile (13bd): To a dry round-bottom flask containing 6a-methyl-2-(1-methyl-1H-pyrrol-2-yl)-3a,4,5,6a-tetrahydrofuro[2,3-b]furan-3-carbonitrile **4bd** (40 mg, 0.17 mmol) in dichloromethane (0.9 mL, room temperature) was added boron trifluoride etherate (22 μL, 0.17 mmol). The reaction was allowed to proceed for 30 minutes. The crude material was purified via flash silica gel chromatography (25% EtOAc/Hexane, R_f = 0.11). **3bd** was afforded as a yellow solid (20 mg, 50% yield. **^{1}H NMR** ^{1}H NMR (300 MHz, $CDCl_3$) δ = 7.12 (d, *J* = 2.9 Hz, 1H), 6.53 (s, 1H), 6.41 (d, *J* = 2.9 Hz, 1H), 4.56 (t, *J* = 6.1 Hz, 2H), 4.19 (s, 3H), 3.08 (t, *J* = 6.1 Hz, 2H), 2.31 (s, 3H). **^{1}H NMR** (300 MHz, Pyridine-d_5) δ 11.66 (s, 1H), 7.51 (d, *J* = 2.6 Hz, 1H), 6.79 (d, *J* = 2.9 Hz, 1H), 4.73 (t, *J* = 6.1 Hz, 2H), 4.37 (s, 3H), 3.15 (t, *J* = 6.0 Hz, 2H), 2.52 (s, 3H), 2.31 (s, 1H). **^{13}C NMR** (75 MHz, Pyridine-d_5) δ = 167.83, 137.35, 133.99, 124.22, 122.02, 117.08, 101.42, 98.63, 69.59, 65.41, 36.32, 30.51, 24.51, 13.52. ^{13}C NMR (75 MHz, Chloroform-*d*) δ 137.35, 133.72, 120.63, 117.17, 101.09, 69.59, 36.48, 24.36, 13.39. **HRMS (EI)** *m/z*: $[M]^+$ Calcd. for $C_{13}H_{14}O_2N_2$ 230.1055; Found 230.1048.

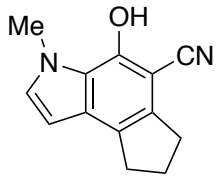

3be

4-hydroxy-3-methyl-3,6,7,8-tetrahydrocyclopenta[*e*]indole-5-carbonitrile (3be): To a dry round-bottom flask containing $Rh_2(PTTL)_4$ (4 mg, 2.5 μmol) and (cyclopent-1-en-1-yloxy)trimethylsilane (256 μl, 1.4 mmol) in refluxing dichloromethane (3.5 mL, 40 °C) was added a solution of 2-diazo-3-(1-methyl-1H-pyrrol-2-yl)-3-oxopropanenitrileoxopropanoate **1b** (100 mg, 0.57 mmol) in dichloromethane (3.5 mL) via syringe pump over 15 minutes. The reaction was allowed to proceed at reflux for 15 minutes and then quenched with a drop of water and the addition of silica. The crude material was purified via flash silica gel chromatography (30% EtOAc/Hexane, R_f = 0.24). **3be** was afforded as a white solid (39 mg, 32% yield. **^{1}H NMR** (300 MHz, Acetonitrile-d_3, 60 °C) δ = 7.02 (d, J = 3.2 Hz, 1H), 6.37 (d, J = 3.2 Hz, 1H), 4.02 (s, 4H), 3.10 (t, J = 7.5 Hz, 2H), 2.95 (t, J = 7.4 Hz, 2H), 2.23 (p, J = 7.4 Hz, 2H). **^{1}H NMR** (300 MHz, Pyridine-d_5) δ = 7.34 (d, J = 3.2 Hz, 1H), 6.78 (d, J = 3.2 Hz, 1H), 4.28 (s, 3H), 3.38 – 3.28 (m, 4H), 2.32 (p, J = 7.6 Hz, 2H). **^{13}C NMR** (75 MHz, Pyridine-d_5) δ = 156.26, 143.74, 135.70, 129.71, 123.67, 120.59, 118.45, 100.45, 81.30, 34.62, 32.66, 30.76, 25.16. **HRMS (EI)** *m/z*: $[M]^+$ Calcd. for $C_{13}H_{12}ON_2$ 212.0950; Found 212.0947.

4.4.3 ^{1}H and ^{13}C NMR Spectra

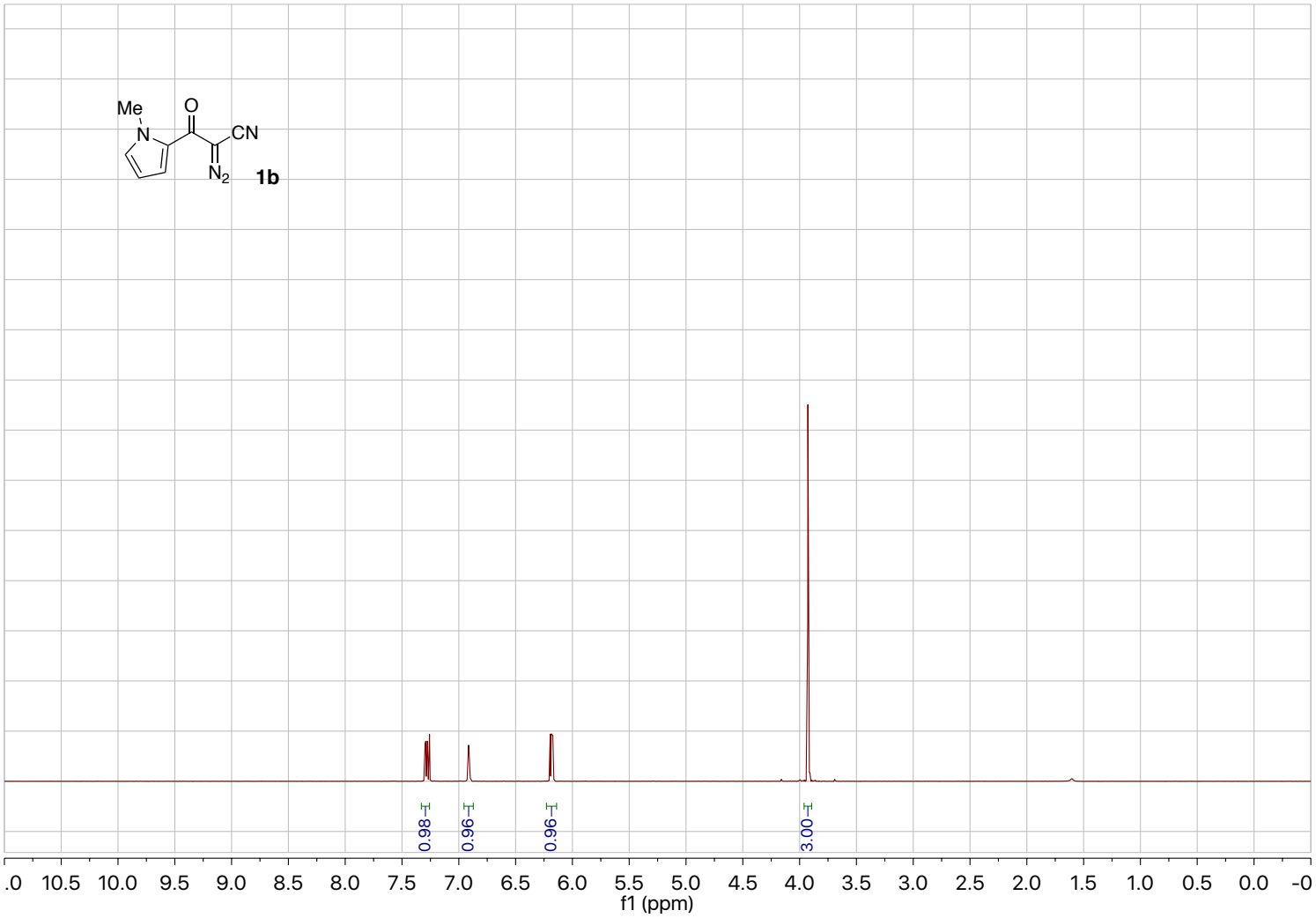
Me
N
O
CN
N2
1b
0.98
0.96
0.96
3.00
.0 10.5 10.0 9.5 9.0 8.5 8.0 7.5 7.0 6.5 6.0 5.5 5.0 4.5 4.0 3.5 3.0 2.5 2.0 1.5 1.0 0.5 0.0 -0
f1 (ppm)

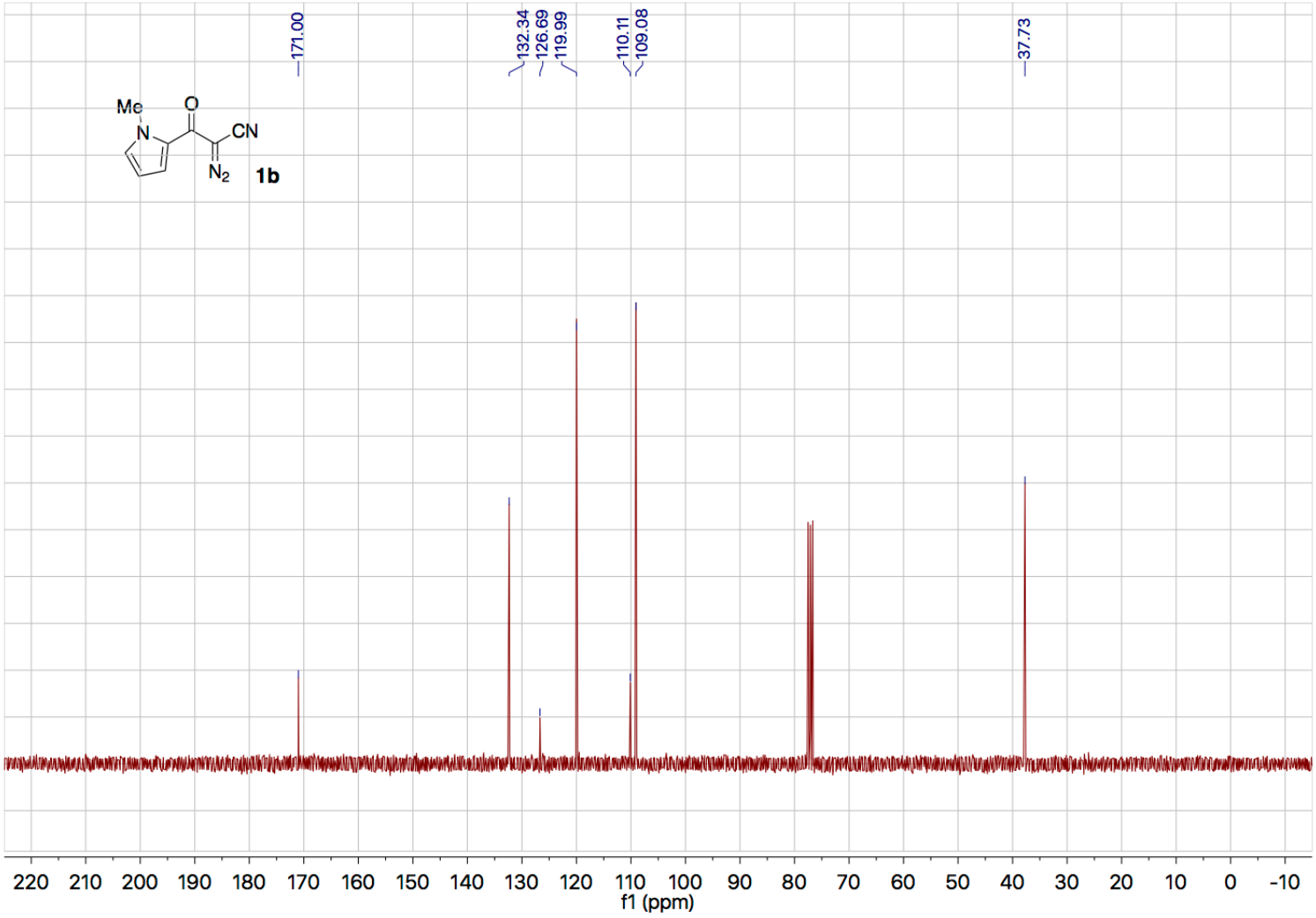
171.00
132.34
126.69
119.99
110.11
109.08
37.73
Me
N
O
CN
N2
1b
220 210 200 190 180 170 160 150 140 130 120 110 100 90 80 70 60 50 40 30 20 10 0 -10
f1 (ppm)

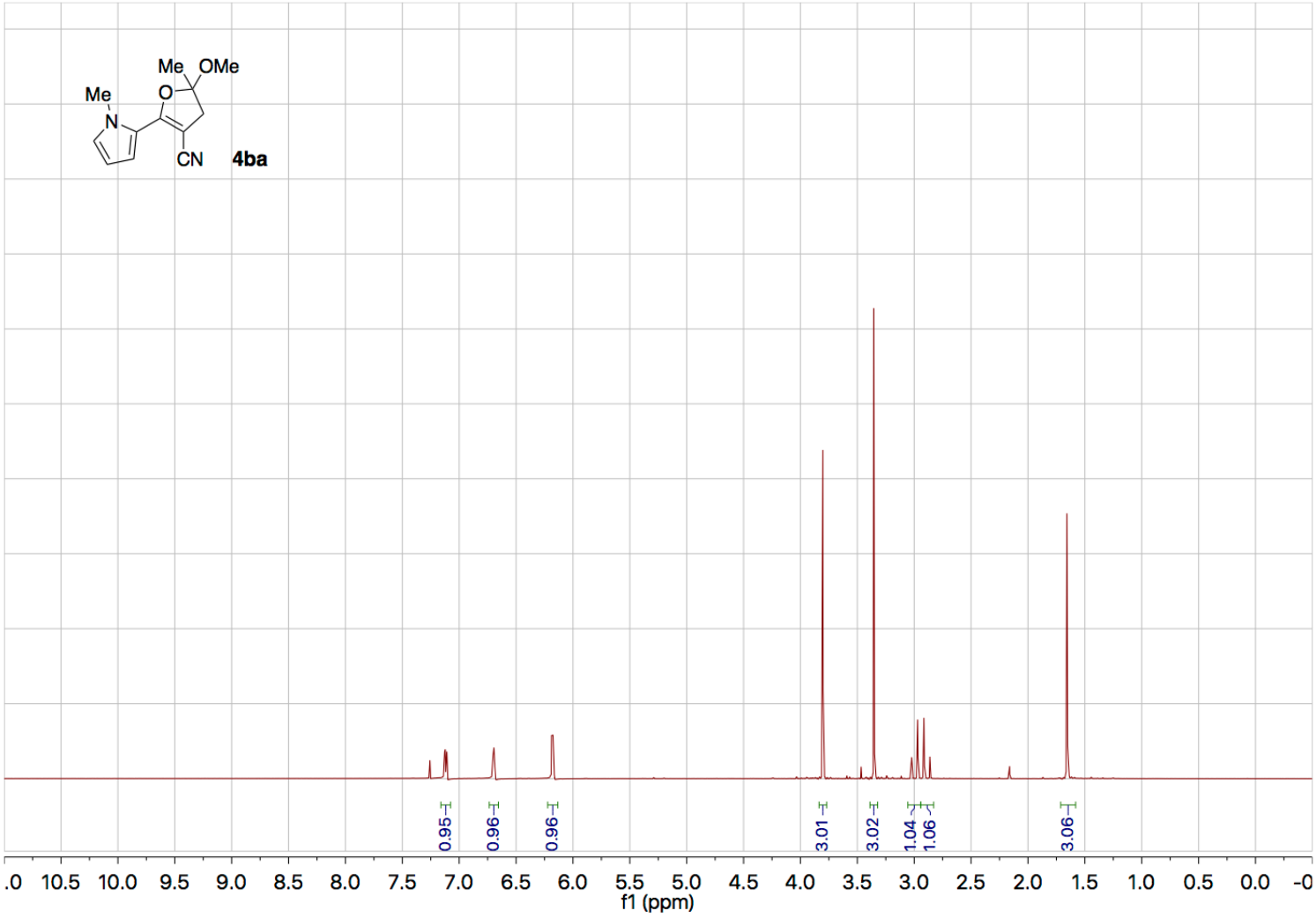
Me
OMe
Me
O
N
CN
4ba
0.95
0.96
0.96
3.01
3.02
1.04
1.06
3.06
.0 10.5 10.0 9.5 9.0 8.5 8.0 7.5 7.0 6.5 6.0 5.5 5.0 4.5 4.0 3.5 3.0 2.5 2.0 1.5 1.0 0.5 0.0 -0
f1 (ppm)

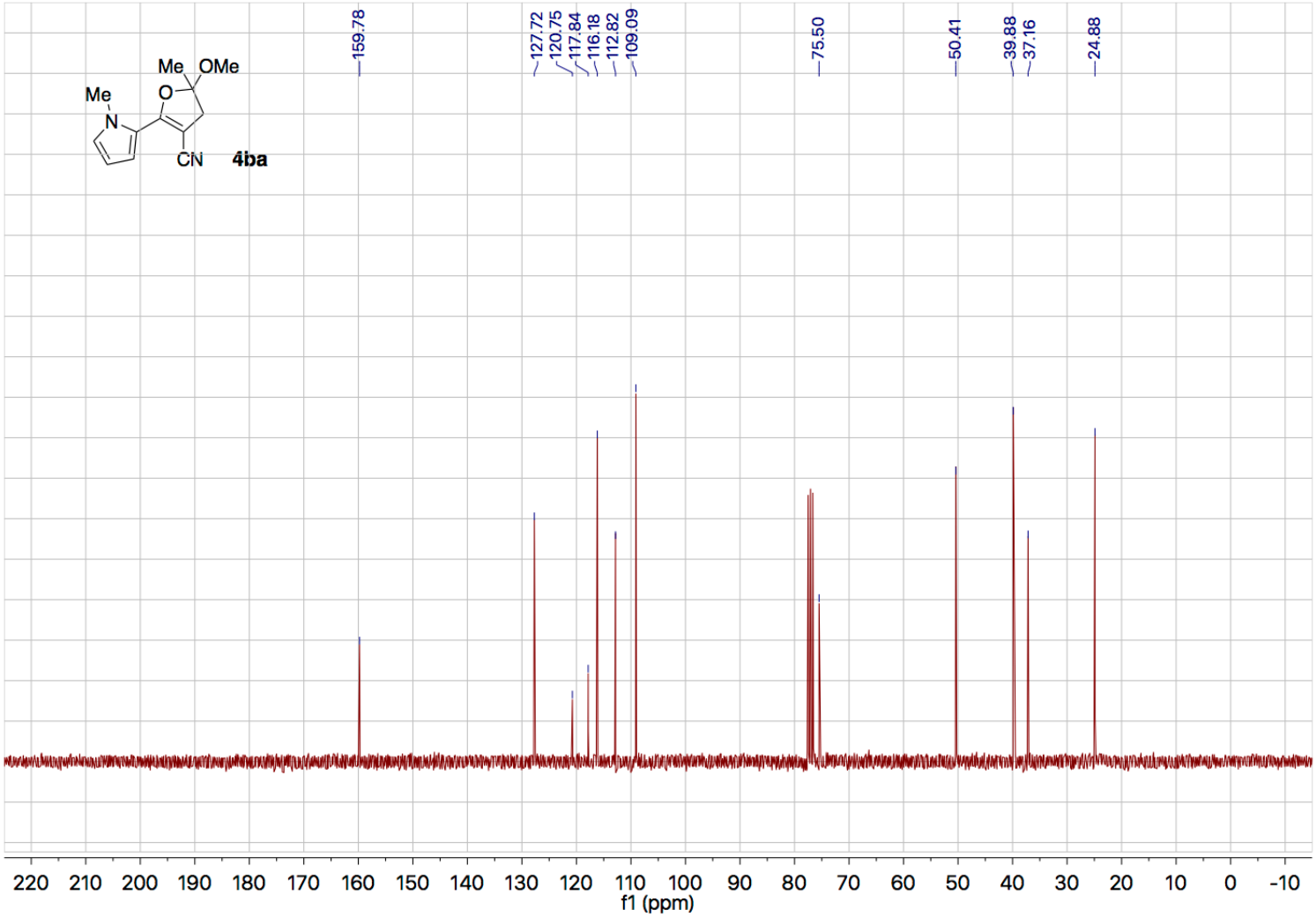
159.78
127.72
120.75
117.84
116.18
112.82
109.09
75.50
50.41
39.88
37.16
24.88
Me
OMe
Me
O
N
CN
4ba
220 210 200 190 180 170 160 150 140 130 120 110 100 90 80 70 60 50 40 30 20 10 0 -10
f1 (ppm)

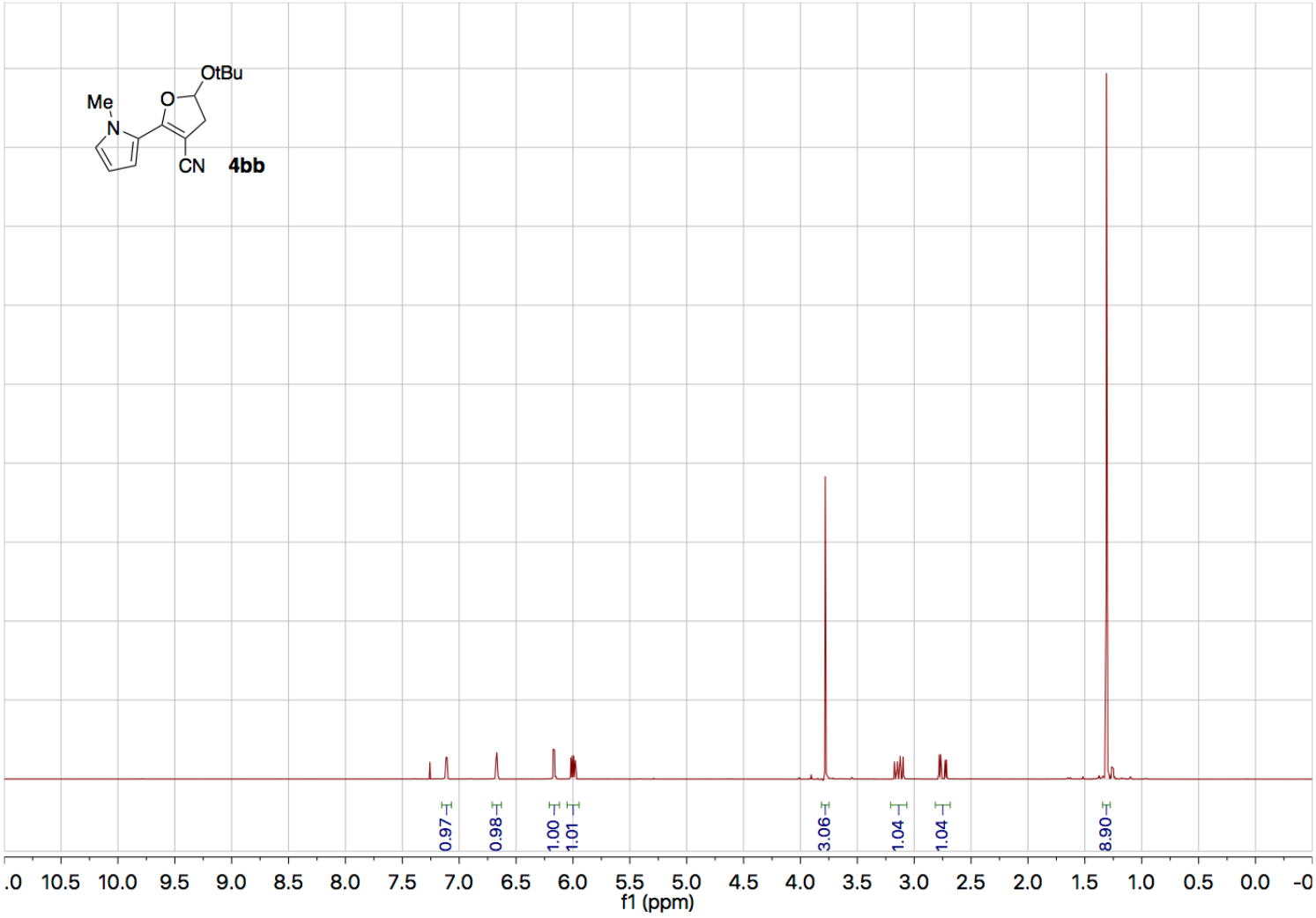
OtBu
Me
N
O
CN
4bb
0.97
0.98
1.00
1.01
3.06
1.04
1.04
8.90
.0 10.5 10.0 9.5 9.0 8.5 8.0 7.5 7.0 6.5 6.0 5.5 5.0 4.5 4.0 3.5 3.0 2.5 2.0 1.5 1.0 0.5 0.0 -0
f1 (ppm)

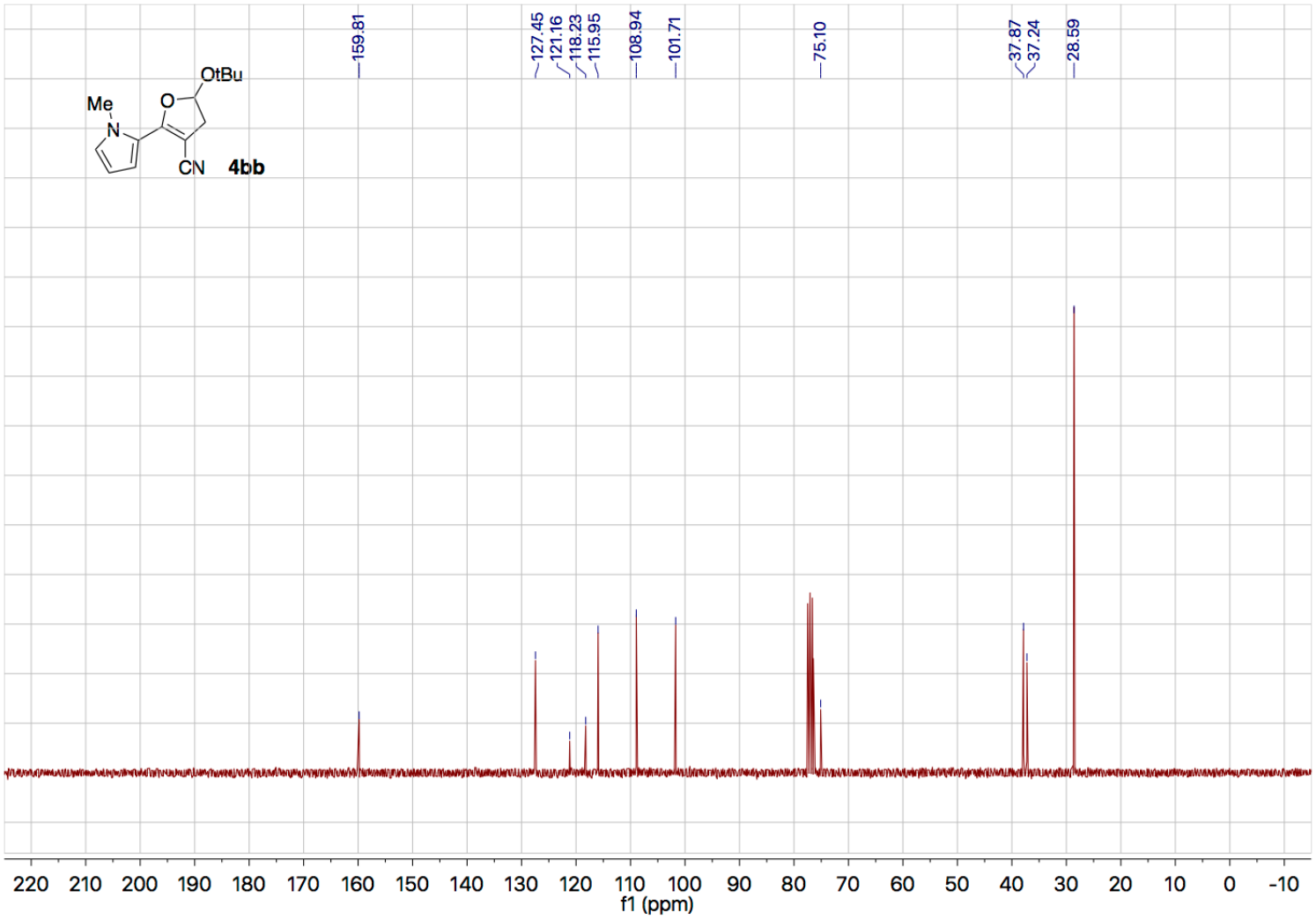
159.81
127.45
121.16
118.23
115.95
108.94
101.71
75.10
37.87
37.24
28.59
OtBu
Me
N
O
CN
4bb
220 210 200 190 180 170 160 150 140 130 120 110 100 90 80 70 60 50 40 30 20 10 0 -10
f1 (ppm)

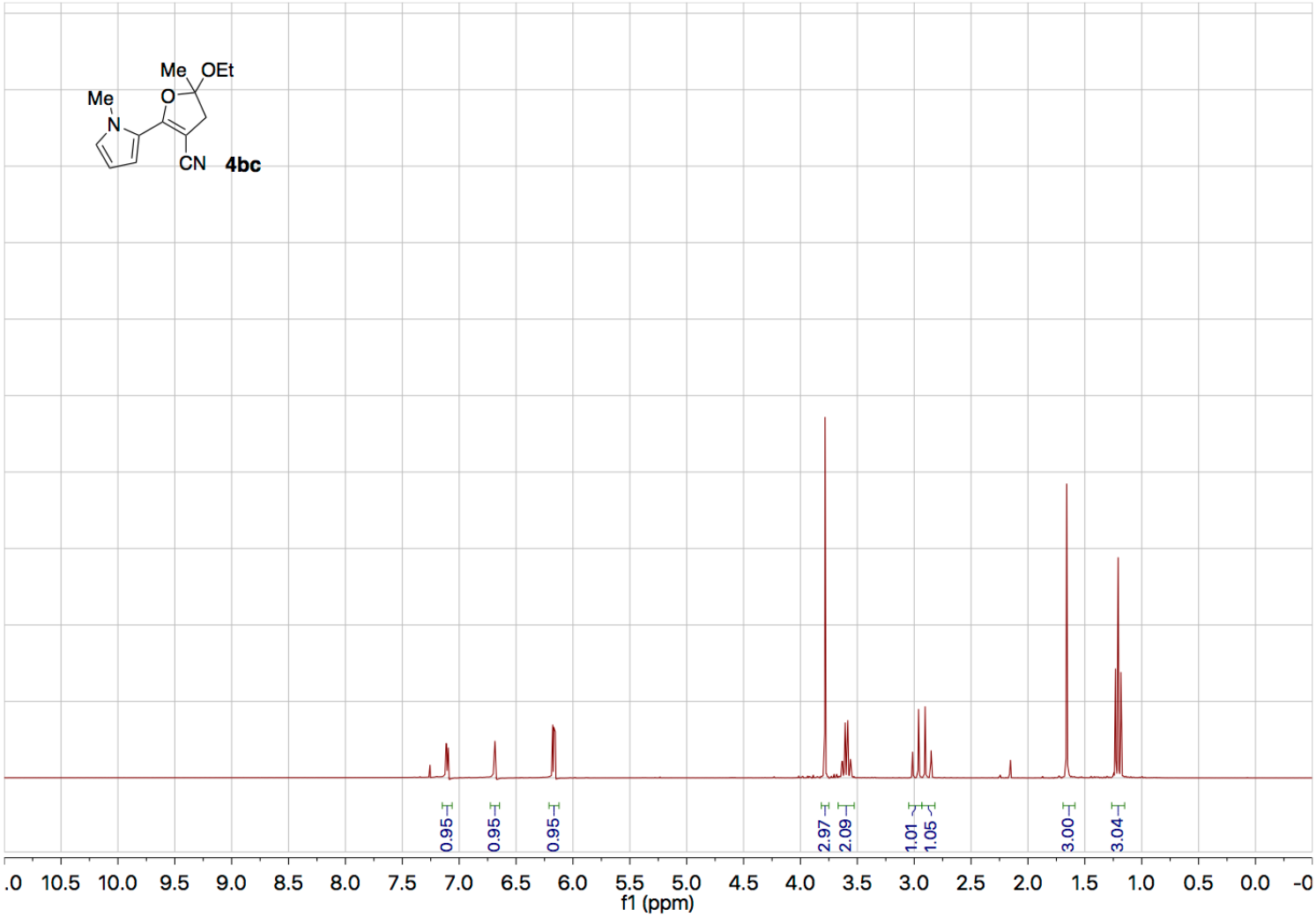
Me
OEt
Me
O
N
CN
4bc
0.95
0.95
0.95
2.97
2.09
1.01
1.05
3.00
3.04
.0 10.5 10.0 9.5 9.0 8.5 8.0 7.5 7.0 6.5 6.0 5.5 5.0 4.5 4.0 3.5 3.0 2.5 2.0 1.5 1.0 0.5 0.0 -0
f1 (ppm)

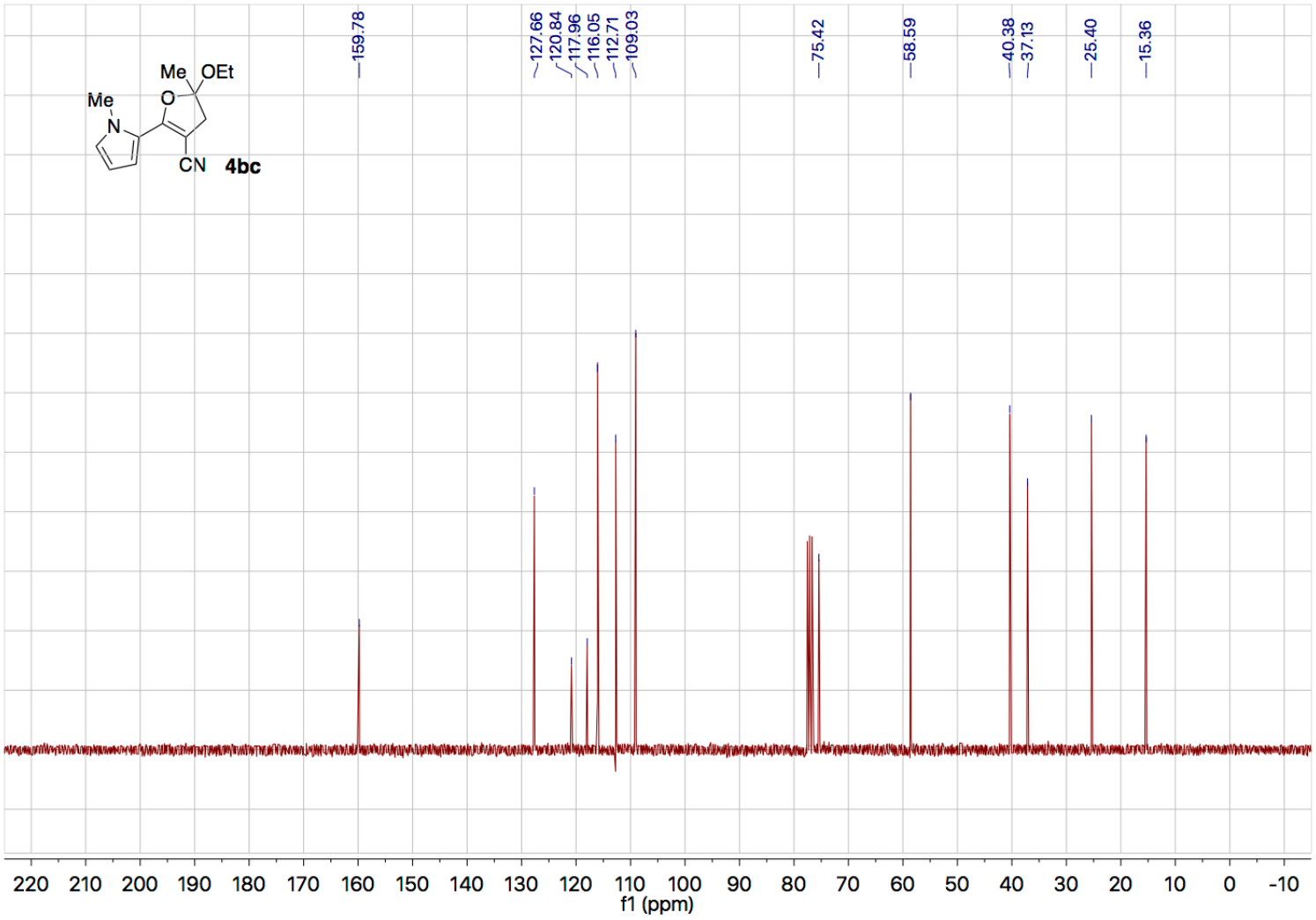
159.78
127.66
120.84
117.96
116.05
112.71
109.03
75.42
58.59
40.38
37.13
25.40
15.36
Me
OEt
O
Me
N
CN
4bc
220 210 200 190 180 170 160 150 140 130 120 110 100 90 80 70 60 50 40 30 20 10 0 -10
f1 (ppm)

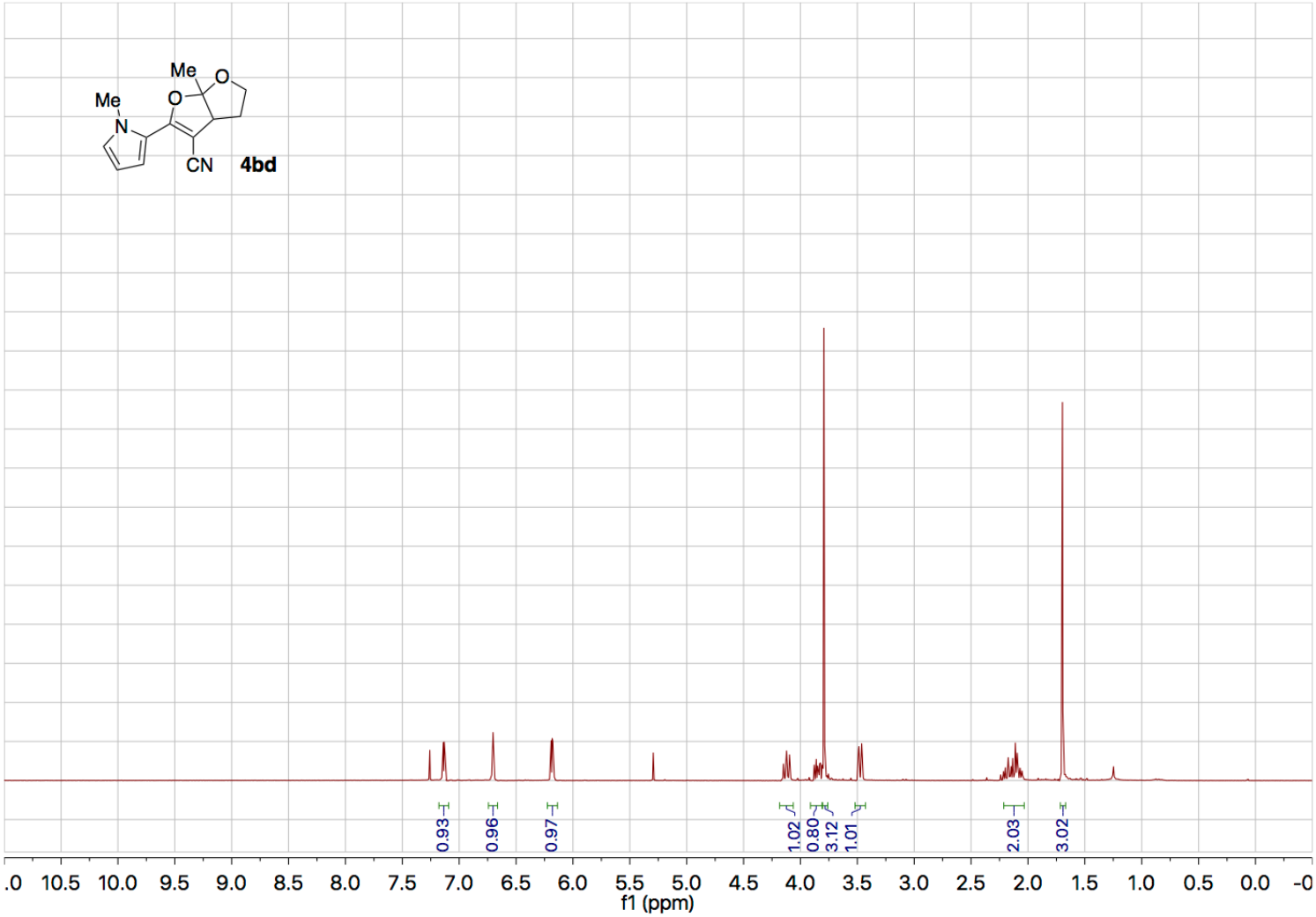
Me
O
Me
O
N
CN
4bd
0.93
0.96
0.97
1.02
0.80
3.12
1.01
2.03
3.02
.0 10.5 10.0 9.5 9.0 8.5 8.0 7.5 7.0 6.5 6.0 5.5 5.0 4.5 4.0 3.5 3.0 2.5 2.0 1.5 1.0 0.5 0.0 -0
f1 (ppm)

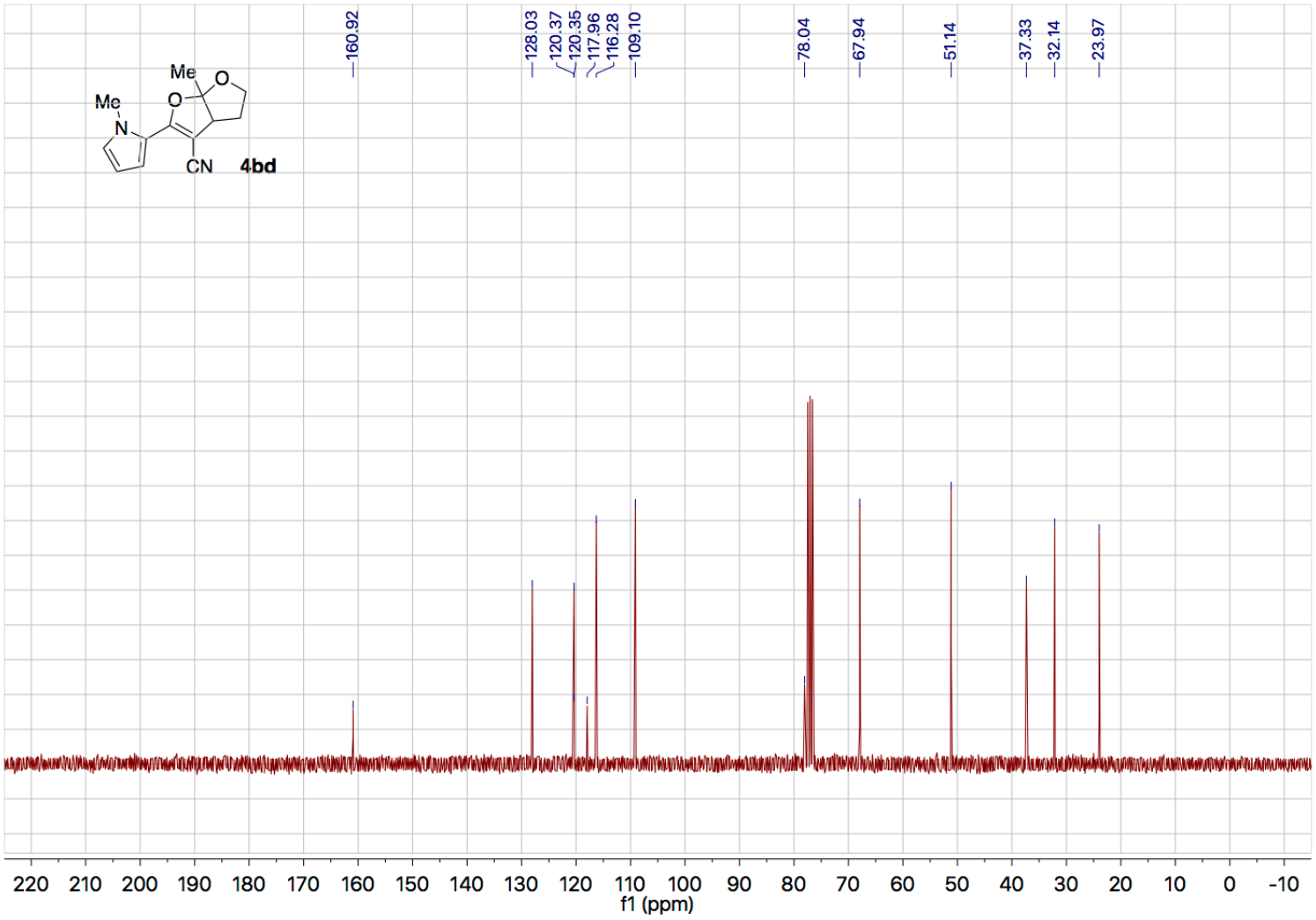
160.92
128.03
120.37
120.35
117.96
116.28
109.10
78.04
67.94
51.14
37.33
32.14
23.97
Me
O
Me
O
N
CN
4bd
220 210 200 190 180 170 160 150 140 130 120 110 100 90 80 70 60 50 40 30 20 10 0 -10
f1 (ppm)

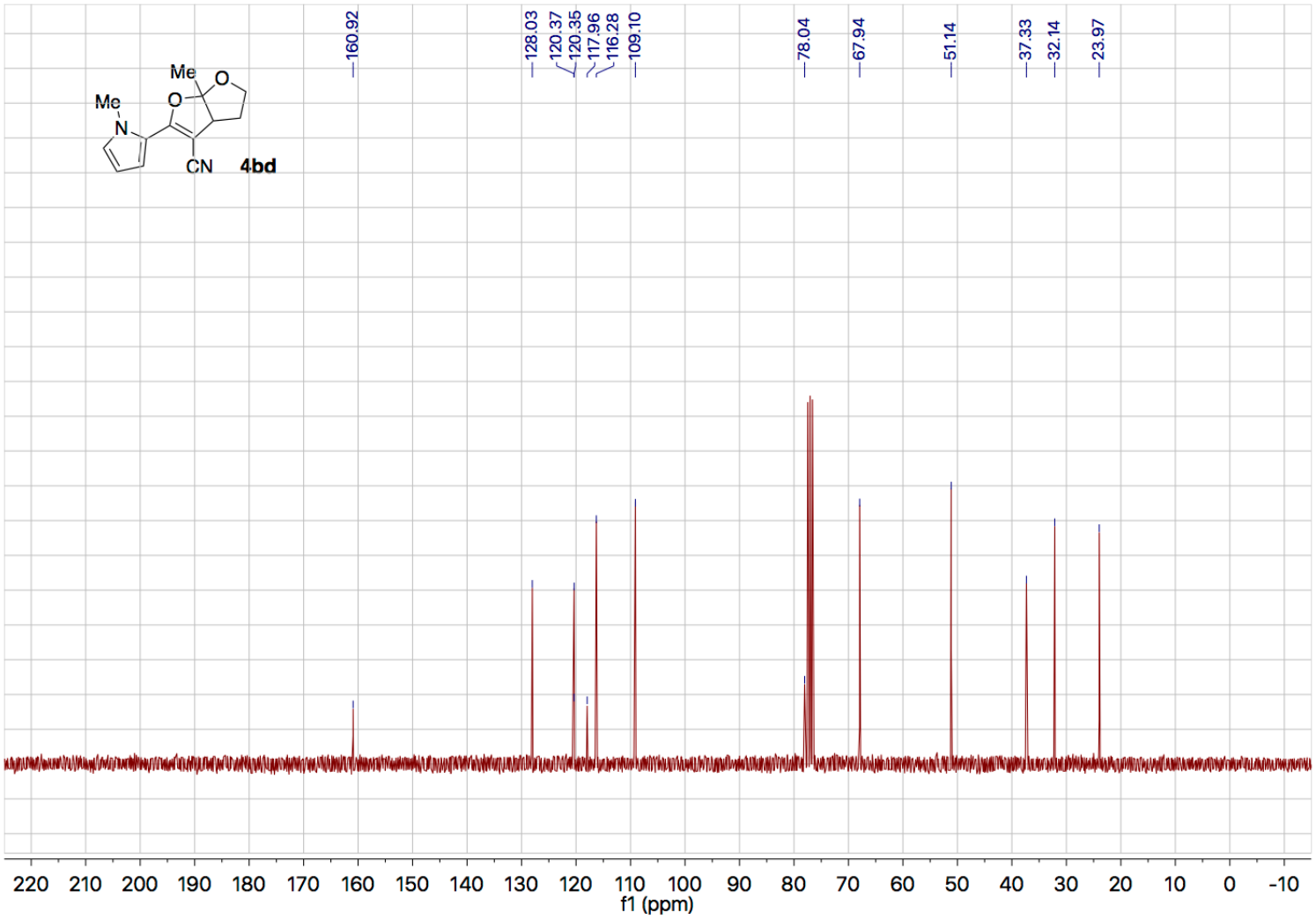
160.92
128.03
120.37
120.35
117.96
116.28
109.10
78.04
67.94
51.14
37.33
32.14
23.97
Me
O
Me
O
N
CN
4bd
220 210 200 190 180 170 160 150 140 130 120 110 100 90 80 70 60 50 40 30 20 10 0 -10
f1 (ppm)

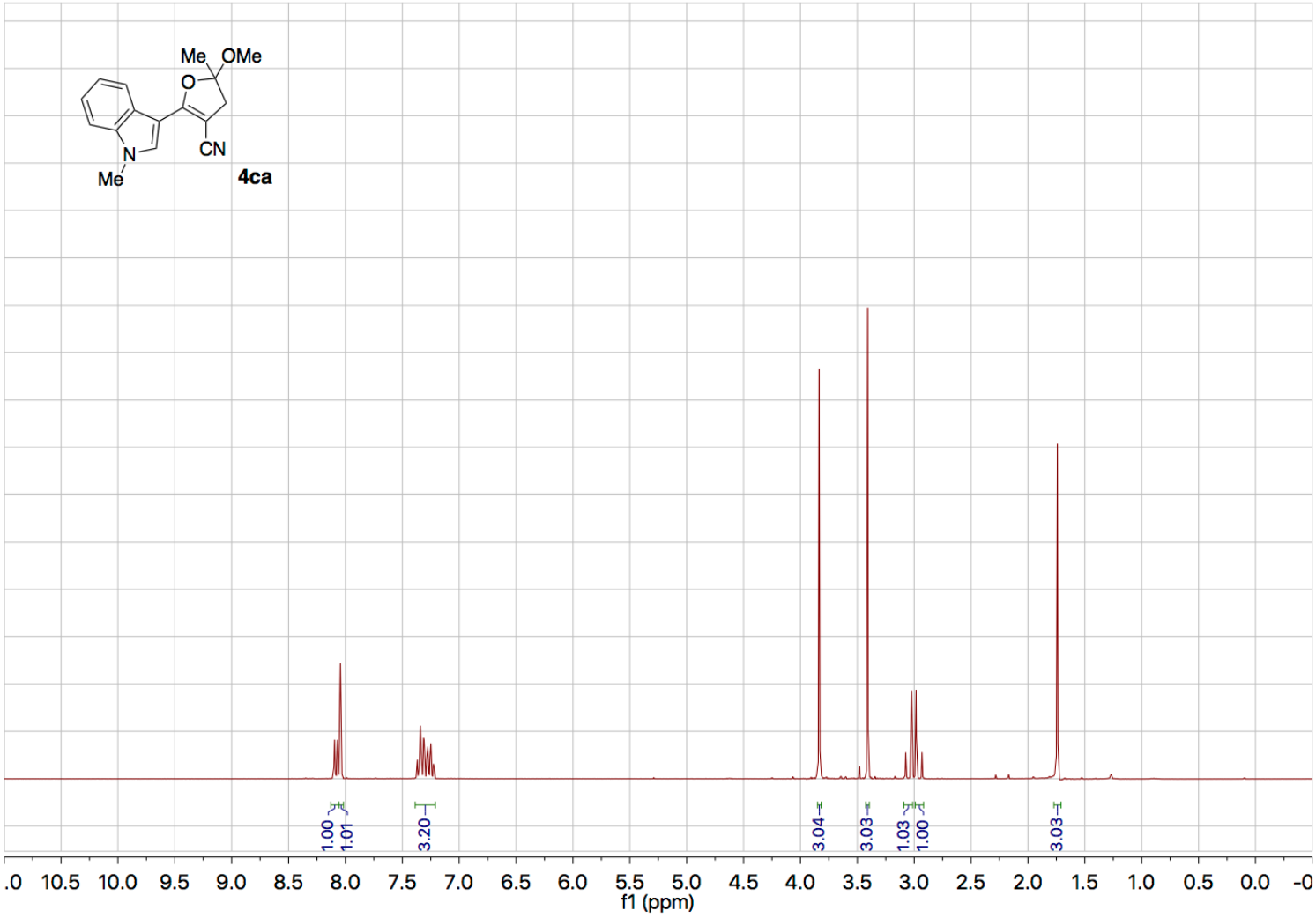
Me
OMe
O
N
Me
CN
4ca
1.00
1.01
3.20
3.04
3.03
1.03
1.00
3.03
.0 10.5 10.0 9.5 9.0 8.5 8.0 7.5 7.0 6.5 6.0 5.5 5.0 4.5 4.0 3.5 3.0 2.5 2.0 1.5 1.0 0.5 0.0 -0
f1 (ppm)

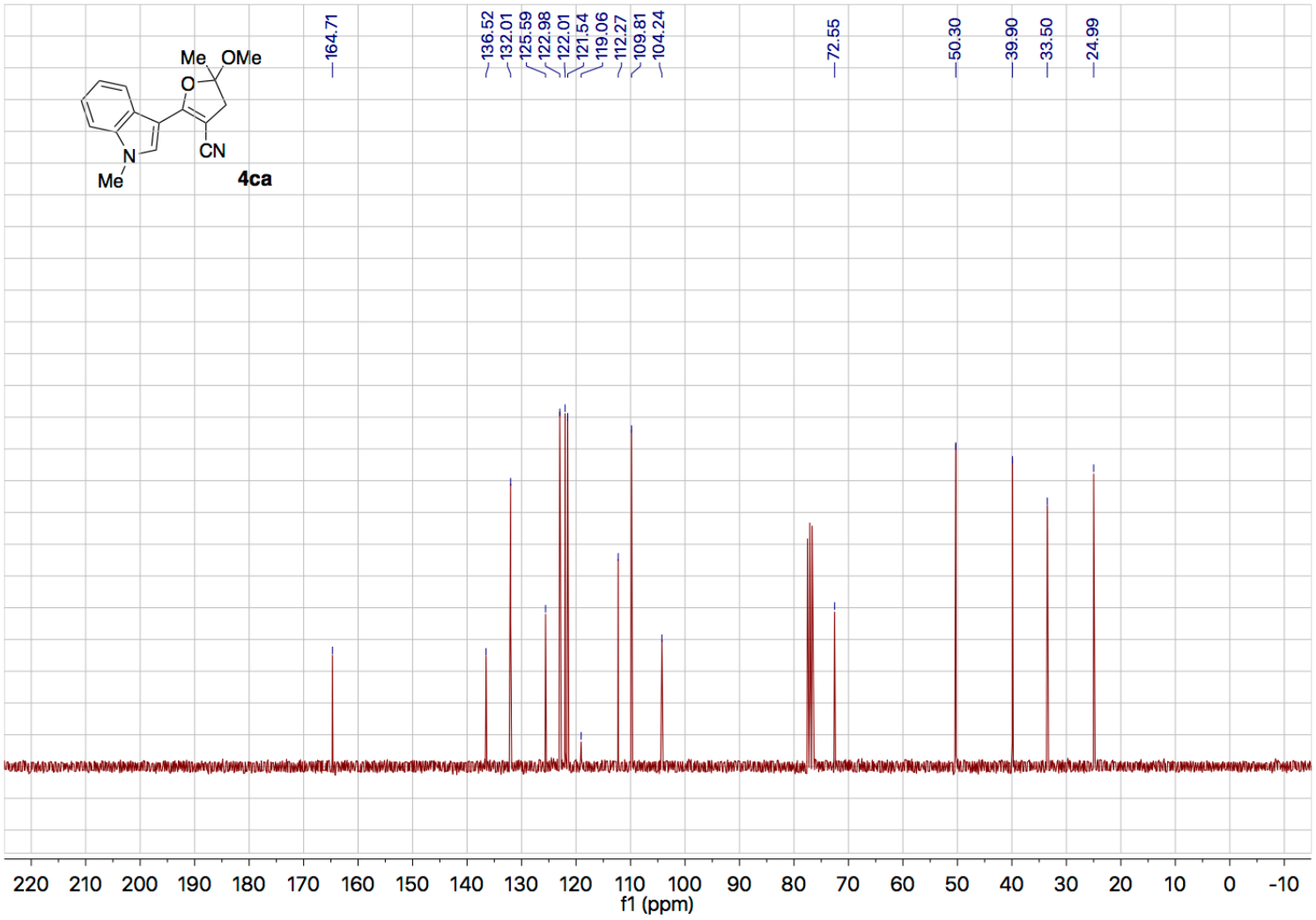
Me
OMe
O
N
Me
CN
4ca
164.71
136.52
132.01
125.59
122.98
122.01
121.54
119.06
112.27
109.81
104.24
72.55
50.30
39.90
33.50
24.99
220 210 200 190 180 170 160 150 140 130 120 110 100 90 80 70 60 50 40 30 20 10 0 -10
f1 (ppm)

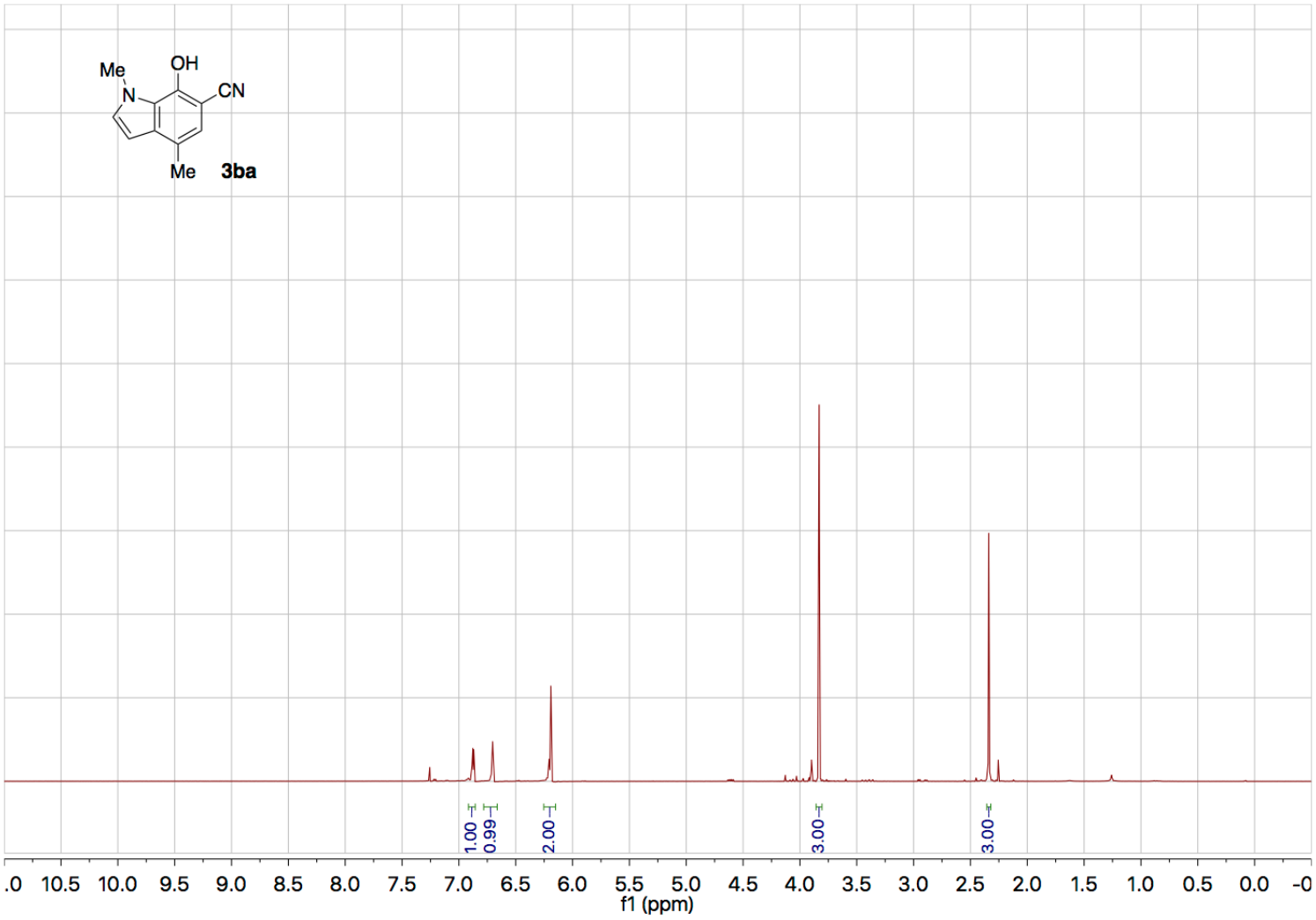
Me
N
OH
CN
Me
3ba
1.00
0.99
2.00
3.00
3.00
.0 10.5 10.0 9.5 9.0 8.5 8.0 7.5 7.0 6.5 6.0 5.5 5.0 4.5 4.0 3.5 3.0 2.5 2.0 1.5 1.0 0.5 0.0 -0
f1 (ppm)

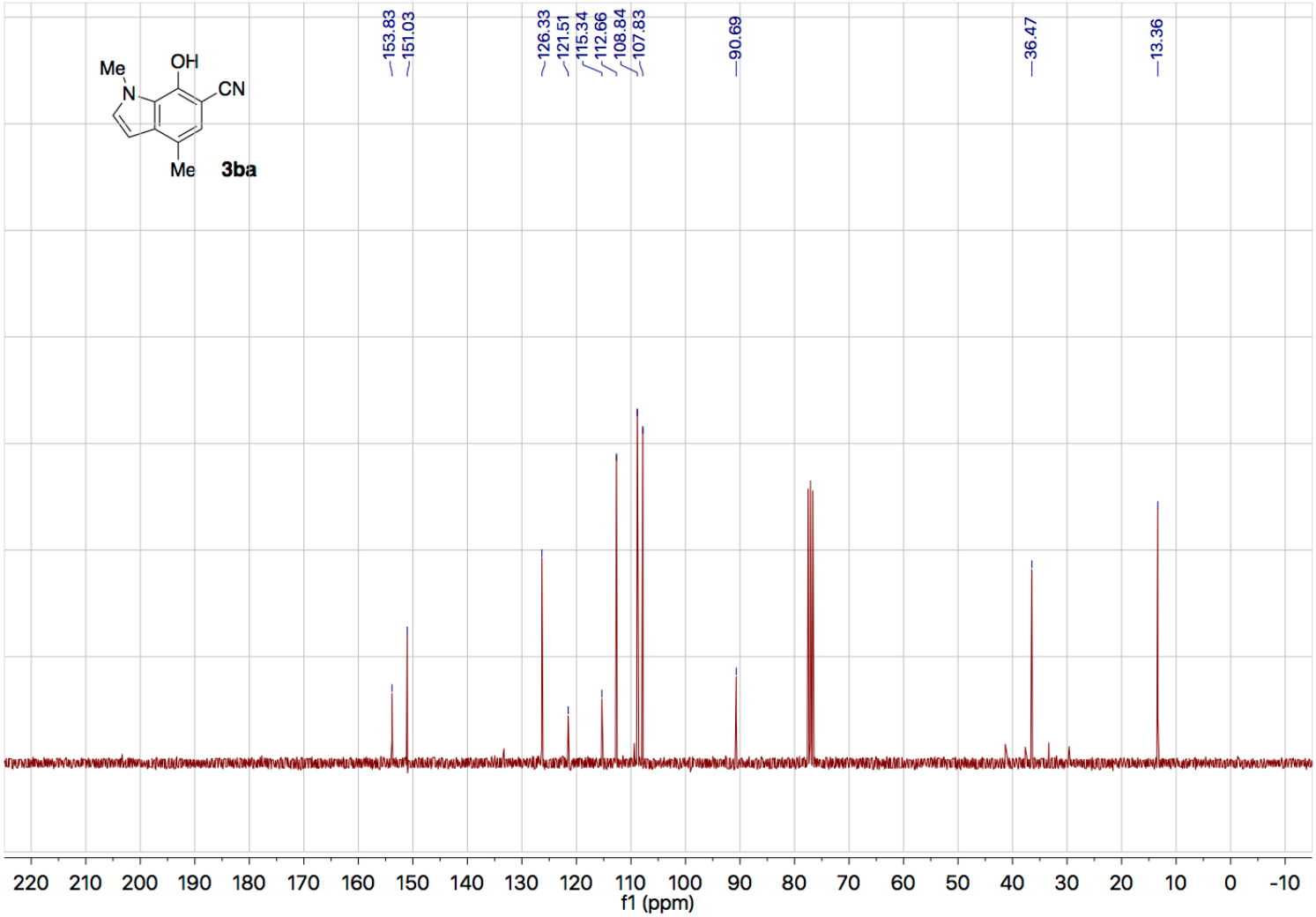
Me
OH
N
CN
Me
3ba
153.83
151.03
126.33
121.51
115.34
112.66
108.84
107.83
90.69
36.47
13.36
220 210 200 190 180 170 160 150 140 130 120 110 100 90 80 70 60 50 40 30 20 10 0 -10
f1 (ppm)

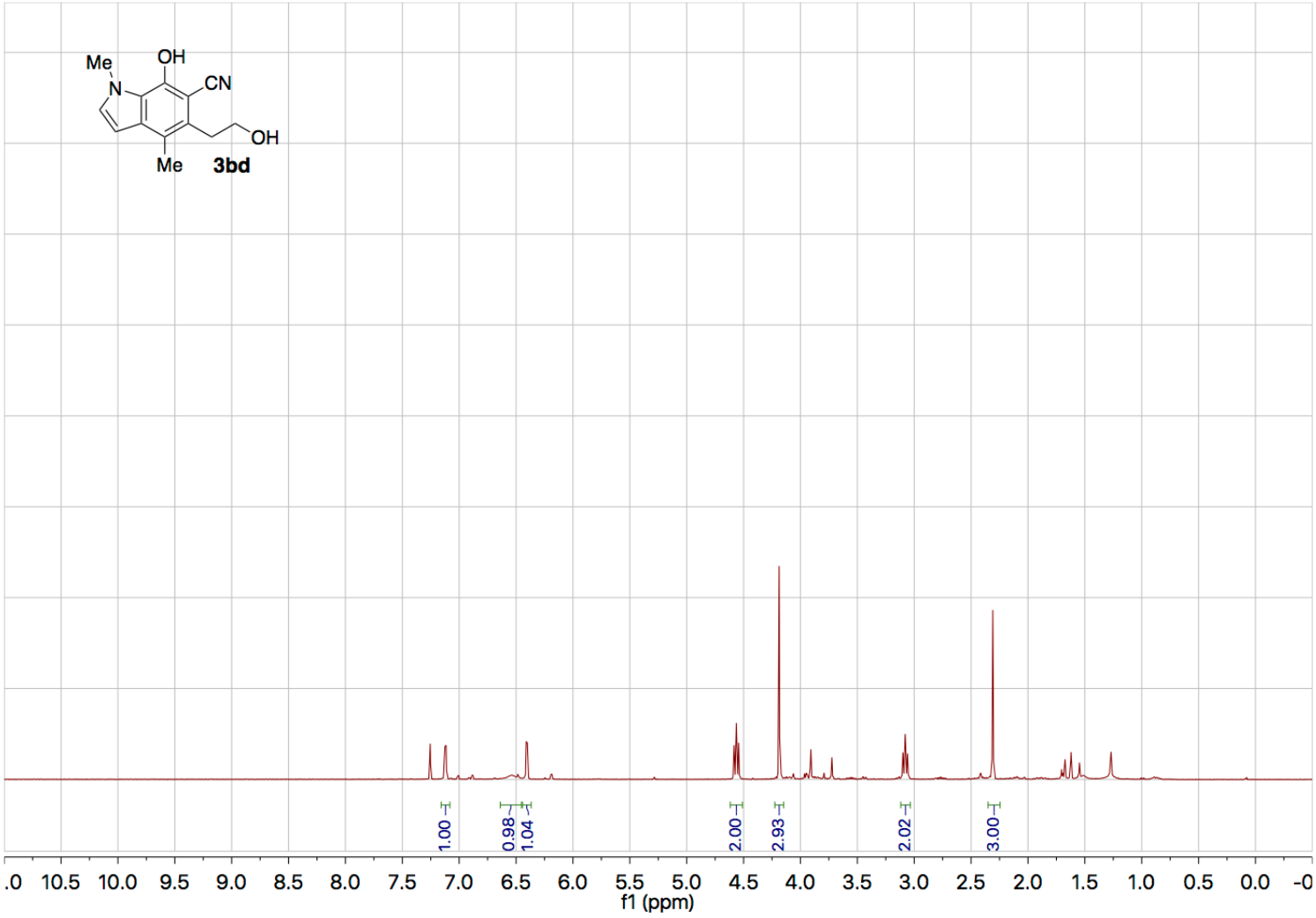
Me
N
OH
CN
OH
Me
3bd
1.00
0.98
1.04
2.00
2.93
2.02
3.00
.0 10.5 10.0 9.5 9.0 8.5 8.0 7.5 7.0 6.5 6.0 5.5 5.0 4.5 4.0 3.5 3.0 2.5 2.0 1.5 1.0 0.5 0.0 -0
f1 (ppm)

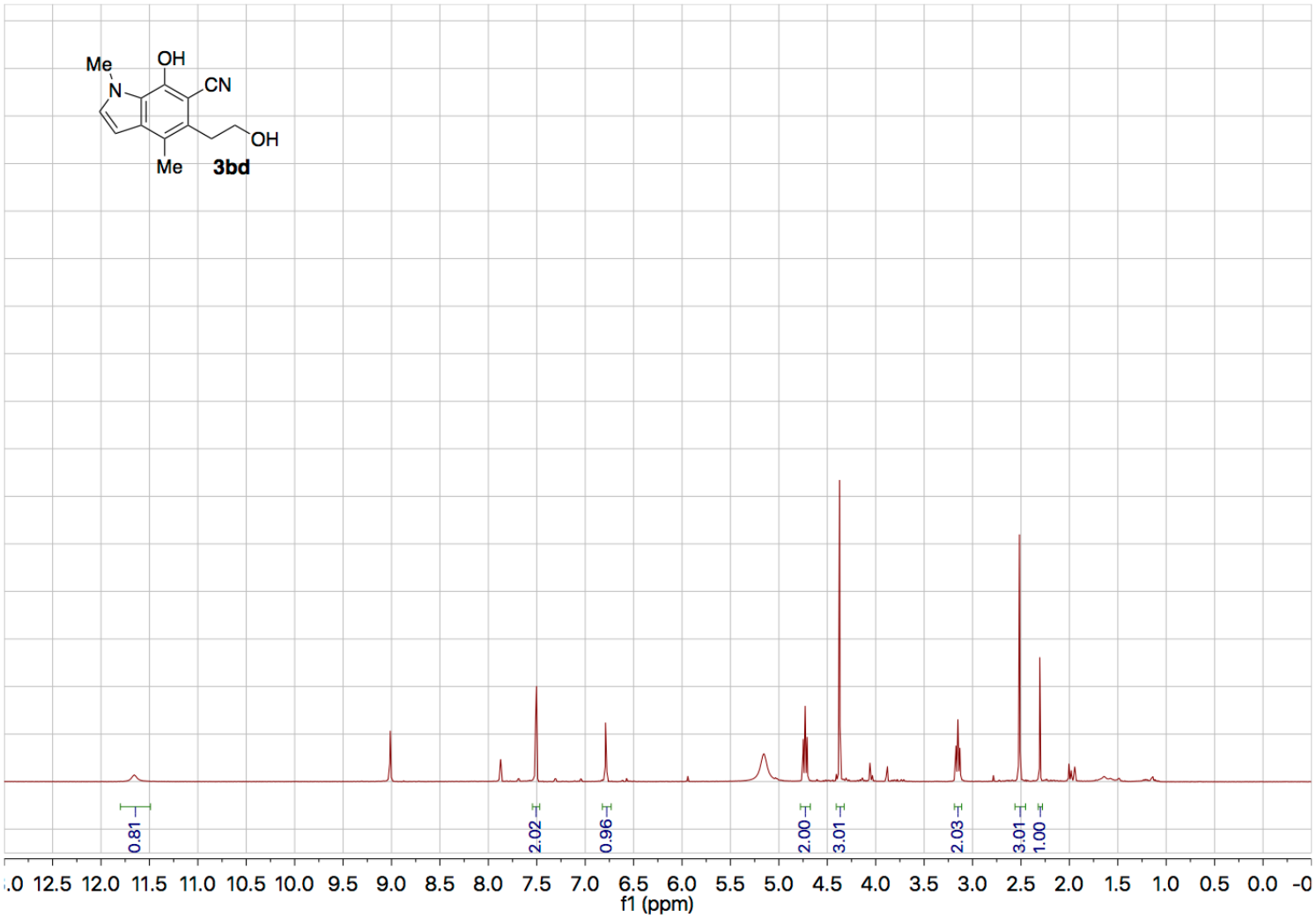
Me
N
OH
CN
OH
Me
3bd
0.81
2.02
0.96
2.00
3.01
2.03
3.01
1.00
.0 12.5 12.0 11.5 11.0 10.5 10.0 9.5 9.0 8.5 8.0 7.5 7.0 6.5 6.0 5.5 5.0 4.5 4.0 3.5 3.0 2.5 2.0 1.5 1.0 0.5 0.0 -0
f1 (ppm)

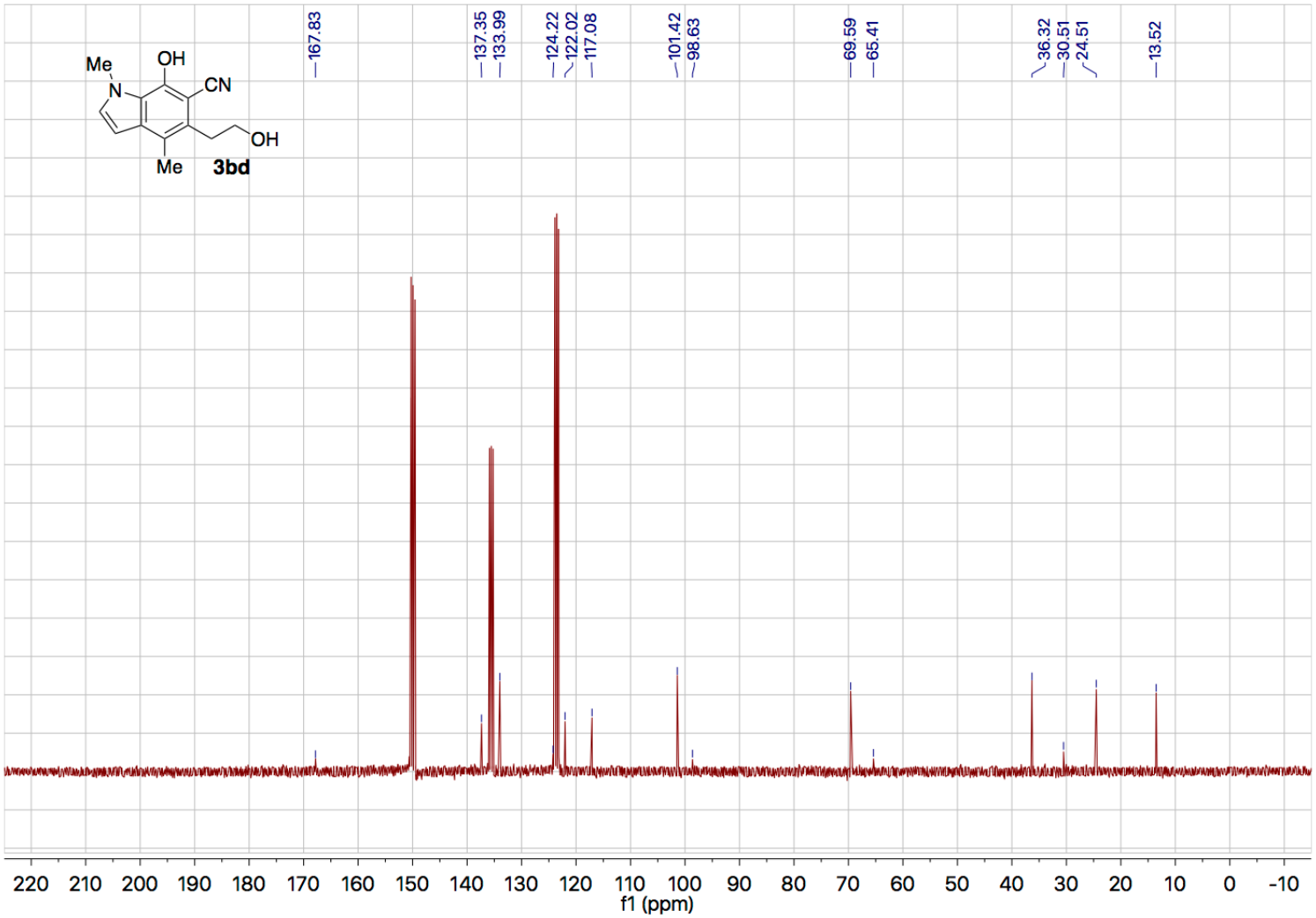
Me
OH
CN
N
OH
Me
3bd
167.83
137.35
133.99
124.22
122.02
117.08
101.42
98.63
69.59
65.41
36.32
30.51
24.51
13.52
220 210 200 190 180 170 160 150 140 130 120 110 100 90 80 70 60 50 40 30 20 10 0 -10
f1 (ppm)

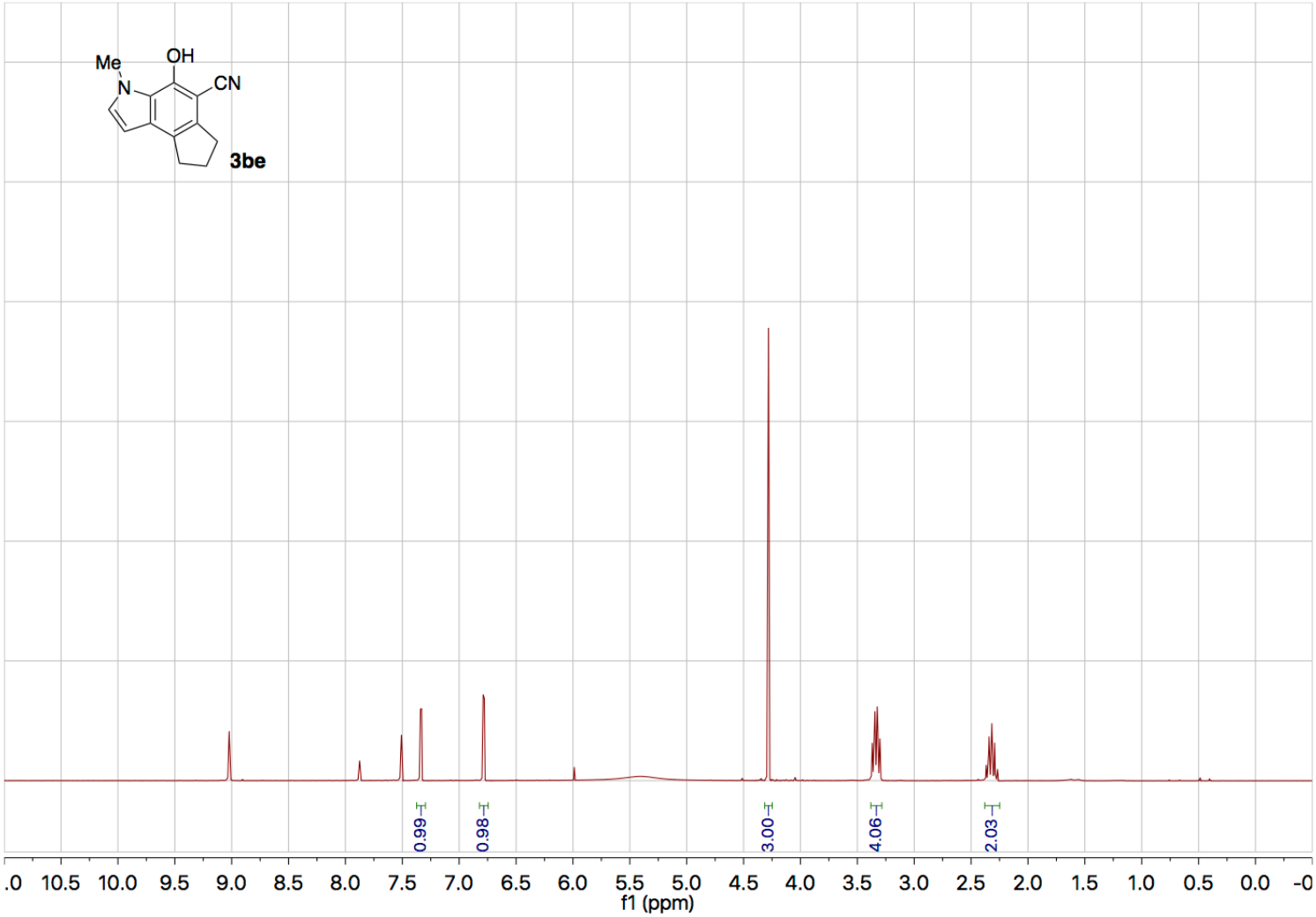
Me
N
OH
CN
3be
0.99
0.98
3.00
4.06
2.03
.0 10.5 10.0 9.5 9.0 8.5 8.0 7.5 7.0 6.5 6.0 5.5 5.0 4.5 4.0 3.5 3.0 2.5 2.0 1.5 1.0 0.5 0.0 -0
f1 (ppm)

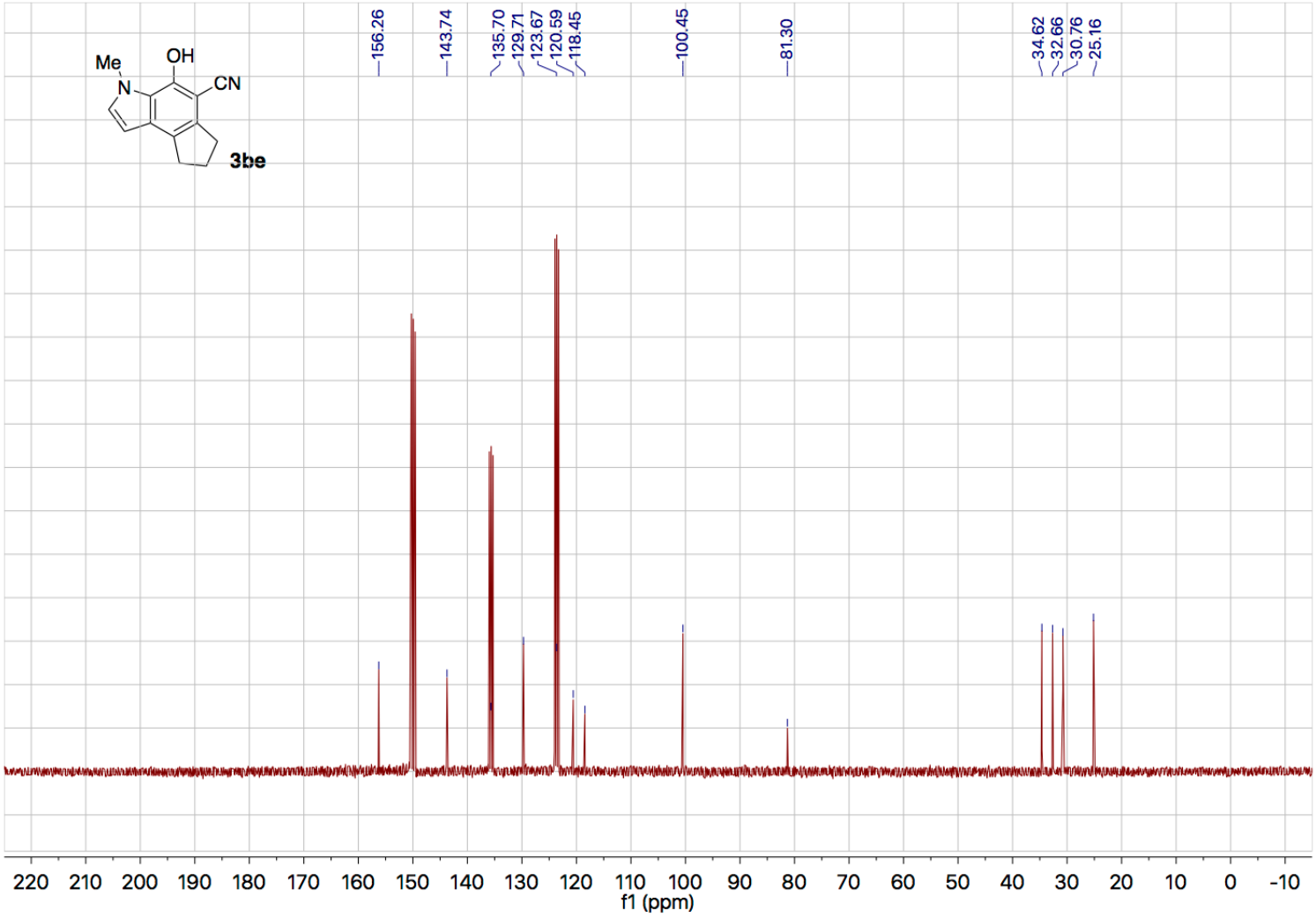
Me
N
OH
CN
3be
156.26
143.74
135.70
129.71
123.67
120.59
118.45
100.45
81.30
34.62
32.66
30.76
25.16
220 210 200 190 180 170 160 150 140 130 120 110 100 90 80 70 60 50 40 30 20 10 0 -10
f1 (ppm)

4.5 References

[1] (a) Kaushik, N. K.; Kaushik, N.; Attri, P.; Kumar, N.; Kim, C. H.; Verma, A. K.; Choi, E. H. *Molecules* **2013**, *18*, 6620; (b) Sharma, V.; Kumar, P.; Pathak, D. J. *Heterocyclic Chemistry* **2010**, *47*, 491; (c) Chadha, N. and Silakar, O. *European Journal of Medicinal Chemistry* **2017**, *134*, 159.

[3] Taber, D. F.; Tirunahari, P. K. *Tetrahedron* **2011**, *67*, 7195.

[3] a) Fischer, E.; Jourdan, F. *Berichte der Deutschen Chemischen Gasellschaft* **1883**, *16*, 2241 (b) Robinson, B. *Chemical Reviews* **1963**, *63*, 373.

[4] Chae, J.; Buchwald, S. L. *Journal of Organic Chemistry* **2004**, *69*, 3336.

[5] Mori, M.; Chiba, K.; Ban, Y. *Tetrahedron Letters* **1977**, 1037.

[6] MacLeod, J. K.; Monahan, L. C. *Tetrahedron Letters* **1988**, *29*, 391.

[7] Yamada, K.; Kurokawa, T.; Tokuyama, H.; Fukuyama, T. *Journal of the American Chemical Society* **2003**, *125*, 6630.

[8] (a) Larock, R. C.; Yum, E. K. *Journal of the American Chemical Society* **1991**, *113*, 6689; (b) Larock, R. C.; Yum, E. K.; Refvik, M. D. *Journal of Organic Chemistry* **1998**, *63*, 7652.

[9] (a) Jones, C. D.; Suarez, T *Journal of Organic Chemistry* **1972**, *37*, 3622; (b) Jones, C. D. *Journal of Organic Chemistry* **1972**, *37*, 3624.

[10] Moskal, J.; van Leusen, A. M. *Journal of Organic Chemistry* **1986**, *51*, 4131.

[11] Arai, M.; Miyauchi, Y.; Miyahara, T.; Ishikawa, T.; Saito, S. *Synlett* **2008**, 122.

[12] Petronijevic, F.; Timmons, C.; Cuzzupe, A.; Wipf, P. *Chemical Communications* **2009**, 104.

[13] Yang, Y.; Gao, P.; Zhao, Y.; Shi, Z. *Angewandte Chemie* **2017**, *129*, 4024.

[14] Leitch, J. A.; Bhonoah, Y.; Frost, C. G. *ACS Catalysis* **2017**, *7*, 5618 and references therein.

[15] Eastgate, M. D.; Schmidt, M. A.; Fandrick, K. R. *Nature Reviews Chemistry* **2017**, *1*, 1-16.

[16] Aponte-Guzmán, J.; Phun, L. H.; Cavitt, M. A.; Taylor, J. E.; Davy, J. C.; France, S. *Chemistry – A European Journal.* **2016**, *22*, 10405.

[17] Currently, a graduate student in our lab is demonstrating success in optimizing an approach to form indole carboxylates from diazoacetates.

[18] (a) Lindsay, V. N. G.; Fiset, D.; Gritsch, P. J.; Azzi, S.; Charette, A. B. *Journal of the American Chemical Society* **2013**, *135*, 1463; (b) B. D. McLarney, M. A. Cavitt, T. M. Donnell, D. G. Musaev, S. France, *Chemistry – A European Journal.* **2017**, *23*, 1129.

[19] Campbell, M. J.; Johnson, J. S. *Journal of the American Chemical Society* **2009**, *131*, 10370.

CHAPTER 5. CONCLUSION

5.1 Summary

This thesis presents three projects that are thematically linked as methods for intermolecular C-H functionalization by A-A diazo compounds. In Chapter 2, a method for constructing the β,γ-unsaturated-γ-heteroatom framework via the $C(sp^2)$-H functionalization of enol ethers, enamides, and enecarbamates was presented. Insight gleaned from density functional theory calculations was utilized to improve the scope of the method. Meanwhile product utility was demonstrated through synthetic derivatizations and the discovery of a Lewis acid catalyzed cyclization protocol.

In Chapter 3, a systematic computational investigation of β-carbonyl-α-carbene esters was presented. This investigation resulted in parameterization of important steric and electronic features of these carbenes which was then used to build a visual chemical space map that describes how activation energy to intermolecular $C(sp^3)$-H insertion varies with the change in steric and electronic components of the carbene. Ultimately, the chemical space guide built in the study was leveraged to discover a new synthetically useful sub-class of H-bonding carbenes.

Chapter 4 detailed a multi-C-H functionalization protocol that utilizes β-keto-α-diazo nitrile and enol ether starting materials to generate 7-hydroxy-indole-6-carbonitriles in two steps. Optimization of both steps was conducted and a preliminary substrate scope was generated. Further work will be conducted by junior graduate students.

5.2 Future Work

Two primary categories of future work exist for this these: (1) inspired studies such as enhancing the scope and performance of the current reactions and models, and (2) developing chemistry enabled by the discoveries in this thesis (Figure 29).

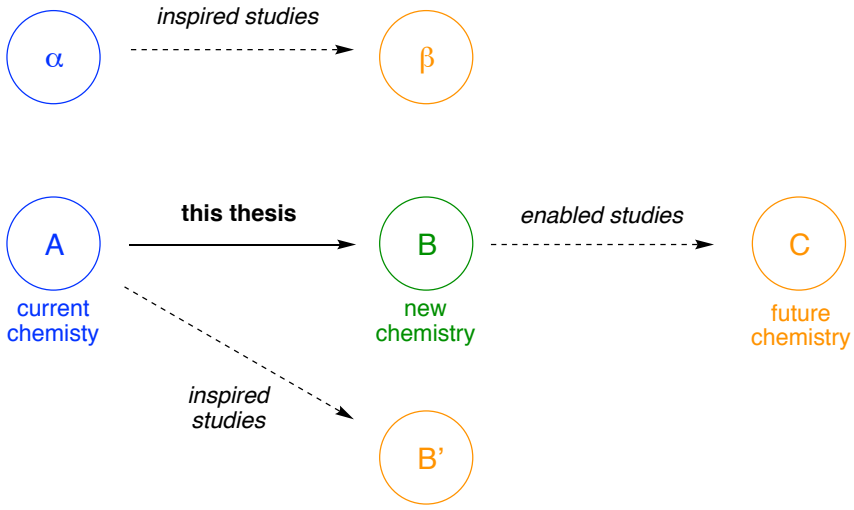

Figure 29 – Categorizing Future Work Related to this Thesis

5.2.1 Inspired Studies: Enhancing Scope and Performance

The overarching theme of this thesis was uncovering the latent, C-H functionalization potential of A-A diazo compounds. Among these species, the most heavily explored in this thesis were α-diazo-β-keto esters followed by α-diazo-β-keto nitriles; as such, opportunity remains for the extension of these chemistries to more exotic A-A species (Scheme 43). Some acceptor group, such as the nitro and ketone groups, would be natural extensions to this work given their structural similarity to esters. Other acceptor groups, such as phosphonate and trifluormethyl groups, will likely require more ground-up approaches beginning with computational investigations akin to those presented in Chapter 3. In this sense, not only should this thesis be used as a launch pad into new

chemical space, but it should be used as a model for interrogating systems from a two-pronged, synthetic and computational approach.

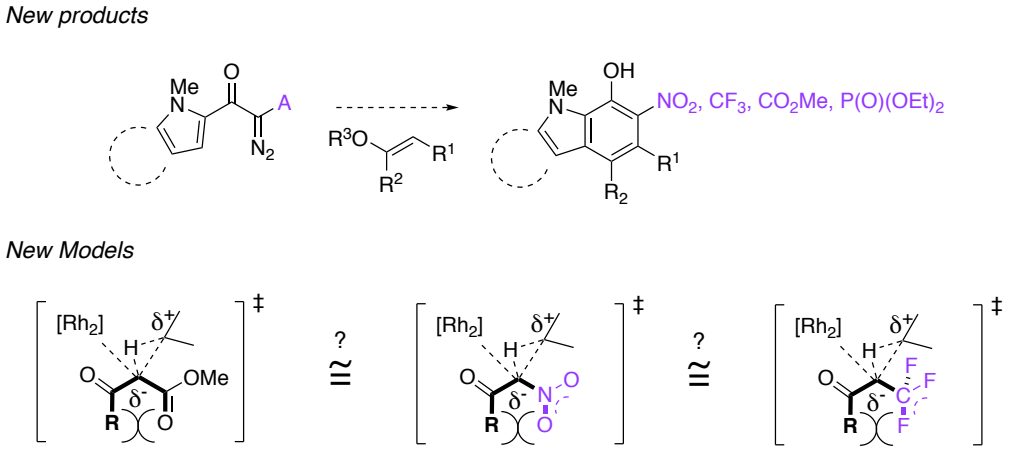

Scheme 43 – Examples of Extending the Chemistry to Other A-A Sub-Classes

In addition to expanding the scope of these reactions, efforts could be made to improve the performance of the methodology by increasing selectivity or, in the case of Chapter 4, developing a one-pot approach from the diazo compound. Significant room for improvement also exists for enhancing the C-H functionalization chemistry of 2° amide diazo compounds (Scheme 44).

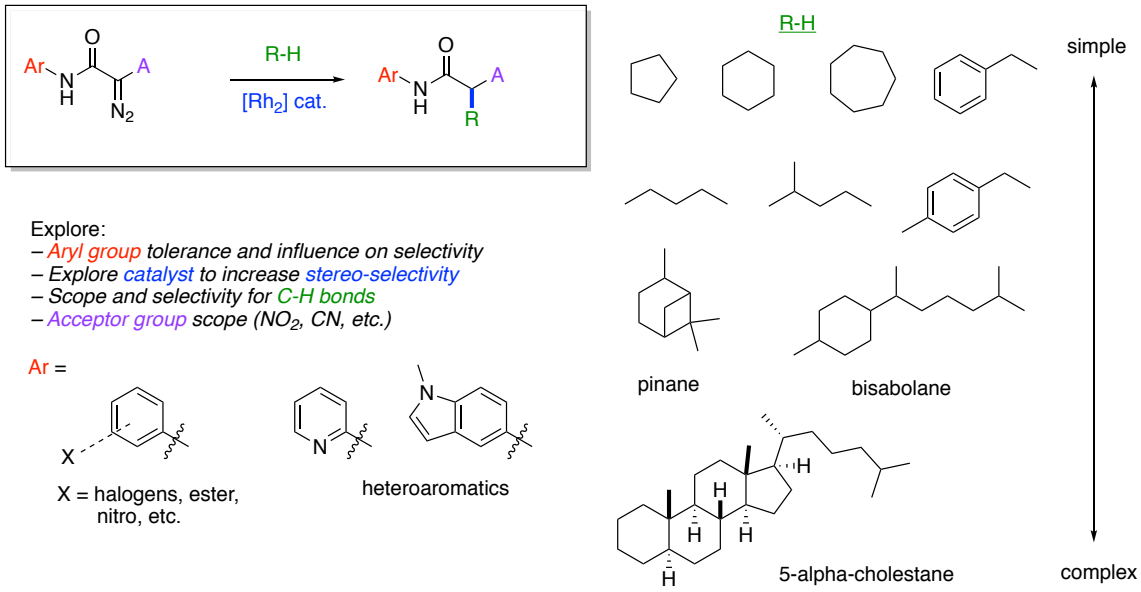

Scheme 44 – Pushing the Limits of 2° Amide Carbene Chemistry

5.2.2 Enabled Chemistry

Each C-H functionalization method presented in this thesis offers access to uncharted chemical space, thus opportunity exists to build chemistry using the product space. For example, Chapter 2 provides access to starting materials that could be leveraged to develop an electrocyclization methodology generating aryl building blocks (Scheme 45 A). Furthermore, Chapter 3 enables studies on auxiliary group directed C-H functionalization, electron deficient amide coupling, pharmaceutical synthesis, cyclopropanation utilizing 2° amide diazoacetates, and H-bonding carbene catalyst development (Scheme 45 B,C,D).

(A) Cyclization of β,γ-unsaturated-γ-heteroatom aryl substituted carbonyls

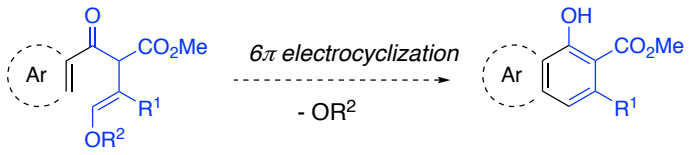

(B)

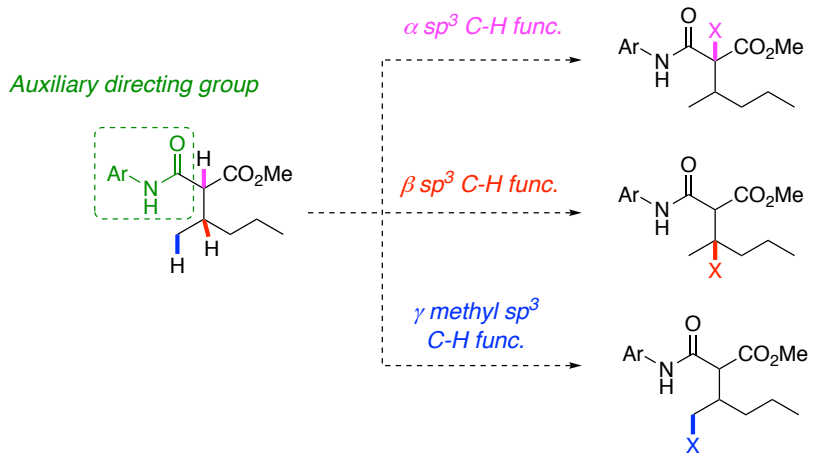

(C) Pharmaceutical synthetsis

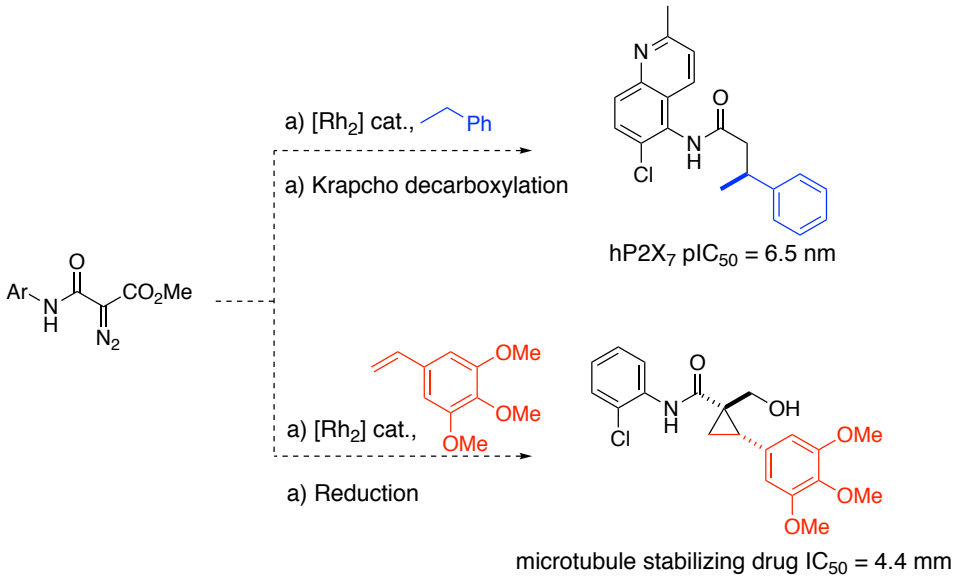

(D) Strategic platform for catalyst development

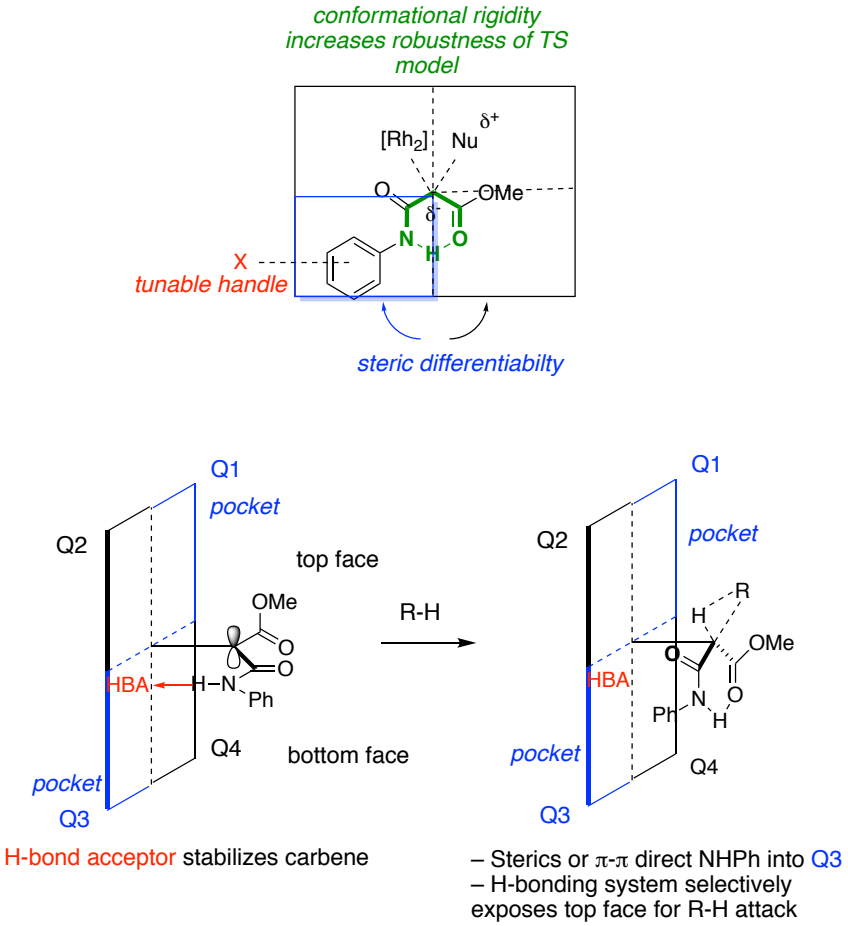

Scheme 45 – Studies Enabled by the Chemistry in this Thesis

5.3 Concluding Statements

This thesis represents a journey for the acceptor-acceptor carbene subclass through the synthetic and computational rigors of intermolecular C-H functionalization methodology (Scheme 46). Once a class of compounds avoided in this field due to their unmanageable reactivity profile, A-A carbenes now have demonstrated potential to selectively functionalize sp^2 and sp^3 C-H bonds under intermolecular manifolds. Furthermore, this reactivity is accompanied by theoretical models to rationalize and predict future behavior. As such, now A-A carbenes are not only useful synthetic tools for their

ability to transform chemical feedstock into complex synthons, but they are also attractive species for further investigation by other groups in this field.

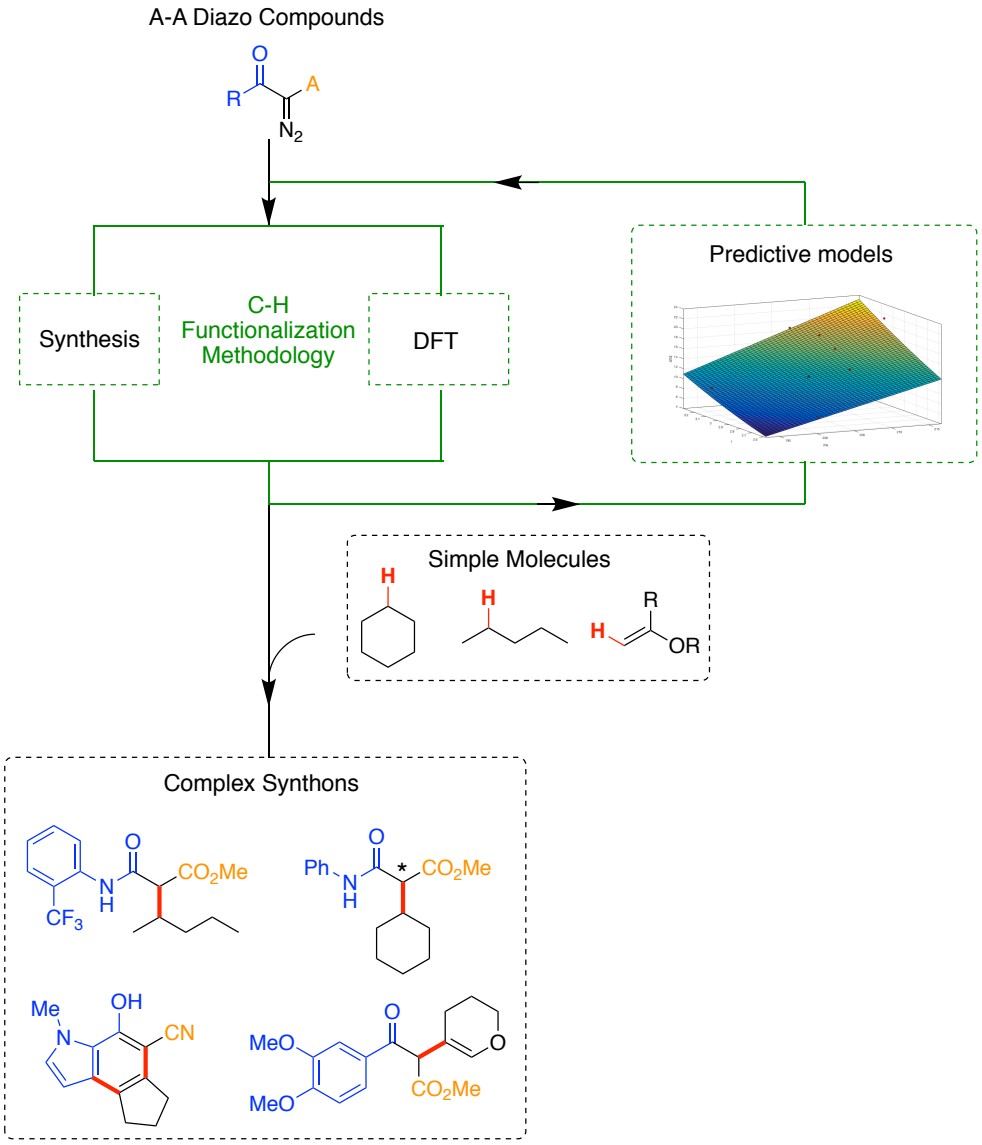

Scheme 46 – Journey of the A-A Carbene Sub-Class in this Thesis

This collection of new chemistries, along with the approaches toward their discovery, are intended to function as a template to guide future research efforts in the field of C-H functionalization.

APPENDIX A. UNDERSTANDING E VS. Z SELECTIVITY IN THE RING-OPENING CYCLIZATION OF CYCLOPROPYL CARBINOLS TO FORM α-ALKYLIDENE-γ-BUTYROLACTONES

With the publisher's permission, this chapter has been adapted from the original manuscript: Sandridge, M. J.; McLarney, B. D.; Williams, C. W.; France, S. A. *Journal of Organic Chemistry*. **2017**, *82*, 10883.

A.1 Introduction

A.1.1 The α-Alkylidene-γ-Butyrolactone Moiety

A.1.1.1 Synthetic Importance of the α-Alkylidene-γ-Butyrolactone Moiety

The α-alkylidene-γ-butyrolactone (ABL) framework represents an important structural motif to both organic and medicinal chemists (Figure 30).

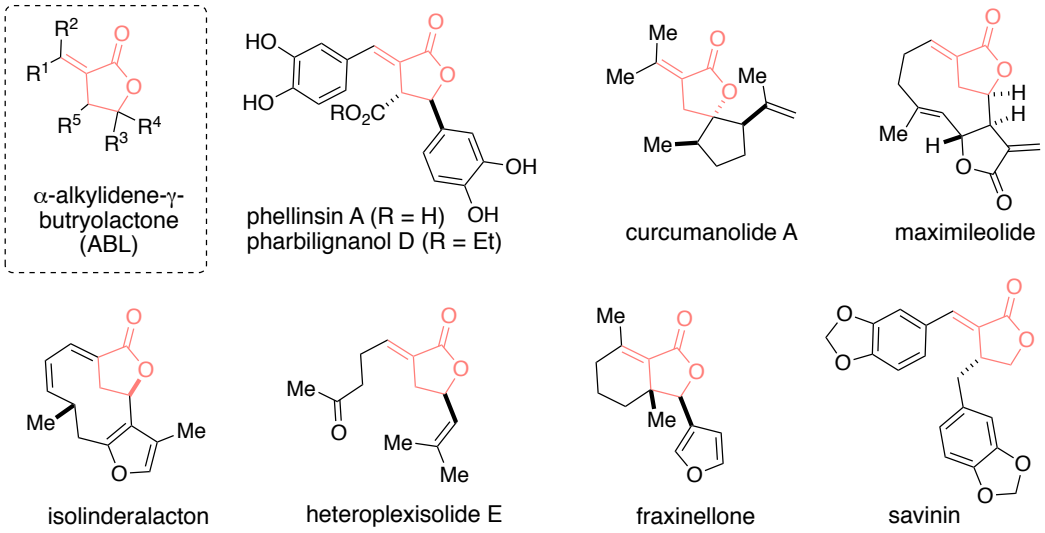

Figure 30 – Biologically Relevant Examples of ABL-Containing Molecules

It is found in a vast collection of natural products and potential therapeutics with significant biological activities including anticancer, anti-inflammatory, antibacterial, antifungal, and antiviral.[1] ABLs are also useful building blocks for chemical synthesis due to their facile derivatization.[2] It was estimated that by 2009 there were more than 5000 identified ABL natural products along with another 9000 synthetic analogues.[3] Synthesis of the ABL framework is an ongoing endeavor for the synthetic community. As such, several reviews have been published highlighting a diverse set of approaches toward the scaffold.[1,3,4]

A.1.1.2 Current Approaches to Generating ABLs

The general synthetic approaches to the ABL core have been classified into the following types: alkylidenation of γ-butyrolactones,[5] various lactonization approaches,[6] tandem or sequential intramolecular C−H insertion/olefination,[7] the Dreiding−Schmidt organometallic approach,[8] cross-metathesis between α-methylene-γ-butyrolactones and

olefins,[9] intramolecular enyne metathesis reactions,[10] Pd-catalyzed cross-couplings,[11] Diels−Alder and retro-Diels−Alder reactions,[12] radical cyclizations,[13] and Baeyer−Villiger reactions on cyclobutanones.[14] Despite the abundant literature, the diversity within the ABLs has made the pursuit of strategic ABL targets and the development of methodologies to access them persistently meaningful endeavors in the synthetic community.[15]

A.1.2 Seminal Work Toward ABL Products in the France Lab

A.1.2.3 Initial Observations

Over the past 10 years, our laboratory has explored a variety of intra- and intermolecular ring-opening cyclizations of small, strained ring systems (e.g. cyclopropanes, cyclopropenes, alkylidene cyclopropanes, and cyclobutanes).[16] In one pertinent example, we disclosed a calcium-catalyzed, dehydrative, ring-opening cyclization of (hetero)aryl cyclopropyl carbinols to form (hetero)aryl-fused cyclohexa-1,3-dienes.[17] Interestingly, we found that when cyclopropyl carbinol **1a** was subjected to the reaction conditions, 14% yield of α-alkylidene-γ-butyrolactone **3a** was obtained in addition to the expected dihydronaphthalenes **2a** and **2a′** (Scheme 47). Product **3a** was unexpected, as no mention of α-alkylidene-γ-butyrolactone formation had been reported in the previous literature for the transformation.[18]

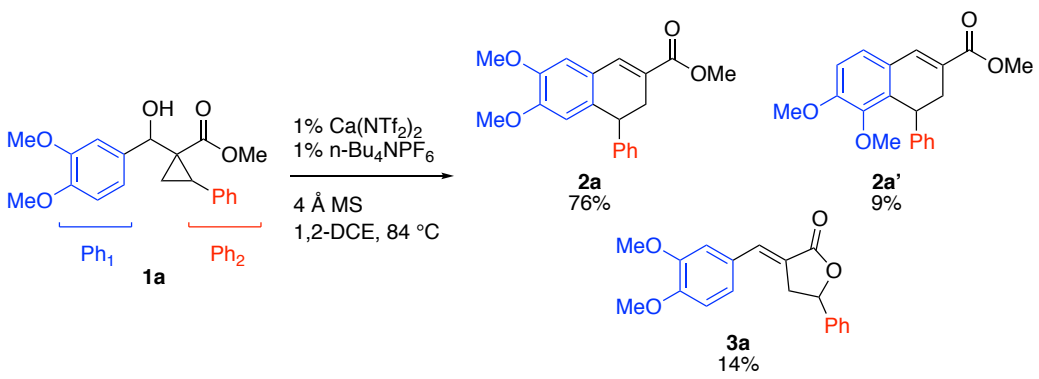

Scheme 47 – Initial Observation of ABL Formation from a Cyclopropyl Carbinol

A.1.2.2 Summary of Sandridge's Synthetic Results

Sandridge optimized reaction conditions for formation of the ABL product and demonstrated utility of the method through an impressive substrate scope. However, the product space exhibited inconsistent selectivity for *E* and *Z* diastereomers, the origins of which eluded intuition. A subset of Sandridge's ABL-forming reaction scope illustrates the variable *E*/*Z* selectivity (Table 18). Notably, while **1a** generated ABL **2a** in 99:1 *E*:*Z* selectivity (entry 1), the selectivity was completely eroded by the transposition of a single methoxy group: **1k** afforded ABL **3k** with no *E*:*Z* selectivity (entry 11). As Sandridge's approach for the construction of ABL products was mechanistically distinct from any in the literature, it required a model through which the selectivity for *E* and *Z* diastereomers could be explained.

Table 18 – Scope of the ABL-Forming Reaction Illustrating Variable E/Z Selectivity

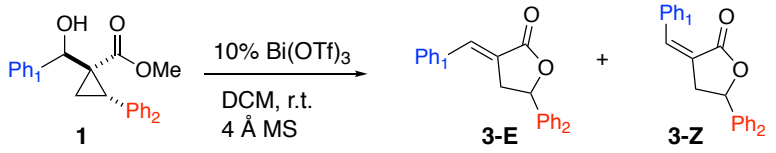

1 **3-E** **3-Z**

Entry[a]	Cyclopropyl Carbinol		ABL Product	E:Z[b]	Yield[c]
1	R = H	**1a**	**3a**	99:1	62%
2	4-Me	**1b**	**3b**	3:1	23%
3	4-Cl	**1c**	**3c**	99:1	81%
4	4-Br	**1d**	**3d**	99:1	87%
5	2-Br	**1e**	**3e**	99:1	72%
6	3-Br	**1f**	**3f**	99:1	89%
7[d]	**1g**		**3g**	99:1	78%
8	R = H	**1h**	**3h**	1:1	60%
9	OMe	**1i**	**3i**	7:1	73%
10	Cl	**1j**	**3j**	1:1	35%[e]
11	**1k**		**3k**	1:1	26%

[a]Reactions were performed with cyclopropyl carbinols **1** (1 equiv.) and $Bi(OTf)_3$ (10 mol %) in CH_2Cl_2 (0.1 M, 23 °C) in the presence of 4 Å molecular sieves. [b]E/Z ratios determined by ^1H NMR analysis of the crude reaction material. [c]Isolated yields. [d]Reaction performed with 20 mol % $Bi(OTf)_3$. [e]Yield determined from ^1H NMR analysis of the crude reaction material using dimethyl terephthalate as an iternal standard.

A.1.3 Approach to Understanding E vs. Z Selectivity in the ABL Chemistry

The approach taken to understand *E* vs. *Z* selectivity in Sandridge's ABL-generating chemistry proceeded through four stages: (1) proposing a mechanistic regime, (2) using the mechanism to formulate a hypothesis about selectivity, and (3) applying DFT calculations to test the hypothesis.

A.1.3.1 Proposing a Mechanism

A mechanism was proposed to accommodate the observed product space with two transition states, **TS1** and **TS2**, available to the cyclopropyl carbinyl cation **(I)** leading to the ABL and aryl dihydronaphthalenes products, respectively (Scheme 48).

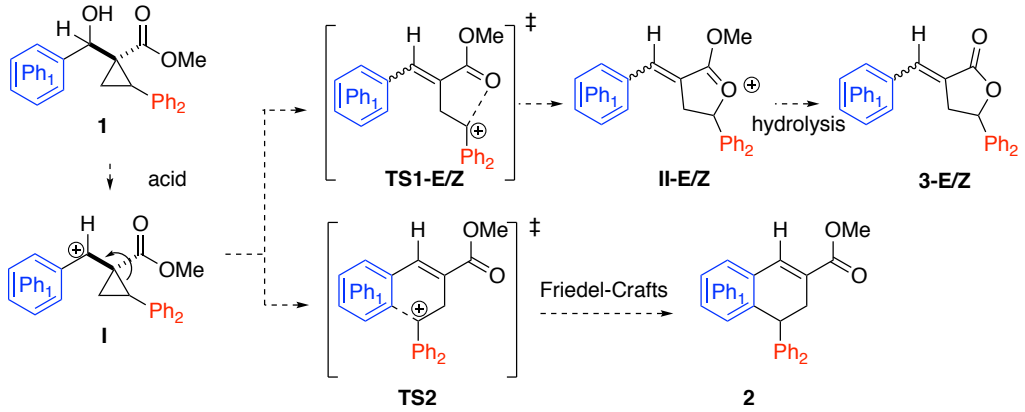

Scheme 48 – Proposed Mechanism Accommodating the Formation of ABL and Aryl Dihydronaphthalene Products from a Cyclopropyl Carbinol

The ABL product would be obtained by traversing **TS1**, and, assuming a comparatively low barrier to rotation about the C_α-C_β bond, the E/Z selectivity would be determined by the $\Delta\Delta G^{\ddagger}$ between transition states **TS1** for the *E* and *Z* conformers (call these **TS1-E** and **TS1-Z**, and $\Delta\Delta G^{\ddagger}_{E/Z}$).

A.1.3.2 Hypothesis Concerning *E/Z* Selectivity

It was hypothesized that we could understand the origins of E/Z selectivity by examining cyclization transitions (from **I** to **II**) from a DFT perspective while interpreting geometric and electronic trends in these transitions through results from the synthetic experiments based on principles of least nuclear motion.

A.1.3.3 DFT Approach to Testing the Hypothesis

The DFT testing of the hypothesis could be broken into two steps. First, transitions from the cyclopropyl carbinyl cation (**I**) to the cyclized, pre-hydrolysis product (**II**) for two species, **1a** and **1h**, that exhibited different selectivity would be modeled. Analysis of an exemplary reaction coordinate for each, a highly selective transformation and an unselective one, would, hypothetically, reveal which characteristics of the transition were most relevant to observed selectivity. After identifying these characteristics, we could validate their relevance by examining their correlation with observed selectivity for other substrates on which Sandridge collected synthetic data.

A.2 Computational Method

All calculations were performed using the Gaussian 09 package at the M06L/6-31g(d,p) level of theory.[30,31] Gaussian's default solvation model, the Polarizable Continuum Model implemented via integral equation formalism (IEF-PCM), was employed to simulate a dichloromethane solvent.[32–34] Transition state calculations were verified to have only one imaginary vibrational frequency.

A.3 Results and Discussion

A.3.1 Understanding E vs. Z Selectivity Through Two Representative Substrates

DFT calculations were employed to examine the cyclopropane-opening transition states between intermediates **I** and **II**, derived from both the 3,4-dimethoxyphenyl-substituted carbinol **1a** (high selectivity, Figure 31) and the phenyl carbinol **1h** (low selectivity, Figure 32). The transformation generally agreed with our proposed mechanistic transformation between **I** and **II**, going through a homoallylic cation partially stabilized through an approaching ester. Consistent with the experimentally observed selectivity, the computations revealed a $\Delta\Delta G^{\ddagger}$ = 3.9 kcal/mol in favor of E isomer formation for the 3,4-dimethoxyphenyl carbinyl cation **I-a**. Meanwhile, $\Delta\Delta G^{\ddagger}$ = 1.3 kcal/mol for **I-h**, which displayed no E/Z selectivity under the optimized reaction conditions.

The more exothermic ring opening for **I-h** suggests an earlier transition state and thus begs the application of Hammond's postulate to rationalize observed selectivity. Indeed, not only is the transformation more exothermic for **I-h**, but the cyclopropane C_{β}–C_{γ} bond in **I-h** is weakened compared to that in **I-a**, 1.73 Å vs 1.65 Å, respectively. In this light, the C_{β}– C_{γ} bond must undergo more elongation to reach the transition state from **I-a**, prompting a later and more selective transition compared to that from **I-h**.

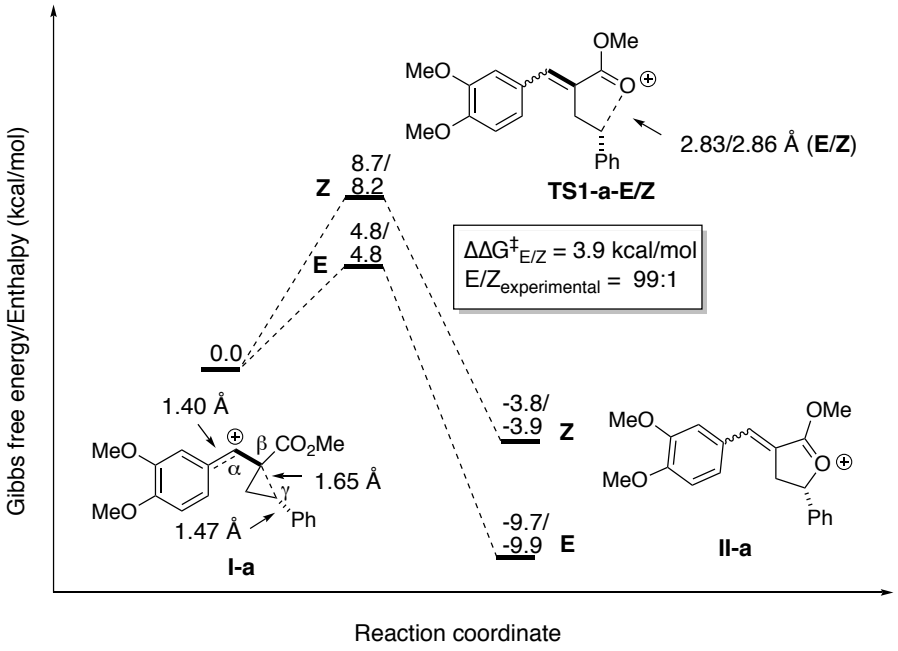

Figure 31 – Reaction Coordinate Diagram for a Selective Cyclopropane-Opening Cyclization Transition

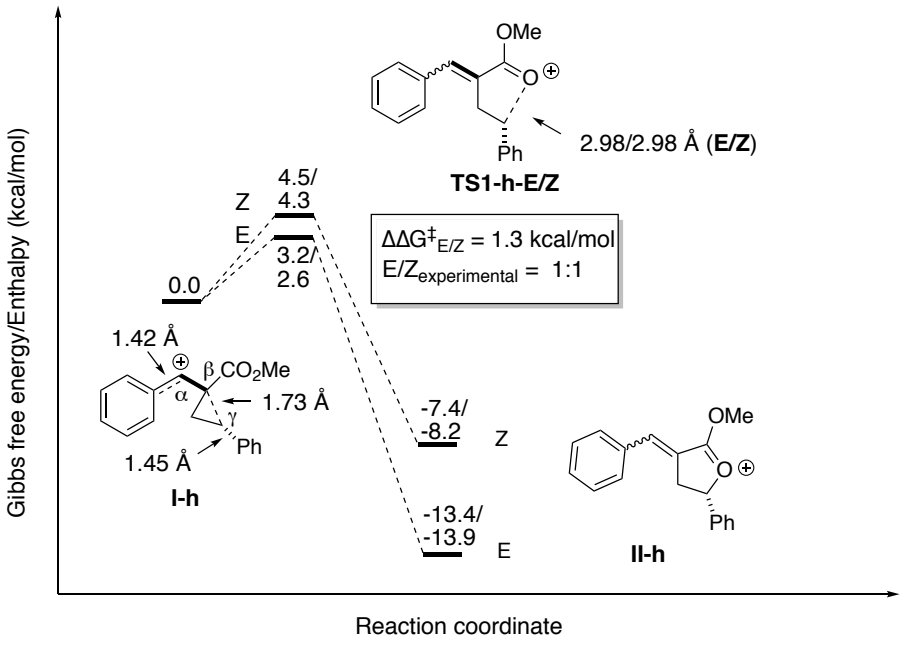

Figure 32 – Reaction Coordinate Diagram for a Nonselective Cyclopropane-Opening Cyclization Transition

Here, the difference in cyclopropane lability arises from the different electron donating potentials of the phenyl rings. Methoxy substitutions at the 3 and 4 positions increase stabilization of the benzylic cation at C_α. With less electron-donating potential on the unsubstituted phenyl ring, **I-h** compensates by elongating the C_β–C_γ bond and delocalizing some of the positive charge onto the benzylic C_γ position. This phenomenon is reflected not only in the elongation of C_β–C_γ but also in the shortening of the Ph–C_γ bond (1.47 Å in **I-a** vs 1.45 Å in **I-h**). Atomic partial charges (δ+) reflect these geometric changes by displaying a shift of positive charge accumulation from C_α to C_γ as the C_β–C_γ length increases.

A.3.2 Validating the Model

Hypothetically, the cyclopropane could be polarized via substitution on the second phenyl ring as well. For example, comparing **I-a** and **I-b** we see that 4-methyl substitution is responsible for elongating C_β–C_γ by 0.02 Å in the ground state (Figure 33); a concomitant drop in *E*/*Z* selectivity from 99:1 to 3:1 is observed in the synthetic experiments.

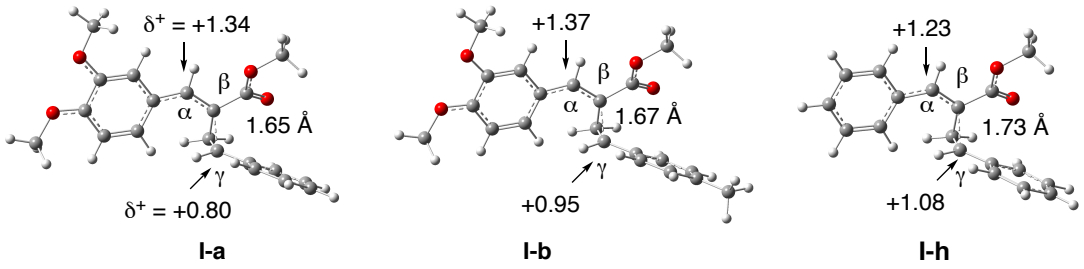

Figure 33 – Geometric Changes in the Cyclopropane as a Function of EDG Substitution on Ph^1 and Ph^2

Holding sterics constant and examining this trend across structures **I-a – I-k** suggests that, as a corollary to Hammond's postulate, electron-donating groups at Ph_1 and electron-withdrawing groups at Ph_2 enhance *E*/*Z* selectivity by strengthening the C_β–C_γ bond in the ground-state carbinyl cation **I** (Figure 34).

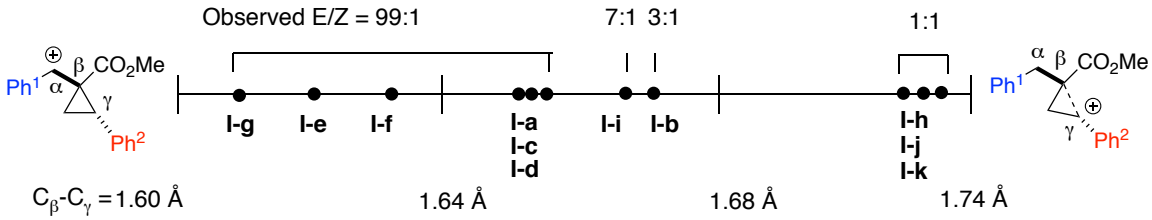

Figure 34 – Spectrum of C_β-C_γ Bond Lengths Correlates with Observed E/Z Selectivity for ABL Formation

A.4 Conclusion

Through comparing the experimental results to DFT calculations, selectivity can be reasonably rationalized by applying Hammond's postulate to the transition from **I** to **II** through **TS1** (Figure 35). Moreover, the *E*/*Z* selectivity and the polarization (as measured by bond length) of the cyclopropyl C_β–C_γ in the ground-state carbinyl cation **I** can then be correlated.

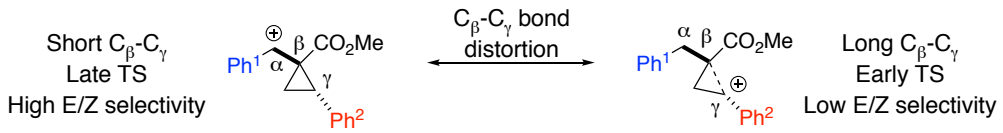

Figure 35 – Easily Calculated C_β-C_γ Bond Lengths Interpreted through Hammond's Postulate Can Be Used to Predict Selectivity for E vs. Z ABL Products

This approach provides an easily accessible calculation (C_β–C_γ bond length in intermediate **I**) as the basis for predicting the *E*/*Z* selectivity in ABL formation and, thus, a useful tool for synthetic chemists targeting ABL-containing molecules via a cyclopropyl carbinol ring-opening cyclization.

A.5 Experimental

For supporting information including general methods, experimental procedures, computed structure geometries and energies, and characterization data, see: Sandridge, M. J.; McLarney, B. D.; Williams, C. W.; France, S. *J. Org. Chem*. **2017**, *82*, 10883-10897.

A.6 References

[1] (a) Kunzmann, M. H.; Sieber, S. A. *Molecular Biosystems* **2012**, *8*, 3061. (b) Ghantous, A.; Gali-Muhtasib, H.; Vuorela, H.; Saliba, N. A.; Darwiche, N. *Drug Discovery Today* **2010**, *15*, 668. (c) Lepoittevin, J.- P.; Berl, V.; Gimenez-Arnau, E. *The Chemical Record* **2009**, *9*, 258. (d) Hoffmann, H. M. R.; Rabe, J. *Angewandte Chemie, International Edition* **1985**, *24*, 94.

[2] For examples of chemical derivatization, see the following. Hydrogenation: (a) Ohta, T.; Miyake, T.; Seido, N.; Kumobayashi, H.; Akutagawa, S.; Takaya, H. *Tetrahedron Letters* **1992**, *33*, 635. Epoxidation: (b) Murray, A. W.; Reid, R. G. *Synthesis* **1985**, *1985*,

35. Conjugate addition: (c) Miyata, O.; Shinada, T.; Naito, T.; Ninomiya, I. *Chemical and Pharmaceutical Bulletin* **1989**, *37*, 3158. Amine addition: (d) Artman, G. D., III; Weinreb, S. M. *Organic Letters* **2003**, *5*, 1523.

[3] Kitson, R. R. A.; Millemaggi, A.; Taylor, R. J. K. *Angewandte Chemie, International Edition* **2009**, *48*, 9426.

[4] For further reviews on synthetic approaches to ABLs, see: (a) Janecki, T. *Targets in Heterocyclic Systems* **2006**, *10*, 301. (b) Lu, X.; Ma, S.; Ji, J.; Zhu, G.; Jiang, H. *Pure and Applied Chemistry* **1994**, *66*, 1501. (c) Samarat, A.; Amri, H.; Landais, Y. *Tetrahedron* **2004**, *60*, 8949. (d) Sharma, R. P.; Sarma, J. C. Heterocycles 1986, 24, 441. (e) Petragnani, N.; Ferraz, H. M. C.; Silva, G. V. J. *Synthesis* **1986**, *1986*, 157. (f) Grieco, P. A. *Synthesis* **1975**, *1975*, 67.

[5] For recent examples, see: (a) Nakamura, T.; Tsuboi, K.; Oshida, M.; Nomura, T.; Nakazaki, A.; Kobayashi, S. *Tetrahedron Letters* **2009**, *50*, 2835. (b) Hirose, T.; Miyakoshi, N.; Mukai, C. *Journal of Organic Chemistry* **2008**, *73*, 1061. (c) Dai, M.; Danishefsky, S. J. *Journal of the American Chemical Society* **2007**, *129*, 3498. (d) Merten, J.; Fröhlich, R.; Metz, P. *Angewandte Chemie, International Edition* **2004**, *43*, 5991.

[6] For representative examples, see: (a) Azarken, R.; Guerra, F. M.; Moreno-Dorado, F. J.; Jorge, Z. D.; Massanet, G. M. *Tetrahedron* **2008**, *64*, 10896. (b) Bandyopadhyay, S.; Dutta, S.; Spilling, C. D.; Dupureur, C. M.; Rath, N. P. *Journal of Organic Chemistry* **2008**, *73*, 8386. (c) Hilt, G.; Paul, A.; Harms, K. *Journal of Organic Chemistry* **2008**, *73*, 5187. (d) Ramachandran, P. V.; Pratihar, D. *Organic Letters* **2007**, *9*, 2087. (e) Elford, T. G.;

Arimura, Y.; Yu, S. H.; Hall, D. G. *Journal of Organic Chemistry* **2007**, *72*, 1276. (f) Mitra, S.; Gurrala, S. R.; Coleman, R. S. *Journal of Organic Chemistry* **2007**, *72*, 8724.

[7] (a) Lloyd, M. G.; D'Acunto, M.; Taylor, R. J. K.; Unsworth, W. P. *Tetrahedron* **2015**, 71, 7107. (b) Lloyd, M. G.; Taylor, R. J. K.; Unsworth, W. P. *Organic Letters* **2014**, *16*, 2772. (c) Shie, J.-Y.; Zhu, J.-L. *Tetrahedron* **2016**, *72*, 1590.

[8] Csuk, R.; Schroder, C.; Hutter, S.; Mohr, K. *Tetrahedron: Asymmetry* **1997**, *8*, 1411.

[9] (a) Moïse, J.; Arseniyadis, S.; Cossy, J. *Organic Letters* **2007**, *9*, 1695. (b) Raju, R.; Allen, L. J.; Le, T.; Taylor, C. D.; Howell, A. R. *Organic Letters* **2007**, *9*, 1699.

[10] Charruault, L.; Michelet, V.; Genet, J.-P. *Tetrahedron Letters* **2002**, *43*, 4757.

[11] Gagnier, S. V.; Larock, R. C. *Journal of Organic Chemistry* **2000**, *65*, 1525.

[12] (a) Lebel, H.; Parmentier, M. *Organic Letters* **2007**, *9*, 3563. (b) Lertvorachon, J.; Thebtaranonth, Y.; Thongpanchang, T.; Thongyoo, P. *Journal of Organic Chemistry* **2001**, *66*, 4692.

[13] (a) Dulcere, J.-P.; Mihoubi, M. N.; Rodriguez, J. *Journal of Organic Chemistry* **1993**, *58*, 5709. (b) Bachi, M. D.; Bosch, E. *Journal of Organic Chemistry* **1992**, *57*, 4696.

[14] Wakamatsu, T.; Miyachi, N.; Ozaki, F.; Shibasaki, M.; Ban, Y. *Tetrahedron Letters* **1988**, *29*, 3829.

[15] For recent examples that highlight the continuous activity of the synthetic community toward α-alkylidene-γ-butyrolactone synthesis, see: (a) Su, X.; Zhou, W.; Li, Y.; Zhang, J. *Angewandte Chemie, International Edition* **2015**, *54*, 6874. (b) Odagi, M.; Furukori, K.;

Yamamoto, Y.; Sato, M.; Iida, K.; Yamanaka, M.; Nagasawa, K. *Journal of the American Chemical Society* **2015**, *137*, 1909. (c) Xu, X.; Wang, X.; Zavalij, P. Y.; Doyle, M. P. *Organic Letters* **2015**, *17*, 790. (d) McCammant, M. S.; Sigman, M. S. *Chemical Science* **2015**, *6*, 1355. (e) Zhang, Z.; Wu, W.; Liao, J.; Li, J.; Jiang, H. *Chemistry – A European Journal* **2015**, *21*, 6708. (f) Karmakar, R.; Yun, S. Y.; Chen, J.; Xia, Y.; Lee, D. *Angewandte Chemie, International Edition* **2015**, *54*, 6582. (g) Xiao, X.; Xu, Z. Y.; Zeng, Q.-D.; Chen, X.-B.; Ji, W.-H.; Han, Y.; Wu, P. Y.; Ren, J.; Zeng, B.-B. *Chemistry – A European Journal* **2015**, *21*, 8351.

[16] (a) Martin, M. C.; Shenje, R.; France, S. *Israel Journal of Chemistry* **2016**, *56*, 499. (b) Shenje, R.; Martin, M. C.; France, S. *Angewandte Chemie, International Edition* **2014**, *53*, 13907. (c) Shenje, R.; Williams, C. W.; Francois, K. M.; France, S. *Organic Letters* **2014**, *16*, 6468. (d) Aponte-Guzmań,J.; Taylor,J. E., Jr.; Tillman, E.; France, S. *Organic Letters* **2014**, *16*, 3788. (e) Cavitt, M. A.; Phun, L. H. *Chemical Society Reviews* **2014**, *43*, 804. (f) Martin, M. C.; Patil, D. V.; France, S. *Journal of Organic Chemistry* **2014**, *79*, 3030. (g) Phun, L. H.; Aponte-Guzmań, J.; France, S. *Angewandte Chemie, International Edition* **2012**, *51*, 3198.

[17] Sandridge, M. J.; France, S. *Organic Letters* **2016**, *18*, 4218.

[18] (a) Sakuma, D.; Ito, J.; Sakai, R.; Taguchi, R.; Nishii, Y. *Chemistry Letters* **2014**, *43*, 610. (b) Yoshida, E.; Nishida, K.; Toriyabe, K.; Taguchi, R.; Motoyoshiya, J.; Nishii, Y. *Chemistry Letters* **2010**, *39*, 194.

[30] Gaussian 09, Revision D.01, M. J. Frisch, G. W. Trucks, H. B. Schlegel, G. E. Scuseria, M. A. Robb, J. R. Cheeseman, G. Scalmani, V. Barone, B. Mennucci, G. A.

Petersson, H. Nakatsuji, M. Caricato, X. Li, H. P. Hratchian, A. F. Izmaylov, J. Bloino, G. Zheng, J. L. Sonnenberg, M. Hada, M. Ehara, K. Toyota, R. Fukuda, J. Hasegawa, M. Ishida, T. Nakajima, Y. Honda, O. Kitao, H. Nakai, T. Vreven, J. A. Montgomery, Jr., J. E. Peralta, F. Ogliaro, M. Bearpark, J. J. Heyd, E. Brothers, K. N. Kudin, V. N. Staroverov, R. Kobayashi, J. Normand, K. Raghavachari, A. Rendell, J.C. Burant, S.S. Iyengar, J. Tomasi, M. Cossi, N. Rega, J. M. Millam, M. Klene, J. E. Knox, J. B. Cross, V. Bakken, C. Adamo, J. Jaramillo, R. Gomperts, R. E. Stratmann, O. Yazyev, A. J. Austin, R. Cammi, C. Pomelli, J. W. Ochterski, R. L. Martin, K. Morokuma, V. G. Zakrzewski, G. A. Voth, P. Salvador, J. J. Dannenberg, S. Dapprich, A. D. Daniels, Ö. Farkas, J. B. Foresman, J. V. Ortiz, J. Cioslowski, and D. J. Fox, Gaussian, Inc., Wallingford CT, **2013.**

[31] Zhao, Y.; Truhlar, D. G. J. Chem. Phys. 2006, 125, 194101.

[32] (a) Tomasi, J.; Mennucci, B.; Cammi, R. *Chemical Reviews* **2005**, *105*, 2999 and references cited therein.

[33] Tomasi, J.; Mennucci, B. Cances, E. *THEOCHEM* **1999**, *464*, 211.

[34] Pascal-Ahuir, J.L.; Silla, E.; Tuñoń, I. *Journal of Computational Chemistry* **1994**, *15*, 1127.